Research Facilities
Design Concepts
Summer 1969

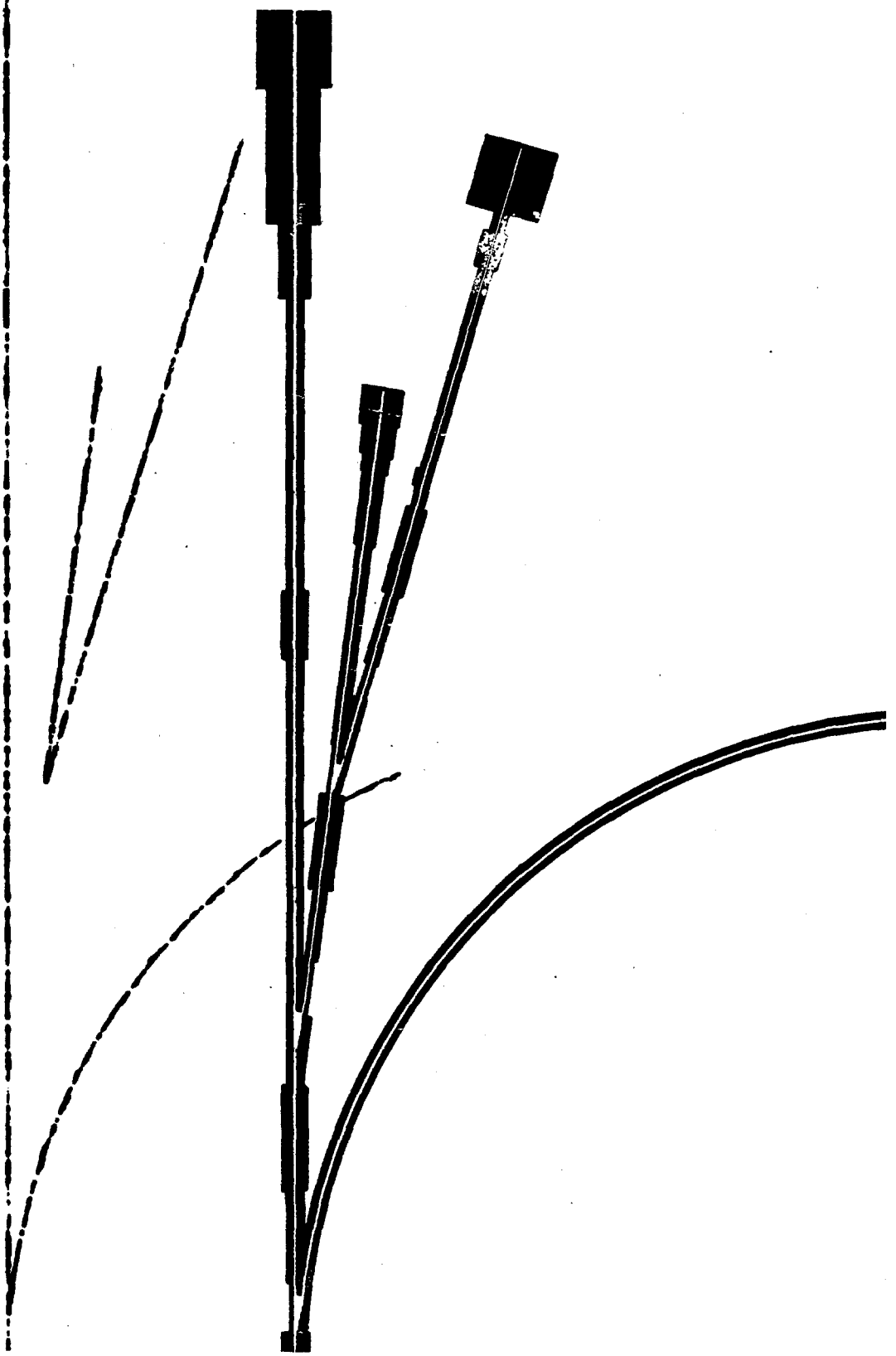

national accelerator laboratory

FERMILAB-TM-0181

NAL RESEARCH FACILITIES DESIGN CONCEPTS

SUMMER 1969

E.J. BLESER, R.A. CARRIGAN, JR., F.A. NEZRICK, A.L. READ, EDITORS

1. INTRODUCTION

This report has been prepared with the principal purpose of acquainting the 1969 Summer Study participants with the activities presently underway to develop experimental facilities at NAL. It consists of a central report supported by a number of appendices. A great deal of the substance of the report has been summarized concisely in Appendix I, "Concepts of the Experimental Areas".

Chapter 2 reviews the plans for the experimental facilities including the overall site plan, the primary beam transfer, the conventional target areas with their secondary beams and shielding, the neutrino-bubble chamber area and the special purpose areas. Chapter 3 surveys the overall equipment needs at NAL and some of the equipment development projects that are underway. These include an extensive program to develop superconducting magnets for the laboratory and an NAL-BNL collaboration on a 25 foot cryogenic bubble chamber. Chapter 4 discusses the organization of the work on experimental facilities and describes some of the liaison activities being carried out.

Many of the appendices consist of more detailed treatment of the material in the main text. In most cases the material in the appendices was developed at an earlier date than the material in the main body of the text. The latter represents later and more consistent information. Appendix I is a review of the conceptual design of the experimental facilities. Appendix II contains two reports covering some aspects of the proton extraction; beam transport, and targeting. Appendix III reviews a preliminary plan for shielding in a conventional

target station. Appendix IV discusses radiation shielding and safety requirements and also gives theoretical production cross sections at 200 BeV. Appendix V is an extensive discussion of the NAL superconducting magnet program. Appendix VI is NAL MM 148 - a discussion of the overall projected experimental equipment needs through 1975. Appendixes VII and VIII review charged particle secondary beam designs for a conventional target station. Appendix IX discusses neutrino beam design concepts in detail. Appendix X contains abstracts of the 1968 Summer Study reports for easy reference. Appendix XI describes target modulated r.f. beam design concepts.

The NAL Design Report[1] contains a discussion of earlier concepts of the experimental areas, along with very useful material on accelerator characteristics which also have particular relevance in the design of experimental areas. The 1968 NAL summer study reports are also available in a three volume set.[2]

The material in this report has been developed by the Experimental Facilities Section along with the assistance of members of some other sections at NAL. In particular, M. Awschalom (Radiation Physics), J. MacLachlan (Accelerator Theory), A. Maschke and R. Mobley (Beam Transfer and Targeting) have made major contributions. A list of the principal contributors to each chapter of this report appears at the start of the chapter. H. Cramer, D. Mery, J. Plese, and A. Gonzales ably assisted in the typing and preparation of the report. R. A. Carrigan, Jr., has handled the compilation of this material into the report. Most of the design concepts for experimental areas described in that report have been developed through the work of E. J. Bleser,

TABLE OF CONTENTS

FIGURES

T. L. Collins, E. L. Goldwasser, A. Maschke, D. Moll (DUSAF), F. A. Nezrick, A. L. Read, and F. C. Shoemaker. Although the work we describe here is the product of many people, we four (E. J. Bleser, R. A. Carrigan, Jr., F. A. Nezrick, A. L. Read) must accept full responsibility.

E. J. Bleser

R. A. Carrigan, Jr.

F. A. Nezrick

A. L. Read

REFERENCES

1. National Accelerator Laboratory Design Report, July, 1968.

2. National Accelerator Laboratory 1968 Summer Study, June, 1969 (3 volumes)

2. EXPERIMENTAL FACILITIES

W. F. Baker, E. J. Bleser, Y. W. Kang, R. Mobley, F. A. Nezrick

The design of the experimental facilities for an accelerator is an iterative process. Starting to design an area with all options open faces the designer with an extremely difficult selection task. Instead, decisions have to be made rather arbitrarily and a definite design started. Then, in the light of detailed studies the earlier decisions can be reviewed and modified if need be. The effect of these modifications on other elements of the design can then be taken into account and the process repeated. Eventually, the process should converge. In the case of NAL, the construction schedule imposes a severe limit on the number of steps that can be taken. In the fall and winter of 1968-69, the master plan for the overall layout of the experimental facilities was reviewed, the present plan was adopted, and it has since undergone several critical reviews. At present, the detailed design of the experimental area is under consideration rather than the present master plan. The 1969 Summer Study is intended to provide a critical review of the detailed designs that exist and of the concepts that were used in generating them. It should also provide guidance for those designs not yet underway. In the fall of 1969, a final review of the details of the master plan will be carried out in the light of the detailed design of the individual experimental areas.

The first part of this chapter discusses the present master plan. In the framework of the master plan, detailed designs of the beam transport system, the beam splitting system, the beam targeting system, the radiation shielding, and the experimental

areas are underway. The beam studies are being carried out at NAL by the Beam Transfer Section as reported in Section 2.2 and Appendix II. The Radiation studies of the Radiation Physics Section are reported in Section 2.3 and Appendix III.

The remaining sections contain reports on the designs of the experimental areas as far as they have gone -- a conventional station, a neutrino-bubble chamber station and a transmission station, an area which does not now appear in the master plan. The second conventional station shown in the master plan is discussed only briefly since no detailed plans yet exist for it.

2.1. Master Plan

The object of the master plan is to distribute the experimental areas on the site so that they are well separated from each other in order to allow ample room for future experimental requirements. On the other hand, it is desirable to have the areas close together to share support services. Most importantly, the transport and bending of beams is very expensive, and it is imperative to minimize this expense.

The master plan as presented in the 1968 Design Study Report envisaged one internal target area, one thin target station and two conventional target stations. Later studies, in part by the 1968 summer study, recommended elimination of the internal target area and emphasized the importance of a large cryogenic bubble chamber coupled with a neutrino beam. The present plan has two conventional target stations, and a third station specially designed to produce neutrino beams and charged particle beams for a bubble chamber. An internal target area is no longer provided. In the

present master plan, only one beam is extracted from the main ring. This single beam will be split by septum devices into beams which can then be targeted or split again. Between 1,000 and 1,500 feet of beam transport are needed between each switching, splitting, or targeting point to re-form the beam.

The configuration which best satisfied the criteria is a design based on a curving main proton beam with experimental areas fanning off the curved line. The design is shown in Figure 2.1 and discussed in detail in Section 2.2 on beam transfer. Its advantages are that the experimental areas naturally fan out from each other giving more space for a fixed number of bending magnets then could be achieved with a parallel arrangement. A different scheme which involved areas alternately to the left and to the right of the main beam results in very complicated road and utility systems. A further advantage of the present arrangement is that the bubble chamber beam is split off before this fast beam goes past any septa, since they could easily be destroyed by a fast pulse which was misaligned.

This master plan uses all the resources allotted to the external areas in the 1968 Design Report. Any additions will be very hard to manage in the present construction package. Any possible economies would be very desirable. The overriding consideration in developing the experimental areas is the great expense involved in bending, shielding and targeting 10^{13} 200 BeV protons. The somewhat constrained and limited scope of the designs in the ensuing sections derives from a realization of the great practical problems which must be mastered with finite resources.

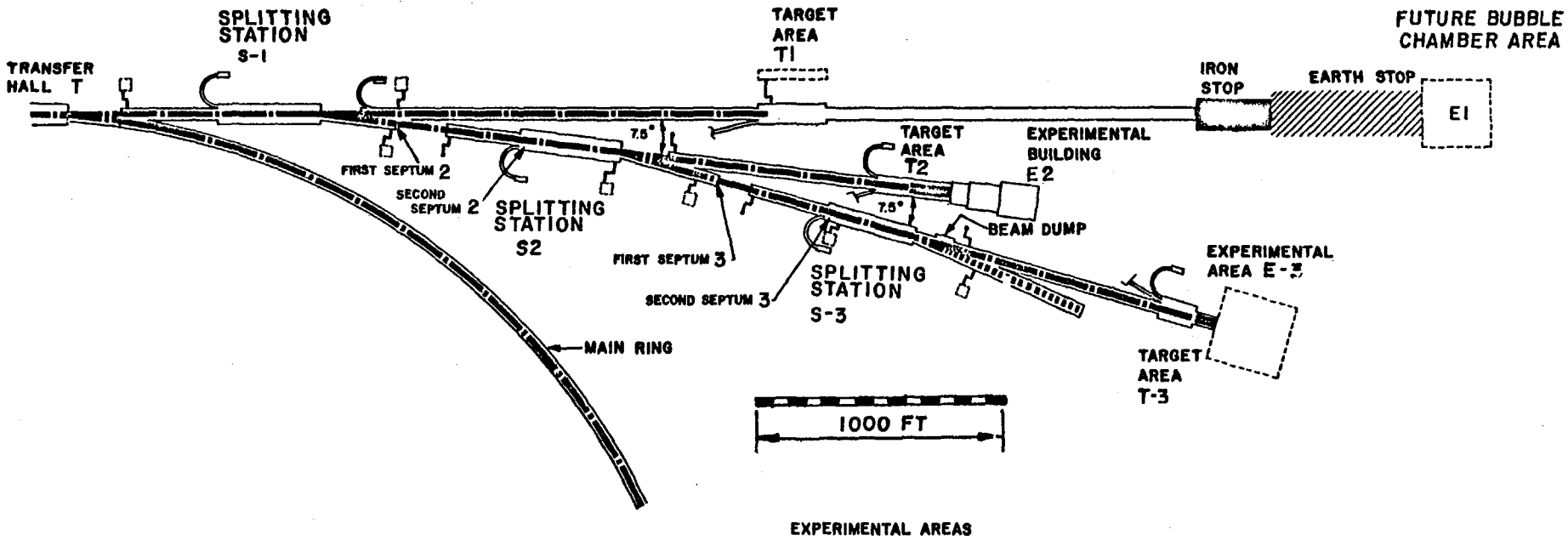

Figure 2-1 - Experimental Areas Master Plan

2.2. Primary Beam Transfer and Targeting

In the proposed plan for the experimental areas, the proton beam is extracted from the main ring in the Transfer Hall (see Figure 1) over a time that can be varied from one revolution period (20 microseconds) up to the full length of the flat-top (1 second). The proton beam is then transported from the Transfer Hall and moves in a straight line along a northeasterly direction to the first splitting station, S1. Beyond this point, the beam-transport system is comprised of a straight section 600 feet in length followed by a bending section of the same length. The beam is split in the straight section, with a fraction extracted from the main transport line to go to a target station and the remainder going through the bending section to be carried to the next splitting station.

The switched portion of the beam is bent through an angle of 7.5°. It travels 1350 feet, past the shops and laboratories of the industrial area, to the second splitting station, S2. Here the beam can be split again, either travelling straight on to the second target, T2, or being bent eastward, again through approximately 7.5°, toward the third target area, 3. The experimental facilities can be expanded in the future, should this prove desirable, by adding more splitting stations and target stations farther along the same curved line. In the concept outlined in the NAL Design Report, the primary beam line was straight; the beam was diverted to targets by the switching stations. The primary advantage of the new concept is that it provides greater lateral space between the experimental areas for the same total amount of bending of the proton beam.

As presently conceived, the bending and focusing in this system are similar to those in the main accelerator. In fact, it is planned that extra main-accelerator magnets will be fabricated for this beam-transport system. Similarly, the housing of the proton beam will make use of the pre-formed sections designed for the main-accelerator enclosure. Sections of small beam-transport pipe will be used immediately downstream of each switching station to decouple the switching stations from each other and to localize radioactivity.

Beam splitting is carried out by the use of a series of septum devices. This system is similar to the one used to extract the beam from the main accelerator. The first thin electrostatic septum is positioned close to the beginning of the straight transport section. The split beam is given a vertical impulse. After a 90° betatron phase advance to achieve maximum amplitude, it clears the septum of the next element which bends the beam further upward to miss the leading magnet at the end of the straight section. The beam is then transported at an upward angle from the 725.5-ft elevation at the switching station to the 753-ft elevation at the target stations, where it is brought back to the horizontal plane. The horizontal distance traversed during this change of elevation is 1000 feet. In this traversal, the beam is focused by a series of quadrupoles spaced 200 feet apart. At the 753-ft elevation, the beam is transported 200 feet to the target. The quadrupoles in this last 200 feet must be moveable in order to provide for changing of target elements.

In the NAL Design Report the following emittance areas are given for the circulating 200 BeV beam at the septum.

$E_v = 0.09\ \pi$ mm - mrad (10 mm x 0.030 mrad)

$E_h = 0.23\ \pi$ mm - mrad (20 mm x 0.035 mrad)

The momentum spread is expected to be $\frac{\Delta p}{p} = \pm 10^{-3}$. The fast switched beam will have essentially these dimensions, plus a dispersion width of:

$$\Delta R = \frac{R}{\nu_{x^2}} \frac{\Delta p}{p} = 2.5 \text{ mm}.$$

In the slow beam, the vertical emittance will be the same or slightly larger due to resonance coupling at extraction. The horizontal emittance is reduced in the extraction process to about:

$$E_h = 0.06\ \pi \text{ mm - mrad (10 mm x 0.02 mrad)}.$$

This number is obtained from the design criterion of a 1 cm/turn growth rate of the beam at the septum, and the fact that the divergence is reduced to ~ 0.02 mrad because the betatron oscillations are locked in phase during the resonant growth.

In uniform acceleration of a beam, the betatron amplitudes are damped as $p^{-1/2}$. The emittance is proportional to p^{-1}. The design report emittances at 200 MeV, 10 BeV, and 200 BeV only roughly correspond to the momentum damping. For example, from 10 BeV to 200 BeV, the quoted emittances are reduced about a factor of 12 rather than 19. The difference is due to allowances for dilution in transfer.

At splitting stations the vertical emittances are further reduced. This may not be useful experimentally since the emittances are already unprecedentedly small. Halos produced by scattering at septa (at most 0.1% is scattered at each septum) will be reduced by cleanup stops.

The proton beam transport system will be able to handle the nominal emittance beam at 50 BeV. Thus, at 200 BeV, it will be able to handle a factor of four in the beam emittances greater than the nominal values given. A number of these concepts are developed at somewhat greater length in Appendix II.

The target stations are the points of greatest radioactivity in the entire accelerator facility. All the technical components associated with the target -- that is, target mechanisms, collimators, and possibly, the first focusing magnets for secondary beams -- are to be mounted in a "target box." The target box is a steel enclosure, approximately 100 feet long and 3 x 3 feet in cross section. The target box itself is fixed in a permanent position and surrounded by massive fixed concrete and earth shielding (unlike the portable shielding of the design report).

Components are brought into it and put in place by a railroad train. The target box contains ledges for the support of components and rails for the train. A target assembly is installed on the train in the target laboratory described below and is moved to the target box, where it is lowered onto the support ledges by remotely operated jacks. The train is then removed from the target box. Thus, a major function of the target box is to provide rigid support for the target assembly. Another important function is to make it possible to locate radiation shielding very close to the target and the proton beam stop.

The target laboratory will probably be a prefabricated steel-frame building similar in size to the temporary laboratories in the Village (10,000 sq ft). It will have an additional area of

approximately 5,000 square feet for power supplies, shops, and light laboratories. The train-rail system inside the building will run between shielding walls. Remote manipulators and a crane will be used to carry out operations on the train with television cameras for viewing.

The target changing operation will probably occur infrequently, but is nevertheless essential. The concepts outlined here are a lean, but expandable design to accomplish this purpose; it is expected that operational experience might well modify the methods used.

2.3. Radiation in the Experimental Areas

The radiation problem at NAL is unique in at least two ways. The beam power in the external beam is about 0.5 megawatt. This is more than two orders of magnitude larger than the beam power handled in existing proton accelerators. The second problem is the need to range out high energy muons. At the primary energies of current proton accelerators the muon range is equal to or less than the required length of the neutron shield, while at NAL the muon shield is much longer. An NAL primary muon shield will require 7m of iron and 136m of heavy concrete in the direction of the beam.

The residual radioactivity situation in the target areas has already been discussed in the beam transfer section of this chapter. The neutrino-bubble chamber area involves additional complications because of the widely spaced elements. These problems are discussed in detail later in this chapter. Appendix IV contains a number of general radiation considerations for the experimental areas in regard to shielding and safety. Appendix III discusses a target station shielding design.

2.4 Conventional Experimental Area

2.4a Introduction In a conventional experimental area, the overall goal is to make the best use of the available funds and building space. With unlimited resources, the problem is easily solved by putting up a building large enough to accommodate any foreseeable needs. In practice, the total floor space of the experimental halls in the initial construction at NAL will be only slightly greater than that presently available at Brookhaven. The projected space will probably be split equally between Areas 2 and 3. Thus, the problem at Area 2 is to accommodate seven experiments each roughly seven times as long as a typical Brookhaven experiment in about one half the space available at Brookhaven.

Various suggestions have been made to accomplish this, such as temporary buildings, air buildings, and outdoor experimental areas. Working outdoors in Illinois in experimental areas which operate twenty-four hours a day raises such problems with the weather that it is not considered further in this report. As for temporary buildings, the savings do not seem to be very great, if there are any at all. A building consists of a number of parts--roof, walls, floor, services, crane coverage, hydrogen safety elements, magnet power, and magnet cooling water. Each part on the list costs about an equal fraction of the total.[1] As a result, savings on a temporary roof and walls represent a fraction of the cost to operate an experiment. Thus, the construction of temporary buildings does not look like a fruitful path to follow.

It does not seem possible to supply facilities which place no restrictions on the experimenter's utilization. To find a solution,

it is helpful to consider the experience at other machines, notably the G-10 area at the A.G.S. This area has had beams built according to user demand, but once a complete set existed they have remained essentially unchanged and subsequent users have simply continued to use the existing facilities. Therefore, the suggested program at NAL is to design a complete set of beams for Area 2. The buildings can then be fitted to the beams. This program loses a great deal of flexibility in possible beam arrangements. The justification for this loss is that in practice once an array of beams is built it is not changed. Therefore, the wisest course is to initially build the best set of beams possible and then accommodate the construction program to this design. This can result in great savings since in the beam transport area, which may be some 500 feet long, the building, power, cooling, control, shielding, and material handling needs are all well defined and can be met by supplying only what is necessary. For instance, if the area is permanent, the material handling demands are only those needed for replacing malfunctioning equipment and not those which would be needed to rebuild the whole area in a short time.

In order to study a concrete example, Area 2 is assumed to contain only conventional beams. This area can then be designed to maximize the number of these beams. In this plan there is no provision for specialized beams such as a hyperon beam, thin target experiments, large angle beams, very high intensity pion, muon, or neutrino beams, or beam dump experiments. All such specialized beams are allocated to Area 3. The problem with many such specialized facilities is that they exclude other beams from a target.

The present plans call for only two targets, other than the bubble chamber target. Consequently, it is necessary to make basic decisions on the following matters:

1) adding target stations, which requires more funding,
2) giving over a target station to a specialized use, which limits the number of operating experiments, or
3) inventing a scheme for accommodating a specialized beam along with a number of general beams at one target.

A particular case of such a specialized arrangement is discussed in the section on the thin target station. The remainder of this section is an examination of one conventional experimental area (Area 2). Area 3 will be the second conventional area. One half of the available resources are allocated to it, but its design is not yet formulated.

2.4b Secondary Beam Elements The present plan has evolved by designing a set of secondary beams and then providing services and buildings for them. In this process the first step is to decide on the beam transport magnets. Superconducting magnets are an attractive possibility which is being actively pursued. It seems quite possible that the experimental areas will be equipped entirely with superconducting magnets.

Chapter III and Appendix V contain extensive information on the NAL superconducting program. This program is centered on using magnets run at up to 20 kilogauss with iron poles and yokes to shape the field. An investigation into the economics of superconducting beam-transport magnets has shown that this is the most

economical installation. In such a configuration, the superconductor is used to magnetize the iron and the ampere turns are kept at a minimum.

The standard superconducting beam transport dipole will have a gap 10 cm wide by 4 cm high, will be 4 meters long and its outside shape will be cylindrical, 30 cm in diameter. The quadrupole will have an inner radius of 3.5 cm, an O.D. of 30 cm, and be 2m long.

Many of the designs in this report have been based on main ring magnets operated d.c. at 9.0 kilogauss. The present emphasis on superconductors indicates magnets will probably run at fields nearer 20.0 kilogauss. In general this does not strongly effect the results of the previous studies.

2.4c Secondary Beams Producing multiple secondary beams from one target presents a problem because the secondary particles are produced in a small forward cone. In this design, no attempt has been made to be elegant. Instead only existing components such as main ring magnets have been used. The solution adopted here is a conservative solution--anything actually built may use any of a number of approaches to produce beams at smaller angles thereby increasing their energy and intensity. The present solution is practical and could be built and operated using existing equipment. It is a useful basis on which to study various configurations of experimental buildings since it provides a sufficient number of satisfactory beams. The actual problem of the front end of the secondary beams has not been solved in detail and deserves a great deal of further study.

The secondary beams in the present designs for the charged particle target stations were designed in three stages. First the original sixteen experiment model in Appendix VI was used to find a reasonable mix of beams, then the 200 and 80 BeV/c beams were designed in some detail, (see Appendix VII) in part to determine the required number of beam elements and their location in the experimental hall, but also to determine alignment and field tolerance requirements for practical beams. Finally, these were systematically scaled (see Appendix VIII) to give the parameters of the other beams and achieve compatibility with the overall target station. In general, the individual beams were designed to clear one another without boring holes through the magnet yokes. The parameters of the main ring bending magnets were used in order to make definite the aperture and other quantities. Enough dipoles were provided so that a nominal beam momentum allows the dipoles to operate at 9.0 kG. These magnets have a limitation because of the beam sagitta (3 cm at 80 BeV/c). In addition, the field quality is probably somewhat better than required. The design of the beams is reviewed in the following paragraphs.

Each beam consists of two sections with a momentum slit separating the two regions. Sufficient momentum resolution is available so that single pion production can be resolved from elastic scattering (0.05% at 200 BeV/c). Small production angles are achieved by allowing the secondary particles to drift some distance before bending (40 to 60 m) rather than by using a dispersing magnet near the target which could lead to difficult shielding problems. An emittance of the external beam of $\Sigma_v = 0.09\ \pi$

mm-mrad and E_h = 0.033 π mm-mrad was assumed, along with a spot with a horizontal size of 1 mm and a vertical spot of 1.4 mm. The parameters of these beams after optimization are given in the appendices. Typically, the 200 BeV/c beam is 300 m long and requires twelve dipoles and eight quadrupoles, while the 30 BeV/c beam is 120 m long and requires two dipoles and eight quadrupoles. The solid angles subtended range from 1.5 to 3.0 microsteradians. With these solid angles, very reasonable intensities of from 10^6 to 10^8 particles per 10^{13} protons can be achieved.

The tolerance for current regulation on the dipoles follows directly from the required momentum resolution. Typically, it will have to be on the order of 10^{-4}. Quadrupole regulation is less important. The most important effect of alignment errors in the dipoles seems to be loss of aperture. A 5 mrad misalignment leads to an aperture loss of 3 cm. The situation is somewhat more critical for quadrupole alignment. There, a displacement of 0.2 mm leads to an addition to a momentum error of 0.037%, because of gradient displacements. Some investigation has been made of second order effects, but none appear to be particularly troublesome.

2.4d Shielding The beam layout described in Section 4.3 has been used to carry out an estimate of the shielding requirements for a conventional target station. (See Appendix III.) In general there are three catagories of shielding to consider:

1) Hadron shield,
2) Beam line shielding,
3) Muon shield.

The hadron shield absorbs the non-interacting primary particles and the secondary particles that do not go down beam paths. This

shield requires the equivalent of 7 meters of iron longitudinally to the beam and 4 meters radially. The present design of the target box buried in a large earth berm provides the radial shielding in an inexpensive way.

The beam line shielding for transverse neutrons is a familiar form of shielding but it will be a major expense item at NAL where beam lines may run for 1000 feet.

The muon shield is a less familiar item. Many mesons are produced at the primary target, some of which decay into muons before they are absorbed in the hadron shield. These muons, which have energies up to 200 BeV, have to be stopped by shielding. Calculations indicate that a length of 140 meters of heavy concrete is needed downstream of the hadron shield to stop them. Thus downstream of each primary target about one million dollars worth of heavy concrete must be piled up to stop muons. On the one hand, the muon shield doubles as shielding along secondary beam lines, but on the other hand, the need to stop the flood of muons greatly complicates the design and shielding of the secondary beams. Appendix III is only the first attempt to deal with a very large problem.

2.4e Experimental Halls 75,000 square feet of experimental halls is available for experimental area E2. Various building configurations can be examined, working with the array of beams and shielding developed in the earlier sections. Figure 2-2 shows a straightforward "Great Hall" design totaling 77,500 square feet. Here the magnets are run at 18Kg. Typical experiments are shown in the four lower energy beams. The two high energy beams have their second foci downstream of the rear wall of the building which means that

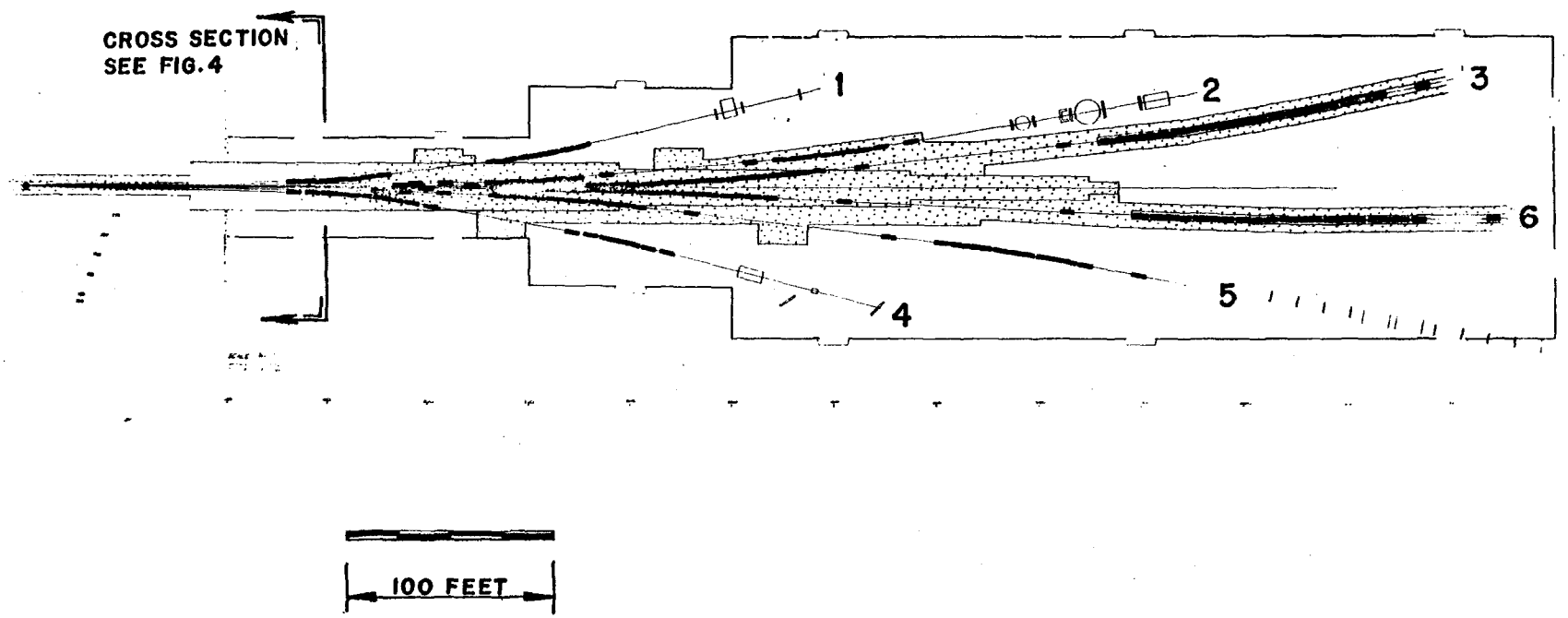

Figure 2-2 - Normal "Great Hall" Layout of Experimental Area 2

experiments in these beams will not be indoors. In this layout much of the available floor space is allocated to beam transport and shielding.

Figure 2-3 shows a different arrangement. The magnets in this plan are run at 9 kilogauss which stretches out the beam length and reduces the lateral displacement of the experiments. Thus this experimental area is a long narrow one with considerable space between the experiments. It lends itself quite naturally to placing one small building at the end of each beam line--each building containing one experiment. The buildings shown here are quite small, in general 30' by 100'. The total floor space is only 27,000 sq. ft. which means there is another 50,000 sq. ft. to be allocated to expanding the buildings shown and providing buildings in the two high energy beams. This design is quite inflexible but it does make efficient use of the floor space available for experiments.

Either of these two designs requires nearly $2 million worth of heavy concrete muon and beam line shielding. Furthermore, over 50 magnets are buried in the shielding. Figure 2-4 shows a cross section of the shielding. Clearly, magnets are inaccessible. This sort of design may prove to have very great maintenance problems. A preliminary design of a third scheme is shown in Figure 2-5. The magnets are all located in tunnels or enclosures so that they are easily accessible when the primary beam is turned off. The heavy concrete shielding is replaced by earth bermes, saving around a million dollars. This scheme is very inflexible. There may also exist serious radiation problems not yet analyzed, but it perhaps indicates a course that could be followed to save money and provide ease of maintenance.

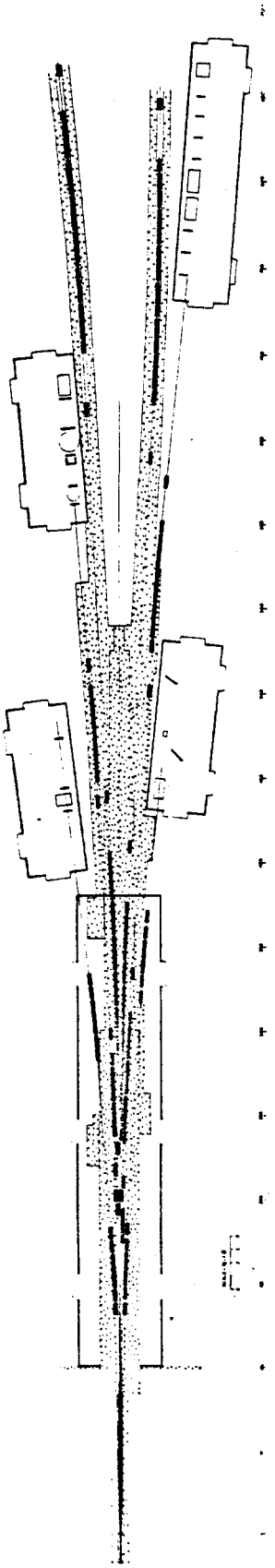

Figure 2-3 - "One Experiment, One Building"

Layout of Experimental Areas.

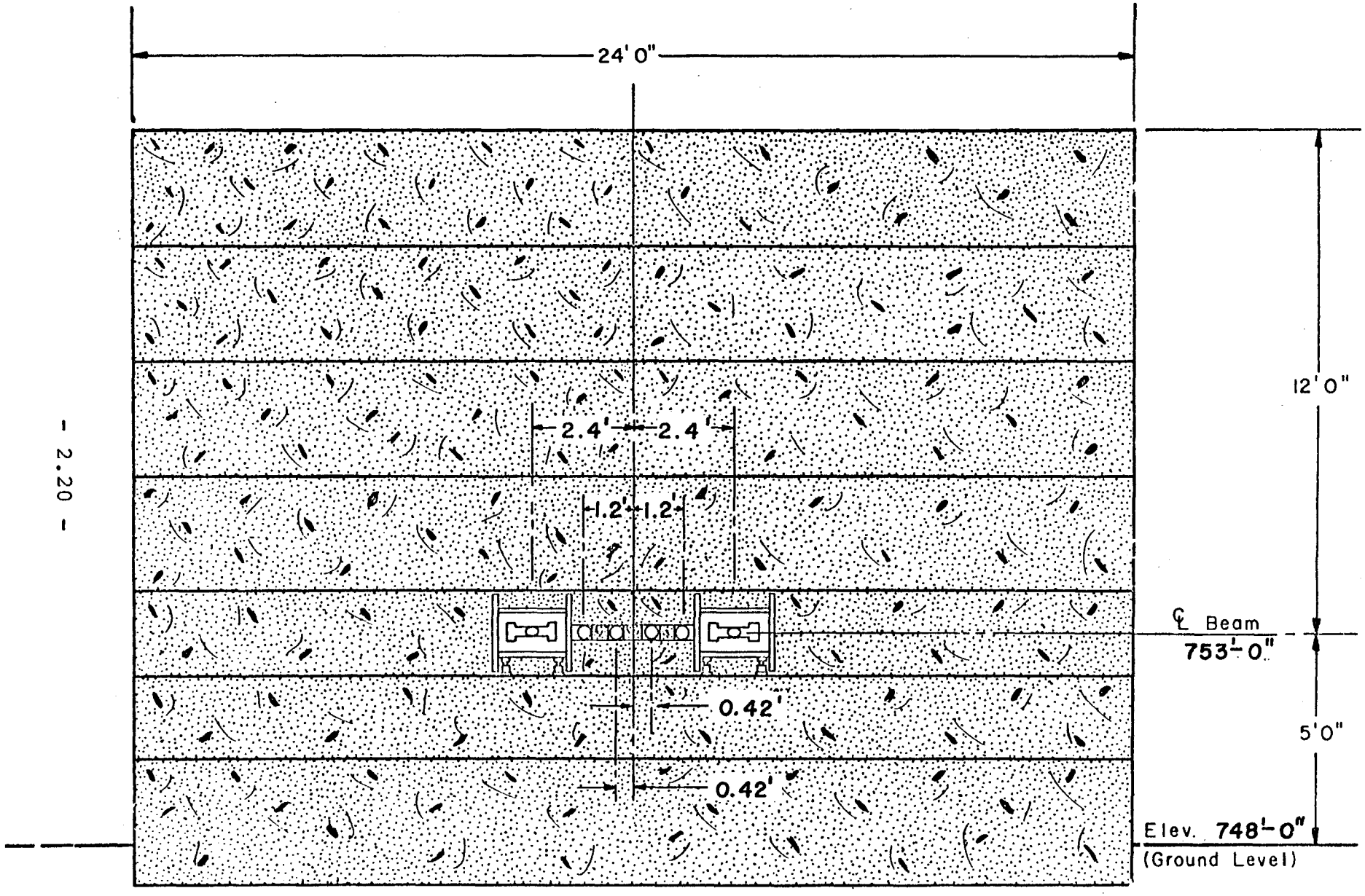

Figure 2-4 - Cross Section through the Muon Shield shown in Figure 2-2.

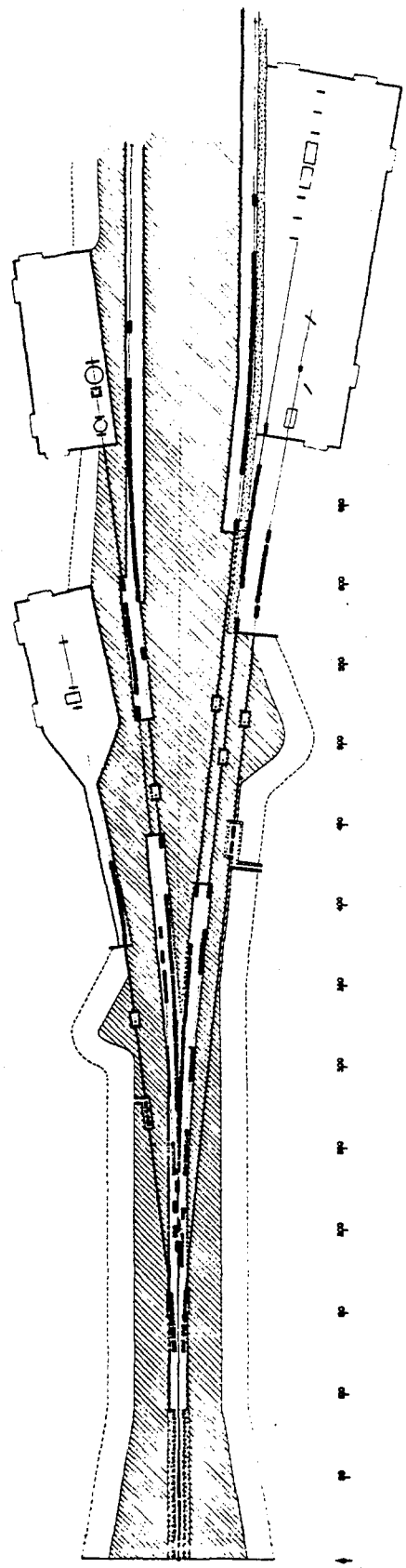

Figure 2-5 - "Tunnel and Earth Shield" Layout of Experimental Areas.

2.5. Bubble Chamber-Neutrino Area

2.5a Introduction The bubble chamber-neutrino area, designated as Area 1 here, is primarily intended to provide secondary beams for use in a bubble chamber. It has been assumed that the specific beams will be a high intensity broad-energy spectrum neutrino beam, an energy-hardened neutrino beam, a low intensity full energy proton beam, and an rf separated π and K meson beam with a momentum range from 15 BeV/c to about 80 BeV/c. The design of the target station and beam area described here is somewhat independent of whether the neutrino beam is provided by a current-sheet focusing system or a quadrupole focusing system and also to the details of the charged beam designs.

Target station T1 has several features which make it unique. First and most important, the neutrino beam elevation is nominally 15 feet below ground level to minimize the cost of muon shield. Second, because there are relatively few transport elements in the neutrino beam, the method of handling these elements and hence the design of the target building will differ materially from that of the target buildings in Areas 2 and 3.

Since it is intended eventually to increase the energy of the accelerator from 200 BeV to 400 BeV, expandability must be allowed for in the design of this area. The two lengths which become important at 400 BeV are the length of the highest energy rf separated beam of interest and the length of the neutrino beam. The latter length is dependent on the neutrino energy region of interest when the machine goes to 400 BeV.

There are three principal boundary conditions on the design of Area 1:

1) Area 1 must be a complete bubble chamber facility within itself, that is, all the bubble chamber beams must originate from the T1 target.

2) The maximum possible flexibility in providing secondary beams to the bubble chamber must be provided. For example, if the bubble chamber were cycling at two pulses per one-second flat top, both a neutrino and a strong interaction exposure could be carried out concurrently with one pulse from each beam on each acceleration cycle.

3) The cost of the area must fit in with the overall project cost. The conventional facilities cost for Area 1, excluding the bubble chamber facilities as outlined in the BNL report 12400[2], must be less than $3.3 million including the neutrino muon shielding for the bubble chamber. The technical equipment cost must be less than $7.1 million excluding the bubble chamber.

The conceptual neutrino beam design is not a completely optimized design, but rather the result of a preliminary study of the basic design parameters. The charged beams have not been studied in detail except to insure that they can originate from the target T1 and still have a sufficient length to the bubble chamber to provide particle separation and momentum resolution.

2.5b Neutrino Beam A greater effort has been expended in the conceptual design of the neutrino beam than in the design of the charged beams since the neutrino beam parameters dominate the physical layout of Area 1. This preliminary design has been obtained using a variation of the CERN neutrino flux program[3], and the following assumptions:

1. It is desirable to construct a wide-band neutrino beam which optimizes the flux above 2.5 BeV.
2. The detector diameter is 3.6 m.
3. The pion production is predicted by the CKP formula.
4. The target thickness is 0.033 of an interaction length.
5. The ratio $\frac{K}{\pi} = 0.15$ at the production target.
6. The muon shield thickness is sufficient to stop the muons by ionization loss alone.
7. To provide an energy-hardened neutrino beam with minimum modification.
8. To provide a short and lengthened short spill so that counter experiments could also be performed in Area 1.
9. All the boundary conditions outlined in the introductory paragraphs should be satisfied.

The neutrino beam is obtained primarily from the two-body decays of the π and K mesons produced at the target. The muons also produced in these decays would be the principal source of background tracks in the neutrino detector if the detector were not adequately shielded. The neutrino flux is enhanced by focusing the mesons so that they are directed toward the detector. The basic elements of the neutrino beam are, therefore, the proton targeting, the meson focusing, the meson decay region, and the muon shielding. An optimal beam design has the correct combination of these parameters to produce a maximum flux passing through the detector in some neutrino energy interval. A detailed study of the neutrino beam parameters is presented in Appendix IX. A summary of the important points of investigations reported there follows.

A set of shielding thicknesses for earth, earth and iron, iron,

and uranium has been assumed to be 600 m, 300 m, 150 m and 70 m, respectively, to shield the detector from 200 BeV muons. For each shield thickness, the integrated neutrino flux above 2.5 BeV and 40 BeV has been calculated as a function of decay length for perfect meson focusing. These results are shown in Figure 2-6. The resulting optimal decay length as a function of shield thickness is given in Figure 2-7. The neutrino energy spectra for several shield-decay length combinations are given in Figure 2-8. Above 15 BeV the fluxes from all the configurations except the earth shield are quite comparable while the earth-shielded beam is much inferior below 15 BeV. The uranium-shielded beam is found to be not much better than the iron-shielded beam, and because of its higher cost will not be considered further.

If the maximum proton energy of the accelerator were 200 BeV, then the preferred beam would include a full length iron shield of 150 m and a decay length of 600 m. However, the maximum proton energy will ultimately be 400 BeV. At present it appears difficult to modify appreciably the position of the target, the beginning of the shielding, and the bubble chamber when the proton energy is increased to 400 BeV. If a single shield thickness and decay length is used at both proton energies, then an ultimate choice of these distances will depend on the neutrino energy regions to be optimized at each proton energy. In lieu of the details of a long-term neutrino program, it was decided to investigate a compromise beam of 600 m decay length and 300 m shield thickness. This longer shield thickness would allow the use of a low cost earth-iron combination at 200 BeV and a full iron shield at 400 BeV. The compromise beam, while being nearly optimal at 200 BeV, is also quite good at the higher

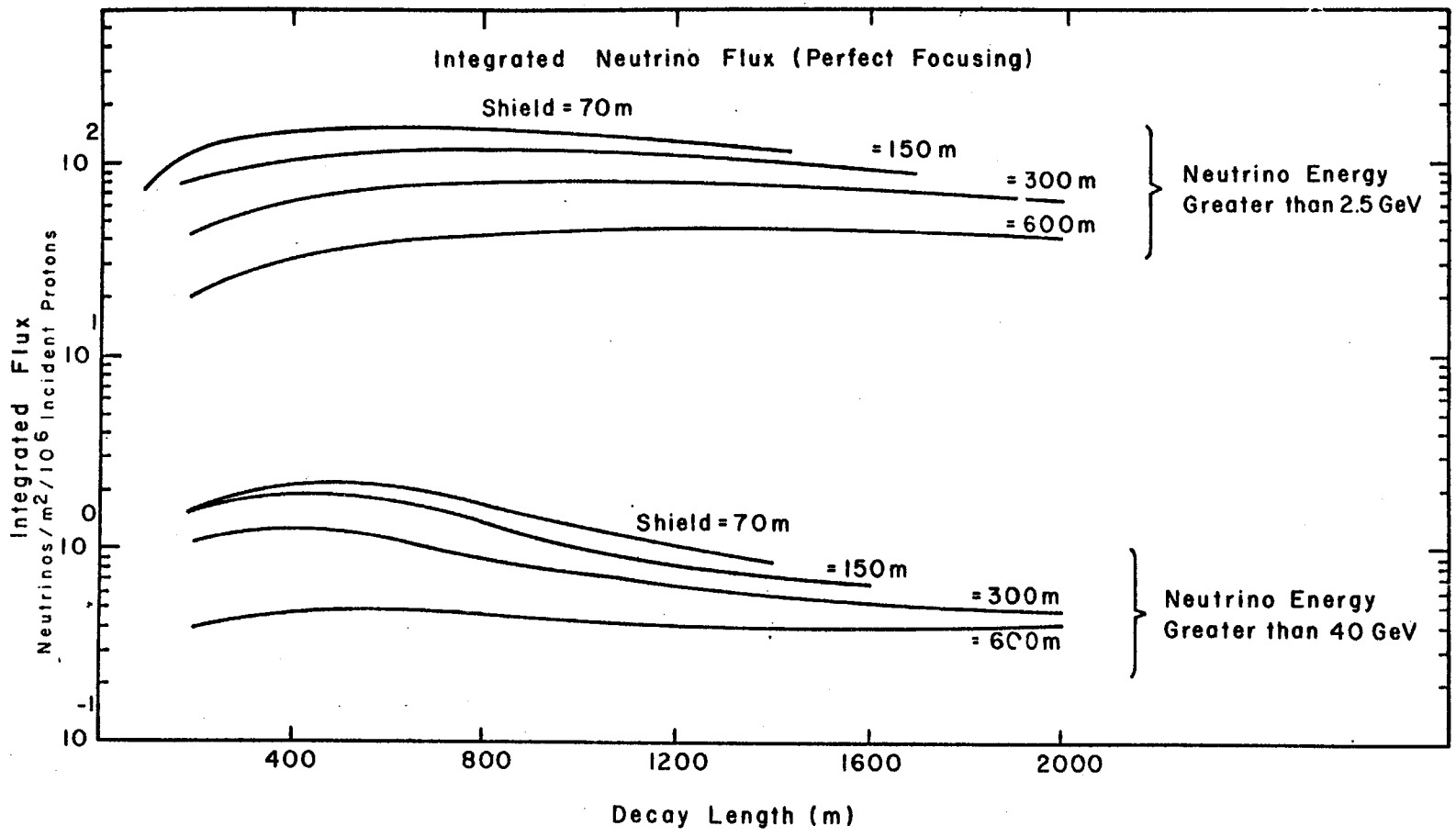

Fig. 2-6 Neutrino Flux Dependence on Decay Length for Different Shield Thicknesses.

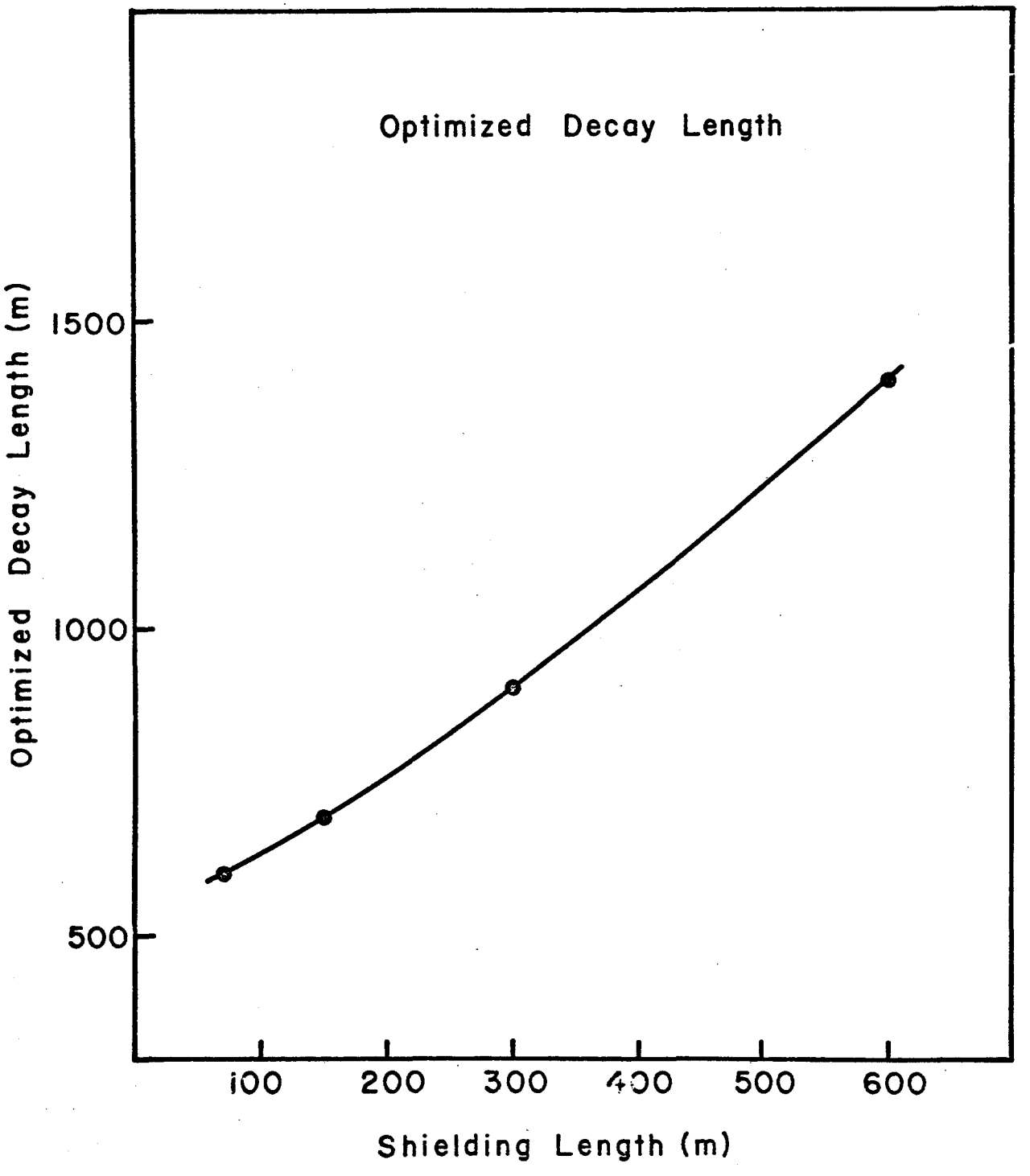

Fig. 2-7 Optimized Decay Length Dependence on Shield Thickness.

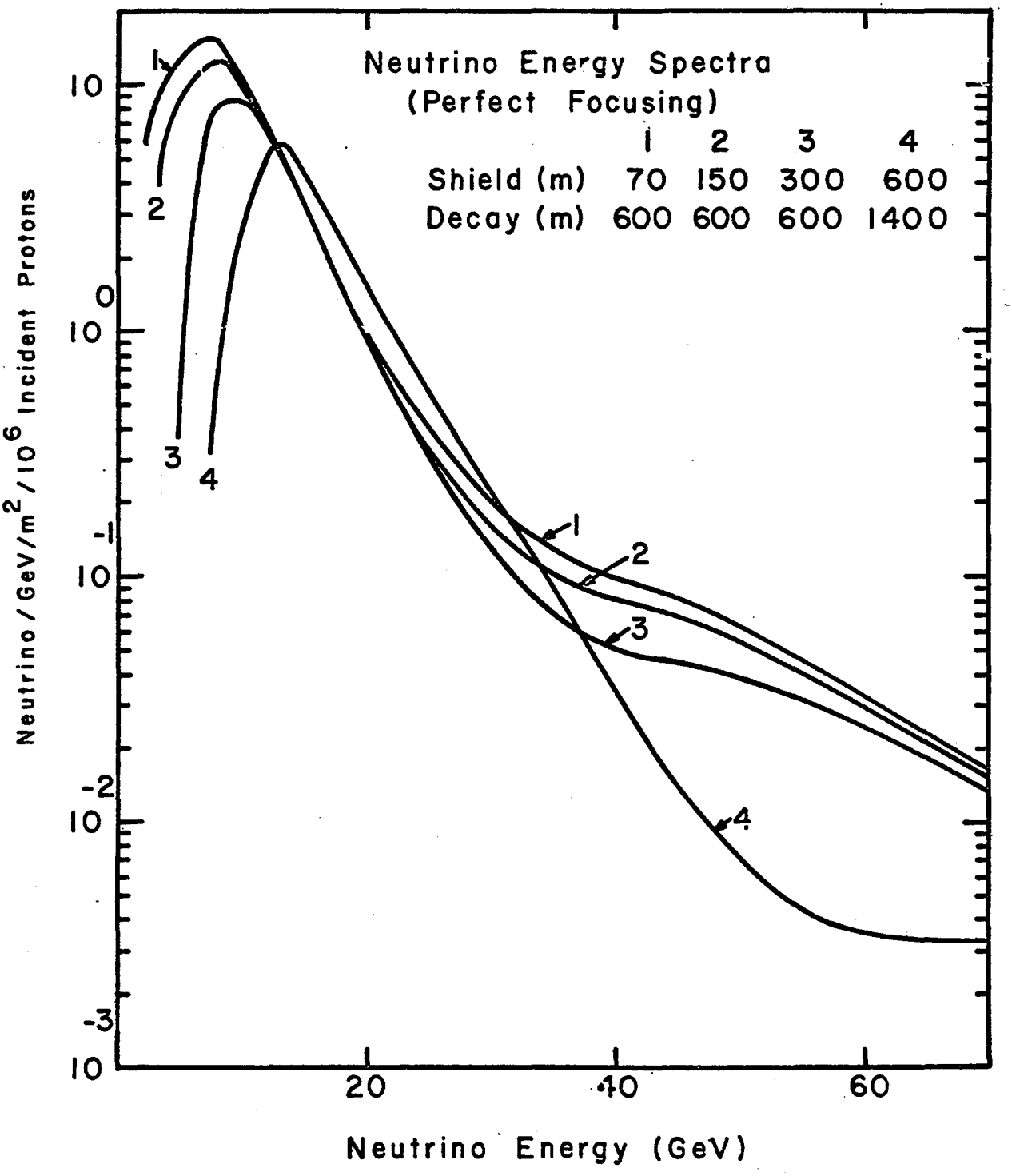

Fig. 2-8 Neutrino Energy Spectra for Four Different Shield-Decay Length Combinations.

neutrino energies when the accelerator is at 400 BeV as shown in Figure 2-9.

All of the above arguments assume that the mesons are perfectly focused along the line connecting the target and the center of the neutrino detector. Two wide-energy-band focusing systems have been investigated, the conventional current sheet (horn type) focusing system, and the strong focusing quadrupole system. The quadrupole system is in a preliminary state of investigation and shall not be further reported here. The focusing system considered in this preliminary design consists of three current sheet focusing elements as shown in Figure 2-10. The energy spectrum of the three element system is compared with the perfect focusing and no focusing systems in Figure 2-11.

The decay length of 600 m corresponds roughly to a collision mean free path in air. The calculated neutrino flux is reduced by approximately 50 percent because of the meson interactions on the air atoms in the decay tunnel. This loss can be reduced substantially by inserting helium bags into the decay tunnel. With the above beam and a helium-filled tunnel, it is estimated that one picture in four from the 25-ft bubble chamber will contain an elastic interaction in deuterium.

2.5c Charged Beams The possible candidates for charged beams to be built in Area 1 within the first few years of machine operation are S1 beam, a low intensity unseparated charged beam of narrow momentum bite which can transport the highest momenta available. S2 beam, a low intensity full-energy proton beam. S3 beam, a low intensity rf separated π and K beam of momentum from 15 BeV/c to about 80 BeV/c S4 beam, a high intensity proton beam to be targeted near the chamber

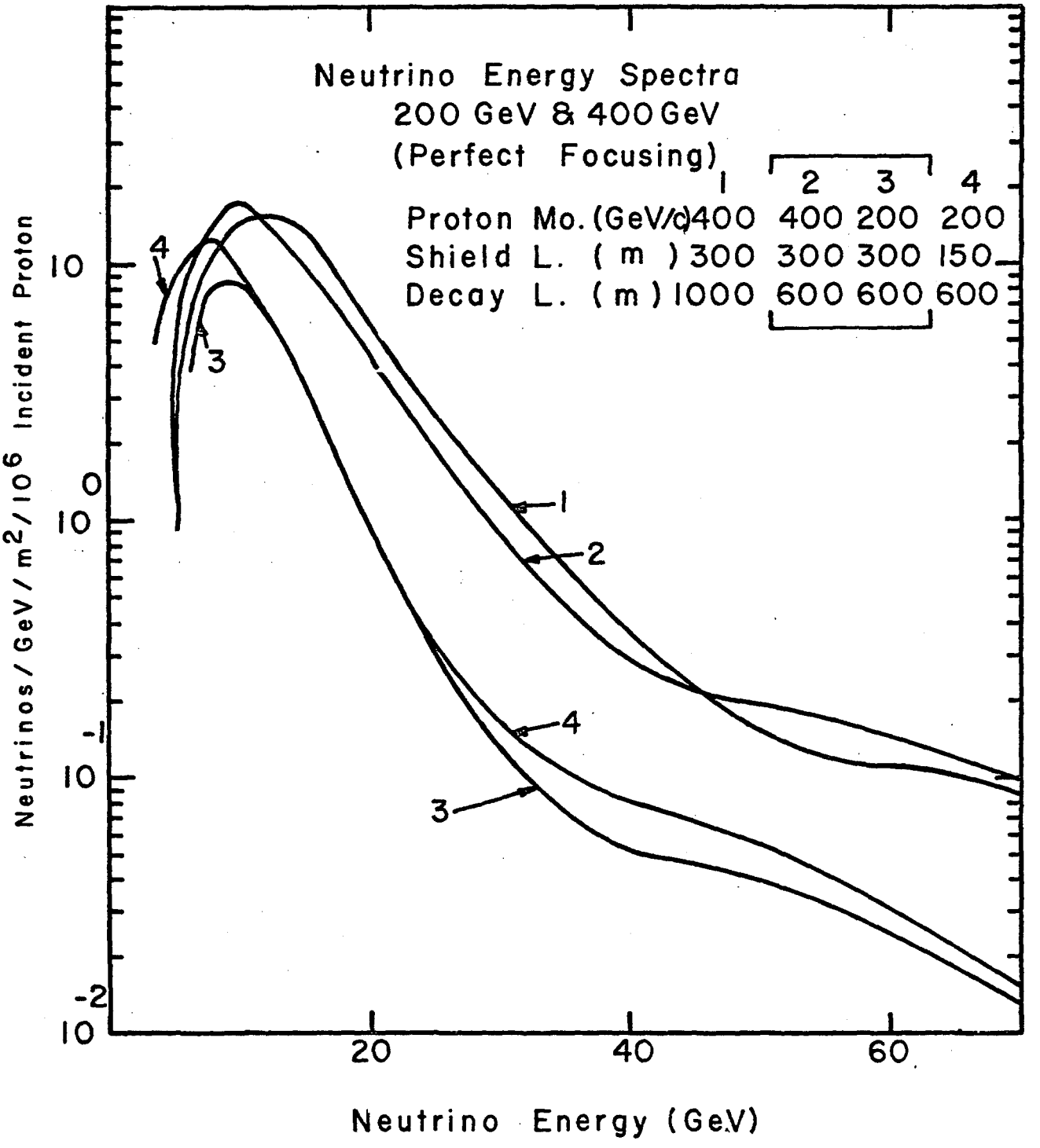

Fig. 2-9 Neutrino Energy Spectra for the Optimized Beams and Compromised Beams at 200 GeV and 400 GeV.

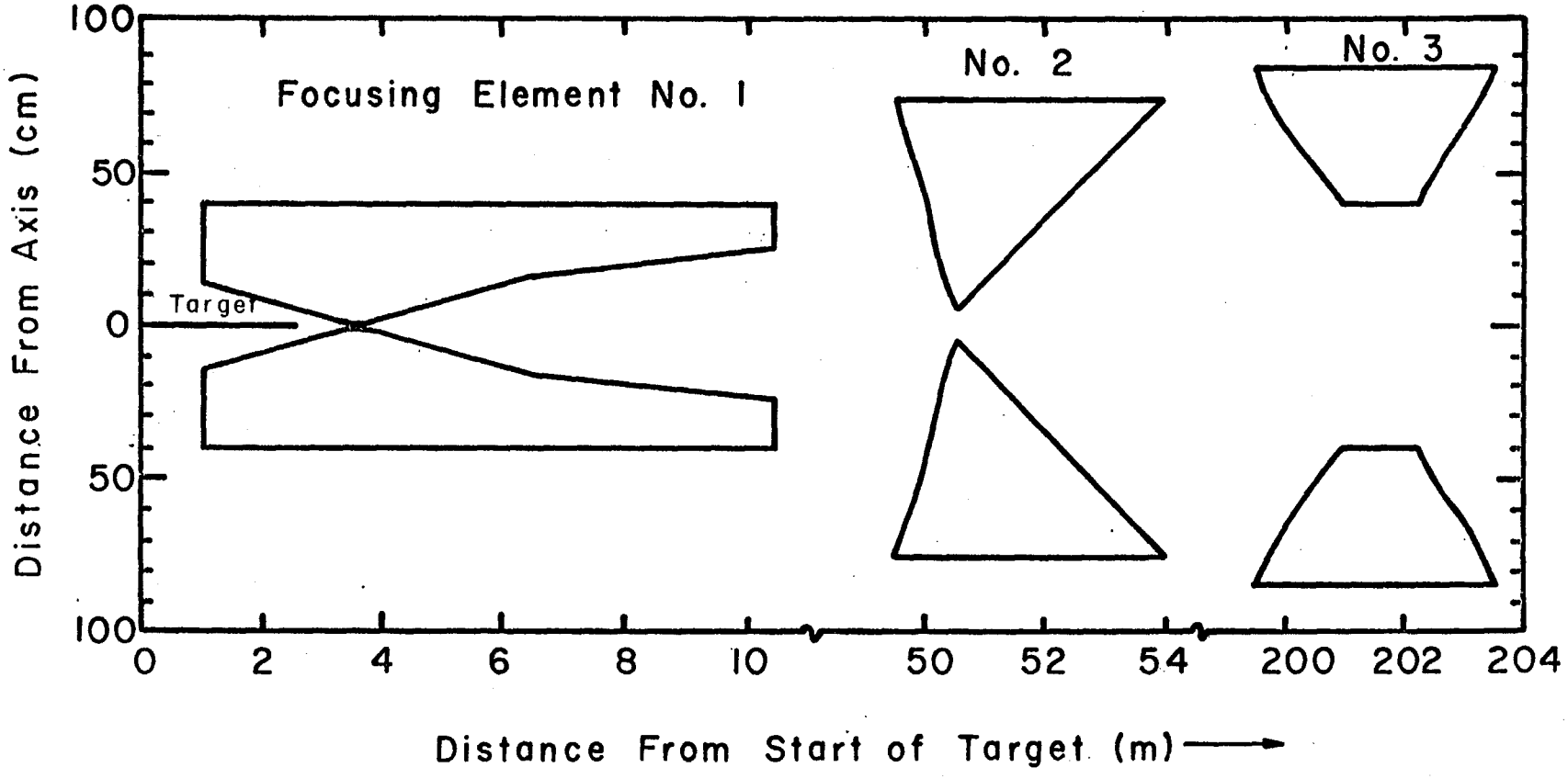

Fig. 2-10 Profile of the Three Element Focusing System.

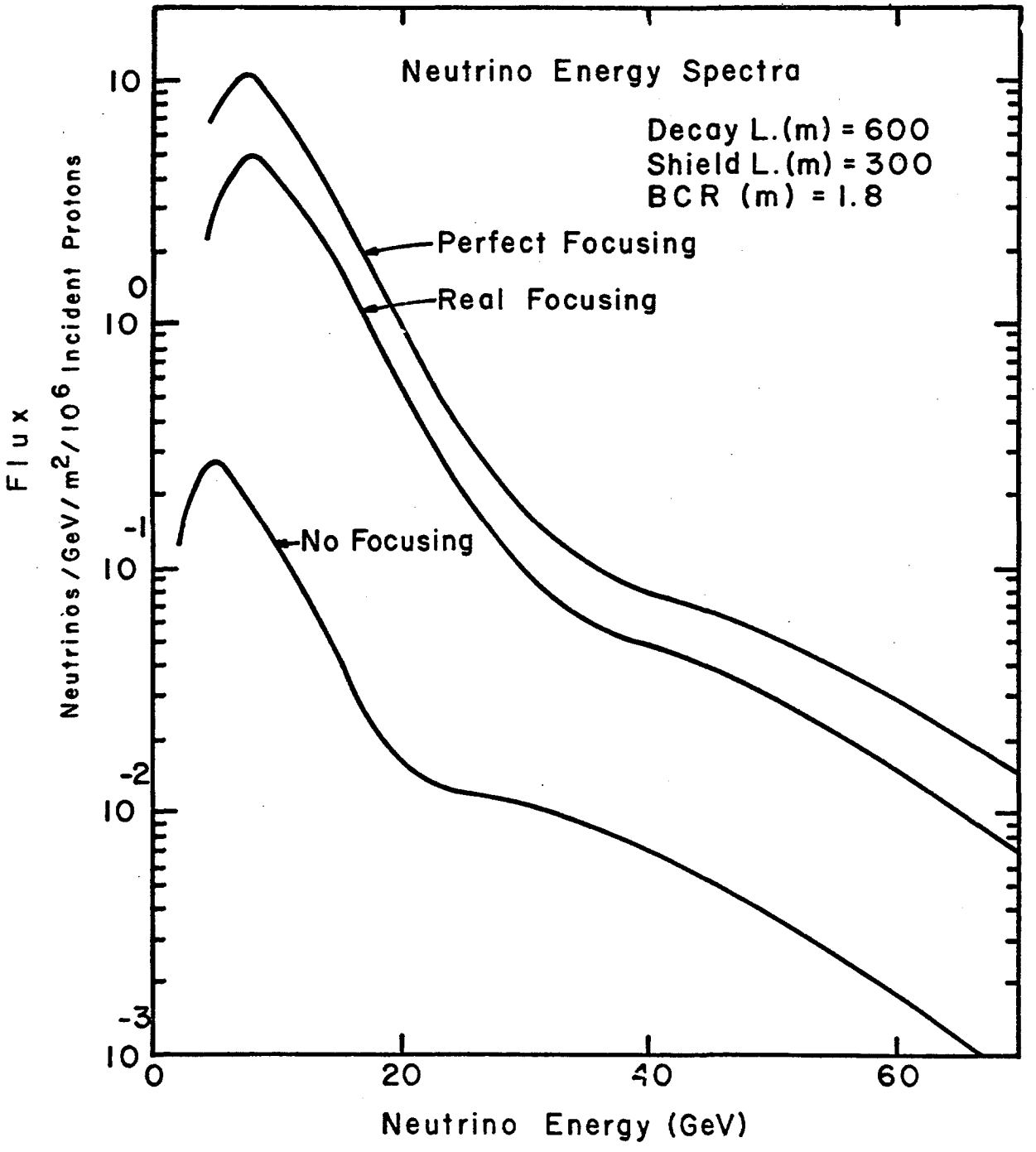

Fig. 2-11 Comparison of Neutrino Energy Spectra From Perfect, Real and Non Focused Beams.

to provide short beams, e.g., hyperon beams. Several designs of these beams have been proposed in previous NAL, UCRL and ECFA high energy accelerator utilization studies.

The S4 beam because of its shielding problems, and the necessity of a second target station has been essentially excluded from the initial design of Area 1. The S1 and S2 beams present few new design problems and beyond the expensiveness of bending high energy beams are very good candidates for construction.

A prime requirement in building a high energy rf separated beam such as S3 is that a sufficient distance be allowed from the target to the detector for the beam. In the conceptual neutrino beam layout, the detector is placed 900 m from the target. A 900 m beam length is sufficiently conservative to allow for a 100 BeV maximum momentum three-state rf separated beam at 10 GHZ or a higher momentum beam ($\geq$ 150 BeV/c) if one goes to a chopped separator or higher frequencies.

The inclusion of beams S1, S2, and S3 appears to be conceptually compatible with the proposed neutrino beam. A possible RF separated beam is covered in Appendix XI.

2.5d Physical Layout of Area 1 The physical layout of Area 1 with respect to the other experimental areas and the main accelerator is shown in Figure 2-1. The fast-extracted proton beam leaves the transfer hall at an elevation of 725.5 feet. The protons travel approximately 1,350 feet to the first switching station, S1, where all or a fraction of the protons can be switched into Area 1. The protons are slightly pitched toward ground level (approximate ground elevation is 748 ft) as they leave S1 so that they arrive at the target area T1, at an elevation of 733.5 ft.

A single target is used at T1. The protons striking the target produce secondaries which are either focused by pulsed current sheets to produce a neutrino beam or deflected into a charged beam channel and transported to the bubble chamber. In the present plan, the elevation of the center of the bubble chamber is 733.5 feet. The main items of Area 1, the target station, decay tunnel, muon shield, charged beam corridor and detector area will be discussed below in more detail.

2.5e Target Station Because of the intense neutrino beam, target T1 has several features that make it unique. To minimize the cost of the muon shield, the proton and neutrino beam elevation is 733.5 ft which is nominally 15 ft below ground level. Since there are few transport elements in the target station T1, a different approach from target stations T2 and T3 is being pursued in its design.

As shown in Figure 2-12, the target building is a 300-foot long enlarged rectangular tunnel. The lowest level of the target station provides a volume five feet square and 300 feet long along the primary proton direction, covered by twelve feet of portable heavy concrete shielding. This lowest level contains the target, neutrino focusing elements, and a magnetic system to deflect charged particles into the charged particle gallery. The proposed method of mounting the target and beam transport elements is to suspend them from concrete mounting pads. These pads are aligned on shelves made in the side walls of the target building five feet above the lowest level. Twelve feet of portable heavy concrete shielding is placed over the mounting pads to partially fill the target building, as shown in Figure 2-12 to provide a lower-background (~ 20 mr/hr) environment on the upper level where electrical and mechanical connections can

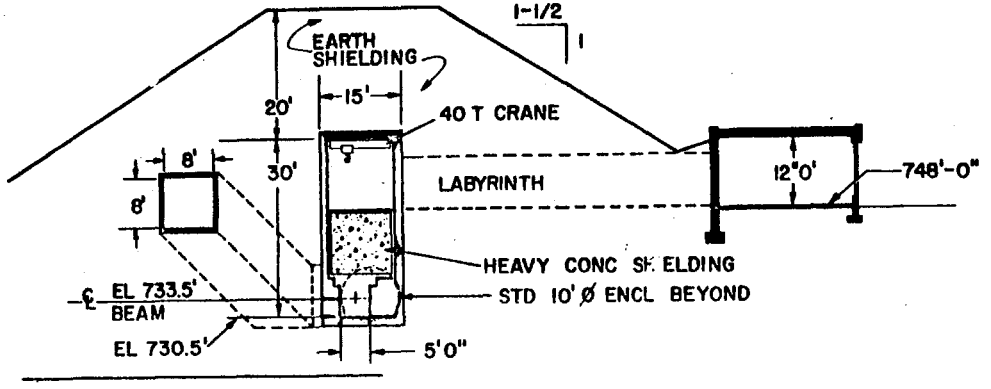

VIEW LOOKING UPSTREAM

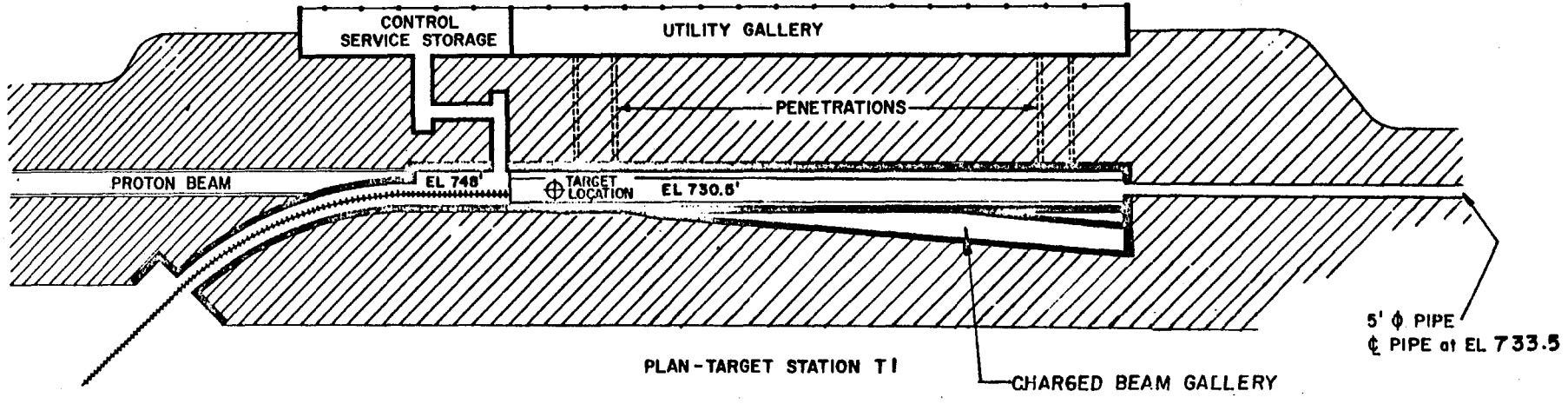

Fig. 2-12 Schematic Representation of Target Station T_1.

be made to the beam elements. Beam elements and portable shielding blocks are of a standard width so that any beam-transport element can be removed by the overhead crane without disturbing the other elements. A radioactive transport element can be safely removed from the target station by the following procedure. The element with its alignment pad is automatically lifted by the overhead crane and transported to the upstream end of the target building where it is deposited into a special casket mounted on a railroad flatcar which enters the station at that end. The railroad car is then removed to the target laboratory where the element is repaired, stored or discarded.

The additional earth shielding over the target station reduces the background around the target station to an acceptable biological level during machine operation. Along the primary proton beam direction, the target station lower level is sufficient to contain a current-sheet neutrino focusing system or the front end of a quadrupole neutrino focusing system.

2.5f Meson Decay Tunnel Because of the long mean decay distances for the π and K mesons (55 meters/BeV and 7.5 meters/BeV, respectively it is necessary to provide a long, low-cost decay path. The total decay length required in the proposed neutrino beam is 600 m. The target station is about 90 m long, thus requiring a 510 m long decay tunnel. Because of the meson decay kinematics, the neutrino flux at the detector increases as the diameter of the decay tunnel increases as shown in Figure 13. This figure shows the flux as a function of diameter for both π and K decays.

A decay tunnel diameter of 1.6 m was tentatively chosen even though it reduces the lower energy neutrino flux somewhat. At the

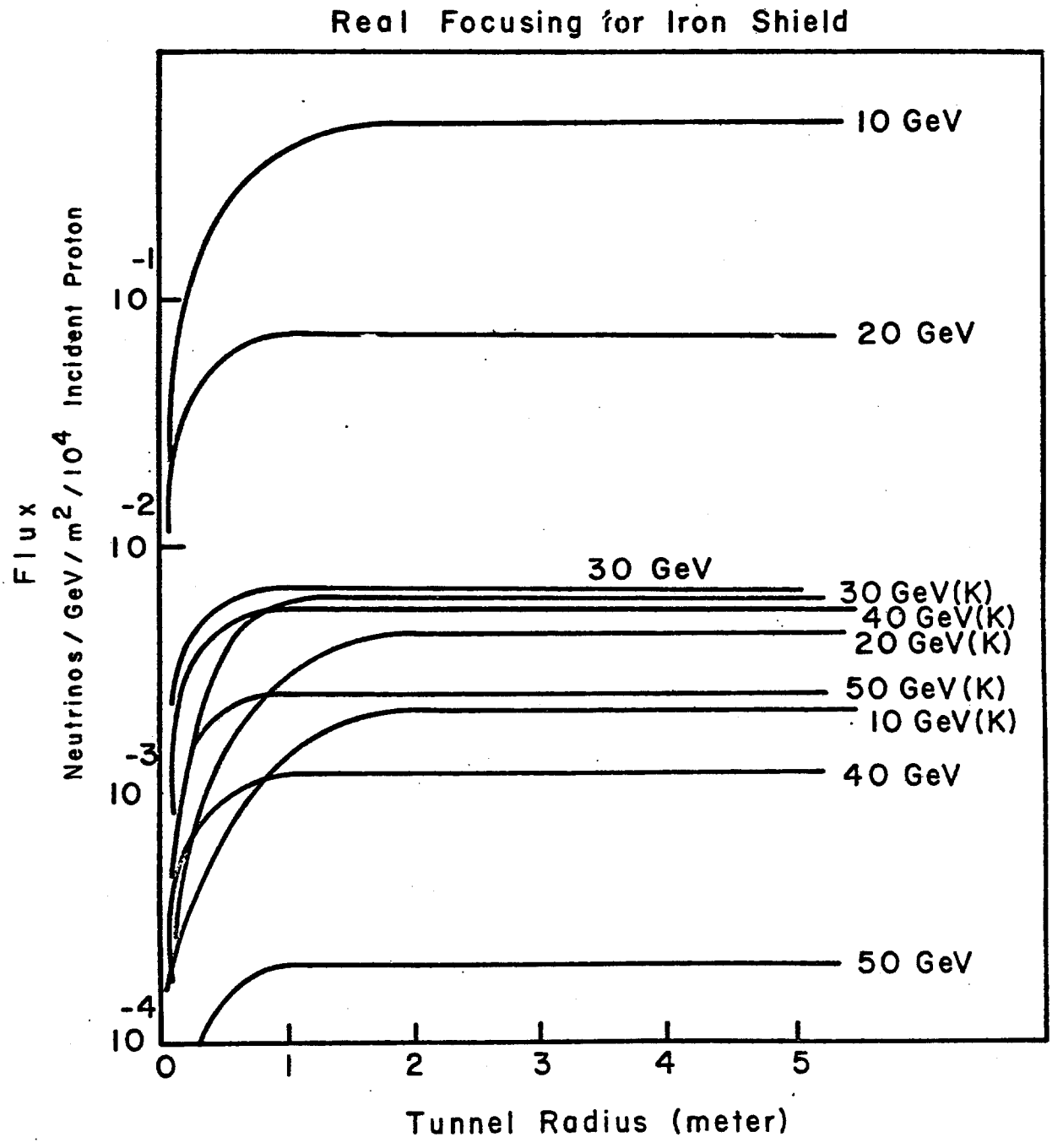

Fig. 2-13 Neutrino Flux Dependence on Decay Tunnel Radius for a Real Focused Beam.

present time, the 1.6 m diameter decay tunnel appears to be a good compromise because the emphasis of interest is likely to be on the higher-energy neutrino interactions and the tunnel diameter also determines the transverse dimension of the muon shielding. The smaller tunnel can significantly reduce the cost of the neutrino beam.

The proposed meson decay tunnel would be made of a 1.6 m diameter steel corrugated pipe with water tight seams and joints. A problem presently under study is to what extent the irradiated salts in the earth around the decay tunnel will be dissolved by the ground water. One possible, but expensive solution would be to imbed the decay pipe in several feet of heavy concrete. This study is still underway.

2.5g Muon Shielding A problem common to all accelerator neutrino experiments is to prevent the muons produced in the meson decays from passing through the neutrino detectors. The methods proposed to date are:

1. Deflect the muons from the detector via magnetic fields.
2. Stop the muons in a full-range shield.
3. Use a combination of the above two by using a magnetized iron shield.
4. Minimize the shield thickness by limiting the maximum meson energy allowed in the decay tunnel.

The muon shielding proposed in the conceptual beam design is the most conservative, that is, a full-range high-density shield to stop the highest possible energy muons by ionization loss only. Two attacks are being pursued to reduce the cost of such an expensive shield. First, the shield density is increased as the primary proton energy is increased. For example, during 200 BeV operation a shield

composed of 100 m of iron plus 200 m of earth is sufficient. At 400 BeV operation, a 300 m iron shield is necessary. This solution saves nothing during the 400 BeV operation, but at 200 BeV, there is 33 percent saving in the necessary amount of iron. Second, since the transverse dimension of the shield, at least the high density part of it, depends on the diameter of the decay tunnel, an attempt is being made to minimize that diameter.

By keeping the neutrino beam axis nominally 15 feet below ground, use is made of the earth around the decay tunnel and around the high density shield as additional muon shielding. Also under study is the possibility of using a very high density (uranium) core on the beam axis in the iron shield.

2.5h Detector Area The detector area extends beyond the muon shield and contains the large bubble chamber and counter detectors set up for neutrino and separated beam experiments. The beam height in the experimental area is nominally 15 feet below the ground level, which means that the detectors must be installed in pits or trenches. The problems of such an arrangement are appreciated and at present, the beam elevation is under reinvestigation. The inconvenience and expense of performing experiments in pits has to be weighed against the expense of building the neutrino beam at the ground level or above the ground.

Other topics related to the detector area which are under study are:

1. A muon sweeping magnet to deflect muons produced by neutrino interactions in the shield so they do not pass through the bubble chamber.

2. A cosmic ray shield over the bubble chamber to reduce the number of muons and soft showers passing through the chambers.

3. A ν_e trino flux monitoring system, e.g., a muon flux sampling system built into the muon shield.

2.5i Charged Beam Gallery A single target mounted in the upstream end of the target building is the source for both the charged and neutrino beams for Area 1. Charged beams are obtained from the target T1 through a collimator mounted in the side wall of the target building on the lower level at a production angle of about 25 mr. The charged beam from the collimator at elevation 733.5 feet is deflected to the ground level so that it emerges from the downstream end of the target building at ground level and about 20 feet from the neutrino beam axis.

A vacuum pipe transports the charged beam between huts, which contain the transport elements, in its flight to the bubble chamber. In the detector area the beams are deflected to the center of the bubble chamber at an elevation of 733.5 feet. Experimental arrangements which would not use the neutrino beam could be constructed at ground level. The charged beams to the bubble chamber contain about 20° of bend. Since the bending of beams (especially the 200 BeV proton beam) is expensive, beam configurations are being investigated that will minimize the total bending angle, the length of charged beam gallery needed, and the muon leakage through the neutrino shield.

2.6. Special Purpose Areas

2.6a Thin Target Station A thin target station has not been included in the present design of the experimental facilities so far.

It was considered unnecessary and not worth its cost. The approximate cost is given here for such a station designed for maximum flexibility.

A thin target is generally considered to be a target which interacts with only a few percent of the extracted proton beam. Often it is a liquid hydrogen or deuterium target in which the primary interactions of the protons are studied, for example, proton-proton elastic scattering. Clearly, the most sensitive cross-section measurements can be performed in the proton beam with its $> 10^{13}$ particles/sec intensity. At very high energies, the cross sections for some channels will be very small (again, in proton proton scattering at large angles).

This station is intended to be placed in one arm of the proton beam preceding an end station for most efficient use of the beam. In the first approximation, it is a section of the proton tunnel with movable shielding and is not intended to produce secondary beams. Figure 2-14 illustrates such a station and its relation to the other facilities. This section would be 200 feet long and covered with an overhead crane in a 100 foot wide building. The beam passes asymmetrically down the hall so that particles in the center-of-mass forward hemisphere can be measured on one side of the hall, while those in the backward hemisphere are detected on the other side which is wider. Concrete pads extend beyond the building to accommodate oversize detection systems; longer for the high momentum particles, wider for the large angle particles.

The shielding configuration shown in Figure 2-14 is for straight through transport of the proton beam. Shielding arrangements for a particular experiment will depend on magnet locations, beam ports

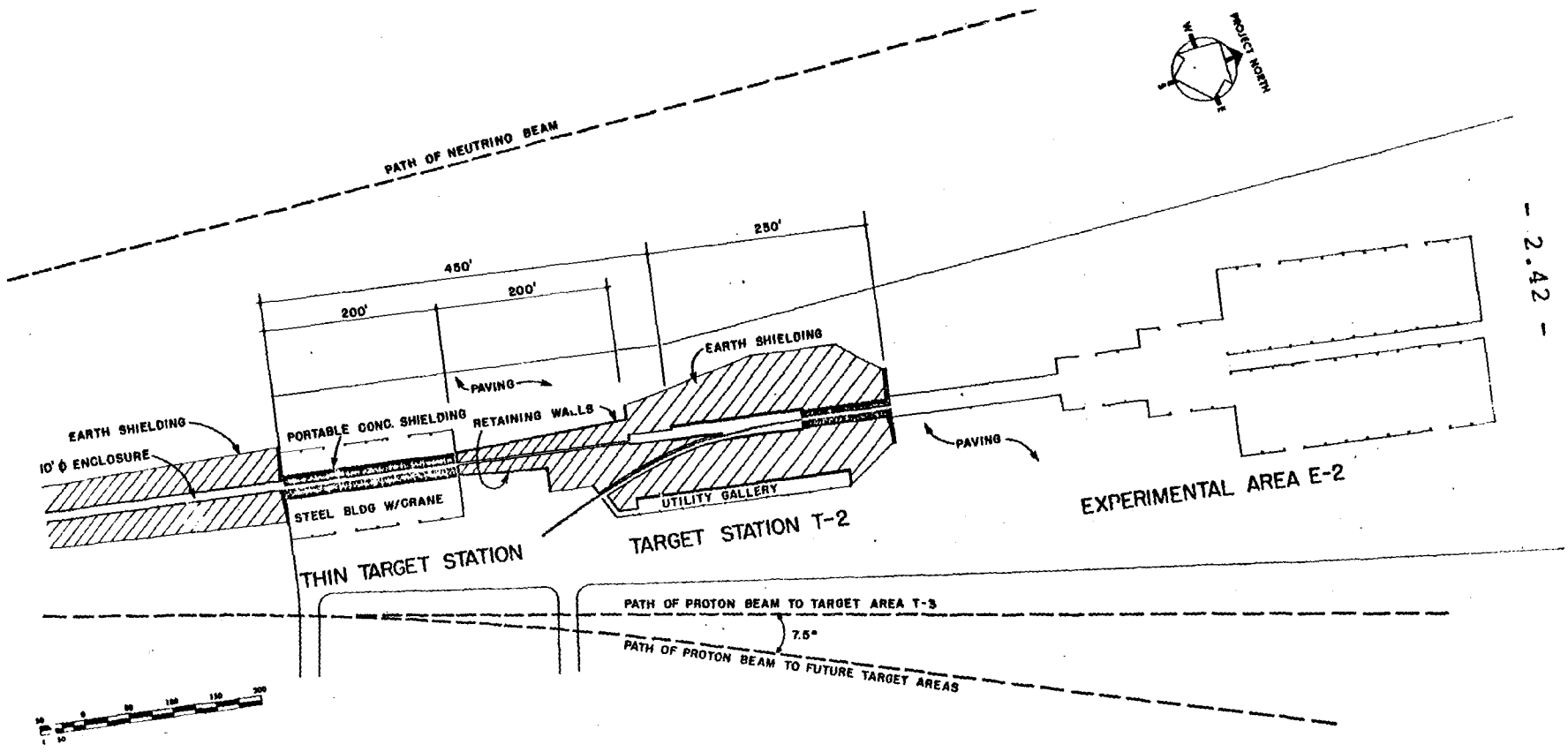

Figure 2-14 - Thin Target Station

and the thinness of the target used. The radiation problems are somewhat different from those of an end station. The number of interacting protons is down a factor of a hundred, each proton interacts only once, the secondaries are sharply peaked forward and since the target is part of a particular experiment, it will be in place a comparatively small fraction of the time. All these factors reduce the handling problems.

After passing the thin target station, the beam can be cleaned up by a constricting tunnel in the same way it is following the septa which split it from the primary extracted beam. The installation moves the end station 2 in Area 2 downstream by 500 feet and, as a by-product, brings it closer to stations 1 and 3. This has the advantage of simplifying services to the three areas. In addition, the extra length has the advantageous effect of giving more transverse space between the stations. The total cost of such a station is $2,200,000, of which $900,000 is for movable shielding, $1,200,000 is for the building with crane and services and $120,000 is to locate the end station 2 downstream. (These numbers include escalation, contingencies, and E.D.I. which represent about one third of the total price.)

2.6b Double Target Box Another variation in the design might be a double target box station. In designing each target complex a prime consideration has been to enable each one to operate independently of the others. Thus when one area is down for maintenance and modifications, the others can operate. This concept makes each station large, elaborate, and expensive. There is a tendency to maximize the beams taken from each target with a corresponding loss of flexibility in experimental set-ups. This problem is implicit

in the discussion of Section 4. The most glaring short-coming of the schemes presented in Section 4 was that user groups will have no easy way of doing experiments using 10^{13} 200 BeV protons. A possible way to rectify this problem is shown in Figure 2-15 which is a detail of Figure 2-2 but modified to include a second target box. The primary beam could be easily switched between the boxes. The primary target box could produce a number of secondary beams. The alternate target box could be used for a single experiment such as a hyperon beam, a beam dump experiment or some other specialized use. The argument is that in general the principal target box would take beam most of the time. The alternate box would be down most of the time to allow for changing experiments or for allowing the experimenters to think about their problems. For not too much money it thus becomes possible to considerably extend the kinds of experiments that can be done easily in the area. The drawbacks are that the second target box will cost money, it will in general not be in use, and the capabilities it will offer would be available by rebuilding the beams from the principal target box.

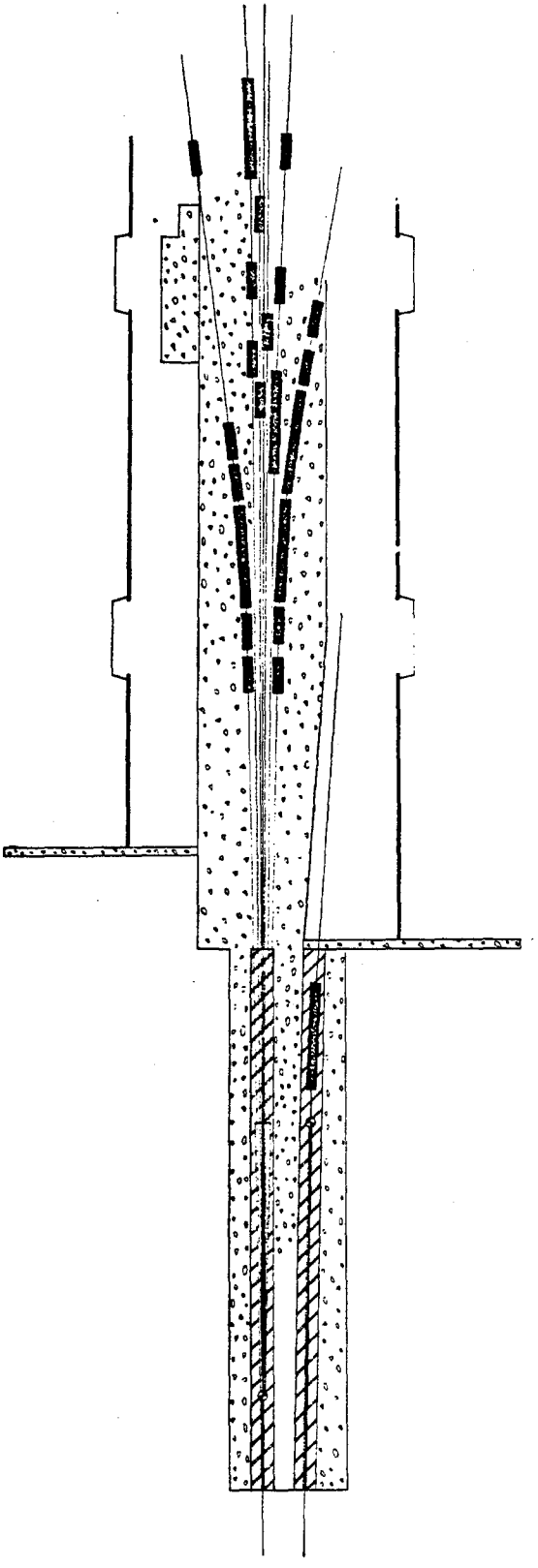

Figure 2-15 - Double Target Box
(Variation of Figure 2-2).

REFERENCES

1. "Experimental Building Costs", J. Sanford, NAL 1968 Summer Study, D1-68-60.

2. "25-Foot Cryogenic Bubble Chamber Proposal", BNL 12400, March, 1969.

3. Private Communication, W. Venus, NPA Division, CERN.

3. EQUIPMENT DEVELOPMENT

M. Atac, E. J. Bleser, F. A. Nezrick,
A. Roberts, J. Sculli, Z. J. J. Stekly

The equipment development program presently underway at NAL has a variety of aspects. (1) There are some items, such as computers and beam transport magnets, which are not strongly related to the needs of a particular experiment. Thus although expensive and complex, their development and acquisition by the laboratory can be undertaken somewhat independently of the development of specific experiments. (2) By way of contrast, the designs of other devices and systems, such as bubble chambers and multiparticle spectrometers, are intimately related to the experimental physics program at the Laboratory. They require the continuous and critical attention of many physicists interested in their future use. (3) There are still other items of equipment which are intended for particular research programs of the NAL staff. Equipment development is underway now in all three of these areas at NAL, and these programs are described in the succeeding sections of this chapter.

In Section 3.1, a general survey of the total needs for experimental equipment at NAL is considered. This discussion serves to place the equipment discussed in succeeding sections in perspective.

Section 3.2 contains a detailed report on the superconducting magnet program being carried out by the Experimental Facilities Section. This program is a serious attempt which looks towards equipping the entire experimental area with

superconducting magnets. This effort will make available the present engineering understanding of what such a system might look like, its cost, and how it will operate. The construction of two prototype bending magnets is at present underway in a joint program at ANL.

In Section 3.3 the present plans for a large bubble chamber are reported -- specifically the 25-ft chamber. The reader is reminded that the Laboratory master plan, described in Chapter 2, incorporates a large chamber facility. This plan includes the technical and conventional facilities necessary to build beams to a large bubble chamber. However, the money for the construction of the bubble chamber itself is not included in the initial construction budget; nor in the projection of the capital equipment costs given in Section 3.2. A separate proposal with request for construction funds for the bubble chamber will be submitted to AEC later this year.

Studies have been made on the feasibility of building a multiparticle spectrometer facility. These are reported in Section 3.4. While a specific facility of this type, as presently envisioned, may well not be built, these studies also raise the question of how large facilities will be provided by the Laboratory or outside groups for general use. Questions of this sort may suggest arrangements which are different from current practice at present proton accelerators, and they deserve serious discussion at this time.

Progress on a beam monitor under development by the Experimental Facilities Section is reported in Section 3.5.

The final section of this chapter (3.6) discusses equipment projects underway which are related to current research programs of the NAL staff. These include: (1) A scanning and measuring facility for bubble and spark chamber experiments, (2) A program of testing and constructing proportional wire planes, (3) A proposal to develop low temperature spark chambers to be used with large hydrogen targets, which is under study.

3.1 Overall Plans for Research Equipment

In the fall of 1968, a detailed study was made of the technical equipment necessary for the experimental areas. For such a study, it is necessary to assume a model and then price the individual items in this model. Although the model may be quite different from what is eventually in the Laboratory program, a study of this sort provides a starting point for considering equipment and unit prices which are fairly accurate. Many of the unit prices were developed by William A. Brobeck and Associates.[1] The overall model of the laboratory equipment was developed by the NAL staff. Altough some details have certainly changed in the ensuing six months, this model still sets the scale of the envisioned facility. This cost estimate has been circulated as NAL MM-148[2] (see Appendix VI).

The cost of the technical equipment is summarized in Table 3-I.

The above numbers include EDIA (Engineering, Design, Inspection, and Administration) where appropriate, but do not include escalation. These expenditures will start in fiscal 1970, and reach a peak at the start of 1973.

TABLE 3-I

COST OF TECHNICAL EQUIPMENT

Secondary Beam Transport	$12,000,000
Spectrometer Magnets	$ 8,000,000
Shielding	$ 4,000,000
Experimental Equipment	$ 3,000,000
Film Analysis Equipment	$ 2,000,000
Computers	$20,000,000
Neutrino Beam Equipment	$ 3,000,000
Superconducting R.F. Beam Equip.	$ 4,000,000
Multiparticle Spectrometer	$10,000,000
Miscellaneous	$ 1,000,000

3.2 SUPERCONDUCTING MAGNET PROGRAM

3.2a Introduction

Superconducting coils have now achieved fields of 140 kilogauss in a 6-inch bore. At the same time very large field volumes, such as the ANL bubble chamber magnet, have been constructed and operated.

Although the state of the art of transverse field magnets has lagged that of solenoids, 40 kilogauss was achieved several years ago, and a 70 kilogauss magnetohydrodyanmics type magnet will be tested within a few months. From a central field point of view, anything below 70 kilogauss can be thought of as achievable with some further development.

While current densities in a superconductor itself may exceed 10^5 A/cm^2, overall winding current densities routinely range up to 15,000 A/cm^2. Current densities up to four times this have been proposed.

The NAL beam transport bending magnets require uniformities of the order of 0.1%. From a technical point of view it is this requirement, rather than the magnitude of the field, which requires more effort to achieve. In carefully designed Nuclear Magnetic resonance experiments with superconducting solenoids uniformities of one part in 10^9 have been achieved. While this experience is not directly applicable to transverse field magnets there is every reason to be optimistic about being able to fulfill the 0.1% homogeneity requirement. However this still needs to be demonstrated experimentally.

The NAL program in superconductivity is aimed at developing superconducting beam transport elements. Up to now the program has been directed mainly toward bending magnets, however the techniques being developed are quite general and they are readily applicable, with slight modifications, to quadrupole magnets.

A desirable superconducting beam transport element has the following characteristics: (These characteristics are developed more fully in Appendix V)

1. A magnet with a field in the neighborhood of 20 kilogauss, employing iron as well as superconductor.
2. A homogeneity of 0.1% over the usable aperture.
3. Designed for minimum refrigeration requirements, since the refrigeration system represents the largest single cost item.
4. Reliable and easy to operate.

It has been these characteristics which have guided the NAL program during the past year. The experimental effort was concerned with three main areas:

1. The construction of a first full-scale model - MKI.
2. The determination of the characteristics of a superconducting "Litz" wire which is promising for use as a conductor.
3. The design of an MKII bending magnet which makes use of the knowledge gained from the MKI magnet.

The MKIII model magnet, which could serve as a prototype, is now in the final design phase. It has the characteristics outlined in Table 3-2, and is shown in Figure 3-1.

TABLE 3-2

MKII SUPERCONDUCTING BENDING MAGNET

Field	18 kG
Ampere turns	70,000
Gap height	4 cm
Gap width	10 cm
Length	90 cm
Refrigeration required	2-5 wattd
Total weight	1000 lbs.

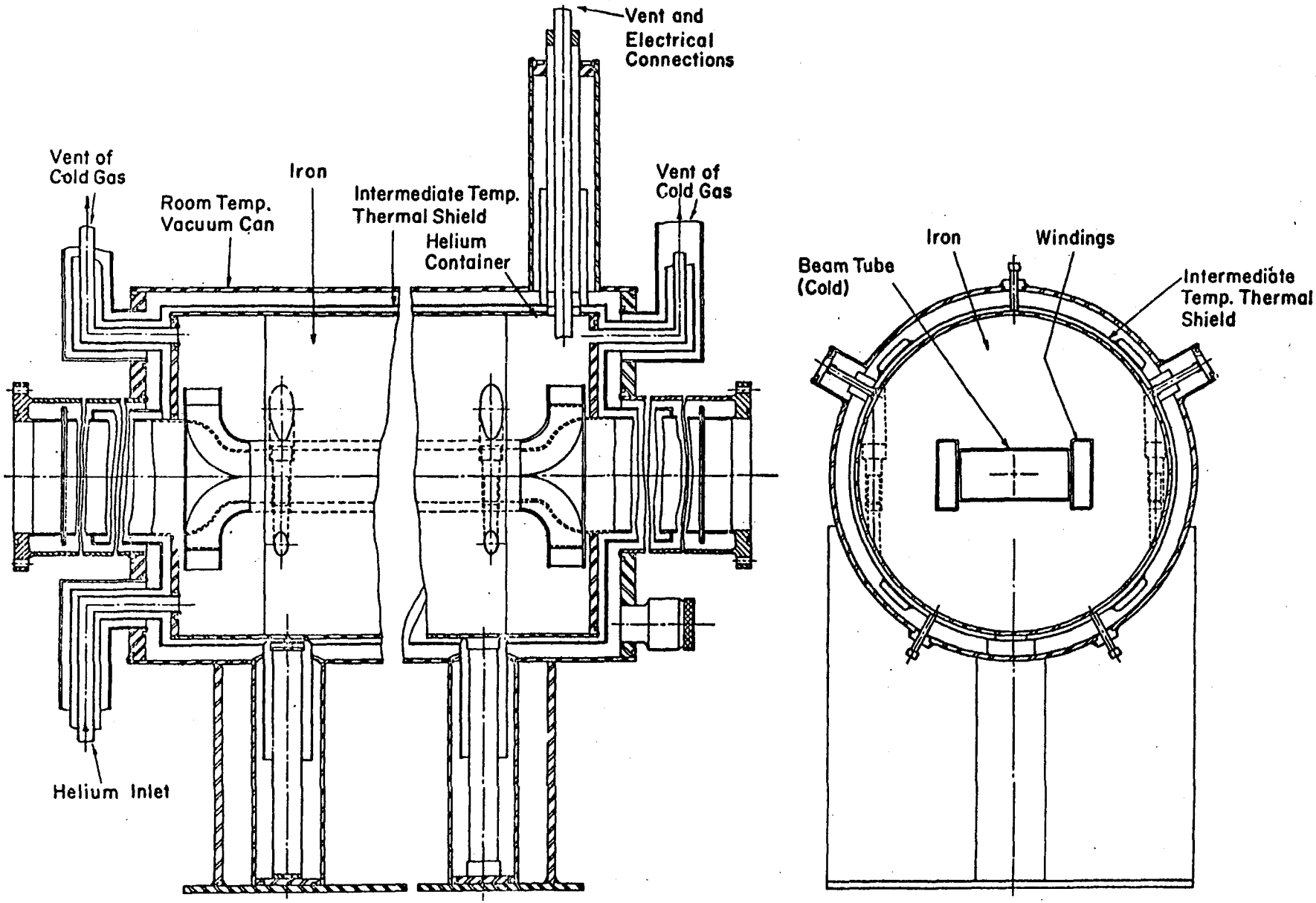

Figure 3-1 Superconducting Beam Transport Magnet

In this design the iron is at helium temperature, as is the beam tube. For regions where thermal loads due to incident radiation are large, other designs with beam tube and iron at higher temperatures may be required.

The "magnet" iron and superconductor are encased in a stainless-steel helium container. Helium liquid at approximately atmospheric pressure is introduced at one end of the magnet and is vented as gas at the other end. Part of the vent gas is returned to the refrigerator, and the rest is first used to reduce the heat leak down the electrical leads.

The helium container is surrounded by a thermal radiation shield cooled to about 80°K by intermediate-temperature helium gas from the refrigerator.

The coils will be wound with superconducting "Litz" wire, which is not only very flexible and easy to wind but exhibits excellent charge rate characteristics. This will result is an energizing current of approximately 200 A and should result in low overall heat load.

3.2b Magnetic Field Qualities

The question of what is the best magnetic field to design for is a complex one which involves technical as well as economic considerations. Fields as high as 140 kilogauss have been reached using superconductors. Therefore any field below this can be considered to be technically feasible.

Superconducting magnets of the type required for beam transport, which consistently produce accurate fields with high

uniformity, have yet to be demonstrated. However the uniformity in a beam transport magnet is determined more by the magnet design and construction than by the superconductor itself.

The geometry of iron magnets energized with superconducting windings has been investigated using the program TRIM to determine whether the required 0.1% uniformity is achievable. Typical computer results for a 20 kilogauss super-ferric magnet are shown in Figure 3-2. This shows the effect of varying the distance between the upper and lower windings. These results indicate that the placement and dimensions of the conductor bundle must be within .006 in. if computer results are to be relied on to predict a given field profile.

In addition to conductor placement and the geometry of the iron the superconductors add one more factor which affects the magnetic field - its diamagnetisim. A thorough study has not yet been made of the effects of the superconductor diamagnetism. Some attemps have been made to include the superconductor diamagnetism in the TRIM computer code, but the introduction of diamagnetism of the windings has resulted in a lack of convergence in the program as it now exists.

Air core bending magnets suffer from the serious disadvantage that the near field external to the windings of a line of magnets decays as the square of the reciprocal of the distance from the axis. Unless other magnets are very far away this external field must be shielded by providing an iron return path.

Below 20 kilogauss the iron can be used very effectively to reduce the ampere turns required as well as to shape the magnetic

Figure 3-2 Field uniformity of 20 kG superferric magnet for various coil arrangements.

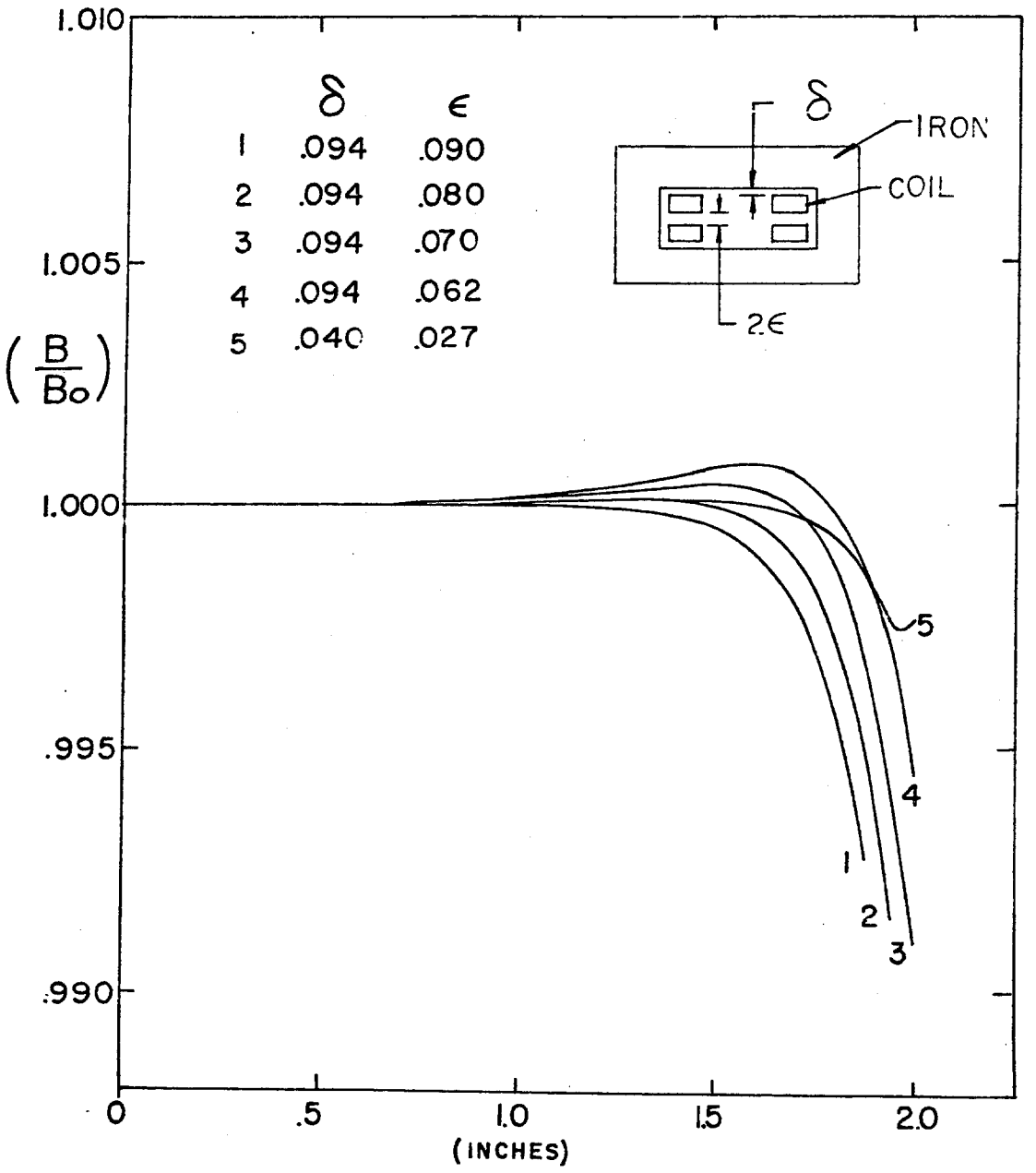

field. Above 20 kilogauss the use of the iron shield falls in one of two categories: (1) The iron is as close as possible to the beam tube and thus makes the iron contribution to the central field as large as possible. This means that the field homogeneity is strongly influenced by the coil as well as the iron. Designs of this type may have field homogeneities which are field dependent. (2) The second category of iron shield is one which surrounds the windings which are designed to produce the required homgeneity. The iron shield is placed at a position so that its surface is at 20 kilogauss. In this approach the distortion of the magnetic field due to the iron shield is minimum, but the net contribution of the iron to the central field is limited to 10 kilogauss.

The 20 kilogauss iron shield magnet (superferric) as shown in Figure 3-1 appears to offer the advantage of using the iron for shielding as well as field shaping, coupled with the economic advantage of considerably reducing the amount of superconductor required.

3.2c Cost Comparison with Conventional Systems

A cost estimate of conventional and superconducting magnets for beam transport has been made by W. M. Brobeck and Associates.[1]

The following table gives the characteristics and quantities of the beam transport magnets:

CHARACTERISTICS AND QUANTITIES OF

BEAM TRANSPORT MAGNETS

	Peak Field	Aperture (inches)	Length (inches)	Quantity
1. Bending Magnets	20	6 x 2	120	200
2. Quadrupole Magnets	15	2 dia.	72	100

A cost comparison between the conventional system and a superconducting system of magnets with identical apertures, fields and lengths gives:

	Conventional System (K$)	Superconducting System (K$)
Dipole magnets	3,440	4,122
Quadrupole magnets	1,720	1,431
Cables, power supplies and controls	4,471	1,204
Vacuum system	205	205
Cooling water system	151	99
Refrigeration system	---	5,800
Total Capital Cost	$9,997	$12,861
Total power during steady operation at peak field	45,285 KW	1050 KW
Yearly power cost (.008 $/KW hr.)	1,587 K$ (50% Duty Factor)	73.5 K$ (100% Duty Factor on refrigeration)

The estimates of initial costs indicate that the cost of the superconducting system is slightly higher. One of the most costly items is the refrigeration system itself.

When one takes into account that this cost depends strongly on the detailed engineering design of the system there is probably more room for improvement of the overall cost picture for the superconducting system. For instance, the operation of magnets in the persistent mode would reduce the heat load on the refrigerator considerably.

The yearly saving in power cost is very large and makes up for the difference in initial cost within two years.

3.2d Refrigeration and Cryogenic System

The total refrigeration load can be broken into the following parts:

1. Conduction down supports and electrical leads.
2. Thermal radiation from high temperature surfaces to cold surfaces.
3. Nuclear radiation impinging on the magnet that causes an addition thermal heat load.

The heat conducted down the supports is proportional to their cross sectional area. Consequently a good design uses supports in tension made as long as possible in order to minimize the heat conduction.

The supports may run directly from room temperature to helium temperature, however more usually they run from room temperature to an intermediate temperature thermal shield (typically at 80°K), where the heat conducted from room temperature is intercepted, and then from the thermal shield down to helium temperature.

Since the cold walls and room temperature walls have vacuum in between (below 10^{-4} mm Hg) the only mechanism for heat transfer across the gap is by thermal radiation.

The design of electrical leads is a compromise between the heat conduction down the lead, and the joule losses. Optimum leads which use the helium boiloff to intercept the heat conduction down the lead require a helium boiloff which is proportional to the current.

Additional thermal load due to nuclear radiation may be present. If an unshielded beam element with an inner radius of 2" and an outer radius of 4" is placed at an angle of 3.5 mrad to a target 60 meters away with $1.5 * 10^{13}$ 200 BeV/c protons interacting on the target per second, then the element will have approximately 18 kwatts passing through it. Only a small fraction of this would be dissipated in the magnet. An iron shield 4 to 7 m thick in front of the magnet would completely eliminate the hadronic flux. In an actual target station there might be somewhere between 25 m to 30 m of iron before the first magnet. If the magnet is an aperture stop for the system, the pole faces will be unshielded. For a 2 m long magnet 300 watts will pass through the pole faces. Very roughly, 5% of this will dissipate in the magnet, leading to a 15 watt thermal load. This indicates that it may be important to provide some modest shielding for the pole faces of the superconducting magnets. After the hadronic contribution is shielded there remains a muon flux which is extremely difficult to reduce. Typical muon shielding calculations give a muon ionization power loss of 2.5 milliwatss for this beam element.

These calculations, which are conservative, (that is they overestimate the radiation dose), indicate that nuclear radiation thermal loading is not an important problem, provided the pole faces are properly shielded.

A summary of typical heat loads is shown in Table 3-3.

Table 3-3

HEAT LOAD SUMMARY*

Supports			
1 foot long 5000 lbs in all directions.		Steel	1.62 watts
		Drawn steel	0.43 watts
		Titanium	0.30 watts
Radiation			
(36 ft^2)		Steel surf.	0.18 watts
		Gold plated	0.086 watts
Electrical Leads			
(500 A)	1.35 ℓ/hr of helium or		4 watts
Nuclear Radiation			
		Unshielded	15 watts
		Shielded	0.003 watts

The power required in an ideal Carnot cycle refrigerator operating between 4.2°K and 300°K is 70.5 watts for every watt of refrigeration at low temperature.

For a refrigerator of 10 watts refrigeration capacity only 5% of the Carnot effectiveness, or 1400 watts of power per watt of refrigeration is usually obtained. At the 100 watts

---

* All heat loads assume an intermediate temperature thermal shield.

refrigeration level, about 10% of the Carnot effectiveness can be achieved or about 700 watts of power per watts of refrigeration is required.

The cost of a refrigerator in dollars can be estimated by the formula $C = 6000\ P^{0.7}$ where P is the input power (not refrigeration capacity) in kilowatts.

The refrigerator system cost for 300 magnets requiring 7 watts of refrigeration and using 10 refrigerators is:

NO. OF MAGNETS	300
NO. OF REFRIGERATORS	10
HEAT/LOAD MAGNET	7 watts
UNIT REFRIG. CAPACITY	210 watts
FRACTION OF CARNOT	0.12
POWER/REFRIGERATOR	125 KW
TOTAL REFRIGERATOR COST	1,750 K$

The above cost is only for the refrigerator. In addition to the refrigerator there are transfer lines, helium piping and systems controls. A study of several systems by Green[3] found a system cost of just below $20,000 per magnet. The 5,800 K$ system cost in the W. M. Brobeck study is based on this number.

The difference between the table and the Brobeck number can be attributed to different assumptions as far as heat load is concerned, and also the inclusion of costs for transfer lines, piping and valving. Nevertheless, even if we double the 1750 K$ to account for the other system costs we are still left with the difference between 6000 K$ and 3500 K$ between the estimated costs.

These variations are real and will not be resolved until the heat loads and systems are more accurately determined.

In any case, we can conclude that the refrigeration system cost does vary as the 0.7 power of the total heat load. Since the cryogenic system is a major cost component, low heat leak cryogenic design of the magnets and transfer lines becomes essential.

3.3 NAL Bubble Chamber Facilities

An agreement has been reached between the National Accelerator Laboratory and Brookhaven National Laboratory to jointly undertake the construction of a large cryogenic bubble chamber to be used in particle beams at NAL. The bubble chamber is described in the BNL report 12400.[4] A proposal was submitted to the AEC during October, 1968, by NAL to begin this bubble chamber project during FY 1970. During May, 1969, the AEC approved the use of Construction, Planning, and Design funds for the Title I design and cost estimates of this project.

Under the terms of the NAL-BNL agreement, BNL will assume the responsibility for the design, construction and assembly of the bubble chamber and for making the bubble chamber a fully operating facility at NAL. NAL has final control of the chamber parameters (e.g., shape, magnetic field, filling liquid, etc.) which affect its research capabilities. NAL will be in charge of the design, construction and assembly of beams, buildings and on-site utilities which are required for the operation of the bubble chamber at NAL.

The basic parameters of the proposed 25-ft bubble chamber described in BNL 12400 are summarized in Table 3-4.

TABLE 3-4

NAL-BNL 25-ft Bubble Chamber Parameters

Volume total	105 m^3
visible (3 cameras)	72 m^3
Shape	see Figure 3-3
Possible filling gasses	H, Ne, D. H-Ne
Magnet	Hollow superconductor (niobium-titanium)
coil o.d.	29 ft 2 in.
coil i.d.	23 ft 6 in.
coil height	4 ft 6 in.
separation of coils	5 ft
average field	40 kG
Optics	140° 27 mm telecentric lenses
bubble demagnification	75 on median plane
Piston	fiberglass-reinforced plastic
diameter	90 in.
stroke	10-in. for 1.0% expansion
Expansion System	hydraulic
expansion cycle time	150 msec
Cost Total	\$17.6 M (inc. D_2 Gas)
Deuterium Gas	\$ 4.0 M
Estimated Construction Time	60 months from Title I request

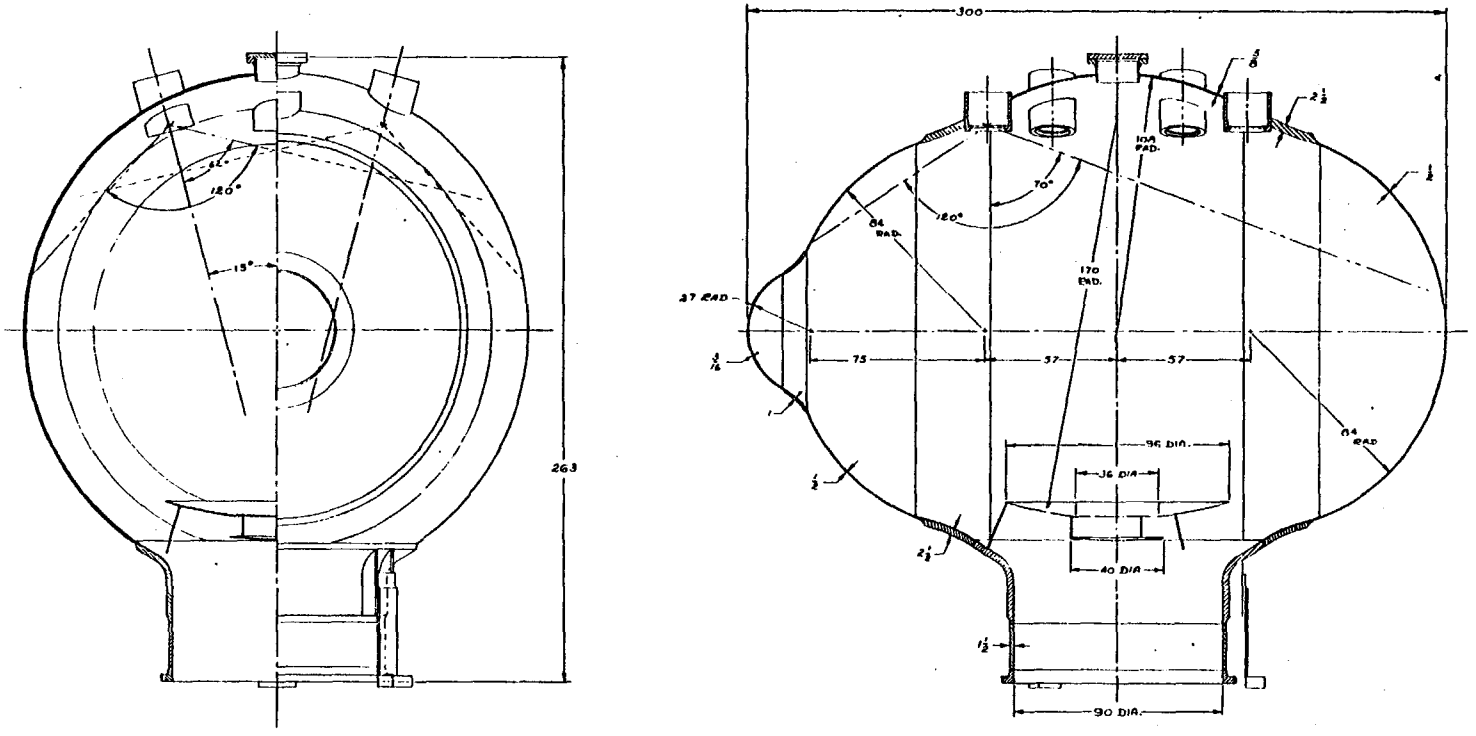

25 FT. BUBBLE CHAMBER
CHAMBER ASSEMBLY
FRONT ELEVATION

25 FT. BUBBLE CHAMBER
CHAMBER ASSEMBLY
SIDE ELEVATION

Fig. 3-3 25 Ft. Cryogenic Bubble Chamber

3.4 STUDIES OF MULTIPARTICLE SPECTROMETERS

The 1968 Summer Study included a considerable amount of work on high-precision systems intended to analyze in detail high-energy particle interactions at energies up to 100 BeV. The first detailed system that was proposed included both spark chambers and a fast-cycling bubble chamber[4] (Summer Study Report 68-12, Fields et al.) and the project, therefore, came to be known as the hybrid spectrometer. In later work the properties of many other systems were explored, and the use of the generic term "multiparticle spectrometer" was adopted.

A series of desirable characteristics and requirements for multiparticle spectrometers has been developed in NAL TM-102,[5] along with an extensive bibliography on relevant Summer Study reports and related material. The desiradata are:

1) Momentum accuracy of 0.1 BeV/c and transverse momentum accuracy of 20 MeV/c.
2) Smallest possible setting error.
3) 150-200 Kgauss-meters for the high momentum spectrometer if a setting error of 0.2 mm is achieved.
4) Field free regions to increase the precision of momentum measurements.
5) Neutral particle detection must be practical.
6) Flexible triggering schemes.
7) Some possibility for essentially "on-line" operation.
8) Modular components capable of operating by themselves.

Three principal varieties of multiparticle spectrometers were proposed during the summer session, and some additional variants were proposed afterward. Among these the most important representatives are the following:

1) The hybrid spectrometer in which a fast-cycling bubble chamber is used both as a target and as a detector for the slow particles emanating from the target vertex; the upper momentum limit is perhaps 5-10 BeV/c. Faster particles, which are predominantly forward, emerge from the bubble chamber through a thin wall, and pass through spectrometers (either one or two, in different versions), which cover the momentum range from 5 or 10 to 100 BeV/c. These are spark chamber spectrometers using either visual or digitized planes to determine trajectories. These spectrometers are supplemented by gamma-ray and neutron detectors to be used when needed. A schematic of the original Fields et al. proposal is shown in Figure 3-4.

2) A principal variant of the above substitutes track-visualizing spark chambers (either narrow-gap assemblies, wide-gap chambers or streamer chambers) for the target bubble chamber. In this variant the primary interaction vertex now withdraws into a hydrogen target, becoming invisible, and must be reconstructed from the emergent particle tracks.

   Additional use of large track-visualizing chambers in the high-energy spectrometer region downstream is also proposed; this improves track positioning accuracy, and also permits observation of downstream decays of hyperons, kaons, etc.

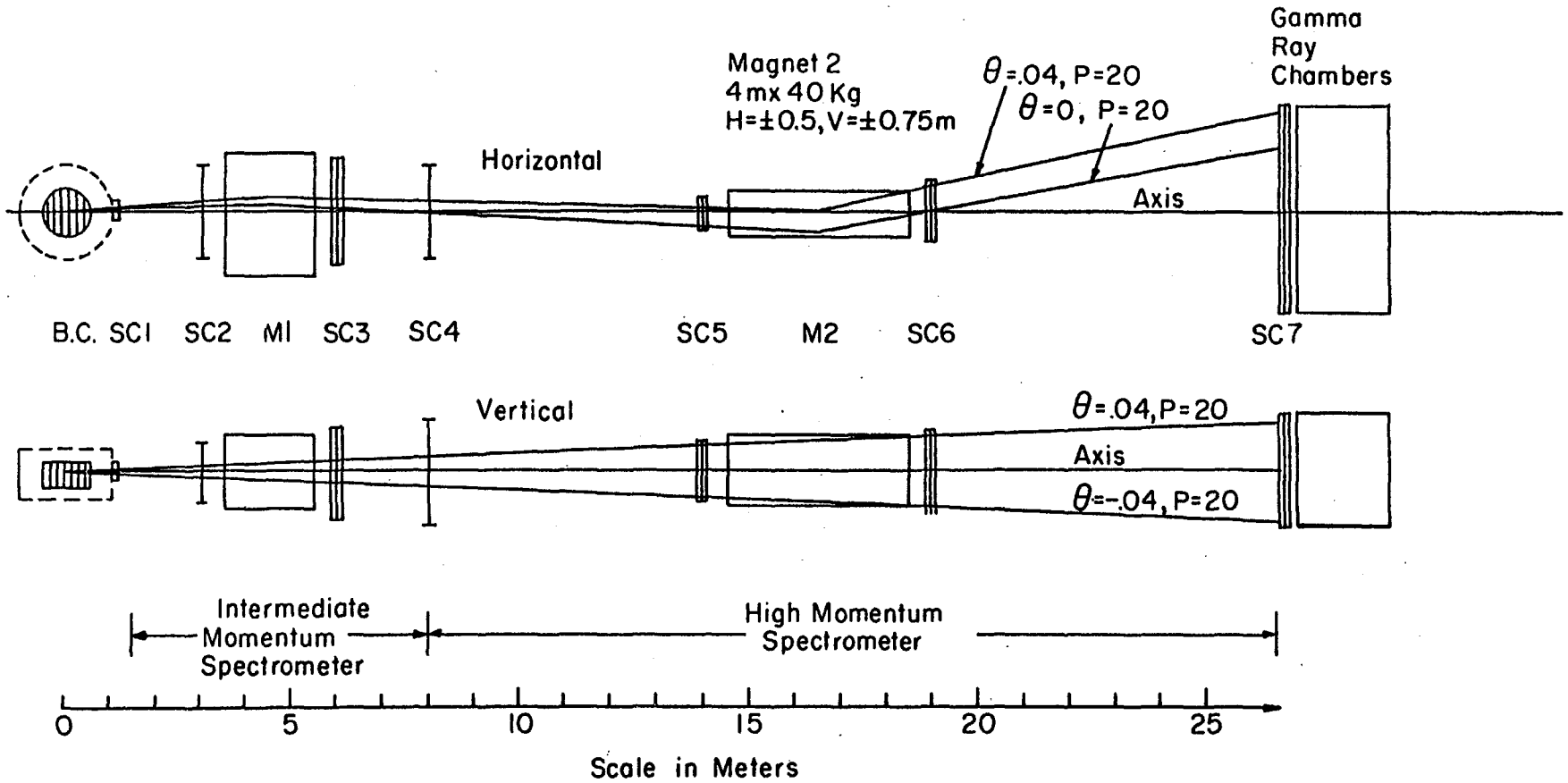

Fig. 3-4 Typical Multiparticle Spectrometer

There are also several all-or-nothing variants. These are:

3) A single large bubble chamber. The number of advocates of this approach is small; the limit of feasible size of bubble chambers has been passed (because of secondary interactions) before 100-BeV events can be profitably analyzed in a single chamber.

4) A single large streamer chamber. A SLAC group has produced a proposal for a 12-meter streamer chamber, in which the charged particle can be seen and measured.[7]

5) A digitized spark chamber spectrometer. This approach is essentially that of the Lindenbaum Mark 2 system,[8] or the Collins group[9]; a multiple spectrometer with wire planes on-line to a very large computer.

6) Another variant, in which narrow- or wide-gap chambers are used, as in the CERN Omega project,[10] is also possible.

Following the Summer Study, an ad hoc committe on multiparticle spectrometers was appointed at NAL by A. L. Read, to consider the suggestions made and to recommend a course of action for NAL. With the cooperation of the NAL Users Group, a discussion on the subject was held at the December, 1968, Users meeting, and after some additional discussion and consultation, the committee made a report which recommended the following:

1) NAL should not abandon consideration of multiparticle spectrometer systems, and should in fact reserve the $11,000,000 mentioned by A. L. Read at the Users meeting for this purpose.

2) No serious design study should be undertaken until at least after the 1969 Summer Study.

3) Final decision on construction should be postponed to the last possible moment to take advantage of the latest technological advances. To this end active liaison with groups working on technical advances should be maintained.

The recommendations were adopted by the Experimental Facilities Section. Since that time, activity has been limited to liaison; however, a proposal has been made to initiate work at NAL on the behavior of spark chambers at low temperatures, especially with regard to seeing whether the expected increase of accuracy of location can be achieved. The size and cost of large spectrometer systems are very closely coupled to the attainable accuracy of location of points on a particle trajectory.

In the fall after the 1969 Summer Study, it is expected that the status of the subject will be reviewed again; and a decision made on future action. In view of the lead time for a large multi-particle spectrometer system (at least three years) delay beyond this fall may delay the operation of such a system significantly beyond initial operation of the accelerator. Consequently, the contribution of 1969 study will be of great importance in determining the course of the project.

3.5 CHARGED PARTICLE BEAM MONITOR

A slow spill charged particle beam intensity measuring device is being developed in the Experimental Facilities Section. The current sensing part of the device consists of two toroidal supermalloy magnet cores. The cores, which are nonlinear devices,

produce even harmonic signals when they are driven by an alternating signal and are biased by a small direct current such as the external beam. The amplitude of the even harmonic signals (mainly second harmonic) is proportional to the d.c. current.

This type of monitor does not interact with the charged-particle beam and does not require calibration when the harmonic effect due to the beam is nulled by a bucking coil. Therefore, the bucking current is a direct measurement of the number of particles passing through the toroids. Similar devices have been been used in magnetometry and direct current stabilization.

The d.c. sensitivity of the device is being tested and improved. It appears that the sensitivity is limited by the Barkhausen effect and thermal noise. The thermal noise can be reduced by minimizing the resistivity of the components. The group plans to study the Barkhausen effect in various ferro-magnetic toroids. The present device can detect one μA d.c. Eventually it may be possible to measure absolute d.c. beam intensities below 1 μA with a few percent error. A simplified schematic of the arrangement is shown in the Figure 3-5.

3.6 EQUIPMENT

3.6a Scanning and Measuring Facilities

The Physics Research Section has started to develop a film analysis facility at NAL. A Hermes film plane measuring machine with track following is being obtained from BNL. This will be modified to increase the stage motion velocity. In addition two

FIGURE 3-5

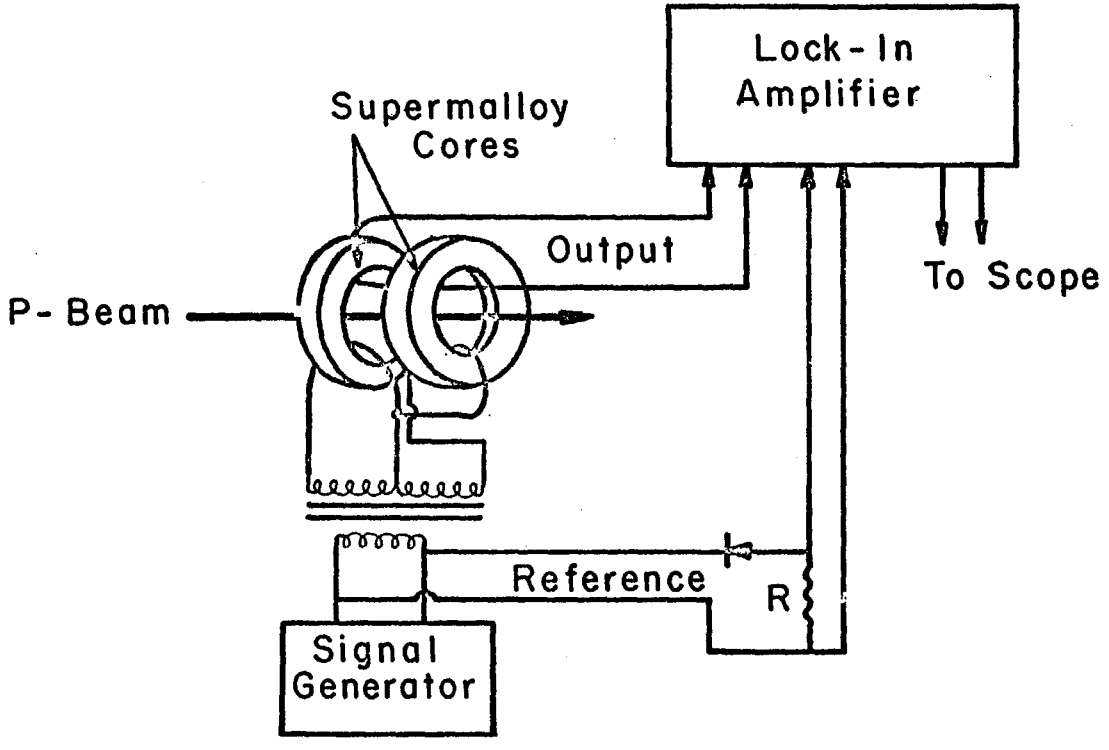

Simplified block diagram of the inductive d.c. beam monitor.

image plane measuring machines will be purchased and will operate on line to a computer. The Hermes will be used for engineering investigations of film from the seven and twelve-foot bubble chambers as well as to perform research measurements. The results of these scanning and measuring activities will help in specifying the next generation of measuring machies needed at NAL. The facilities will be used to carry out bubble chamber measurements at NAL for experiments performed under the Physics Research Section.

3.6b Low Temperature Spark Chamber Investigation

The Experimental Facilities Section has considered the possibility of designing and constructing a test stand for the operation of spark chambers at low temperatures (down to liquid hydrogen temperature). The purpose of such a test facility would be to extend presently available data on the low-temperature performance of optical and digitized spark chambers. The operation of spark chambers in thermal equilibrium with liquid hydrogen targets opens some interesting experimental possibilities, chief among which is the possibility of constructing spark chamber systems for neutrino investigations using very large amounts of liquid hydrogen as a target.

Such a system provides an alternative to bubble chamber detection of high-energy neutrino events. It could be a modular system, capable of operating on a small scale, and of revision, improvement, and expansion if it proves successful. It could supplement bubble chamber operation for certain types of neutrino events; on a sufficiently large scale, it could increase the amount of hydrogen available as a target by an order of magnitude over that provided

by the 25-ft bubble chamber, without costing nearly as much. Such an increase would make possible experiments, such as strange particle production by high energy anti-neutrinos, which would be very much more difficult in the 25-ft bubble chamber.

Another area of interest to NAL is the construction of high-precision spectrometers. It appears likely that spark chambers operated at low temperature should allow higher intrinsic accuracy of track location than room temperature operation. This is because, ultimately, the accuracy is limited by electron diffusion in the gas. Decreasing the temperature and increasing the density should decrease the diffusion length and allow the possibility of increased accuracy.

It is now known that helium, hydrogen,[11] and neon[12] work well at increased pressures at room temperature, and that helium at atmospheric pressure works well at liquid nitrogen temperatures.[13] "Working well" means only that it has been observed that the expected increases in gap efficiency are found, and in addition the tendency of narrow-gap sampling chambers to become delineating has been confirmed; the sparks start to follow the particle trajectories. No attempts to run streamer chambers at low temperatures seem to have been recorded. An early, vigorous investigation of these properties could have a substantial beneficial effect on the planning of a multiparticle spectrometer facility and a neutrino facility.

3.6c Proportional Plane Development

The benefits to be realized from increased detector spatial resolution, particulary in the intrinsically fine optics of NAL beams, were stressed by L. Lederman at last year's Summer Study.[14] Great strides have recently been made in integrated circuits which offer the hope of operating wire planes in the proportional rather than the spark mode, and thereby gaining better spatial resolution. At the very least, these developments guarantee a higher rate capability ($\sim 10^5$/wire sec.) than conventional wire planes. In addition, it appears possible to operate the planes near high magnetic fields. In the last few months, a group in the Experimental Facilities Section have begun a program of instrumentation research for proportional planes. A wire plane made from 20 micron gold-plated molybdenum wire with 3 mm wire spacing has been constructed, and many of the measurements performed at other laboratories have been repeated with comparable results. A second plane with 1 mm spacing is presently being assembled for continuing studies. A variable spacing wire winding machine has been constructed. At present, cost estimates of $8-10/wire for amplifiers and associated logic are still prohibitive if one is contemplating large systems.

REFERENCES

1. "Cost Estimate of Experimental Equipment", William M. Brobeck and Associates Report No. 200-1-R7, January, 1969.

2. NAL MM-148, February, 1969. (See Appendix VI).

3. "Refrigeration for Superconducting Magnets in the 200 BeV Accelerator", M. A. Green, G. P Coombs, J. L. Perry, Arthur D. Little, report June 1968.

4. "25-Foot Cryogenic Bubble Chamber Proposal", BNL 12400, March, 1969.

5. "A High-Accuracy, Large Solid Angle Detector for Multiparticle Final States at 100 GeV", T. Field, A. Roberts, D. Sinclair, J. Vandervelder, and T. G. Walker, NAL 1968 Summer Study, A3-68-12.

6. "An Approach to Establishing the Characteristics of a Flexible Modular Large-Scale Detection System for the Study of Complex High-Energy Events", A. Roberts, NAL TM-102, November, 1968.

7. "An Evaluation of the 12-Meter Streamer Chamber", A. Roberts, NAL TM-101, November, 1968.

8. "Large Digitized Spark Chamber Spectrometer and On-line Computer System", S. J. Lindenbaum, BNL report 13130, October, 1968.

9. "Study of Multiparticle Production in P-P Interactions at 28 GeV/c", BNL-VPI proposal, G. B. Collins et al., October, 1968.

10. "The Omega Project", Omega Project Working Group, NP Division, CERN, Internal Report 68-11, May 1968.

11. G. L. Schnurmacher, Nuc. Inst. & Meth. 36, 269 (1965).

12. G. S. Akopyan et al., Instr. and Experim. Techn. 516 (May, 1967).

13. E. F. Beall and V. Cook, Unpublished Report BeV 770 A, (Nov. 1962).

14. "Influence of Detector Spatial Resolution in the Scaling of NAL Experiments", L. Lederman, NAL 1968 Summer Study, C3-68-65.

4. EXPERIMENTAL FACILITIES ORGANIZATION AND LIAISON ACTIVITIES

A. W. Key, A. L. Read, A. Roberts

The development of the overall experimental facilites is carried out by a number of sections at NAL. The first part of this chapter describes how the effort is shared.

The Experimental Facilities Section maintains almost day-to-day contact with potential users. These contacts occur through user committees, individual visits to the laboratory, and visits of our staff to other research groups. These liaison activities have been quite successful, both from the standpoint of assisting NAL in planning and informing the users of current activities at the laboratory.

In addition, the Experimental Facilities Section has participated in several other large scale liaison activities. A large summer study has been carried out at the Aspen Institute for Physics in 1968 and will be repeated in 1969. A Canadian physicist has joined the section as a visitor, in part to help in formulating a Canadian plan for participation in NAL. These activities are discussed in more detail in the following sections.

1. Organization

Three sections at the National Accelerator Laboratory are concerned with developing the experimental facilities. These are the Experimental Facilities, Radiation Physics and Beam Transfer Sections. This section describes how the facilities development effort is distributed in NAL.

The Experimental Facilities Section (J. R. Sanford, Section Leader) is responsible for the design, fabrication and operation of the equipment in the secondary beam and experimental areas. This does not include detectors and associated equipment used by individual experimenters. Additionally, it is the responsibility of the EF Section, together with the Architectural Services Division (T. L. Collins, Associate Director for accelerator services) to provide design criteria for the conventional experimental facilities at NAL to DUSAF (the architectural liaison at NAL) which in its turn is responsible for the design and management of construction of these facilities. The conventional facilities consist of secondary beam buildings, experimental buildings, utilities, roads, cranes, and other conventional equipment. The EF Section presently consists of fifteen professional people and six others. One year ago, it consisted of five people.

The Beam Transfer Section (A. W. Maschke, Section Leader) is in charge of designing, fabricating and operating the beam extraction equipment for the main accelerator and the external proton beam transport, splitting, switching, and targeting systems. Together with the Architectural Services Division, the Beam Transfer Section provides design criteria to DUSAF for the conventional structures and equipment required by the above technical systems.

The Radiation Physics Section (M. Awschalom, Section Leader) is responsible for shielding and radiation monitoring in the experimental areas. The RP Section also has the responsibility to insure that the design and construction of the conventional facilities, managed by DUSAF, satisfy all the requirements of the NAL policies on radiation.

2. Aspen Summer Study

The 1968 summer study was set up with the main purpose of providing a mechanism for prospective users of the 200 BeV Accelerator to participate in studies upon which some of the important decisions concerning the experimental facilities will be based. Aspen, Colorado was chosen because of the existence of the facilities at the Aspen Center for Physics and the congenial location.

In 1968 over 100 reports were written on this summer study work, many of which have now been collected and published in three volumes.[1] A list of all the reports written, with a short account of their contents, is appended. (Appendix X) The topics included:

1. The design of bubble chambers for use at NAL and their application to specific high-energy physics experiments.
2. Hybrid spectrometers, consisting of combined bubble-chamber and spark-chamber systems, in order to take advantage of target-vertex visibility in the bubble chamber and the measurement accuracy achievable in the spark chamber.
3. Streamer-chamber spectrometers.
4. Proton-proton scattering experiments using the extracted proton beam in specially constructed target stations.
5. New and less costly schemes for targeting and dumping the external proton beam and for shielding in the target areas.

6. New suggestions for master plans of experimental areas, including the question of the internal-target area.
7. The design of a wide variety of secondary-particle beams, for example, neutrino and antineutrino beams, pion beams, separated K beams, and of specific experiments that require the availability of these beams.
8. Experiments to search for intermediate bosons, quarks, and Dirac monopoles.
9. Applications of superconducting techniques to secondary-particle beams.

The concrete accomplishments of the 1968 summer study were impressive, as may be seen from the published reports. Some of the most noteworthy conclusions of the 1968 study were the following:

1. The agreement that the internal target area should be abandoned.
2. The observation that large-hydrogen bubble chambers would only have limited usefulness for the detailed analysis of high-energy interactions above 50 BeV/c, but would perform a vital survey function below that energy.
3. Clarification of the muon background in neutrino experiments involving large-cryogenic bubble chambers.
4. The generation of a set of requirements and specifications for detection systems to be used for the detailed study of such high-energy interactions, such as requirements on transverse momentum resolution.

5. A preliminary examination of the properties of hybrid, streamer chamber, and other multiparticle large spectrometer systems for this purpose.

6. The production of sample designs for a number of different types of beams, and of several different target station experimental area and beam layouts.

7. The design of many different experiments to be performed, with resulting feedback concerning the facilities required to make them feasible. (These designs were used for a number of the experiments used in the cost study model.)

The 1969 summer study has been planned based on the impressive success of the 1968 study. In the 1969 summer study, some of the same topics will again be studied, and some new ones added. In general the approach is to study fewer topics in greater depth. The formal topics are:

First Session

1. Specific and detailed beam designs (cf. also 4).
2. Hybrid spectrometers and other large-scale detection systems; new detection systems or detectors.
3. On-line experiments and their analysis.

Second Session

4. Neutrino experiments and facilities (including beams to the 25-ft hydrogen bubble chamber).
5. Further study of high-energy strong interactions in the 25-ft chamber.
6. Film analysis problems.

Of these, (3) and (4) were not considered last year. Laboratory design and engineering work is already started on (1); during the coming year decisions will be taken upon what to do relative to (2), (4), and perhaps (3), and (6).

3. Canadian Participation in NAL

In 1968 the Canadian 200 GeV Study Group,* with the aid of a grant from the Canadian National Research Council, embarked on a detailed examination of the feasibility of Canadian participation in NAL. A. W. Key (University of Toronto) was employed by the Group to provide liaison with members of the NAL staff and to assist in the preparation of a report on the study. This report, entitled "A Particle Physics Program for Canada," appeared in March 1969.[2]

The report concludes that Canada's sole contribution should not consist of a single item such as an additional experimental area or a large streamer chamber. Instead, it is recommended that Canada become a full partner in NAL with joint responsibility with the U S.A. for constructing, equipping and operating the laboratory.

Several different calculations indicate that a figure of $4,000,000 annually would be a reasonable Canadian contribution. This amount is compatible with Canada's expenditure in other similar areas of scientific research, and, due to the initially limited scope of NAL, could achieve a disproportionately large improvement in the experimental exploitation of the accelerator. The report

---

*Members of the Study Group are E. P. Hincks, Chairman (Carleton University), B. Margolis and D. G. Stairs (McGill University), and J. D. Prentice and W. T. Sharp (University of Toronto)

considers participation in NAL as one aspect of an overall program for particle physics in Canada for the next five years, the other of which is continued and increasing support for the user groups.

The report recommends that the Canadian funds be granted to an organization formed by interested Canadian universities, and that they remain in a separate account placed at the disposal of the Laboratory Director in an arrangement similar to the way the U.S. funds are administered. The Director would then be free to direct the Canadian contribution to the areas of greatest need for the laboratory, while being encouraged to spend the Canadian dollars in Canada. A major appendix to the report indicates that Canadian industry is qualified to supply up to about $37,000,000 worth of the equipment required for the accelerator and the experimental areas.

It is hoped that the National Research Council of Canada will consider in detail the recommendations of the report at its forthcoming meeting in June, and that it will send the proposal for Canadian participation in NAL forward to the next governmental level with its support.

Three Canadians have been invited to participate in the 1969 Summer Study at Aspen, Colorado, and the community of Canadian particle physicists will hold an "Experiment's Design Program" at McGill University in July to keep themselves informed on and provide ideas for experimental planning at NAL. An additional grant from NRC has been obtained to support two Canadian physicists at NAL for 1969-70.

REFERENCES

1. National Accelerator Laboratory 1968 Summer Study, June 1969 (3 volumes)

2. "A Particle Physics Programme for Canada", Canadian 200 GeV Study Group, NRC, March, 1969.

national accelerator laboratory

TM-175
2000

APPENDIX I

CONCEPTUAL DESIGN OF THE EXPERIMENTAL AREAS

E. J. Bleser, T. L. Collins, A. Maschke, D. Moll (DUSAF),
F. A. Nezrick, A. L. Read and F. C. Shoemaker

May 1969

ABSTRACT:

This report describes an updated conceptual design for the external proton-beam lines, target facilities and experimental areas which are planned to be included in the initial program of research at the NAL 200-BeV synchrotron.

1. Introduction

The facilities described in this report will carry the proton beam from the main-accelerator extraction in the Transfer Hall of the Main-Ring enclosure to the Target Stations. Conventional facilities (structures, paved areas, and utilities distribution) are provided for secondary-beam transport and detection equipment beyond the target stations. What is described herein would provide for an initial research program of the same overall scope as that outlined in the NAL Design Report (Section 14.2), January 1968, and in the 200-BeV Accelerator Construction Project Schedule 44, which was submitted to the U.S. Atomic Energy Commission in 1968.

Technical equipment for secondary beams, which is beyond the scope of the accelerator facility and of this report, has been discussed elsewhere.[1] Here we will discuss secondary beams and detectors only as they relate to this conceptual design of the experimental areas.

It is to be emphasized that the concepts discussed in this report are subject to change in many details during the design period that is to follow. We believe that the broad outlines of these concepts are firm enough to serve as a basis for the design.

Initial thinking on design concepts for experimental areas is described in the National Accelerator Laboratory Design Report[2] in Chapters 13 (particularly Sec. 13.3), 14,

and 15 (particularly Sec. 15.3). Since publication of the Design Report, considerable effort has gone into reviewing, refining, and revising these concepts. The work has included a Summer Study held at Aspen, Colorado, in July and August 1968, with participation of many high-energy physicists from all parts of the United States.

This report describes an updated conceptual design of the experimental areas which has been developed subsequent to the 1968 Summer Study. It is on the basis of these design concepts that NAL has received, in May 1969, AEC authorization to proceed with detailed design specification (Title I Design) of the experimental areas.

During and immediately following the 1968 Summer Study two major decisions concerning experimental areas were reached by the NAL staff.

The first decision concerns the internal-target area previously planned to be at Long Straight-Section B. It had been thought that the properties of internal targets such as multiple traversals by the circulating proton beam might be significant in improving secondary particle yields for certain specific experiments. Extensive investigations in the Summer Study failed to unearth any experiments for which internal targets are crucial, and it has therefore been decided to drop them from the plans, both because the same funds can be used more efficiently for a corresponding expansion of the external-beam target facilities, and because their use as a

general facility would produce a level of radioactivity in the main ring that would make maintenance extremely difficult and expensive and would lower the reliability of accelerator operation.

Should a specific research need for an internal target arise in the future, however, the design of the Main-Ring Enclosure has been carried out to preserve the option of constructing an internal-target station and associated experimental area at some later time.

The second major decision concerns a large bubble chamber. There has been considerable discussion as to the usefulness of a bubble chamber for strong-interaction physics in the new higher energy range. Investigations in the 1968 Summer Study showed that bubble chambers will be useful for strong-interaction experiments, at least up to secondary particle energies of approximately 70 BeV, but that their major unique capability will probably be in neutrino-interaction experiments. In these experiments, a very large hydrogen-deuterium bubble chamber will be a unique tool capable of providing data hitherto unavailable. It has therefore been decided to provide for targeting and secondary beam facilities for such a large bubble chamber, with these facilities to be designed to produce both neutrino and separated charged-particle beams. The bubble chamber itself, and those facilities and items of equipment specifically related to its operation as

a detector are not included herein, and are the subject of a separate proposal.[3]

With these two decisions made, the Laboratory staff has concentrated its efforts on developing a conceptual layout of the experimental areas. In this work, the size of the research program and number of secondary beams as discussed in Sec. 14.2 of the Design Report have been regarded as minimum conditions to be met. These minimum goals may be summarized as follows:

Number of experiments set up	12
Number of experiments in operation	9
Number of "electronic" setups	10
Number of "electronic" experiments per year	20
Number of bubble chamber setups	2

It is expected that about one-fourth of the research program will be carried out by resident staff and about three-fourths by visiting users. On the basis of the conceptual design studies described in this report, we believe that the experimental areas can be constructed with a potential scope for the initial research program that is at least equivalent to the scope described in the

NAL Design report and summarized above. All of the experimental areas described here will be constructed within the expected total construction authorization of $250 million.

The conceptual designs presented in this report will be reviewed at the 1969 Summer Study. Different designs which may be developed during the summer of 1969 could be incorporated into the plans for any of the experimental areas 1, 2, or 3, if subsequent detailed studies by the Laboratory staff indicate that the new concepts would be more suitable than the design concepts outlined in this report.

2. General Description

The proposed layout of the external-beam lines, target stations, and experimental areas on the site is shown in the master plan of Figure 1. Figure 2 is an expanded view of the experimental areas. After acceleration, the proton beam is extracted from the main ring in the Transfer Hall at point T over a time that can be varied from one revolution period (20 microseconds) up to the full length of the flat-top

(1 second). The beam emerges from the Transfer Hall and moves in a northeasterly direction. The beam line runs 1350 feet to the first splitting station at S1. Here the beam can be split, with part or all of it being sent straight ahead to a target at T1 to make secondary particles for a bubble chamber at E1; while the remainder of the proton beam is deflected eastward toward the other experimental areas.

The split portion of the beam is bent through an angle of 7.5°. It travels 1350 feet, past the shops and laboratories of the industrial area, to the second splitting station, S2. Here the beam can be split again, either travelling straight on to the second target station, T2, or being bent eastward, again through 7.5°, toward the third target area, 3. The experimental facilities can be expanded in the future, should this prove desirable, by adding more splitting stations and target stations farther along the same curved line. In the design concept outlined in the Design Report, the primary beam line was straight; and the beam was diverted at the splitting stations to the targets. The principal advantage of the new concept is that it provides greater lateral space between the experimental areas for the same total amount of bending of the proton beams.

As presently conceived, the bending and focusing of the proton-beam line will be carried out by magnets either identical to or very similar to those of the main accelerator. Similarly, the housing of the proton beam will make use of the pre-formed sections designed for the main-accelerator enclosure. Sections of

beam-transport pipe will be used immediately downstream of each splitting station to decouple the splitting stations from each other and to localize radioactivity.

The target stations are the points of greatest radioactivity in the entire accelerator facility. With the present design concepts, the targets and nearby equipment will be surrounded by massive shielding and will be removable by rail to a target laboratory for maintenance and repairs.

The three target stations and secondary-beam areas will differ from each other, in order to provide a variety of facilities. The first area, (1), will provide beams to a bubble chamber. The main purpose of this station is to provide a neutrino beam. The beam must be very long, will be a dominant feature of this area and will determine its characteristics. Counter-spark-chamber experiments may also use the neutrino and charged-particle beams at area 1. The second area (2) will be a conventional area providing an assortment of about six charged and neutral particle secondary beams for counter-spark-chamber experiments. It will consist of a large experimental hall with overhead-crane coverage and will be similar to the experimental areas that exist at present-day accelerators. It is expected that in this area the experimenter will use the secondary beams that are available and that the beams will not be rebuilt for special purposes.

The third area will also be for counter-spark-chamber

experiments, but this area will be more flexible than the second area and will be capable of accommodating a more varied array of secondary beams. Since we do not yet have a detailed picture of what the experimental demands will be, this area is discussed as though it were very similar to the second area. Thus half the available resources are allocated to it but its form remains somewhat undefined. These three areas are described in more detail in Sections 4 and 5 below.

3. Beam Transport and Splitting Stations

The proton beam is transported from the Transfer Hall in a straight line to the first splitting station, S1. Beyond this point, the beam-transport system is comprised of a straight section about 600 ft in length followed by a bending section of about the same length. The beam is split in the straight section, with a fraction extracted from the main transport line to go to a target station, T1, and the remainder going through the bending section to be carried to the next splitting station, S2.

Beam splitting is carried out by use of a series of septum devices. The system is similar to the system used to extract the beam from the main accelerator. The first thin electrostatic septum is positioned close to the beginning of the straight transport section, as shown in Figure 2. The split beam is given a vertical impulse. After a 90° betatron phase advance to achieve maximum amplitude, it clears the septum of the second

device shown in Figure 2, which bends the beam further upward to miss the leading magnet at the end of the straight section. The beam is then transported at an upward angle from the 725.5-ft elevation at the splitting station to the 753-ft elevation at the target stations, where it is brought back to the horizontal plane. The horizontal distance traversed during this change of elevation is one thousand feet. In this traversal the beam is focused by a series of quadrupoles spaced 200 ft apart. At the 753-ft elevation, the beam is transported 200 ft to the target. The quadrupoles in this last 200 ft must be moveable in order to provide for changing of target elements.

The unsplit part of the beam is bent 7.5° in the curved section toward the next splitting station.

4. Areas 2 and 3

Areas 2 and 3 are designed primarily for use with counter-spark-chamber experiments and share common target-station features, which are discussed here. As we have mentioned previously in this report, neither the equipment to accomplish the research experiments nor the secondary beam transport equipment are included in this conceptual layout of experimental area facilities.

a. Target Stations T2 and T3. All the technical components associated with the target - target mechanisms, collimators, and possibly the first focusing magnets for secondary beams -

are to be mounted in a "target box." The target box is a steel enclosure, approximately 100 ft long and 3 ft by 3 ft in cross section. The target box itself is fixed in a permanent position. It is surrounded by massive fixed concrete and earth shielding.

Components are brought into it and placed by a railroad train. The target box contains ledges for the support of components and rails for the train. A target assembly is installed on the train in the target laboratory described below and is moved to the target box, where it is lowered onto the support ledges by remotely operated jacks. The train is then removed from the target box. Thus, a major function of the target box is to provide rigid support for the target assembly. Another important function is to make it possible to locate radiation shielding very close to the target and the proton beam stop.

The target laboratory is envisaged as a prefabricated steel-frame building similar in size to the temporary laboratories in the Village (10,000 sq ft). It will have an additional area of approximately 5,000 sq ft for power supplies, shops, and light laboratories. The trainrail system inside the building will run between shielding walls. Remote manipulators and a crane will be used to carry out operations on the train, with television cameras for viewing.

It is estimated that approximately one target-box changing

operation will be carried out per year. The concepts outlined here are a lean but expandable design to accomplish this purpose; it is expected that operational experience might well modify the methods used.

b. Design Basis. The variety of facilities required for the counter-spark-chamber experiments is very great. On the basis of past experience, there will be, on the one hand, a large and continuing demand from users for what might be called conventional beams, while on the other hand, some experiments will demand a wide range of specialized beams that will pose complicated design problems.

A workable conceptual design using conventional elements to produce an array of conventional secondary beams has been carried out. This tentative design is taken as the basis for the layout of area 2. The underlying assumption is that there will always be a demand for conventional beams, that a satisfactory selection can be designed and built, and that the experimenters will use these beams as they are without requiring extensive rebuilding. Based on these assumptions, it is possible to design a beam-transport area that is very crowded with magnets, power, water, shielding, collimators and controls, but that is relatively inexpensive to build and operate because it is designed as a unit, and buildings and facilities have to be provided only for a specific array of magnets. This has been the intent behind the design of area 2. Such an area is not well suited to

experiments requiring the full-intensity primary beam, very short hyperon or K° beams, or maximum-intensity beams of pions, muons, or neutrinos as they are presently understood. Therefore, more specialized beams have been allocated to area 3 while the area 2 has been designed to produce a large number of conventional beams as inexpensively as possible.

c. Secondary Beam Layout. In addition to the studies on main-ring magnets to be used for the primary proton beam transport, and as a guide to laying out the experimental areas, a detailed beam-design program has been undertaken using main-ring magnets. These magnets are moderately well matched to the problem. Their quality is slightly better than what is needed to produce high-energy beams of 100 MeV/c resolution. Thus, this design is entirely realistic and could certainly be built. A design that might actually be constructed would incorporate a number of obvious improvements, such as specialized magnets at the front ends of beams to increase the solid angle. Table I lists the properties of the six beams as presently conceived. Figure 3 shows a possible layout of these beams in the building together with the shielding necessary to absorb muons from pion decays near the primary target and to shield the beam lines. The experimental hall shown has approximately 75,000 sq ft of floor area. Figure 4 is a cross section through the muon shield 120 ft downstream from the primary target.

Table I. Yields of Secondary Particle Beam for 10^{13} Interacting Protons and a 100 MeV/c Momentum Bite
(after T. G. Walker, NAL 1968 Summer Study, Report No. B5-24)

Beam Number	Production Angle (mrad)	Momentum (GeV/c)	π^- Yield	Proton Yield
1,4	20	30	3×10^6	10^6
		20	10×10^6	10^6
2,5	10	80	3×10^5	2×10^6
		40	4×10^6	10^6
3,6	3.5	200	-	2×10^9
		150	5×10^4	3×10^7
		100	10^6	2×10^7
		50	5×10^6	3×10^6

5. Area 1

This area is primarily intended to provide secondary beams for use in a bubble chamber. It is assumed that the specific beams provided will be a high-intensity broad-energy-spectrum neutrino beam and an rf-separated π and K meson beam with a maximum momentum of approximately 80 BeV/c. The designs of the target station and beam area described herein are somewhat independent of whether the neutrino beam is produced by a current-sheet (magnetic-horn) focusing system or a quadrupole focusing system and also of the details of the rf-separated beam design.

Target-station T1 has several features that make it unique. First and most important, the neutrino-beam elevation is set at 733.5 ft, which is nominally 15 ft below ground level, to minimize the cost of the muon-stopping shield. Second, because there are relatively few transport elements in the neutrino beam, the design of this target building will differ materially from that of the buildings in target areas 2 and 3.

a. Target Building T1. The proposed method of mounting the target and beam-transport elements is to suspend them from concrete mounting pads. These pads are aligned on ledges in the side walls of a concrete trench 300 feet long and 11 feet wide, as can be seen in Fig. 5. Portable shielding is placed over the mounting pads to fill the trench partially, as can be seen also in Fig. 5, so as to provide a lower-background environment where electrical and mechanical connections can be made to the beam elements. Beam elements and portable shielding blocks will be of standard widths so that any beam-transport element can be removed by an overhead crane without disturbing the other elements. A radioactive transport element can be removed from the target station in a special casket mounted on a railroad flatcar that enters the target building at the upstream end, in a manner similar to that used in stations 2 and 3. Along the primary proton-beam direction, a space 300 feet long by 5 feet by 5 feet is available in the target-station building and could contain either a current-sheet meson-focusing system or the front end of a quadrupole meson-focusing system.

A single target might be the source of both the neutrino beam and the charged particle beam. It is possible to envision an extraction system for the circulating protons that would give a high-intensity fast-extracted proton burst at the beginning of the flat-top, followed one second later by a low-intensity burst. If both these bursts were extracted into target station T1, this target station could, without moving beam-transport

elements and using only one target, produce a neutrino beam followed one second later by a charged-particle beam to a bubble chamber. It would also be possible to transport slow-extracted protons into area 1, for counter-spark-chamber experiments using the neutrino or charged-particle beam.

It might at some future time be desirable to transport 200-BeV protons to a target close to the bubble chamber, for the production of short beams of short-lived particles. For moderate proton beam intensities $\lesssim 10^9$/burst, the charged-particle secondary transport channel at area 1 might be modified for this purpose.

b. Neutrino Beam. The neutrino beam might, for example, have two or three pulsed focusing elements mounted in the 300-ft long target station. These elements would produce a nearly parallel π and K meson beam of one sign while defocusing particles of the opposite sign. The neutrino beam is provided by the decays of these parent mesons. To provide a long, low-cost decay path for the mesons, a 5-ft diameter pipe is extended for 1,650 ft beyond the target-station building. This provides a total decay length of 1,950 ft. Following the decay region is a shield of iron and earth to stop all known particles except the neutrinos. The 5-ft diameter decay pipe somewhat reduces the lower-energy neutrino flux, but at present it appears to be a good choice because the emphasis is likely to be on the higher-energy interactions. The pipe diameter also determines the transverse dimension of the muon shield and significantly

affects the cost of that part of the beam. A more detailed investigation of this optimization will be made. The present design basis of the muon shield is that its thickness shall be kept constant and its average density increased when the proton energy is increased from 200 to 400 BeV. A shield thickness of 970 ft has been chosen tentatively. At 200-BeV operation, the shield thickness would be 1/3 iron and 2/3 earth.

c. Charged Beams. Charged beams can be obtained from target T1 through the collimator mounted in the sidewall of the target-station trench at a production angle of about 25 mrad. The charged beam from the collimator at elevation 733.5 ft is deflected to ground level where it emerges from the downstream end of the target-station building about 20 ft from the neutrino-beam axis. A vacuum pipe transports the beam at ground level to the bubble chamber, where it is deflected to the center of the bubble chamber at elevation 733.5 ft.

To continue a study of resonances and other strong interaction effects, a three-stage rf-separated beam of 80 BeV/c maximum momentum is proposed. Such a beam can easily be constructed in the 2700 feet available from the target T1 to the bubble chamber. Since the bending of high energy beams is expensive, beam configurations are being investigated that will minimize the total bending angle, the amount of extra tunnel needed, and the muon leakage through the neutrino shield.

6. Superconducting Beam-Transport Magnets

A significant fraction of the cost of the experimental areas will be in the installation of electrical power and cooling-water systems for magnets in the secondary beam areas. However, extensive use of superconducting magnets could potentially save much of these installation costs. This report therefore contains a brief discussion of the superconducting magnet program at NAL. The reader is reminded that the superconducting magnets for secondary beam areas are not included in the $250M construction authorization, but will be funded from a separate capital equipment budget.

An investigation into the economics of superconducting beam-transport magnets has revealed that the most economical installation would make use of iron magnets operating at or below 20 kG. In such a configuration, the superconductor is used to magnetize the iron and the ampere-turns are kept at a minimum. Operation of the beam-transport magnets at higher fields does not appear to offer significant advantage in the experimental areas, but this point needs more investigation.

The main problems of field uniformity and superconductor magnetization are minimized by the fact that the volume of superconductor is small and the field is shaped mainly by the iron.

Figure 6 is a proposed configuration for a superconducting bending magnet. Table II shows the pertinent magnet parameters.

Table II. Superconducting Magnet Parameters

Field	18 kG
Ampere-turns	70,000
Gap height	4 cm
Gap width	10 cm
Length	4 m
Refrigeration required	5-10 W
Power required for operation	3.5 kW
Total weight	4,000 lb

The iron is at helium temperature, as is the beam tube. For regions where thermal loads due to incident radiation are large, other designs with beam tube and iron at higher temperatures will be required.

The "magnet" iron and superconductor are encased in a stainless-steel helium container. Helium liquid at approximately atmospheric pressure is introduced at one end of the magnet and is vented as gas at the other end. Part of the vent gas is returned to the refrigerator, and the rest is first used to reduce the heat leak down the electrical leads.

The helium container is surrounded by a thermal radiation shield cooled to about 80°K by intermediate-temperature helium gas from the refrigerator.

The magnet is energized with leads running from room temperature to helium temperature. These leads are optimized for minimum heat leak and require 3 liters of liquid helium per 1000 amperes per pair of leads. This heat leak is proportional to current and consequently favors lower-current conductors.

7. Physical Plant

The general configuration and technical components of the beam-transport system and the experimental areas have been described above. This section describes the physical plant in these areas.

a. Structure. Proton beams extracted from the accelerator will be carried underground through a beam-transport enclosure of the standard 10-ft diameter cross section. At critical points, because of radiation, the standard enclosure will be replaced by 200-ft long sections of transport pipe 12 in. by 18 in. in cross section. This system of beam-transport enclosure and pipe will connect with a concrete splitting station of rectangular cross section and about 300 ft long. The splitting station is designed to allow the beam either to travel ahead, rising to a target, or to pass to the next splitting station through a similar system of beam-transport enclosures and pipes.

Target-station T1 will be located in a narrow concrete enclosure about 350 ft long and buried in earth shielding. This enclosure will have two levels. The target will be located in the lower level at elevation 733.5 ft, separated from the upper level by blocks of portable shielding. The portable shielding will be handled by a 40-ton crane located at the ceiling of the upper level.

Targets T2 and T3 will be located in the steel target boxes. These target boxes will be cast in heavy concrete 16

feet in thickness, covered with 25 ft of additional earth shielding. Each target box and its pre-target box area will be located at the grade elevation of 748 ft. The beam-transport system connecting the pre-target box area at grade with the respective splitting station below ground will necessarily be inclined.

The beam-transport enclosures, splitting stations, and the three target statiors will all have a system of vehicle and personnel accesses and utility buildings and galleries, which will be located at the existing grade. The size and construction methods will follow those determined by the main-ring design for similar buildings. The present site plan also includes in the experimental areas one special access for each of the target-handling systems, seven utility buildings, two utility galleries, four major vehicle-access buildings, 2 minor vehicle-access buildings, and four personnel emergency exits.

The major experimental areas, E2 and E3, will be located immediately downstream of target stations T2 and T3 at the approximate existing grade elevation of 748 ft. The experimental area E2, following target station T2, will consist of a 750-ft long building designed to enclose a fan-shaped configuration of secondary beams. The total area of this building will be about 75,000 sq ft of experimental space with an additional 10,000 sq ft of enclosed support area. The experimental space will be serviced by a 40-ton crane or other

materials-handling devices of similar capacity. There will be a paved area of 200,000 sq ft immediately surrounding experimental building E2.

The experimental complex E3 is less well defined at this time, but it is thought that the array of secondary beams will be housed in a series of smaller buildings extending for more than a thousand feet. Total areas of these buildings may reach 100,000 sq ft. Four hundred thousand square feet of paving will be provided to accommodate this complex.

b. Mechanical Equipment.

General. Mechanical-equipment requirements for the experimental areas include conditioned-air purge for beam-transport enclosures, splitting stations and Target Station T1. Heating and ventilation will be required for Target Stations T2 and T3 and the experimental buildings E2 and E3. Cooling water for magnets and other equipment will be distributed throughout the experimental areas. Industrial water will be distributed for fire protection and toilet rooms.

LCW Systems. A distributed low-conductivity water (LCW) system for experimental-area equipment cooling will be designed on a local cooling basis. It is planned to utilize cooling tower stations supplying 96° LCW.

Air-Purge Systems. Equipment will be local, using package systems. These systems will be located in typical utility buildings, similar to those of the main accelerator, located at convenient points along the beam line.

Building Heating and Ventilating. Winter heating for target-station and experimental area buildings will be by local systems within the respective buildings served. Ventilation will be supplied by louvered air intakes and roof exhaust fans.

c. Power Distribution. Electrical power will be distributed underground at 13.8 kV, 3 phase, 60 Hz, from the main substation to stationary unit-load substations and plug-in stations, located near the splitting stations, target stations and experimental areas, supplying ac power for the magnets at 480 V, 3 phase, 60 Hz. The distributed power capacity for experimental use is approximately 60 MW, the maximum power available at the main substation for experimental use is limited to 30 MW. Several portable substations rated at 2500 kVA will be provided to supply power to non-fixed experimental loads.

Electrical power for facility requirements will be supplied by separate feeders connected to a number of unit load substations located for distribution at approximately 480/227 V for motor and lighting loads. Dry transformers will be used for 120/208 V power requirements.

8. Schedule

It is planned to design and construct the experimental areas in three parts, corresponding to the three areas, 1, 2, and 3. Table III shows the principal milestones for each of these areas.

Table III. Schedule Milestones

	Begin Design Specification	Begin Construction Design	Begin Construction	Complete Construction
Area 2	9-1-69	4-1-70	11-1-70	4-1-72
Area 1	12-1-69	12-1-70	7-1-71	7-1-72
Area 3	9-1-70	12-1-71	7-1-72	7-1-73

9. Acknowledgements

The conceptual design for experimental areas at NAL, is the product of the work of many individuals in addition to the authors of this report. Other contributors to the design work include E. L. Goldwasser, R. A. Carrigan, Y. W. Kang, A. W. Key, Z. J. J. Stekly, T. O. White, R. Mobley, J. Simon, and P. V. Livdahl. We also acknowledge the assistance of several others in the preparation of this report, including F. Cole, P. Reardon, J. Sanford, and members of our engineering and secretarial staffs.

[1]National Accelerator Laboratory Memo MM-148, "Projected Experimental Equipment Costs FY 1969-1975," E. J. Bleser and A. L. Read (unpublished).

[2]National Accelerator Laboratory Design Report, Second Printing July 1968, Universities Research Association, under the auspices of the United States Atomic Energy Commission.

[3]Brookhaven National Laboratory Report No. 12400, "25-Foot Cryogenic Bubble Chamber Proposal," March 1969.

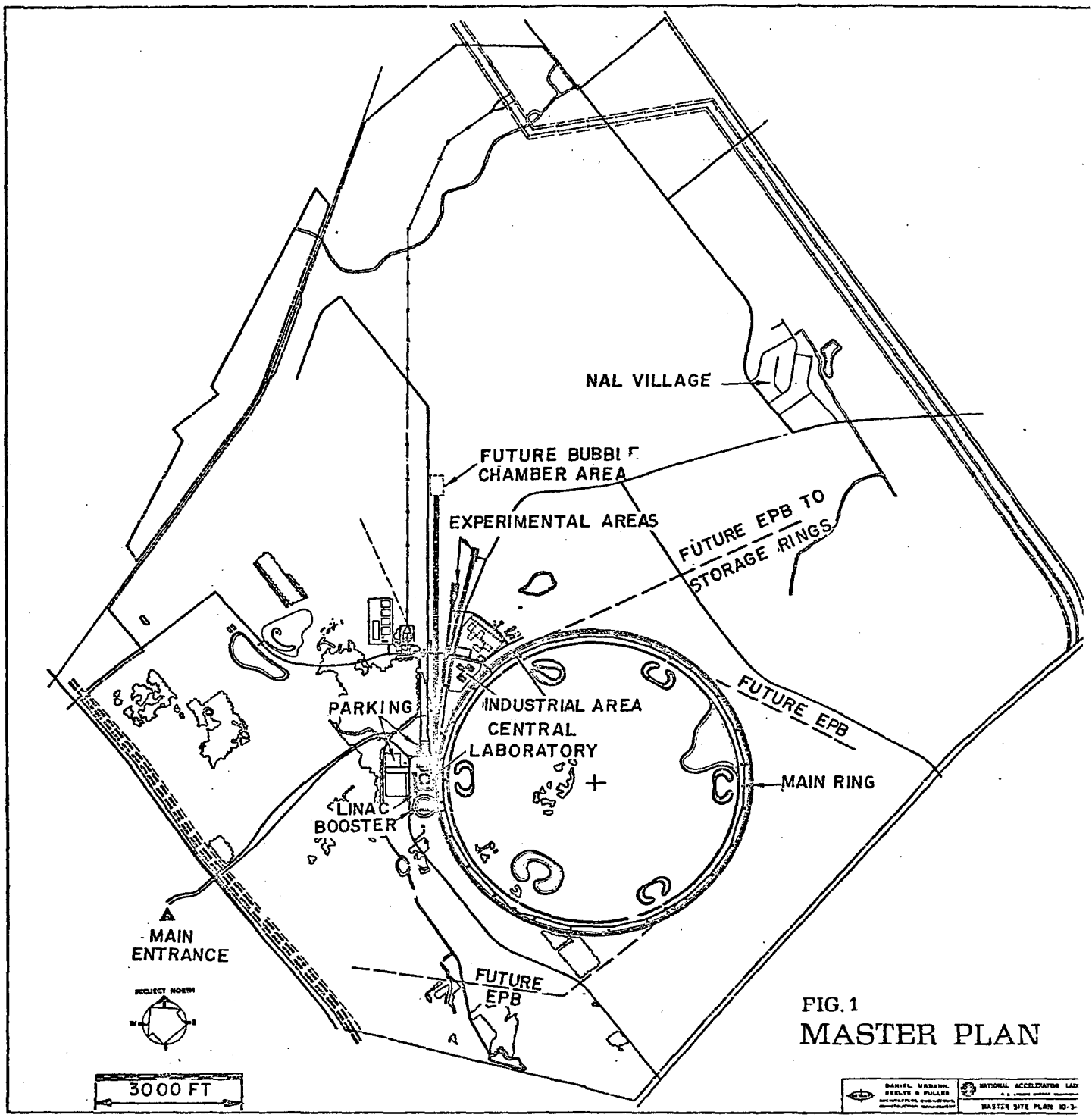

Figure 1 - Site Master Plan

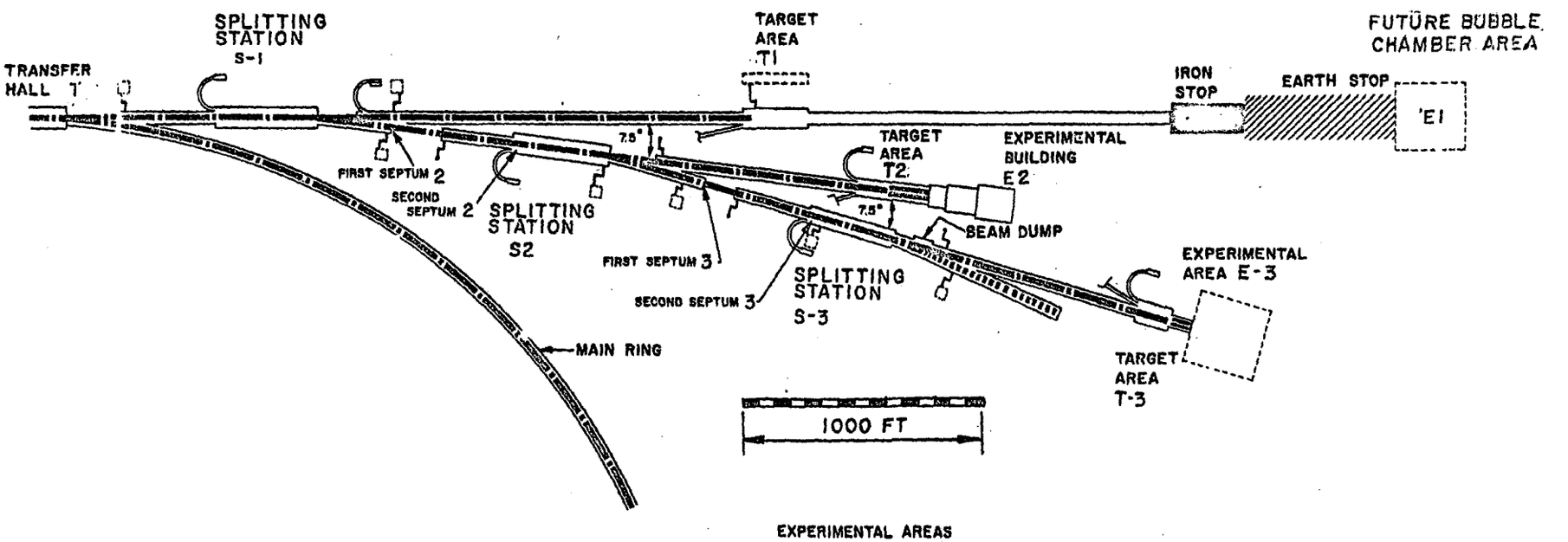

Figure 2 - Experimental Areas Master Plan

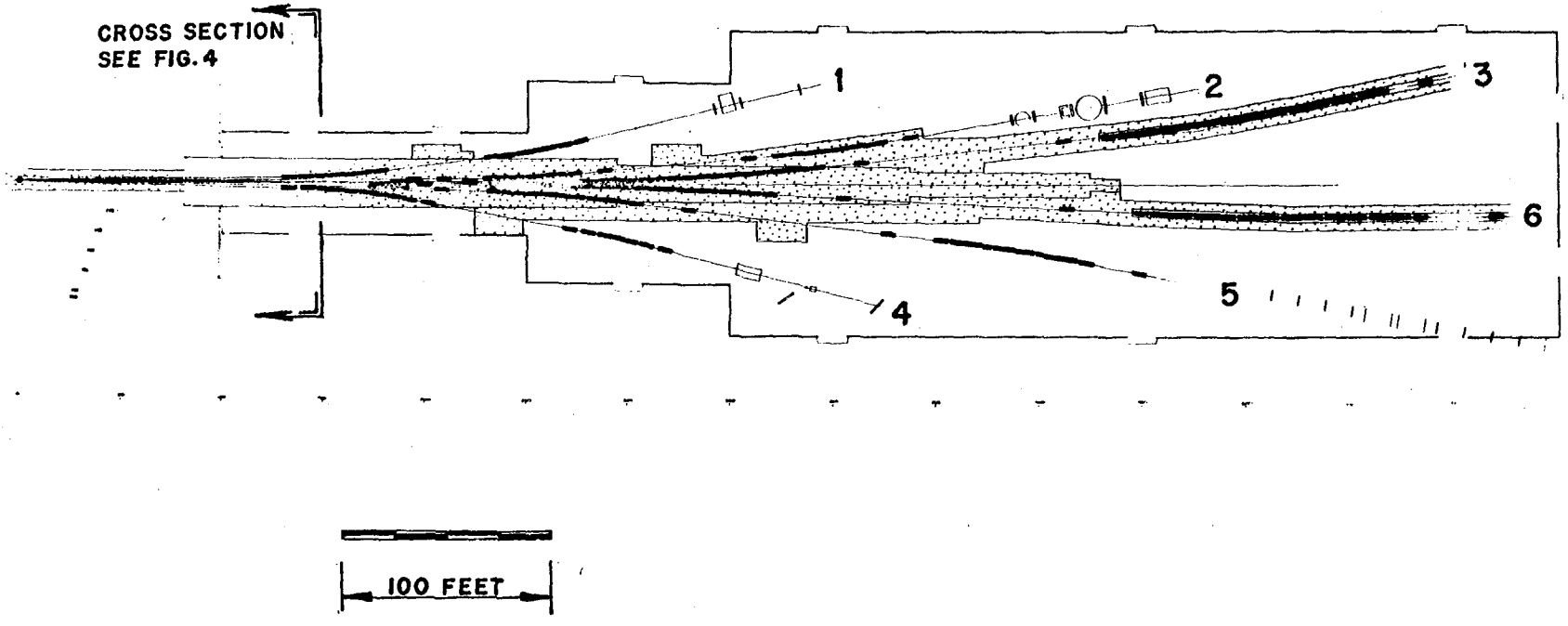

Figure 3
Experimental Area 2

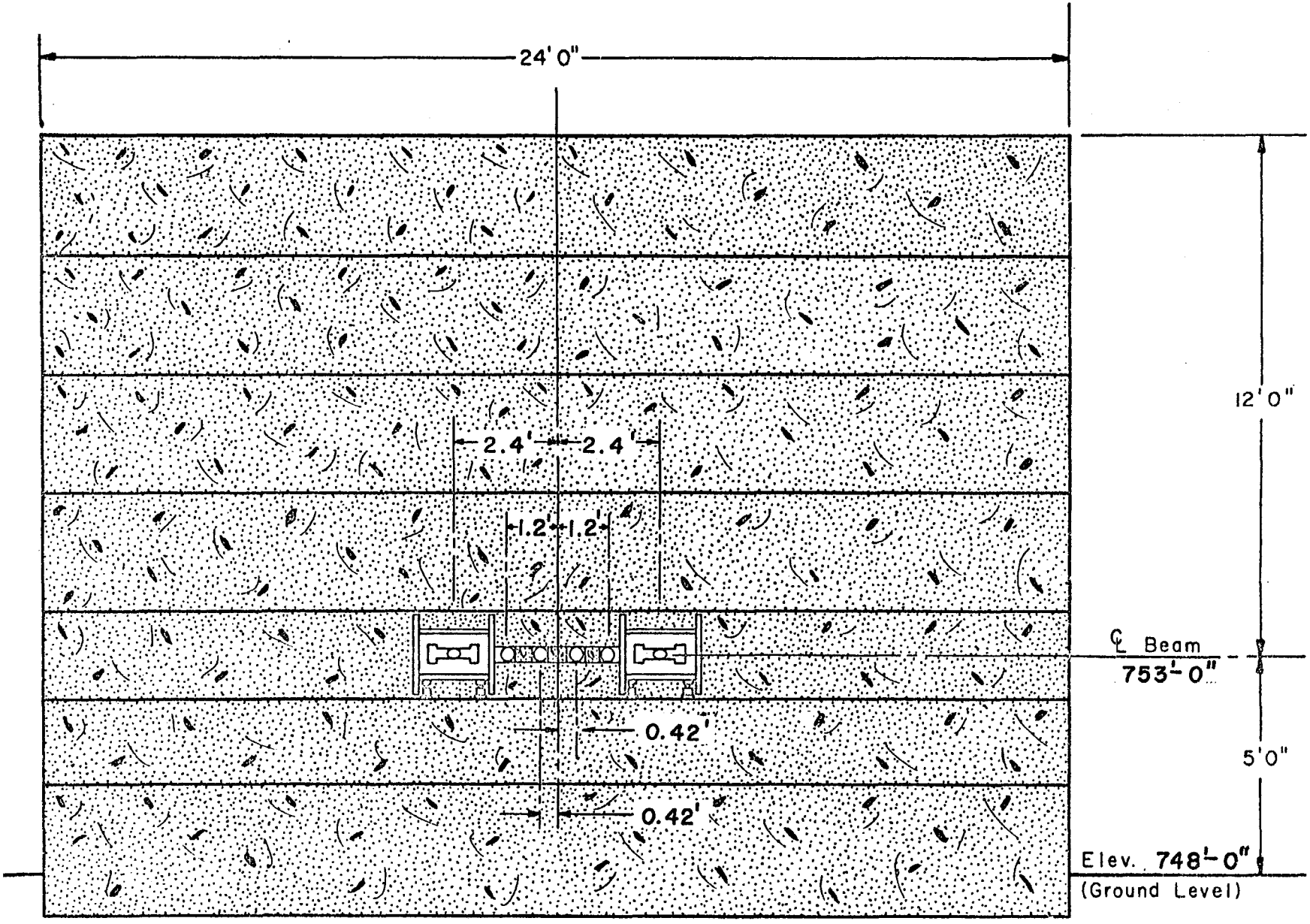

Figure 4 - Cross Section through
Muon Shield in Area 2

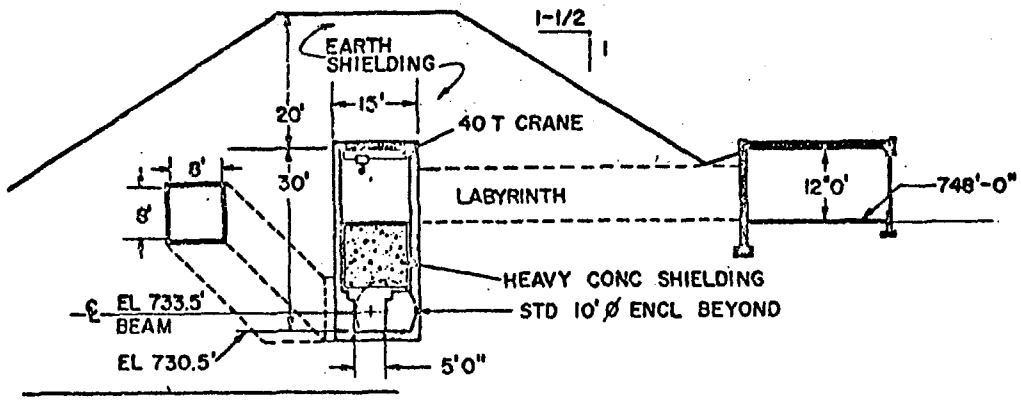

VIEW LOOKING UPSTREAM

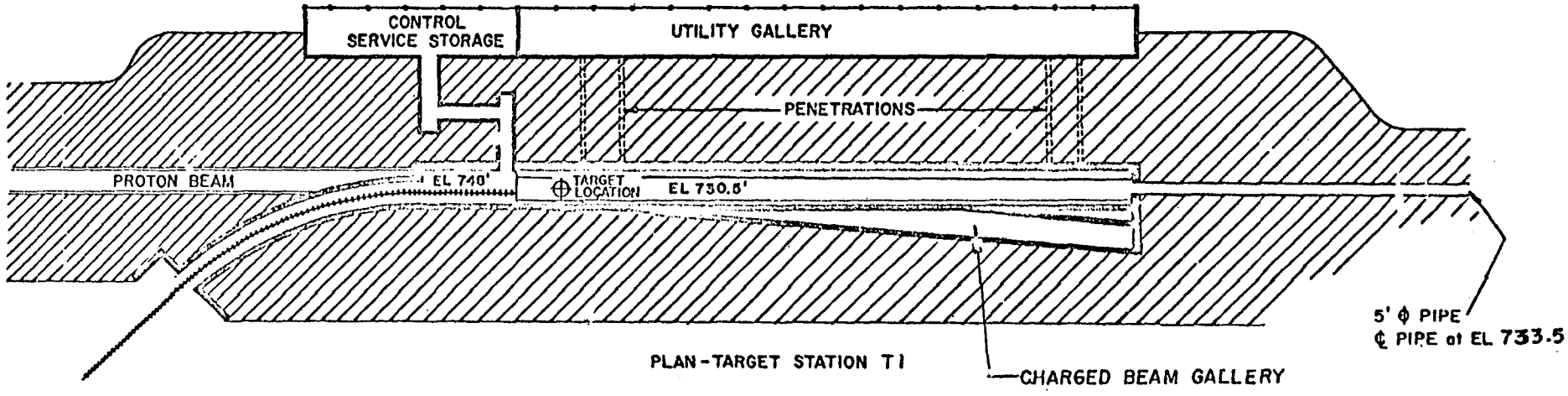

Figure 5 - Target Station T1

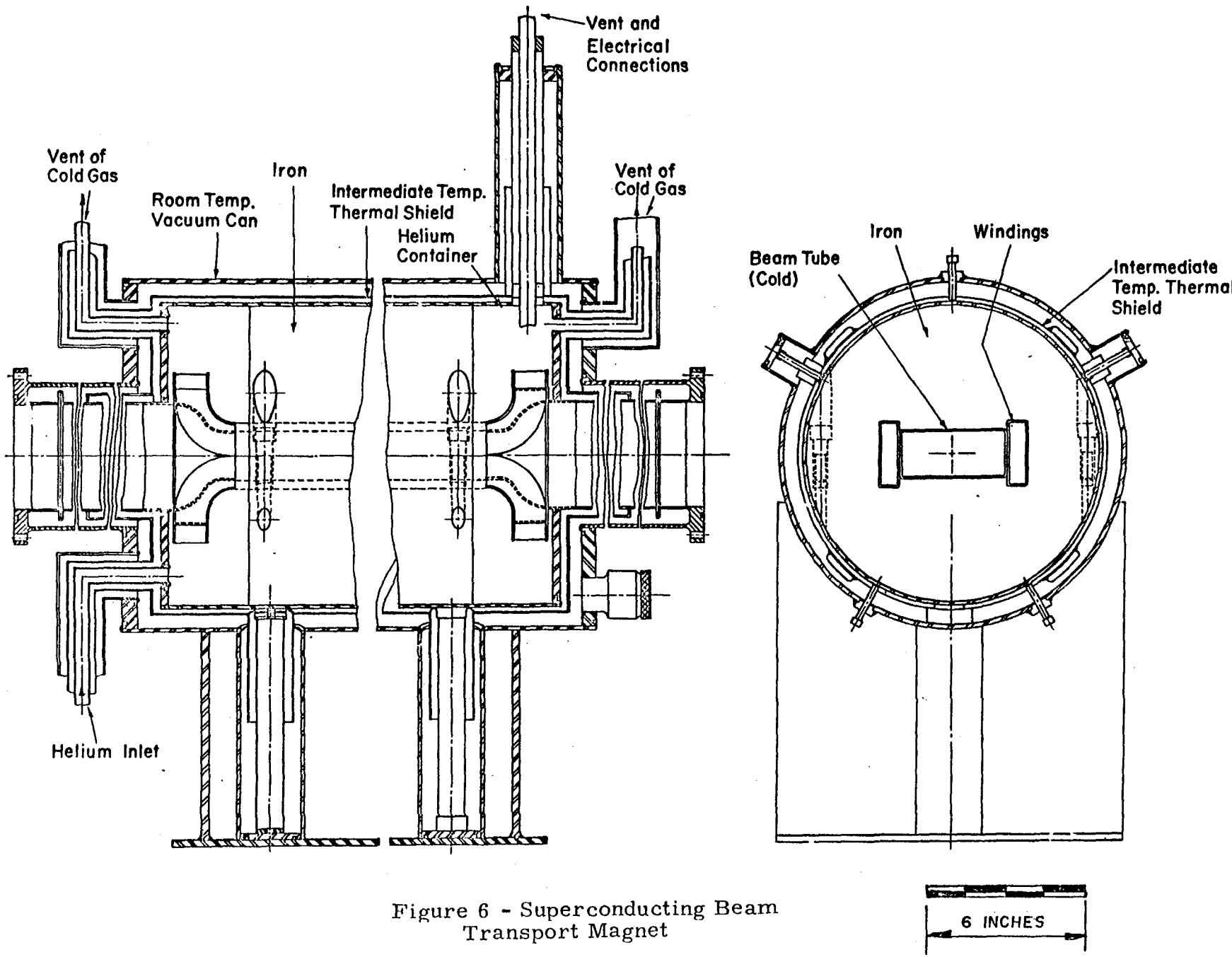

Figure 6 - Superconducting Beam Transport Magnet

APPENDIX II

A BENDING AND FOCUSING STRUCTURE FOR THE EXTERNAL PROTON BEAM

A. Garren and R. Mobley

March 25, 1969

This note proposes a particular structure that may be appropriate for the type of curved external beam line currently envisaged by the Beam Transfer group. The general layout is sketched in Fig. 1. The beam is ejected from the main ring at position 0. Between 0 and 1 the beam is matched to the betatron functions of the FODO cell of Fig. 2, at a mid-F position, and the momentum dispersion is brought to zero, both in displacement and angle.

The first section, or 'superperiod' of the transfer line consists of two parts, each with transfer matrix equal to -1 in both planes. The first part, from 1 to 2, contains the vertical electrostatic beam splitter E, magnetic septum magnets M, and two quadrupole doublets. The second part consists of two FODO type cells, each with 90° phase advance. Eight bending magnets are distributed symmetrically about the junction point 2 between the two parts 1 - 2 and 2 - 3. Likewise eight magnets are centered about point 3, and the dispersion is thereby restored to its original zero value as the beam goes into section B. Further details of a superperiod can be seen in Fig. 2.

Each of the sections A, B, and C are identical except that there is no bending at point 1 at the start of section A.

The scheme proposed has the following advantages:

1) At each beam splitter E the momentum dispersion is zero.
2) At the splitters the vertical β-function is very large, which minimizes beam loss on the septum.
3) The long field-free length after the splitter can be used to shield downstream components from radiation.
4) E and M are 90° in phase and a large distance apart, beam separation is large at M, which can therefore have a large septum thickness, high field, and short length.
5) The length of the two FODO cells is as small as possible for the desired bending, consistent with restoring the dispersion to zero at the splitters. The resulting concentration of bending increases the separation between the target area TA, TB and TC.
6) The phase advance between beam splitters is 2π, so each splitter is exactly imaged on the next one.

Parameters suggesting a possible concrete realization of the proposed system are given in Table I.

Table I

Total length of section between beam splitters	Ls	381	m
Total length of π-insertion (1)-(2)	Lπ	261	m
Free length	L'	113.13	m
End length	ℓ'	28.97	m
Short end length	ℓ'e	2.4016	m
Quadrupole separation	a'	8	
Length of π quadrupoles QF', QD'		4.685	m
Total length of cell	Lc	60	m
Lengths of drifts spaces	a	.3048	m
	ℓ	.92967	m
	L	27.05614	m
Length of quadrupoles QF/2, QD/2		1.31953	m
Length of bending magnet B		6.0706	m
Gradient in QF', QD' (400 GeV)		112.39	kG/m
Gradient in QF/2, QD/2		247.59	kG/m
Bending magnet field		18.02	kG
Bending magnet magnetic radius		742.0	m
Bending angle per section		7.5	dey
Phase advance per section		2π	
Phase advance π-insertion		π	
Phase advance per cell		π/2	
Betatron functions βx, βy, Xp			
Starting at (1)		101, 18, 0	m
QF'		133, 271, 0	m
QD'		58, 608, 0	m
QF'		320, 114, 0	m
(2), (5)		101, 18, -	m
(3)		18, 101, -	m
(4)		101, 18, 5.5	m
(6)		58, 606, 0	m

FIG. 1
SCHEMATIC OF BEAM LINE
—— NOT TO SCALE ——

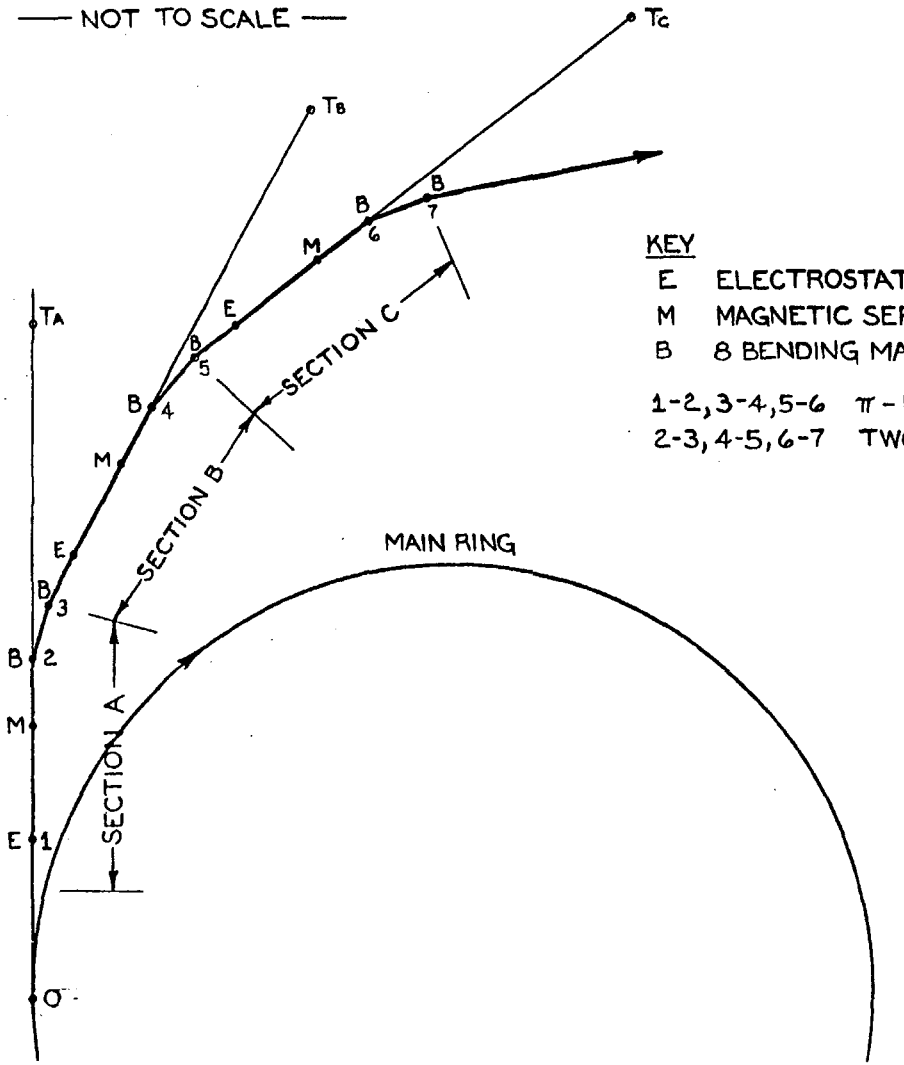

KEY

E ELECTROSTATIC SEPTUM-VERTICAL BEAMSPLITTER
M MAGNETIC SEPTUM MAGNET-VERTICAL
B 8 BENDING MAGNETS, 3.75° BEND

1-2, 3-4, 5-6 π-INSERTIONS
2-3, 4-5, 6-7 TWO 90° FODO CELLS

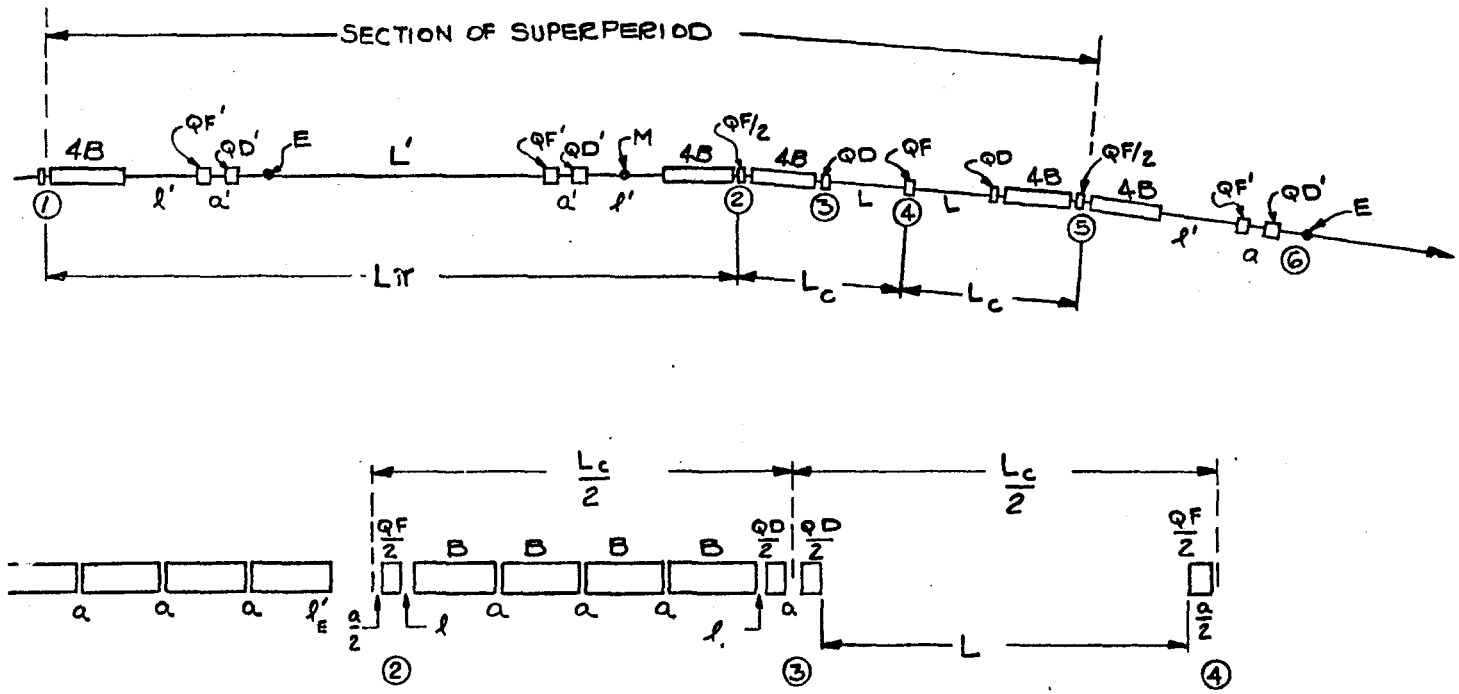

DETAIL OF FODO CELL STRUCTURE

E--ELECTROSTATIC SEPTUM DEFLECTOR
M--MAGNETIC SEPTUM MAGNET

FIG. 2

Appendix II - Continued

DESIGN OF THE 200 GEV SLOW EXTRACTED BEAM AT NAL

R. A. Andrews, R. M. Mobley, A. W. Maschke

and C. H. Rode

National Accelerator Laboratory

Batavia, Illinois

Reported to the

Particle Accelerator Conference, Washington, D.C.

March, 1969

SUMMARY

The design criteria for the slow beam are given, and the methods for achieving high-extraction efficiency are discussed.

INTRODUCTION

As is the case with all accelerator extraction systems, the overriding requirement in the design of the NAL system is high extraction efficiency. The extraction efficiency of the NAL slow beam will be 99.9%. This is far beyond the point of diminishing returns for the experimental program, but it is merely adequate for prevention of severe radiation problems due to beam losses at 200 GeV.

Two features of the NAL machine aid in attaining high efficiency:

a) The emittance of the beam is small. In the radial phase plane, the emittance is $\sim 10^{-4}$ cm-rad, which is composed of 2 cm width and 5×10^{-5} radians divergence.

b) Special cells in the lattice structure have long straight sections ~170 feet in length. One of these, the Main Ring Transfer section, is used for both injection and

extraction.

In brief, the slow extraction is to be accomplished by sextupole excitation of the one third-integral resonance at $\nu_x = 20\ 1/3$. The extracted particles are first split from the coasting beam by an electrostatic deflector which has a septum width of 0.002 inches. All subsequent bending is done by septum magnets aligned in the shadow of the first septum.

This report is confined to the slow beam with spill time of 1 second, but most of the extraction components will also be used for the fast beam and in switching stations. The aspects of our design and development program which are discussed are the resonance extraction technique, the layout of the transfer section, the electrostatic deflector design, and the magnetic septum design and development.

THE ONE THIRD-INTEGRAL RESONANCE TECHNIQUE

The nominal horizontal and vertical tunes of the main ring are $\nu_x = 20.23$ and $\nu_z = 20.27$. For extraction, trim quadrupoles sweep the band of particle frequencies (due to the momentum spread $\nabla p/p = 2 \times 10^{-3}$) through $\nu_x = 20\ 1/3$. An appropriately placed array of sextupole magnets resonantly perturbs the orbits and the amplitude of the horizontal betatron motion grows faster than exponentially. The sextupole field components $B_z \propto (x^2 - z^2)$ drive the resonance $\nu_x = m/3$ for integral m. Components $B_x \propto xz^2$ drive the vertical resonance $\nu_x \pm 2\nu_z = n$. It is possible to place the sextupoles so as to minimize the terms driving the vertical resonance $\nu_x = 20\ 1/3$, $\nu_z = 20\ 1/3$.

Analytical[1] and numerical calculations show that horizontal growth rates of 1 cm/turn can be obtained at a radial distance

3 cm from the equilibrium orbit. At this point the particle crosses the electrostatic septum and is extracted. Beam cleanup stops located around the machine prevent particles of the wrong betatron phase from reaching the extraction components.

The width of the resonance is an order of magnitude narrower than the particle frequency spectrum width. Thus, the spill may be regulated by changing the rate of sweep accross ν_x = 20 1/3 using an external beam monitor signal to servo the trim quadrupoles. The response of the feedback system should be fast enough to compensate for magnetic field ripple at frequencies up to 720 Hz. Orbit studies of the interplay between quadrupole currents, quide field ripple, etc. and the spill rate are planned.

THE MAIN RING TRANSFER SECTION

The location of the transfer hall on the master plan is shown in figure 1. The layout of the lattice cell containing the long straight section is shown in Figure 2. The components are subscripted i and e to indicate injection and extraction service. The upstream D_e element is the electrostatic deflector. The next D_e element is ~30° advanced in betatron phase and is to be an edge-cooled magnetic septum. The third and fourth D_e elements are center-cooled septum magnets. The total bend required of the four septum devices is 22 milliradians.

Conceptual diagrams of the four septum devices S1-S4 which correspond to the four D_e elements are shown in Figure 3. Table I gives the proposed dimensions and fields of S1-S4. The most critical elements are S1 and S2, which are described separately below.

THE ELECTROSTATIC SEPTUM DESIGN

If the septum thickness is to be less than 0.010 inch, the maximum obtainable magnetic field is so low that an electrostatic deflector becomes more effective than a magnetic deflector. The width of S1 largely determines the extraction efficiency. We provide a radial growth rate of 1 cm/turn at the septum, so a foil with 0.002" thickness and perfect mechanical alignment would allow 99.5% extraction efficiency for a hypothetical parallel beam. The beam divergence is a factor, however, (in fact determining the optimum septum width to be about 0.002")[2] and the extraction efficiency is correspondingly reduced to 98.5%. Losses at the septum may be further reduced by introducing a specially designed shield septum ahead of it.[3] This shield septum is made of a low-density, high-Z material; e.g., a line of 2-mil tungsten wires spaced at approximately 150-mil intervals, and a few feet long. Particles that enter the leading edge of the septum will tend to be Coulomb-scattered out of the shield septum before reaching the electrostatic septum. It is estimated that 95% of the protons will be scattered out before making a "strong" interaction in the material, thereby reducing radiation levels around the septum by a factor 20 and raising the extraction efficiency to 99.9%.

The difficult aspects of S1 are those of mechanical tolerance, alignment, and resistance to deformation or wrinkling of the septum under radiation heating. One approach which we are investigating involves a heavy C-shaped form with a precision machined face. A 0.001-0.002 inch tungsten wire is wound along a convenient length, clamped, and then bead-welded in place. The wires are then prestressed to compensate for thermal expansion by releasing interior bolts which had been squeezing the C. The circulating

beam passes through the grounded C with the extracted beam and negative electrode outside. This system has great appeal from the mechanical viewpoint. However, the field emission level occurs at a 40% lower voltage due to the field variation at the wires, and sparks depositing the stored capacitive energy on one or several wires could vaporize them.

An alternative scheme involves the use of a stretched molybdenum foil. Here the problem is stretching the foil in two dimensions and leaving two open edges. Protecting against thermal deformation by stretching is necessary since the forming of ripples on heating would lead to quick destruction by the beam. This effect can be simulated with a blowtorch and it is quite striking.

THE MAGNETIC SEPTUM DESIGN

The S2 septum is shown schematically in Figure 4 and a 2-foot long prototype has been built. The cooling rods are 1/4 x 1/4 in^2 extruded aluminum with a 1/8 inch hole and a 0.0015 inch anodized coating for insulation. The thermal resistance across the coating is a small fraction of the thermal resistance from the copper septum to the cooling water. The prototype has been run at currents of 800 amps per vertical centimeter. The magnetic field corresponding to this current is 1.0 kilogauss. The field uniformity inside the gap is about 1%, and the field outside the septum at 1/8" is about 5 gauss. Fine adjustment of the septum position should improve the external field values.

It is hoped to operate all septum magnets in a d.c. mode for reliability of operation.

FIGURE CAPTIONS

Fig. 1. NAL master plan. The transfer hall is tangent to the top of the main ring in this view.

Fig. 2. Layout of main ring magnets (in outline) and inflection and extraction elements (in black).

Fig. 3. Cross-sections of extraction septum devices.

Fig. 4. Schematic of S2 magnet with 1/32 inch copper current septum.

REFERENCES

1. K. R. Symon. "Beam Extraction at a Third-Integral Resonance". NAL Internal Reports FN-130, 134, 140, 144. April-May, 1968.

2. A. W. Maschke. "Effective Width of Septa". NAL Internal Report FN-96. October, 1967.

3. A. W. Maschke. "Casting Shadows on Septa". NAL Internal Report FN-100. December, 1967.

Table I. Parameters for 200 GeV Extraction Elements

Element	Type	Field	Septum Thickness (in.)	Length (in.)	Deflection (mrad)
1.	Electrostatic	40 kV/cm	0.002	200	0.1
2.	Magnetic	1-2 kG	0.03-0.06	200	1
3.	Magnetic	6 kG	0.2-0.4	200	5
4.	Magnetic	9 kG	1.0-2.0	480	16

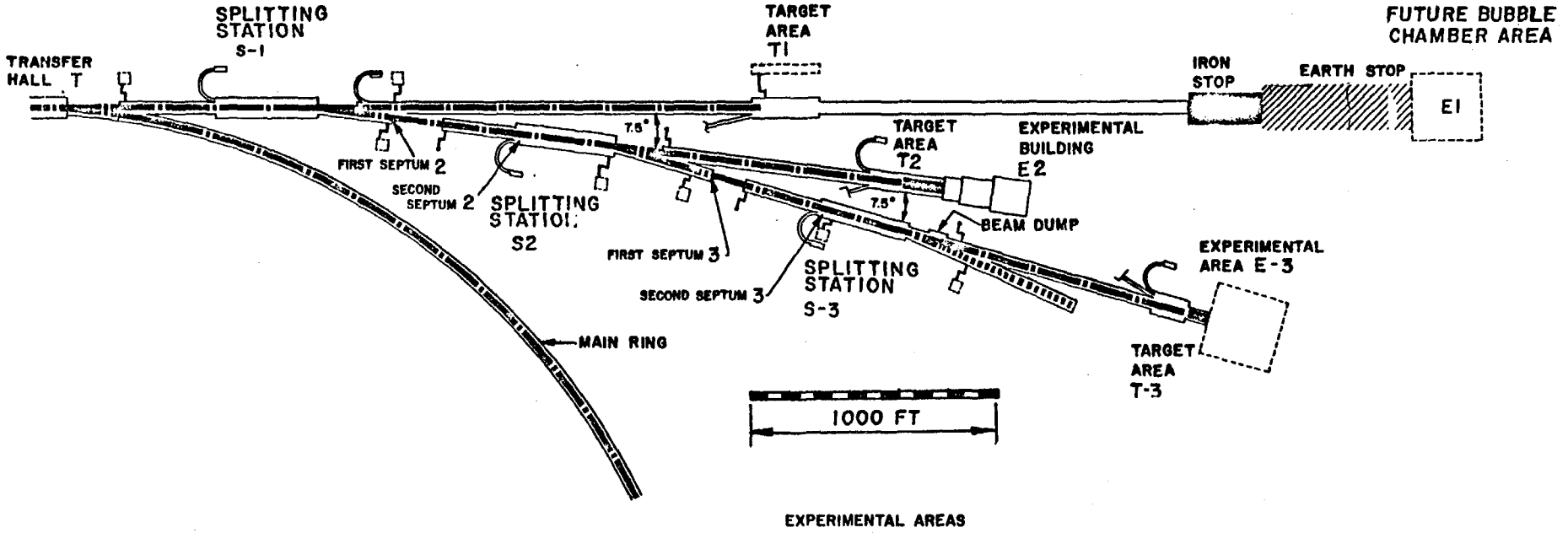
SPLITTING STATION S-1
TARGET AREA T1
FUTURE BUBBLE CHAMBER AREA
TRANSFER HALL T
IRON STOP
EARTH STOP
E1
7.5°
TARGET AREA T2
EXPERIMENTAL BUILDING E2
FIRST SEPTUM 2
SECOND SEPTUM 2
SPLITTING STATION S2
7.5°
BEAM DUMP
EXPERIMENTAL AREA E-3
FIRST SEPTUM 3
SECOND SEPTUM 3
SPLITTING STATION S-3
MAIN RING
TARGET AREA T-3
1000 FT
EXPERIMENTAL AREAS

Figure 1

Upstream End of Straight Section

Elevation of Upstream End

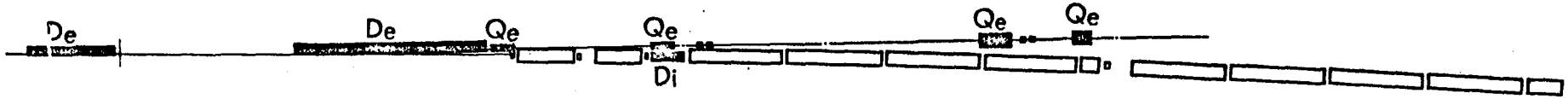

Downstream End of Straight Section

Main Ring Transfer Section

Figure 2

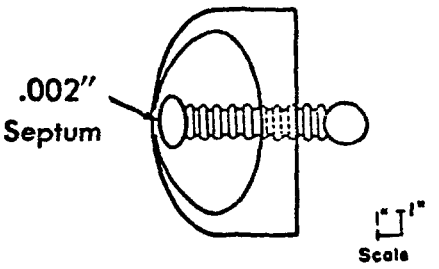

Electrostatic Deflector S1

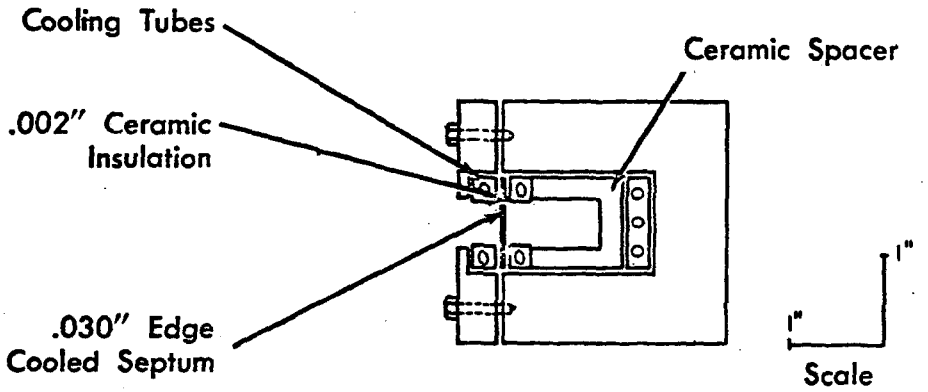

S2

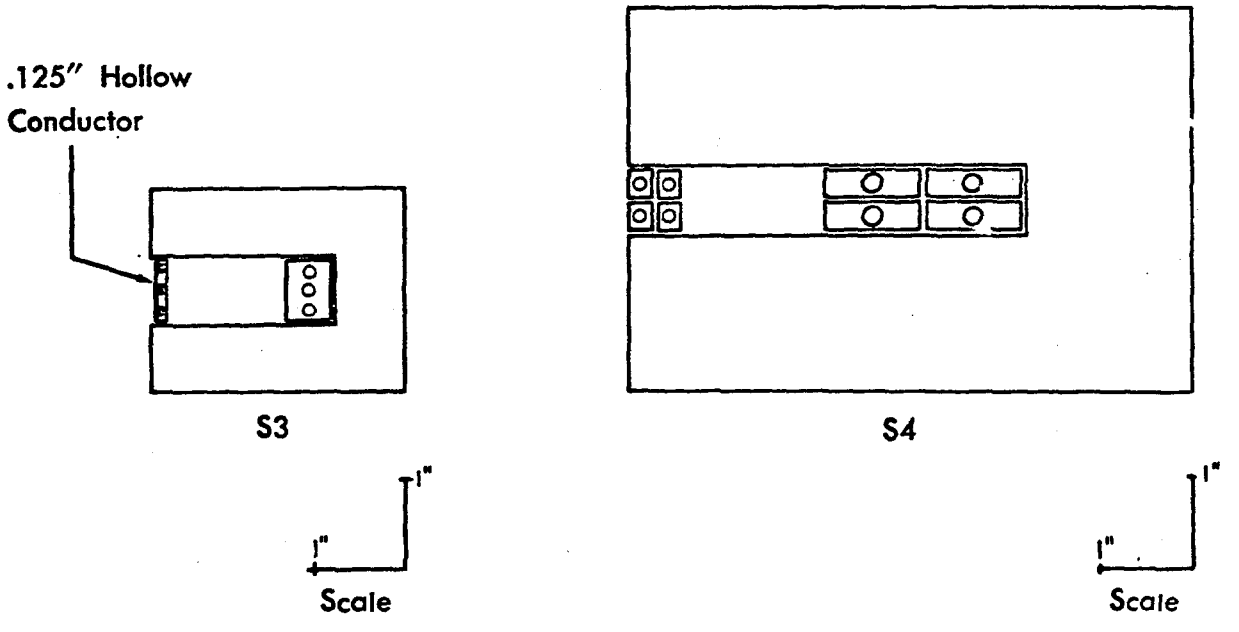

S3

S4

Extraction-System Magnets

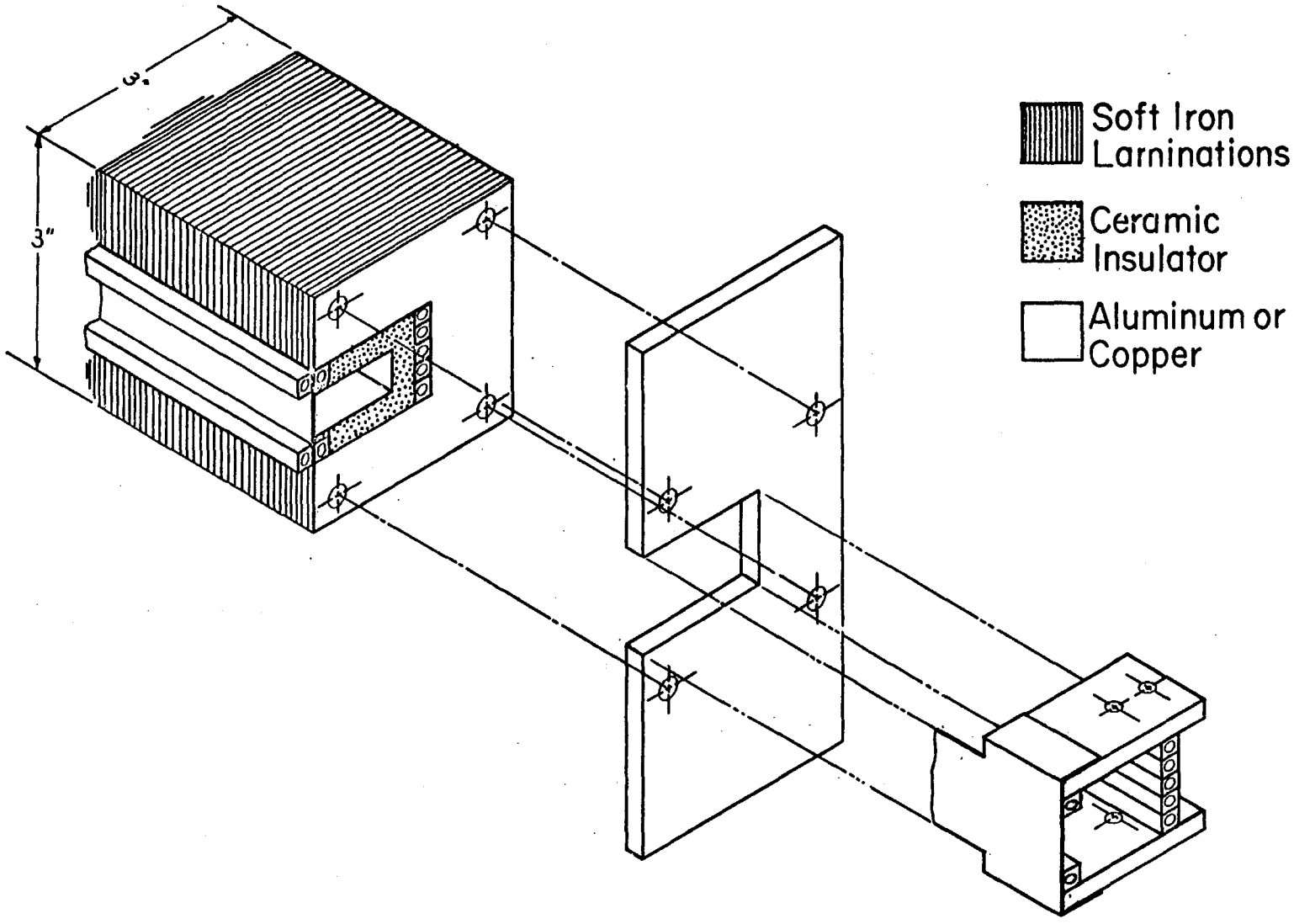

Edge-Cooled
Septum Magnet

Figure 4

APPENDIX - III

A Preliminary Design for Shielding for a Conventional Target Station

R. Carrigan, T. White

The shielding of target stations and secondary beams at the 200 BeV machine is sufficiently expensive to justify unprecedented effort in its design. Accordingly, during the past year, members of the Experimental Facilities and Radiation Physics Sections have begun a program to develop and modify the appropriate Monte-Carlo and analytical shielding design techniques. However, it is not necessary to wait until the results of this work are in hand before making a useful approximation to the shielding for the Conventional Target Station and secondary beams. Instead a preliminary design has been undertaken using a number of approximations. The following assumptions are used. A 200 BeV/c proton beam was assumed to interact completely on a target, with an intensity of $1.5 * 10^{13}$ protons/sec. The target was contained in a box, completely filled with iron having a 75% packing fraction. Its dimensions were 1m wide by 30m long with the target 6m from the upstream end. The box in turn was covered by a 1m thick layer of concrete ($\rho = 3.6$) which was then covered by 11m of earth ($\rho = 1.8$). The relative thickness of concrete and earth in the final design will depend on the results of soil activation studies now in progress. The basic reference for hadron shielding was Ranft.[1] From time to time the assumptions were modified to suit the available material. No attempt was made to be exact. Instead, the approach was to form a simple, general picture of the overall shielding required.

The Hadron Shield for the Primary Beam: Ranft's curves for 300 BeV/c and 10^{13} protons/sec. were used. The dose rate was set at 1mrem/hr. (This corresponds to 40% of a maximum permissible dose for a 40 hour week.) To obtain this a radial shield of 3250 gm/cm^2 iron equivalent and a longitudinal shield of 5400 gm/cm^2 iron equivalent are required. This sets the size of the dirt fill over the box. A more detailed calculation shows the shield can be tapered like an arrowhead pointing downstream.

The Muon Shield for the Primary Beam: Alsmiller's shielding calculation[2] for 200 BeV/c incident protons, and heavy concrete with a 5m drift space was used. The muon dose was set at 4 μ/cm^2 - sec., corresponding to about one-fifth of the maximum permissible dose for a 40 hour week. The concrete shield itself was assumed to have a packing fraction of 90%. The profile after the iron box is then:

Length (m)	Radius (m)
136	0.56
123	1.67
109	2.2
50	3.3

Notice that the effective radial thickness of the hadron shield is greater than the muon shield.

General Remarks on the Shielding of the Secondary Beams: The shielding for the secondary beams breaks naturally into a number of parts. Up to the first momentum slit the beam is intense and the transverse neutron shield needs to be quite thick. The exact calculation is made difficult by the need for some model of the beam loss. Here a loss of 1% per 100m has always been assumed.

At the slit, essentially assumed to be a hadronic shield, the beam is reduced by a factor of about 100. Beyond the slit the transverse neutron shield is considerably reduced. It is also necessary to calculate a muon shield associated with the slit. In addition, off-momentum muons moving along the beam line can be deflected by the magnet and must be stopped. Ultimately secondary beam dumps must be constructed, but that has not been considered here.

Transverse Neutron Shielding: Neutron shielding transverse to the secondary beams has been estimated using an expression given in the ECFA Studies[3]:

$$t\ (gm/cm^2) = 300 \log_{10} \frac{pie}{LD} - 900$$

where p = fraction of beam lost in L cm

i = beam intensity (protons/sec)

E = beam energy in BeV

D = dose rate required at shield surface in mrem/hr.

Notice that this does not take into account any differences between materials. It agrees with Ranft's calculations for low Z but underestimates iron. It also agrees with the main ring shielding calculations to within 20%. The resulting estimates are as follows, using concrete:

Beam	Type	(Intensity/pulse) Before Slit	After Slit	Energy	Transverse Shielding (meters) Before	After
1	p	$2.9*10^{10}$	$8*10^{8}$	200	2.8m	1.5
2	π	10^{8}	$2*10^{6}(\pi^{+})$	80	0.3	0
3	π	$2.25*10^{8}$	---	40	0:4	0

(These beams were from a preliminary target station design with rather small lateral displacements.)

In the case of beams 2 and 3 sufficient transverse shielding is generally already provided by the presence of the main muon shielding.

Slit Hadronic Shield: The upstream beam was assumed to be directly incident on the slit. For 200 BeV/c, Ranft's 300 BeV/c hadronic iron shield was used, properly renormalized for heavy concrete.

Ranft's 70 BeV/c proton values were used for 80 BeV/c pions. It was necessary to interpolate Ranft's tables for the 40 BeV/c case. The values are:

200 BeV/c		80 BeV/c		40 BeV/c	
Z (m)	r (m)	Z(m)	r(m)	Z(m)	r(m)
9.6	1.8	7.3	0.0	6.1	0
8.0	3.9	3.7	3.2	1.1	3.5
6.0	4.5	1.1	3.8	0.0	2.9
0.0	5.3	0.0	3.2		

Muon Shields for the Slits:

In the case of the slits there is effectively no drift space between the target and the shield. In addition several different primary energies are used. The calculations of Keefe and Noble[4] have been used here.

The first beam requires a shield of heavy concrete 70m long with a radius of approximately 1.5m. However, the downstream transverse shielding plus the primary muon shielding adds just this much.

The 80 BeV/c muon shield is less than 10m long and 1/2m wide. The hadronic shielding plus the other material present is sufficient. For beam 3 no further shielding is required.

The Problem of Muons not Produced at the Main Target:

Two cases have been considered. "On" momentum muons produced in the pion beams follow the pion beam and are later difficult to stop. Note, however, that this is handled at the secondary beam dump and can be treated by giving the beam a slight downward bend with a magnet. For the second beam the intensity is approximately $2*10^4$ at the first slit. Direct exposure would result in a dose of about 100 times tolerance over the area of a man's chest.

A second, potentially more serious problem is "off" momentum muons. The third beam with a production angle of 1^o was used to analyze this because the muons can most easily escape from it. Pion production cross sectionswere estimated for several momenta. In turn these pions will decay to muons and then will be deflected by the first magnet (Bending 40BeV/c 40 mrad). (The "trapping"effect of reverse fields in the magnet return yokes was ignored).

The ranges were estimated using Keefe and Noble's energy loss curves. The results are:

p (BeV/c)	Yield (muons/pulse)	R (heavy concrete-m)
10	$4.8*10^7$	16m
60	$5.6*10^5$	78m
120	$5.9*10^2$	143m
180	0.6	206m

In most cases this amount of concrete was already present in the existing shield and nothing further was required.

The overall shielding makes no provision for beam plugs, labyrinths, incorrectly set or turned off magnets, secondary dumps, etc. Nevertheless, it constitutes a reasonably satisfactory framework for conceptual purposes. It has been estimated that the shielding shown plus beam dumps for the 6 secondary beams would cost $1.7 M.

REFERENCES

1. J. Ranft, CERN/ECFA 67/16 Volume II, 311, 1967
2. R. G. Alsmiller, private communication to M. Awschalom
3. CERN/ECFA, 67/16 Volume I, 26, 1967
4. D. Keefe and C. M. Noble, UCRL 18117 (1968).

APPENDIX IV

RADIATION SAFETY CONSIDERATIONS IN BEAM DESIGN

M. Awschalom and T. White

The information given here is intended as a GUIDE ONLY to experimental high energy physicists trying to design the hadron shielding for secondary beam layouts.

The accompanying data will be helpful in setting the shielding requirements in the "right ball park".

Note that nothing is said about muon shielding. This omission is due to our lack of simple design formulae or graphs at this time.

1. The experimental areas must be safe under all beam transport and spectrometer magnet conditions. This means: magnets OFF, ON at all possible currents both direct and reversed. Safe experimental areas means that occupation areas surrounding the beams would normally have dose rates not greater than about .25 mrem/hr.

2. The beam shall include a safety beam plug(s) (it may be combined with collinator slits) to permit work on most, if not all, the particle detectors and as many magnets as possible without turning off the primary proton beam at the target station.

3. The beam transport magnets, access doors to beam areas, and safety plug(s) shall be interlocked with radiation actuated safety interlocks to assure maximum personnel protection.

4. The shielding of beam plugs and slits will be done along the same lines as for a beam stop. This shielding may be designed with the aid of curves given in figure 1. These curves are surfaces of constant dose rate. Each one represents one order of magnitude reduction in the flux and dose. For a given incident hadron power, the table on the figure indicates the curve corresponding to a dose rate of 1 mrem/hr. These curves represent half-sections of a solid of revolution around the axis ("incident protons"). These curves are given in gram/cm^2 and were initially calculated for solid iron. However, they should be good for heavy concrete (ρ=4.0 g/cm^3).

5. It must be remembered that beam transport magnets, as well as walls, may become radioactive and a source of radiation exposure.

6. The shielding for beam lines, away from plugs, slits, and stops, may be designed with the aid of the curve given in

figure 2. This curve is derived from

$$DE(X,R,E,di/dl) = 1.146 * 10^{6} * E * (di/dl) * B(X) / R \quad (mrem/hr.)$$

where

E = hadron energy in GeV
di/dl = hadron loss per cm sec
B(X) = build-up conversion factor
R = distance from beam line to subject
X = thickness of shield in g/cm^2

for 400 $g/cm^2 \leq X \leq$ 1300 g/cm^2, $B(X) = 1.935 \times 10^{-7} \exp(-X/135)$.

The curve is drawn taking for DE 1 mrem/hr. and 2 1/2 ft. of air space were assumed to exist between beam line and shield.

7. Note that no reference is made to muon absorption behind lateral beam shields in general and beam stops in particular. This omission is due to the present lack of convenient "rules of thumb" for such situations. However, figure 3 gives muon ranges in heavy concrete and iron as a function of muon momentum.

5/27/69

RADIATION SAFETY DATA

MAXIMUM PERMISSIBLE DOSES: WHOLE BODY EXPOSURE

1 1/4 rem per quarter, or

3 rem per quarter, provided 5(N-18)rem is not exceeded where N=age in years at latest birthday.

This M.P.D. leads to such rules of thumb dose rates as 2.5 mrem/hr. (40 hour/week), 20 mrem/day and 100 mrem/week. There are no legal maximum permissible dose rates.

PARTICLE FLUXES FOR 1 MREM/HR.

Energy Gev	Neutrons/ $cm^2 sec$	Protons*/ $cm^2 sec$	Electrons/ $cm^2 sec$	Photons/ $cm^2 sec$
0.02	6.2	---	9	2.9×10^3
0.2	5.2	.6	5.1	3.3×10^2
2	3.8	1.4	2.6	65
20	2.7	n.a.	1.7	7
200	2.0	n.a.	1.4	n.a.

*Critical organ = eye.

FIGURE 1

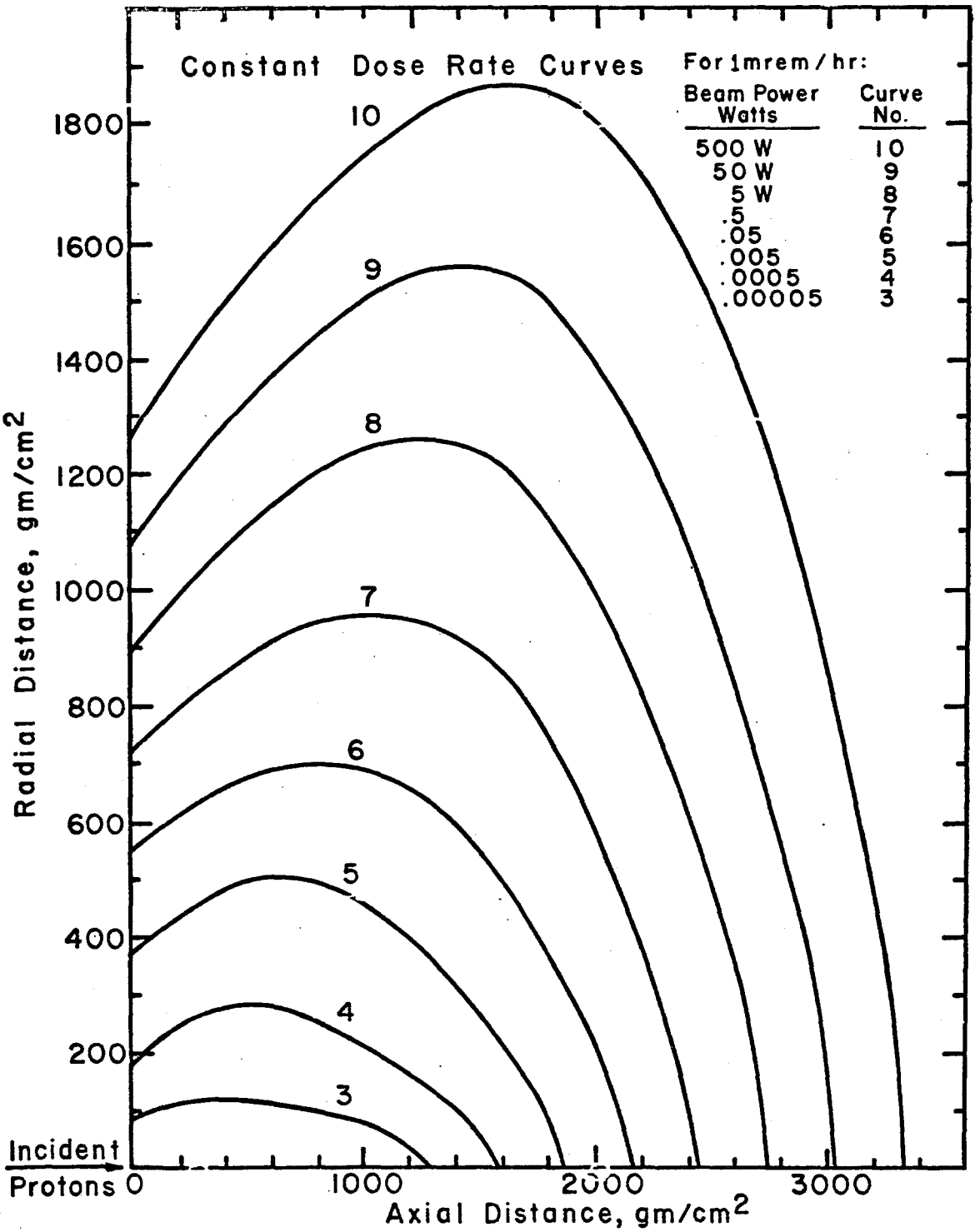
Constant Dose Rate Curves
For 1 mrem/hr:
Beam Power Watts
Curve No.
500 W 10
50 W 9
5 W 8
.5 7
.05 6
.005 5
.0005 4
.00005 3
Radial Distance, gm/cm2
1800
1600
1400
1200
1000
800
600
400
200
10
9
8
7
6
5
4
3
Incident Protons
0
1000
2000
3000
Axial Distance, gm/cm2

FIGURE 2

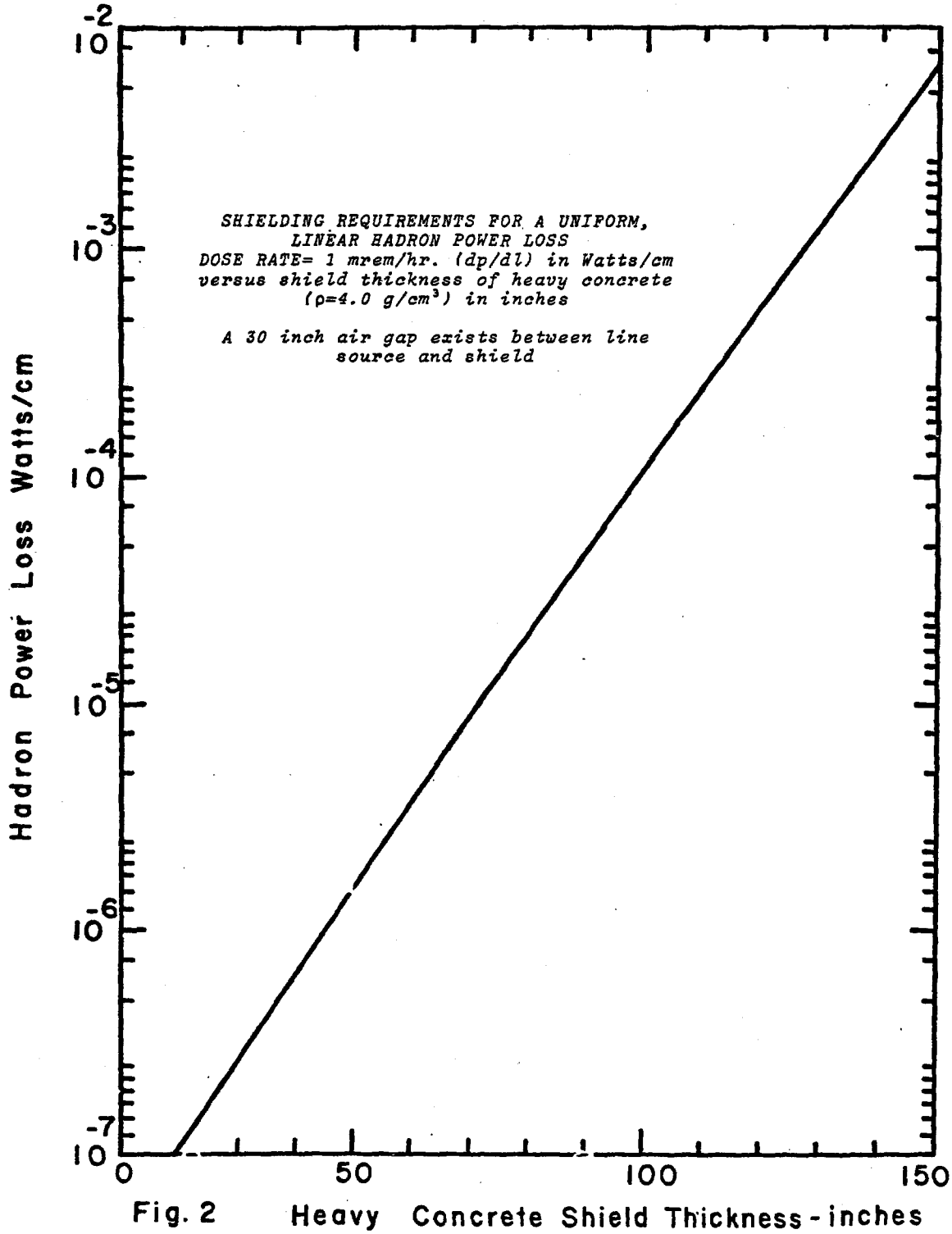

Fig. 2

FIGURE 3

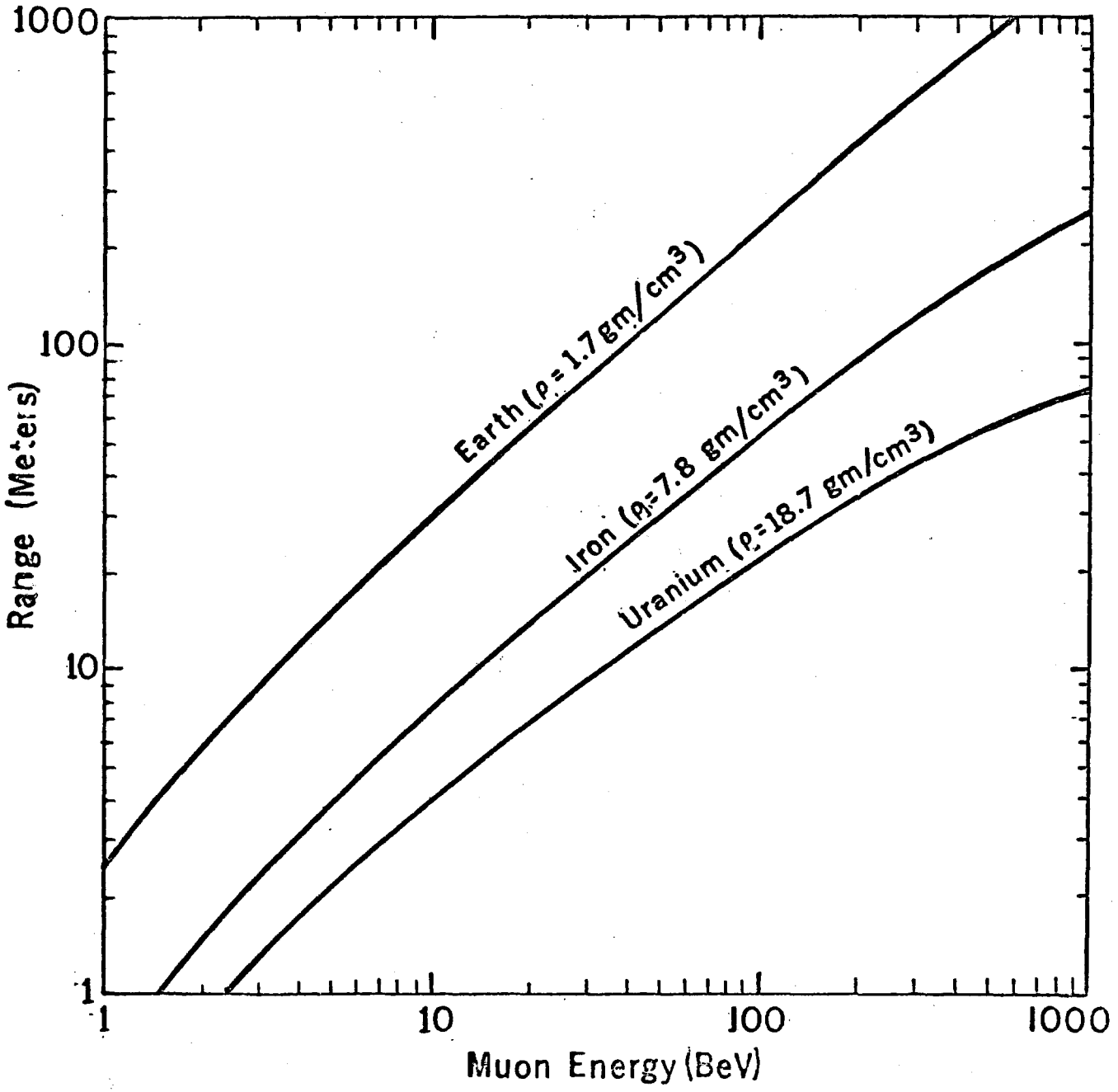

Range of Muons

APPENDIX V - NAL SUPERCONDUCTING MAGNET PROGRAM

Z. J. J. Stekly, R. W. Fast and C. Cohn

1. INTRODUCTION

Since 1960 the state of the art of superconducting coils has advanced rapidly. Figure 1 is a summary of the current state of the art of solenoids and shows the diameter versus magnetic field that has been achieved.

Although the state of the art of transverse field magnets has lagged that of solenoids, 40 kilogauss has been achieved several years ago, and a 70 kilogauss MHD transverse field magnet will be tested within a few months. Any central field below 70 kilogauss can be thought of as possible with some further development.

While current densities in the superconductor itself can exceed 10^5 A/cm^2 the overall winding current densities being obtained on a regular basis range up to 15,000 A/cm^2, although current densities up to four times this have been proposed. The need for high current density varies with the magnetic field and with the size of the aperture. In general so long as the ampere turns required and the mass of iron are not too sensitive to current density a lower current density does not penalize the design. Once the windings increase in size to the point where the far turns are less effective in generating magnetic field, or the bulk of the windings requires increase in the iron cross section, current density becomes an important variable.

The NAL beam transport bending magnets require uniformities of the order of 0.1%. From a technical point of view it is this requirement, more than the magnitude of the field itself, which requires effort to achieve. In carefully designed nuclear magnetic resonance experiments with superconducting solenoids uniformities of one part in 10^9 have been achieved. While this experience is not directly translatable to transverse field magnets there is every reason to be optimistic about being able to fulfill this homogeneity requirement. However this still needs to be demonstrated experimentally.

From an economic point of view, taking into account only the superconducting magnet system, for a given total value of magnetic field times length the optimum magnetic field is approximately 20 kilogauss.

Economic comparisons between a superconducting beam transport system and a conventional one show that within the accuracy of the comparison the superconducting system is equal to that of the conventional system. The economic minimum is achieved by using a "superferric magnet" - an iron magnet with superconducting windings to magnetize the iron. This design minimizes the amount of superconductor used, and uses low fields where its current carrying capacity is highest. If all the beam transport magnets were superconducting the estimated yearly saving in power is of the order of $1.5 million assuming a 50% duty factor.

The choice of 20 kilogauss, coupled with an estimated aperture size of 4 cm x 10 cm in the bending magnets, means that

current densities required are no higher than are readily achievable with "conventional" superconducting windings.

Development work at NAL has concentrated so far on bending magnets. Two models have been worked on, both of the superferric type. The first one of these is essentially finished and will provide test data in the near future - it has iron at 77°K with windings at 4.2°K and a room temperature beam tube. The second model which is in the later stages of design has the iron as well as the beam tube at 4.2°K.

The main problems in the superconducting beam transport elements are the attainment of the required uniformity and the operation in the nuclear radiation environment.

From a system viewpoint a helium temperature refrigeration system of the size required to make all or a significant fraction of the experimental area beam transport magnets superconducting is beyond anything which has been done so far. There is no reason to believe that any insurmountable difficulties will arise. It is nevertheless necessary to obtain operating experience with several magnets coupled to a closed cycle refrigerator to uncover any unforeseen problem areas.

Superconducting magnets have been used for solid state research since the early 1960's. While most of these are cooled down a few times a month there are many instances of coils being kept cold for periods of several months to a year and being in use daily without any detectable deterioration. Once the operating characteristics are understood transition to the normal state is

a rare occurence and is usually due to accidental operation of the coil outside of its operating range.

Operation of superconducting coils so far has been almost exclusively with helium liquid, and instances of operation with closed cycle helium refrigerators are rare. One instance where closed cycle refrigeration was used reliably for years has been with superconducting maser magnets in the Telstar Space Communication System.

2. OPTIMUM MAGNETIC FIELD

The question of what is the best magnetic field to design for is a complex one which involves technical as well as economic consideration. Fields as high as 140 kilogauss have been obtained using superconductors so that any field below this can be considered to be readily achevable.

Superconducting magnets of the type required for beam transport, which consistently produce accurate fields, have yet to be demonstrated. However, superconducting solenoids have achieved field homogeneities as high as a few parts in 10^9 in Nuclear Magnetic Resonance work. In practice the uniformity in a beam transport magnet is determined more by the magnet design and construction than by the superconductor itself.

In general one can say that higher magnet fields result in shorter beam transport systems with the attendant economies in buildings and size of cryogenic system.

We shall now proceed to compare several superconducting bending magnet types.

The air core configurations suffer from the serious disadvantage that external to the windings the field decays as the reciprocal of the square of the distance from the axis for a long line of magnets. Unless other magnets are very far away this external field must be shielded by providing an iron return path.

The iron return path can be designed with one of two philosophies - 1) to place the iron as close as possible to the windings and thus make maximum use of the iron in the generating field. This would, in most cases, result in saturating the iron (at fields above 20 kG) and probable distortion of the magnetic field; or, 2) to place the iron around the windings far enough away so that the surface field is less than 20 kG so that it does not saturate. In this approach the distortion of the magnetic field due to the iron is a minimum. If this is the approach, it can readily be shown that the net contribution of the iron to the magnetic field is one-half of the saturation value, or about 10 kilogauss.

An additional magnet configuration has been proposed* very similar in design to conventional bending magnets. This configuration is shown in Figure 2. At NAL this configuration is called superferric. One of the very significant advantages of a superferric magnet over a conventional magnet of the same type is that the higher superconductor current density reduces the winding window to such a point that the overall dimensions are

---

* R. R. Wilson

reduced to a minimum. Up to 20 kilogauss the superconductor is used to magnetize the iron, and the ampere turns required are determined by the height of the air gap. Above 20 kilogauss the pole tip saturates, but nevertheless the iron still significantly reduces the ampere turns required for a given field.

The superferric magnet is a superposition of the air core field of the coil and the field due to magnetized iron. If we assume all the iron is magnetized to saturation or above we can calculate the iron contribution to the total field. The result is plotted in Figure 3. Also shown in Figure 3 are results obtained from detailed field plots determined by using the computer code, TRIM, to calculate the magnetic fields.

The iron contribution to the field varies with the field itself and the aspect ratio of the window in the iron. The higher the aspect ratio the higher the contribution of the iron. The increase in the field contributed by the iron with increasing field is a result of the fact that for a given aperture the cross sectional area of iron increases with increasing magnetic field. Approximate relative iron sizes are shown in Figure 4. The direction of magnetization becomes more favorable, the larger the iron cross section area, consequently the contribution to the central field increases with field and exceeds the saturation value of 20 kG. This effect is very similar to that which occurs in laboratory type magnets with tapered pole tips where the iron contribution can also considerably exceed the 20 kilogauss saturation field of the iron.

Figure 5 shows the required ampere turns to produce a given magnetic field for several bending magnet configurations - air core and with an iron return path.

It is evident that a very significant saving is possible if full use is made of the iron as in the superferric magnet. Also evident from the figure is the fact that current density affects the coil design much more at higher fields than at lower fields. In general if the winding thickness is kept comparable to or smaller than the aperture dimensions then no serious penalty is paid for lower current density. However as the winding size grows to dimensions comparable with the bore the effectiveness of the far away turns decreases and a penalty in additional ampere turns is required.

The relative costs of various configurations are shown in Figure 6 as a cost per unit length of the particular configuration as a function of magnetic field. Since in a beam transport system we are interested in a given product of magnetic field times distances, we can divide the vertical axis by the magnetic field to get the unit cost per kilogauss meter. This plot is shown in Figure 7.

The cost includes superconductors, iron and dewar. The refrigeration system will in general be only a weak function of magnetic field in a transport system because of the following:

1. The total system weight of a shielded system is approximately constant (for a given number of kilogauss meters) so that the total support cross sectional area required remains

roughly constant. The total support heat load is therefore constant to first order.

2. A major source of heat leak is the electrical leads to the coils. This heat leak can be minimized by running coils in series with cold connections from coil to coil as much as is feasible. If slightly different currents are required, then in addition to the single set of main power leads, leads to the individual coils need be sized only for the required turn currents in each of the coils.

In any case the lead heat leak is not directly tied to the magnetic field, and is more a function of the detailed required operating modes and the value of the energizing current rather than the magnetic field itself.

3. The surface area thermal radiation from room temperature decreases with increasing magnetic field, however the decrease is only small in magnets with an iron return path since a larger cross section - and consequently larger perimeters - are required.

The only major change with magnetic field in the cryogenic system is the length of the transfer lines for the helium. However in most lines the losses occur at the piping connections so that this increase in transfer length will not have a major effect on total system heat leak.

The total refrigeration system cost is then approximately independent of magnetic field.

Returning again to Figure 7, we note that the costs per unit kg-m are flat below 20 kG and rise with increasing field above this value.

If we now consider other items such as building costs, piping, power, then all of these increase, the longer the length. However the net possible change in overall length (not magnetic field length) is relatively small due to the fixed amount of muon shielding required. The result is that while higher fields do tend to decrease the building lengths, piping lengths, and refrigeration required, the variation with magnetic field is small.

We conclude that an optimum economic field must be between 20 and 30 kilogauss, where the costs of the magnets themselves per unit kilogauss meter begin to increase rapidly.

(For cases where buildings, utilities and refrigeration requirements can be shown to vary rapidly with magnetic field the optimum will shift to higher fields.)

Based on the above discussion of economics plus the fact that very good use can be made of iron in shaping the magnetic field, the NAL superconductivity program is aimed mainly at 20 kilogauss superferric type superconducting bending magnets. The higher field superferric bending magnets have also been studied, but the experimental program has been aimed at 20 kilogauss.

3. HOMOGENEITY

In addition to conductor placement and the geometry of the iron the superconductors add one more factor which affects the magnetic field - diamagnetism. A thorough study has not been made of the effects of the superconductor diamagnetism. Attempts have been made to include the superconductor diamagnetism in the

TRIM computer code, however the introduction of diamagnetism of the windings has resulted in lack of convergence in the computer code as it now exists.

The geometry of superferric magnets has been investigated using TRIM to determine whether the required 0.1% uniformity is achievable. Two cases were investigated: 1) a bending magnet with a maximum field of 20 kG, and, 2) a bending magnet with a maximum field of 50 kG, both having apertures of 10 cm x 4 cm. Typical computer results for the 20 kG superferric magnet are shown in Figure 8 which shows the runs where the distance on the center planes between the windings is varied. It is important to note that variations of the order of .03 in. (from .062 in. to .090 in.) approximately span the range of acceptable magnet fields (B/B_o = 0.001 at about 1.65 inches). The dimensional accuracy of the conductor bundle must be less than .03 in. by at least half an order of magnitude ($\sim$ .006 in.) if computer results are to be relied on.

The fact that uniformities of this order are attainable on a computer still does not mean that they will be attained in practice, (especially when one takes into account the diamagnetism of the superconductor), however it is encouraging that the required uniformities can be calculated for reasonable geometries.

As was stated already, attempts were made to include the diamagnetic effects in the computations. At first this was done by introducing a relative permeability (μ/μ_{air}) equal to 0.9 in the windings, a value which was arrived at by assuming

that the superconductor was completely diamagnetic and that it occupied 10% of the winding volume. The computer did not converge on a solution when this was done.

To get a qualitative measure of the effect a non-current carrying sheet with a low relative permeability was introduced at the surface of the winding next to the aperture. The results of computer runs for a particular geometry with and without the diamagnetic sheet are shown in Figure 9. The effect on the magnetic field is not negligible when one is trying to achieve 0.1% homogeneity. Also the effect is likely to be history dependent. From these preliminary runs it can be tentatively concluded that the diamagnetism must be taken into account when computing the magnetic field, however there is every reason to believe that the required uniformity can be achieved if it is.

The 50 kilogauss superferric computations were done for two reasons: 1) to provide accurate field plots which could be used to determine how much the iron contributes to the magnetic field, and 2) to get an estimate of the homogeneity at high fields.

Figure 10 shows the results of computer runs for a magnet designed for operation at 50 kilogauss at several different central magnetic fields. The resultant uniformity is a few percent, and does vary somewhat with magnetic field. The particular geometry chosen has not been optimized but it is the result of a first order correction from a previous geometry. As such the homogeneity can probably still be further improved although it is not known how much the uniformity can be improved.

4. REFRIGERATION LOAD

The total refrigeration load can be broken into the following:

1. Conduction down the supports and electrical leads.
2. Thermal radiation from high temperature surfaces to cold surfaces.
3. Nuclear radiation impinging on the magnet that causes an additional thermal heat load.

4.1 Supports

The heat conducted down the supports is proportional to their cross sectional area. Consequently a good design uses supports in tension made as long as possible in order to minimize the heat conduction.

The supports may run directly from room temperature to helium temperature, however more usually they go from room temperature to an intermediate temperature thermal shield (typically at 80°K), where the heat conducted from room temperature is intercepted and from the thermal shield down to helium temperature.

A rough estimate of the heat leak due to supports in tension is arrived at as follows:

The heat conducted is:

$$q = kA \frac{\Delta T}{\ell}$$

The support should be capable of carrying a total load F:

$$F = \sigma A$$

where σ is the stress and A is the cross section area.

Dividing:

$$\frac{q}{F} = \frac{k}{\sigma} \frac{\Delta T}{\ell}$$

The following table gives the heat conducted per unit force down a support 1 foot long for steel and titanium:

TABLE OF HEAT LOAD PER UNIT FORCE (WATTS/LB)

	Steel	Drawn Steel	Titanium Alloy
From 300°K to 4.2°K	158×10^{-6}	42.1×10^{-6}	29.3×10^{-6}
From 80°K to 4.2°K	27×10^{-6}	7.2×10^{-6}	5×10^{-6}
Working Stresses (1/2 yield) psi	20,000	75,000	72,500

Typically a magnet might weigh 5,000 lbs. If we assume the magnet need support in six directions (tension supports do not work in compression), and assume twice the weight as the support strength then we calculate the following heat load:

HEAT LOAD (WATTS)

	Steel	Drawn Steel	Titanium Alloy
300°K to 4.2°K	9.48	2.5	1.76
80°K to 4.2°K	1.62	0.43	0.3

These are typical values and show that provided as intermediate temperature shield is present the heat load will be of the order of a fraction of a watt if high strength steel or titanium are used.

4.2 Thermal Radiation

Since the cold walls and room temperature walls have vacuum in between (below 10^{-4} mm Hg) the only mechanism for heat transfer across the gap is by thermal radiation.

The following is a table of heat transfer rates per unit area:

RADIATION OF HEAT TRANSFER (W/ft^2)

	Steel Surf.	Gold Plated
300°K to 4.2°K	1.2	0.6
77°K to 4.2°K	.005	.0024

A typical magnet may be 12 ft long and have a perimeter of 3 ft, thus having a wall area of 36 ft^2. The resultant heat loads would be:

TYPICAL RADIATION HEAT LOADS (W)

	Steel Surface	Gold Plates Surface
300°K to 4.2°K	43.2	21.6
77°K to 4.2°K	0.18	0.086

The radiation heat leads to 4.2°K are excessive, however the intermediate temperature shield at 77°K reduces the heat transfer to a fraction of a watt.

4.3 Electrical Leads

The design of electrical leads is a compromise between the heat conduction down the lead, and the joule losses. Optimum leads which use the helium boiloff to intercept the heat conduction down the lead require a helium boiloff which is proportional to the current:

HELIUM BOILOFF = 2.7 liters/hr per 1000 A

for 1 pair of leads.

So if we are using an optimum pair of leads to energize a coil which operates at 500 A, the resulting boiloff will be 1.35 ℓ/hr. In terms of the latent heat of helium liquid 1 watt is equivalent to 1.4 ℓ/hr so 1.35 ℓ/hr is slightly less than 1 watt.

The effect of removing 1.35 ℓ/hr out of the cold gas stream returning to the refrigerator must be taken into account, since the sensible heat of the 1.35 ℓ/hr is used to cool the leads and is not available to exchange heat in the heat exchanger. This increases the effective heat load (as far as power input to the refrigerator is concerned.) This increase in heat load can be from a factor of 3 to 5 so that the effective heat load of 1 pair of 500 A leads is 3 to 5 watts, which is considerably larger than the estimated heat loads for either the supports or by radiation from the walls provided an intermediate temperature shield is used.

4.4 Nuclear Radiation Effects in Beam Transport Elements

The nuclear radiation environment in a target station may significantly affect the operation of unconventional beam elements, such as superconductors. This could occur through mechanisms such as radiation damage or even direct thermal power dissipation in the element. Studies reviewed at Stanford[1] indicate that a nuclear radiation environment may even increase the current carrying capability in a low field superconductor. However in view of the modest size of the

refrigeration requirement anticipated on the individual elements (5 watts) and the large amount of total power in the beam (500 kwatts) it is useful to examine the thermal problem from the radiation in some detail.

If an unshielded beam element with an inner radius of 2" and an outer radius of 4" is placed at an angle of 3.5 mrad to a target 60 meters away with $1.5 * 10^{13}$ 200 BeV/c protons interacting on the target per second, then the element will have approximately 18 kwatts passing through it. Only a small fraction of this would be dissipated in the magnet. An iron shield 4 to 7 m thick in front of the magnet would completely eliminate the hadronic flux. In an actual target station there might be somewhere between 25 m to 30 m of iron before the magnet. If the magnet is an aperture stop for the system, the pole faces will be unshielded. For a 2 m long magnet 300 watts will pass through the pole faces. Very roughly 5% of this will dissipate in the magnet, leading to a 15 watt thermal load. This indicates that it may be important to provide some modest shielding for the pole faces of the superconducting magnets. After the hadronic conctribution is shielded there remains a muon flux which is extremely difficult to reduce. Typical muon shielding calculations give a muon ionization power loss of 2.5 milliwatts for this beam element.

These calculations, which are conservative, (that is they overestimate the radiation dose), indicate that nuclear radiation thermal loading is not an important problem, provided the pole faces are properly shielded.

The calculations performed are of a preliminary nature and need to be confirmed. The thermal loading may affect the design of the beam element, since a large thermal load would more than likely require a design where the iron is at an intermediate temperature (typically 80°K) where the refrigerator power required to remove the heat load is considerably reduced.

5. CRYOGENIC SYSTEM

The power required in an ideal Carnot cycle refrigerator operating between 4.2°K and 300°K is 70.5 watts for every watt of refrigeration at low temperature.

Figure 11 reproduced from a paper by Stobridge[2] shows the percent of the Carnot cycle effectiveness which is achieved in actual refrigeration systems as a function of the refrigeration capacity. The range of interest for the beam transport is from 10 watts (approximate size of a single refrigerator for each magnet) to a few hundred watts where several magnets are operated from the same refrigerator.

At the 10 watts range we would expect about 5% of the Carnot effectiveness, or 1400 watts of power/watt of refrigeration. At the 100 watt refrigeration level we would expect about 10% of the Carnot effectiveness or about 700 watts of power/watt of refrigeration.

In the same paper, Stobridge plots a curve of cost versus installed refrigerator input power (not refrigeration capacity) which is reproduced in Figure 12 and is approximated by $C = 6000\ P^{0.7}$ where P is in kilowatts.

If we compute the refrigerator cost for 300 magnets each

requiring 7 watts of refrigeration, and using 10 refrigerators overall, then we have the following:

NO. OF MAGNETS	300
NO. OF REFRIGERATORS	10
HEAT LOAD/MAGNET	7 watts
UNIT REFRIG. CAPACITY	210 watts
FRACTION OF CARNOT	0.12
POWER/REFRIGERATOR	125 KW
TOTAL REFRIGERATOR COST	1,750 K$

In addition to the refrigerator there are transfer lines and helium piping. A study of several systems by Green[3] found a system cost of $20,000 per magnet which would result in 6,000 K$ as the total system cost.

The difference can be attributed to different assumptions as far as heat load is concerned, and also the inclusion of costs for transfer lines, piping and valving. Nevertheless, even if we double the 1750 K$ to account for the other system costs we are still left with a difference between 6000 K$ and 3500 K$ between the estimated costs.

These variations are real and will not be resolved until the heat loads and systems are more accurately determined.

In any case, we know that the refrigeration system cost varies as the 0.7 power of the total heat load. Since the cryogenic system is a major cost component low heat leak cryogenic design of the magnets and transfer lines becomes essential.

6. COST COMPARISON WITH CONVENTIONAL SYSTEM

A cost estimate of conventional and superconducting magnets has been made by W. M. Brobeck Associates.[4]

The following tables gives the characteristics and quantities of the beam transport magnets:

CHARACTERISTICS AND QUANTITIES OF BEAM TRANSPORT MAGNETS

	Peak Field	Aperture (inches)	Length (inches)	Quantity
1. Bending Magnets	20	6 x 2	120	200
2. Quadrupole Magnets	15	2 dia.	72	100

The following table is a cost comparison between the conventional system and a superconducting system of magnets with identical apertures, fields and lengths:

	Conventional System (K$)	Superconducting System (K$)
Dipole Magnets	3,440	4,122
Quadrupole Magnets	1,720	1,431
Power Supplies	3,680	600
Magnet Controls	329	450
Cables	472	154
Vacuum System	205	205
Cooling Water System	151	99
Refrigerator System	---	5,800
	$9,997	$12,861

	Conventional System	Superconducting System
Total power during steady operation at peak field.	45,285 KW	1050 KW
Yearly power cost (.008 $/KW hr.)	1,587 K$ (50% Duty Factor)	73.5 K$ (100% Duty Factor on refrigeration)

The estimates of initial costs indicate that the cost of the superconducting system is slightly higher with one of the most costly items being the refrigeration system itself.

When one takes into account that this cost depends strongly on the detailed engineering design of the system there is probably room for improvement for the superconducting system. For instance, the operation of magnets in the persistent mode would considerably reduce the heat load on the refrigerator.

The yearly saving in power cost is very large and makes up for the difference in initial cost within two years.

7. NAL PROGRAM IN SUPERCONDUCTIVITY

The NAL program in superconductivity is aimed at developing superconducting beam transport elements. The program has up to now been concerned mainly with bending magnets. however the know how being developed is quite general and is readily applicable, with slight modifications, to quadrupole magnets.

It has been shown in previous sections that a desirable superconducting beam transport elements has the following characteristics:

1. A field in the neighborhood of 20 kilogauss, and consists of iron as well as superconductor.
2. Has a homogeneity of 0.1% over the usable aperture.
3. Is designed for minimum refrigeration requirements, since the refrigeration system represents the largest single cost item.
4. Is reliable and easy to operate.

It has been these characteristics which have guided the NAL program during the past year. The experimental effort was concerned with three main areas:

1. The construction of a first full-scale model - MKI.
2. The determination of the characteristics of a superconducting "Litz" wire which is promising for use as a conductor.
3. The design of an MKII bending magnet which makes use of the knowledge gained from the MKI magnet.

7.1 MKI Model Bending Magnet

The MKI model bending magnet is a joint NAL-ANL program. The schematic diagram of the MKI superconducting bending magnet is shown in Figure 2. A summary of its characteristics is given in the following table.

MKI BENDING MAGNET CHARACTERISTICS

Room temperature bore tube	1-1/4 x 3-1/4
Conductor	.05 x .125 252 strands of NbTi in Copper
Iron gap	2.5 x 7.0
Length of iron	36 in.
Overall length	46-1/2
No. of turns	114
Design current at 20 kG	890 amps
Weight	800 lb. (estimated)

The coil itself is wound from .05 x .125" conductor consisting of 250 strands of Nb-Ti in copper. The turns are insulated from each other by intermittent insulation covering approximately 50% of the conductor surface. The coil is wound on a stainless steel form lined with insulator. The coil form is then welded shut to form the helium container.

The helium temperature container is separated from the 77°K iron by vacuum, and the separation is maintained by supports at either end of the magnet. In this design the iron at 77°K serves as an intermediate temperature thermal radiation shield as well as part of the vacuum can. The 77°K iron is insulated from room temperature by foam (this can easily be replaced by a room temperature vacuum can and super insulation).

For simplicity the windings for this model are turned up on both ends and no serious attempt at achieving uniformity has been made in this magnet. The conductor used was one

already on hand. It operates at a current of the order of 1000 A which is high from a heat load point of view.

Difficulty in winding the ends with the .05" x .125" conductor resulted in several shorts in the windings. It is not expected that this will affect the critical current, only the charge rate sensitivity of the coil.

The windings operate at atmospheric helium. The helium liquid is introduced at one end of the magnet. It then flows axially through the windings to the other side where it is vented along the electrical leads.

The first test was performed only after 20% of the necessary welding had been completed. The welding was then completed and the coils retested to determine whether any damage to the coils had occurred. The first tests exhibited more charge rate sensitivity than the subsequent tests. This change is probably due to handling of the winding which may have resulted in opening up of some of the shorts.

Final assembly and testing are now underway.

It is expected that this model will provide information on field reproducibility as well as on how well the actual field profile can be predicted by computer. It has also resulted in design techniques for iron at a temperature higher than 4.2°K - a design which may be necessary if the thermal load due to Nuclear Radiation exceeds a few watts. The heat load will be higher than in a beam transport system mainly due to the use of the high energizing current of 1000 A.

4.2 Superconducting "Litz" Wire

The conductor used in the MKI model was stiff, relatively hard to wind and had a critical current of the order of 1000 A at the operating field. From a construction standpoint, a more flexible conductor was desirable, while from the heat leak standpoint a lower operating current was needed.

These requirements, coupled with the advantage of small superconducting strands electrically insulated from each other, prompted the investigation of the behavior of coils wound from a cable with 21 strands of individually insulated .005" O.D. copper conductors with a single core of Nb-Tin approximately .0025" in diameter.

Three test solenoids were made:

1. The first was wound with cable made up of strands with very thin Formvar insulation. This resulted in a coil with strand-to-strand as well as turn-to-turn shorts.
2. The second solenoid used the same cable as the first solenoid, except that the cable was insulated with nylon strands to eliminate turn-to-turn shorts.
3. The third solenoid was wound with cable made with strands having a heavier coating of Formvar, which eliminated the shorting problem.

The solenoids were designed for a low field between 10 and 20 kilogauss, so that problems with stability, if they existed, would show up.

The first solenoid exhibited considerable charge rate sensitivity. This was attributed to the turn-to-turn shorts in the coil. When this coil was unwound and the cable reinsulated the low charge rate critical current dropped, but the second coil wound with this cable did not exhibit any charge rate sensitivity within the limits of the power supply. It was felt (although this has not been substantiated) that the additional handling of the cable (three times through the insulating machine) to put nylon around it may have caused damage.

The third solenoid with heavier Formvar to begin with, exhibited the expected critical current and no charge rate sensitivity.

7.3 MKII Model Magnet

The MKII model magnet is now in the final design phase. It has the characteristics outlined in the following table, and is shown in Figure 13.

MKII SUPERCONDUCTING BENDING MAGNET

Field	18 kG
Ampere turns	70,000
Gap height	4 cm
Gap width	10 cm
Length	90 cm
Refrigeration required	2-5 watts
Total Weight	1000 lbs.

The iron is at helium temperature as is the beam tube. For regions where thermal loads due to incident radation are large, other designs with beam tube and iron at higher temperatures will be required.

The "magnet" iron and superconductor are encased in a stainless-steel helium container. Helium liquid at approximately atmospheric pressure is introduced at one end of the magnet and is vented as gas at the other end. Part of the vent gas is returned to the refrigerator, and the rest is first used to reduce the heat leak down the electrical leads.

The helium container is surrounded by a thermal radiation shield cooled to about 80°K by intermediate-temperature helium gas from the refrigerator.

It differs from the MKI model magnet already described in several important ways:

1. The beam tube is at 4.2°K. This means that no thermal insulation is required as in the warm beam tube case, and maximum use can be made of the magnetic field volume (assuming of course that the required uniformity is achieved). A cold beam tube also has the additional advantage that it provides cryopumping. A necessary requirement for the use of a cold beam tube is that the thermal load due to nuclear radiation is tolerable and that the beam does not hit the wall. The ends of the magnet are designed with a temperature gradient so that the connection to an extension of the beam tube or another magnet can be made at room temperature.

2. The iron is at helium temperature, and is not part of the vacuum can. It is made circular for ease of assembly. Operation of the iron at 4.2°K not only minimizes the gap, but also provides the necessary support for the windings. This gain is feasible only if the thermal load due to nuclear radiation is tolerable.
3. The coils will be wound with the superconducting "Litz" wire mentioned above, which is not only very flexible and easy to wind but exhibits excellent charge rate characteristics. This will result in an energizing current of approximately 200 A and should result in a low overall heat load.

REFERENCES

1. "Radiation Effects on Superconducting Magnets" by H. Brechna, SLAC-PUB-469, August 1968.
2. "Refrigeration for Superconducting and Cryogenic Systems" by T. R. Stobridge. Presented at 1969 Particle Accelerator Conference, March 5-7, 1969. To be published in IEEE Transactions on Nuclear Science.
3. "Refrigeration for Superconducting Magnets in the 200 BeV Accelerator by M. A. Green, G. P. Coombs and J. L. Perry, Arthur D. Little Report, June 1968.
4. "Cost Estimates of Experimental Equipment", Eilliam M. Brobeck and Associates Report No. 200-1-R7, January, 1969.

FIGURE CAPTIONS

Figure 1 State of the art of superconducting solenoids.

Figure 2 Superferric magnet with iron at liquid nitron temperature.

Figure 3 Field contribution of iron in superferric magnet for various air gap aspect ratios.

Figure 4 Relative sizes of high field iron magnets.

Figure 5 Excitation required for air core and superferric magnets.

Figure 6 Relative cost per unit length of superferric magnets as a function of field.

Figure 7 Relative cost per kilogauss-meter of superferric magnets as a function of field.

Figure 8 Field uniformity of 20 kG superferric magnet for various coil arrangements.

Figure 9 Enhancement of field uniformity of superferric magnet achieved with superconducting sheets.

Figure 10 Field uniformity of 50 kG magnet operated below design fields.

Figure 11 Relative Carnot effectiveness of 4.2°K refrigerator as function of refrigeration capacity.

Figure 12 Cost of 4.2°K refrigeration as a function of input power.

Figure 13 NAL MKII Model Magnet with iron at 4.2°K.

Figure 1

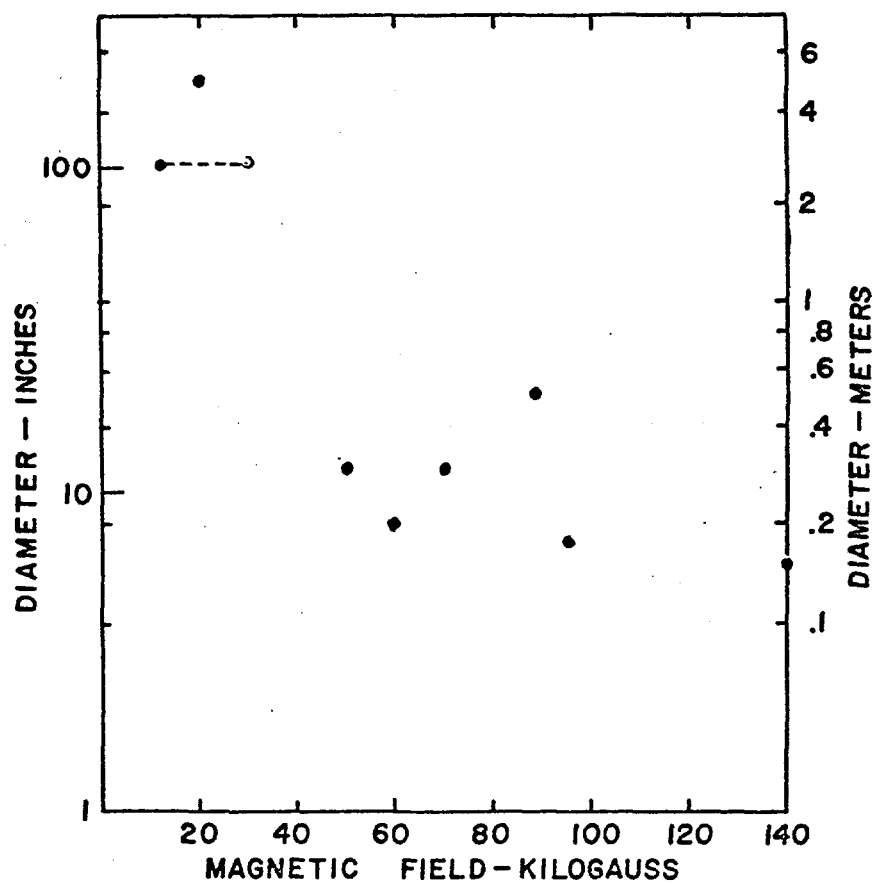
DIAMETER – INCHES
100
10
1
6
4
2
1
.8
.6
.4
.2
.1
DIAMETER – METERS
20
40
60
80
100
120
140
MAGNETIC FIELD – KILOGAUSS

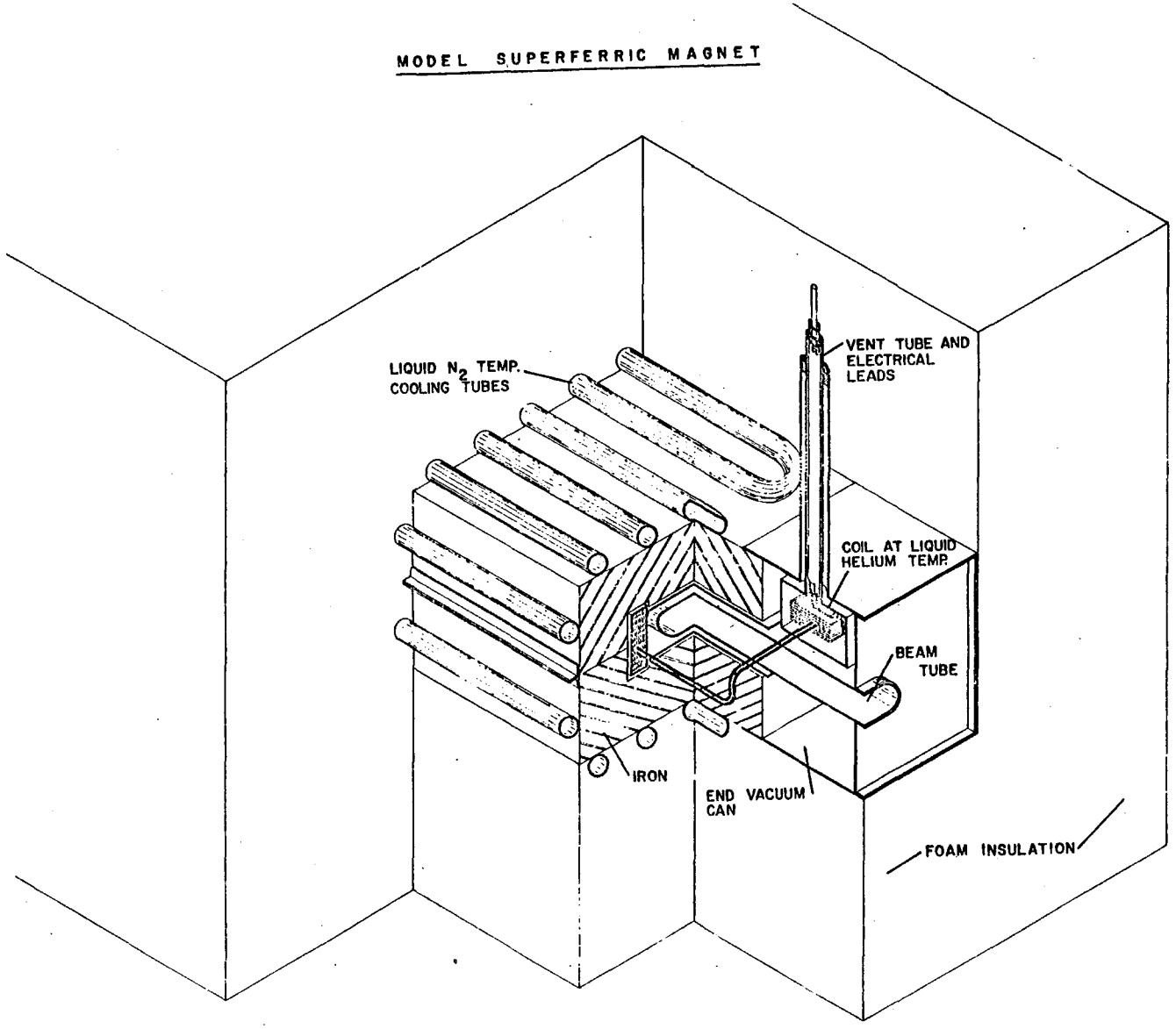
MODEL SUPERFERRIC MAGNET
LIQUID N_2 TEMP. COOLING TUBES
VENT TUBE AND ELECTRICAL LEADS
COIL AT LIQUID HELIUM TEMP.
BEAM TUBE
IRON
END VACUUM CAN
FOAM INSULATION

Figure 2

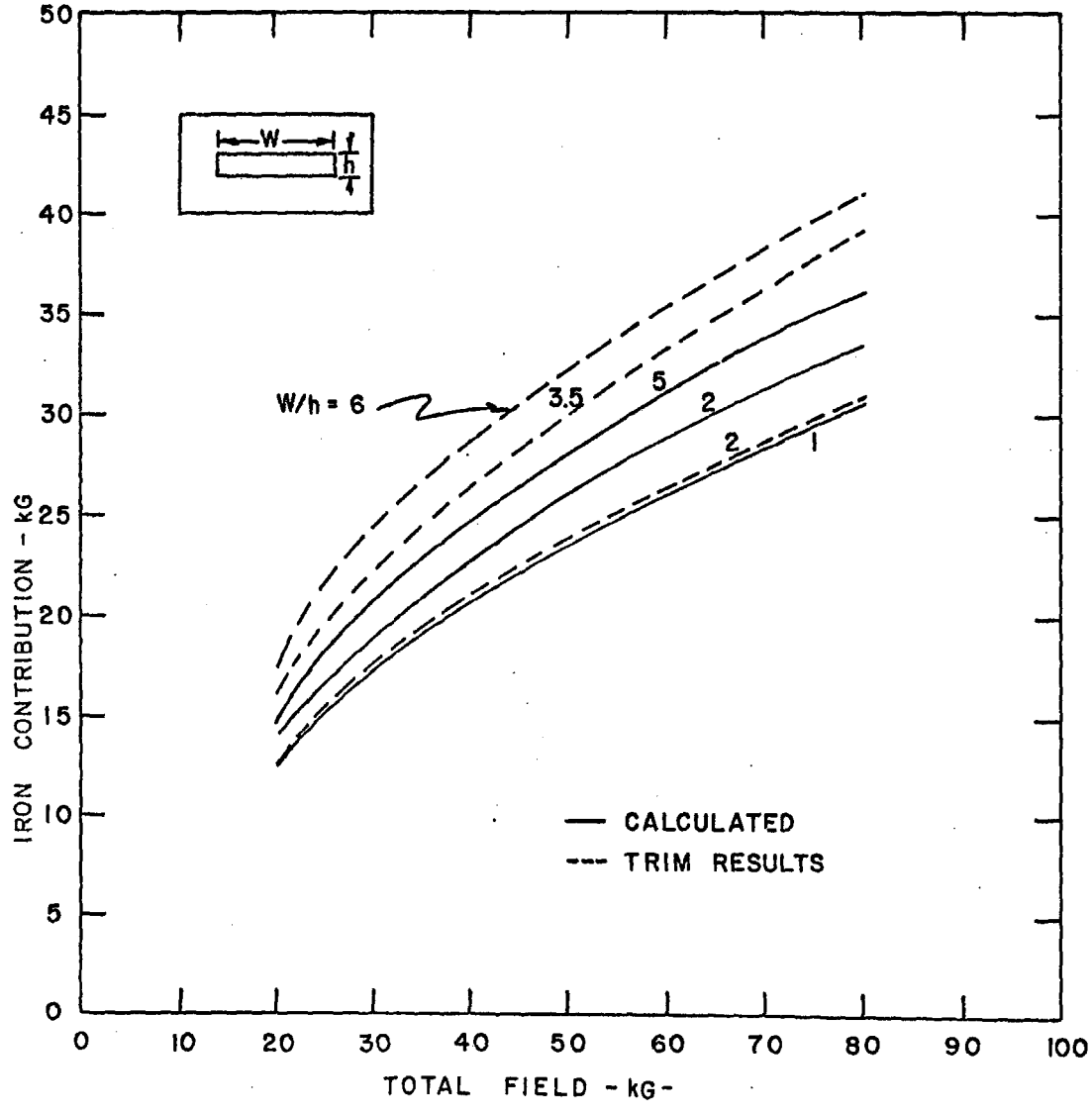
W
h
W/h = 6
3.5
5
2
2
1
CALCULATED
TRIM RESULTS
IRON CONTRIBUTION - kG
TOTAL FIELD - kG -
0
5
10
15
20
25
30
35
40
45
50
0
10
20
30
40
50
60
70
80
90
100

Figure 3

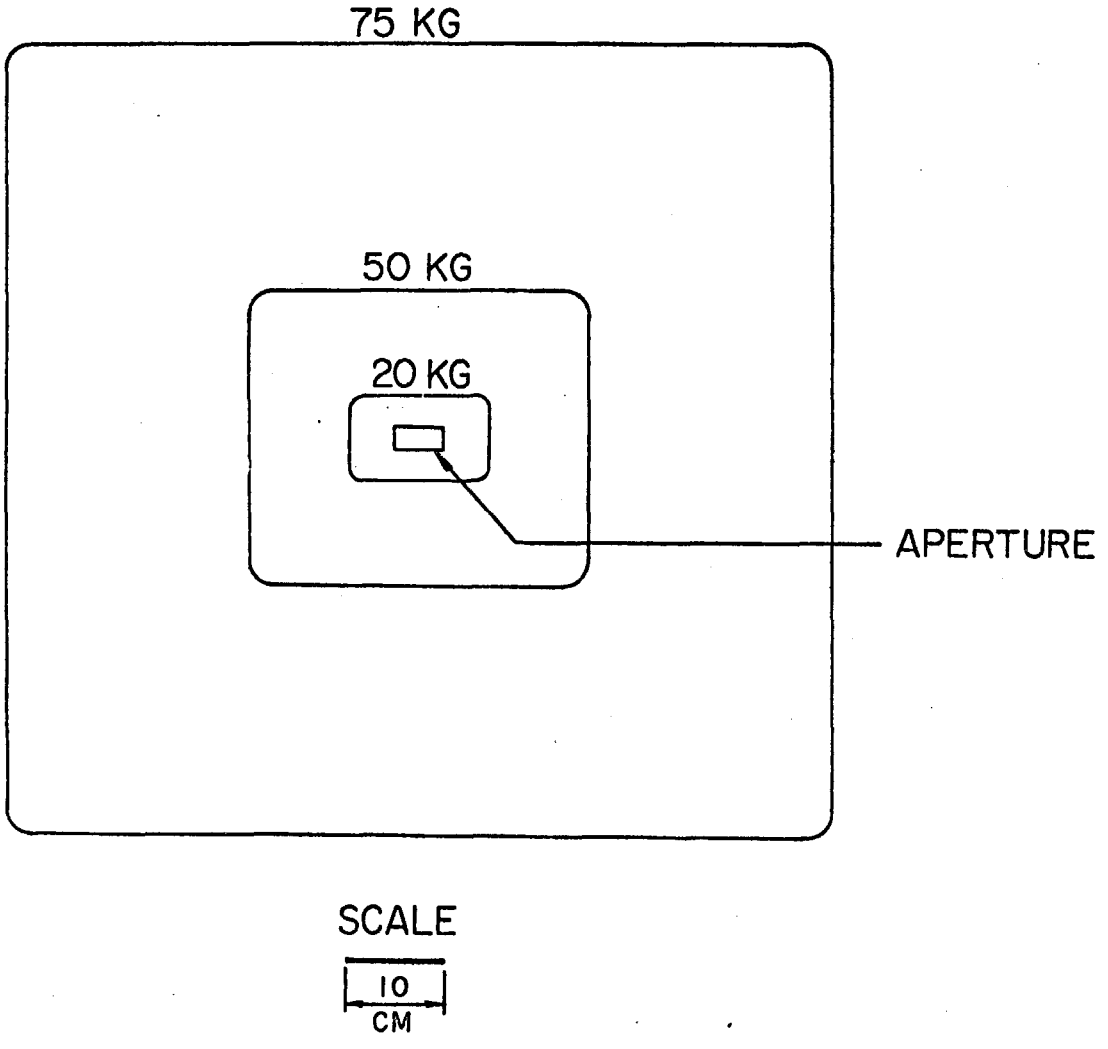

Figure 4

Figure 5

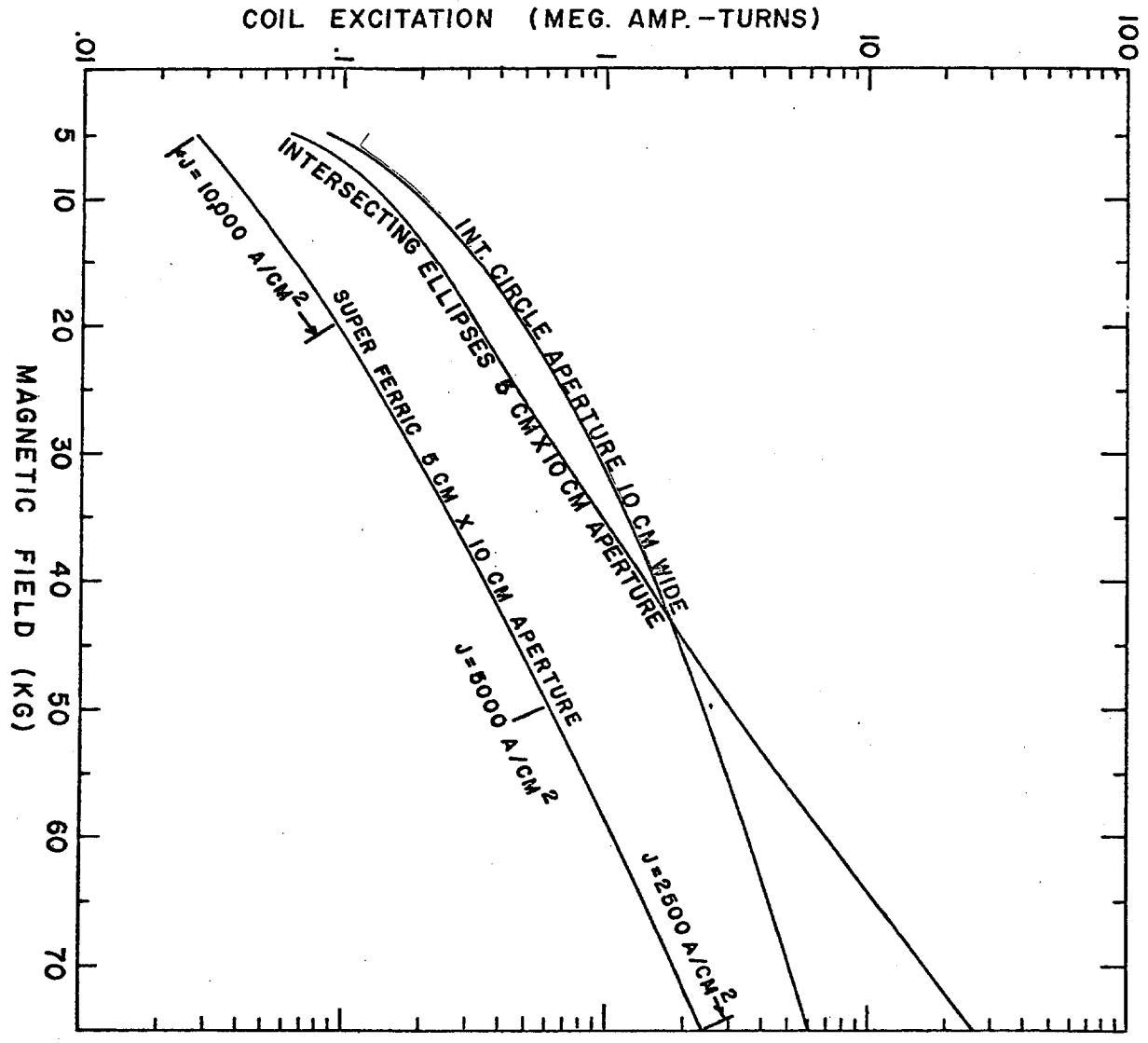
COIL EXCITATION (MEG. AMP.-TURNS)
.01
.1
1
10
100
MAGNETIC FIELD (KG)
5
10
20
30
40
50
60
70
INT. CIRCLE APERTURE 10 CM WIDE
INTERSECTING ELLIPSES 6 CM X 10 CM APERTURE
SUPER FERRIC 6 CM X 10 CM APERTURE
J=10,000 A/CM2
J=5000 A/CM2
J=2500 A/CM2

Figure 6

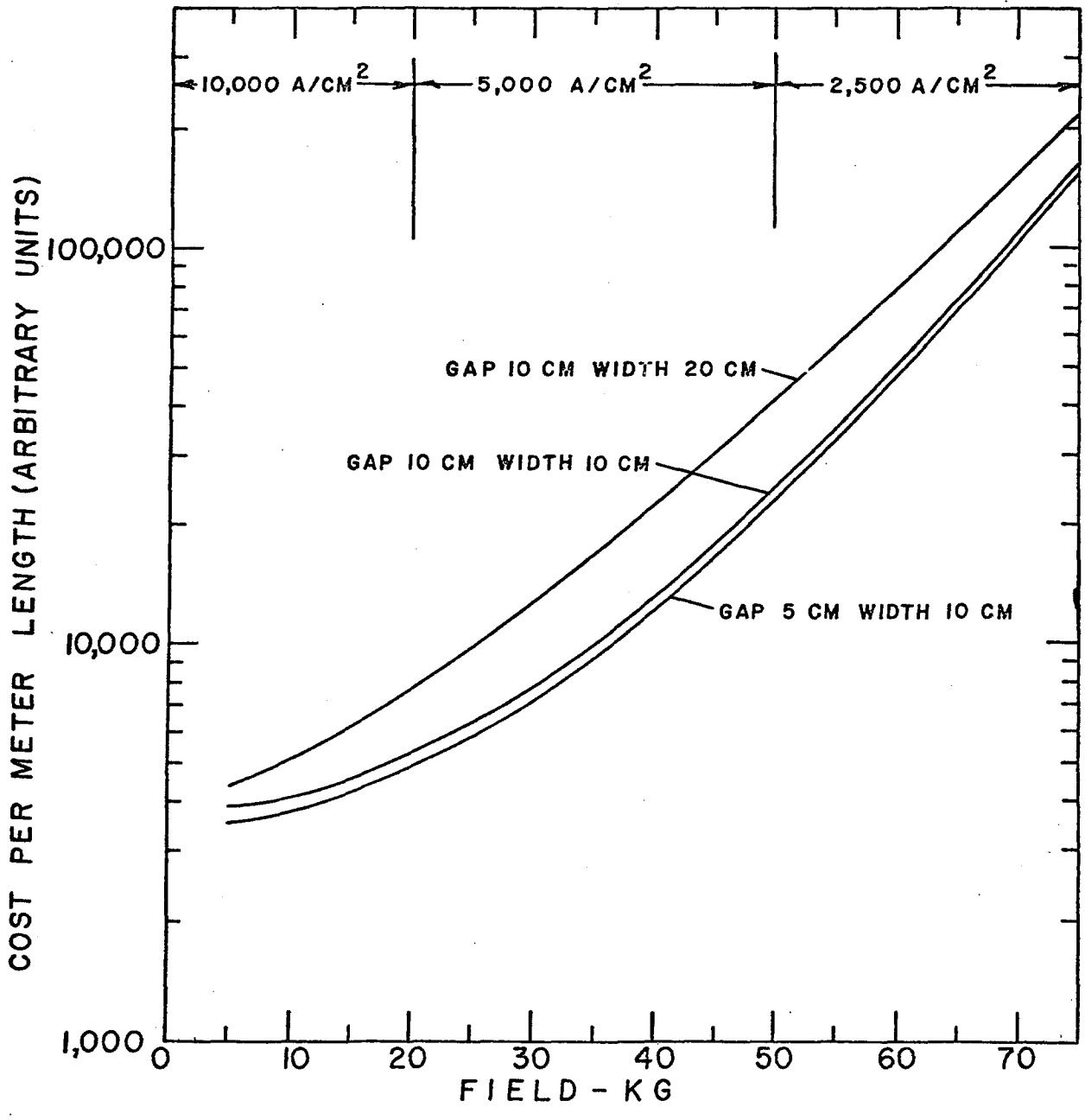
10,000 A/CM2
5,000 A/CM2
2,500 A/CM2
GAP 10 CM WIDTH 20 CM
GAP 10 CM WIDTH 10 CM
GAP 5 CM WIDTH 10 CM
COST PER METER LENGTH (ARBITRARY UNITS)
100,000
10,000
1,000
0
10
20
30
40
50
60
70
FIELD - KG

Figure 7

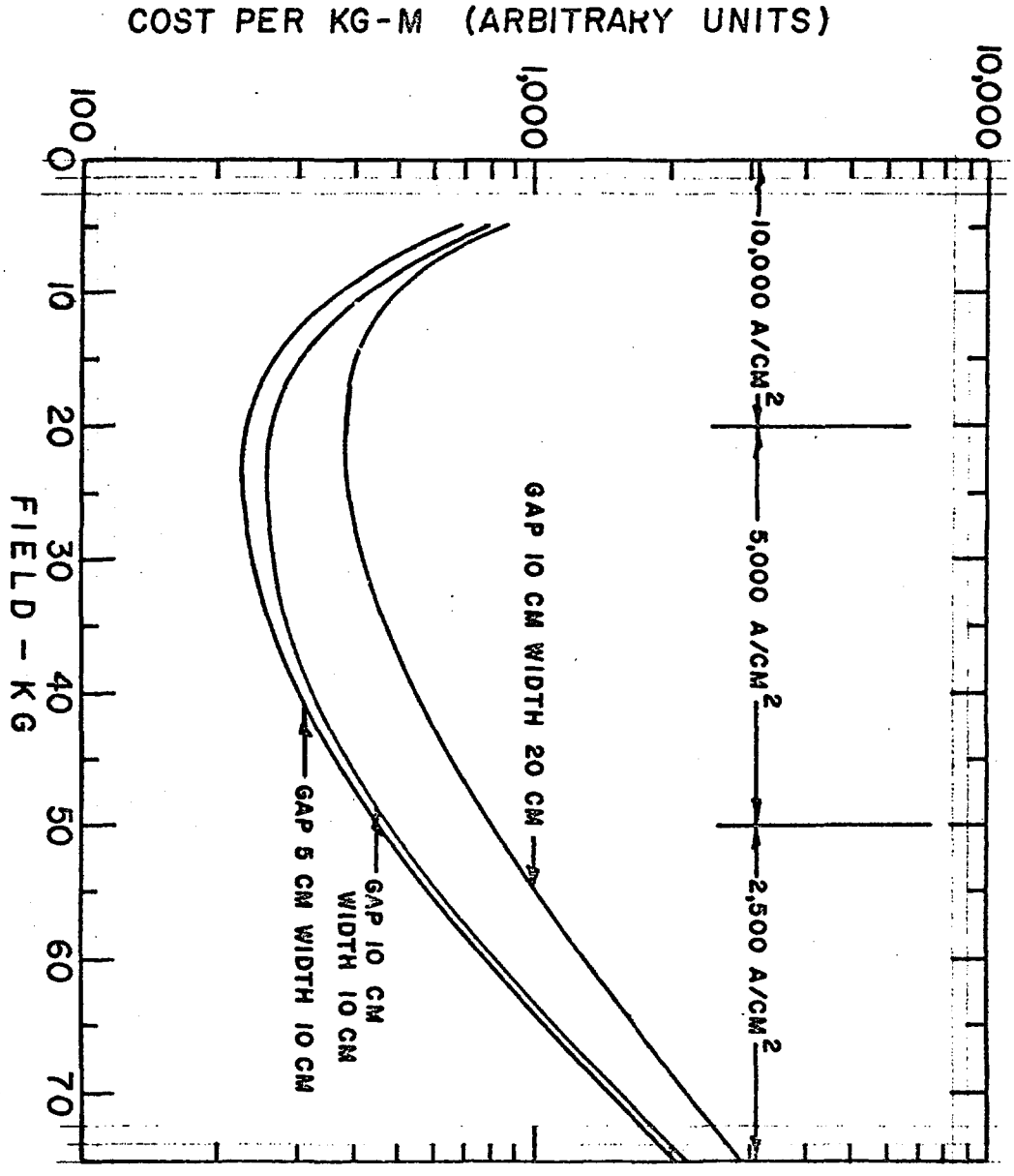
COST PER KG-M (ARBITRARY UNITS)
100
1,000
10,000
FIELD - KG
0
10
20
30
40
50
60
70
10,000 A/CM²
5,000 A/CM²
2,500 A/CM²
GAP 10 CM WIDTH 20 CM
GAP 10 CM WIDTH 10 CM
GAP 5 CM WIDTH 10 CM

Figure 8

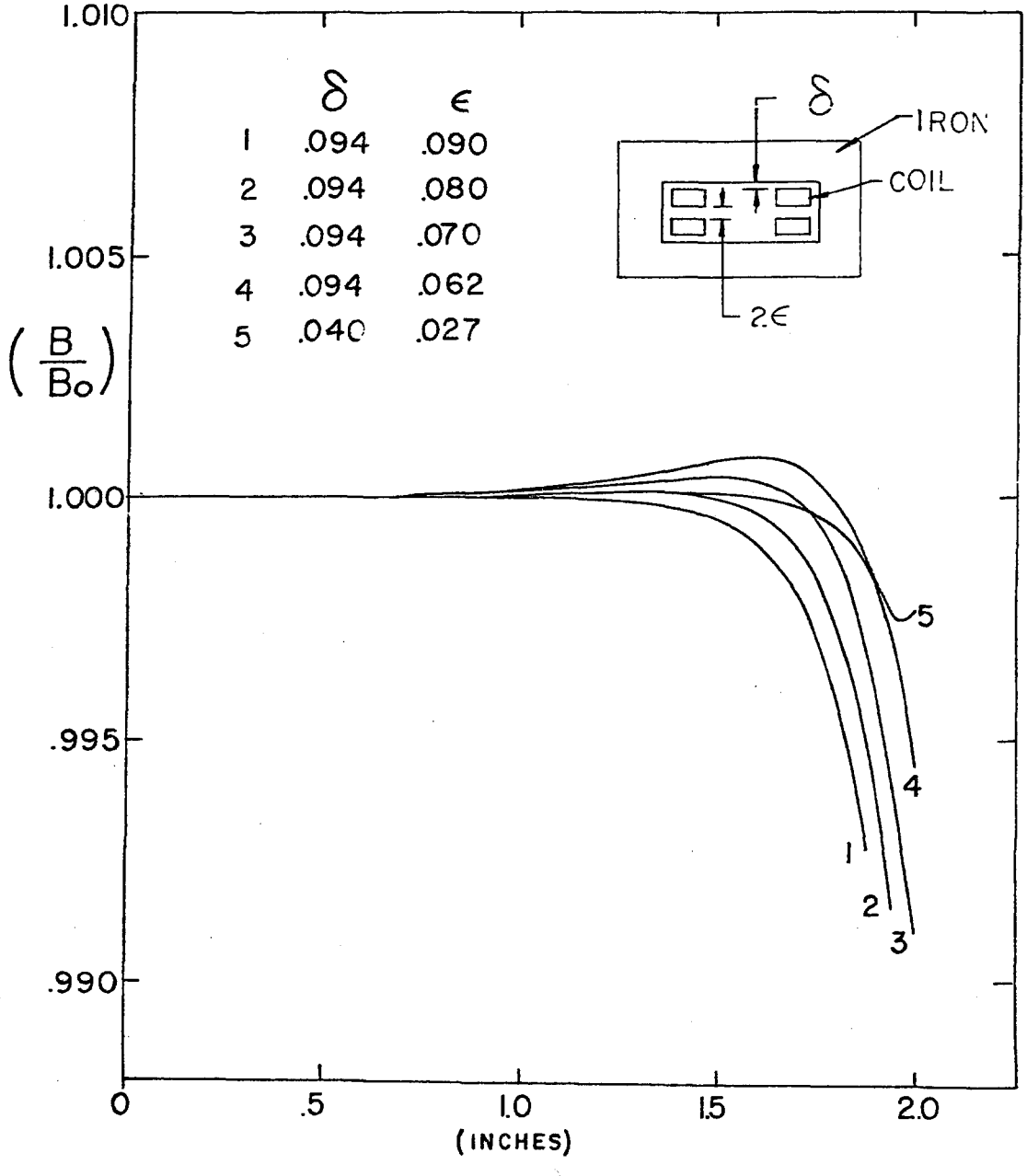
1.010
1.005
1.000
.995
.990
(B/Bo)
δ ∈
1 .094 .090
2 .094 .080
3 .094 .070
4 .094 .062
5 .040 .027
δ
IRON
COIL
2∈
5
4
1
2
3
0
.5
1.0
1.5
2.0
(INCHES)

Figure 9

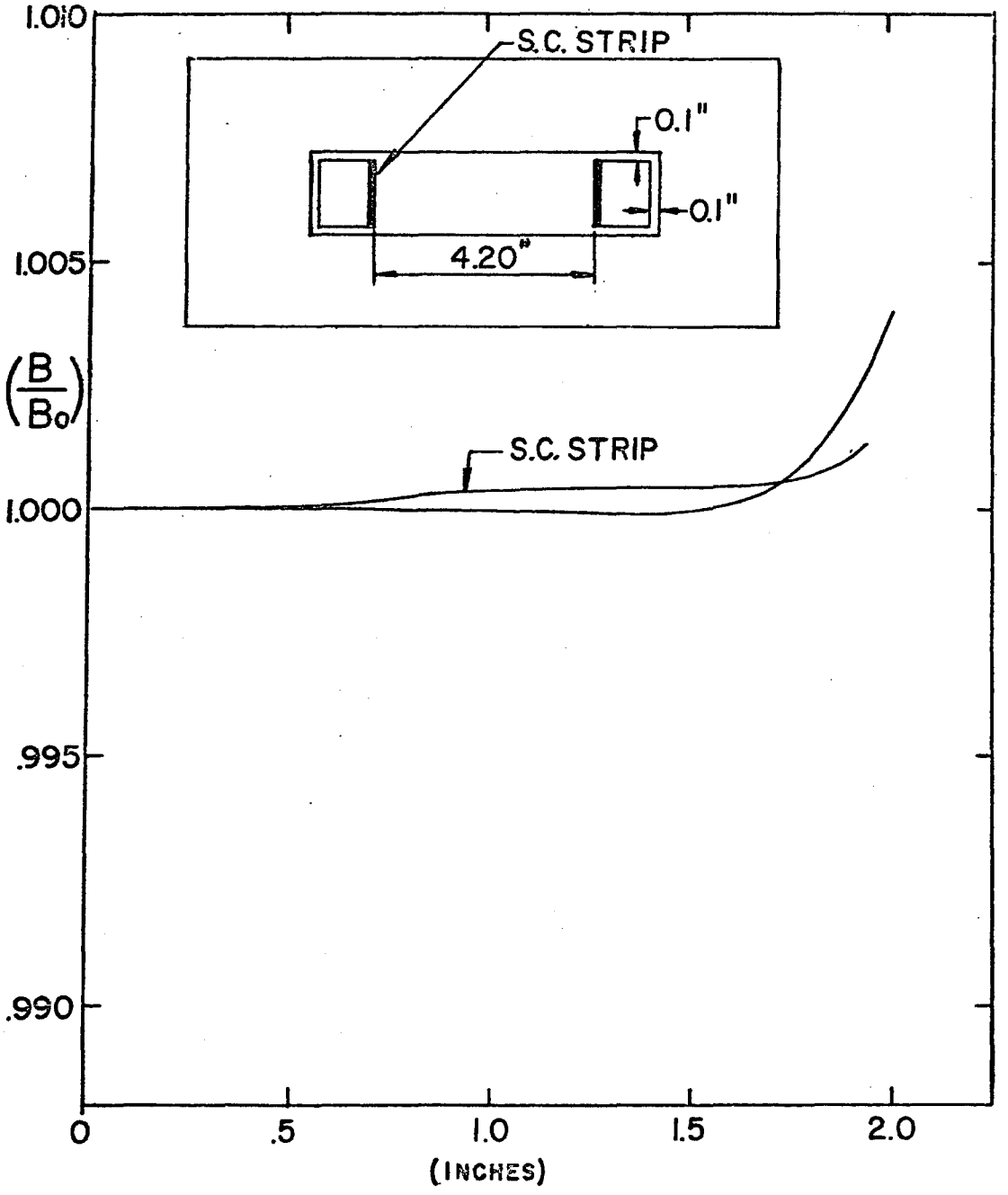
1.010
1.005
1.000
.995
.990
(B/Bo)
S.C. STRIP
0.1"
0.1"
4.20"
S.C. STRIP
0
.5
1.0
1.5
2.0
(INCHES)

Figure 10

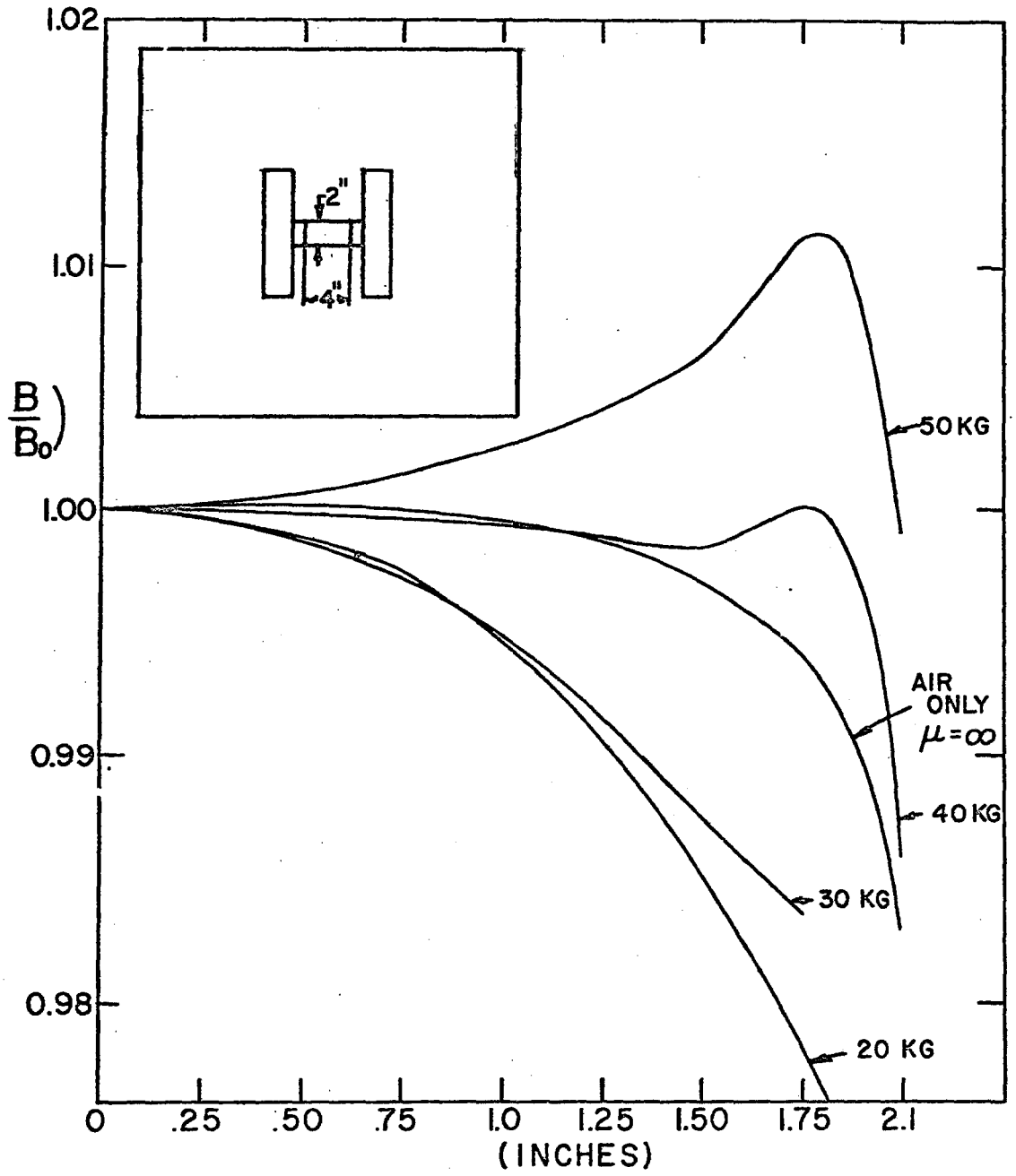
1.02
1.01
1.00
0.99
0.98
B/B0
2"
4"
50 KG
AIR ONLY μ=∞
40 KG
30 KG
20 KG
0
.25
.50
.75
1.0
1.25
1.50
1.75
2.1
(INCHES)

FIGURE 11 (From Stobridge)

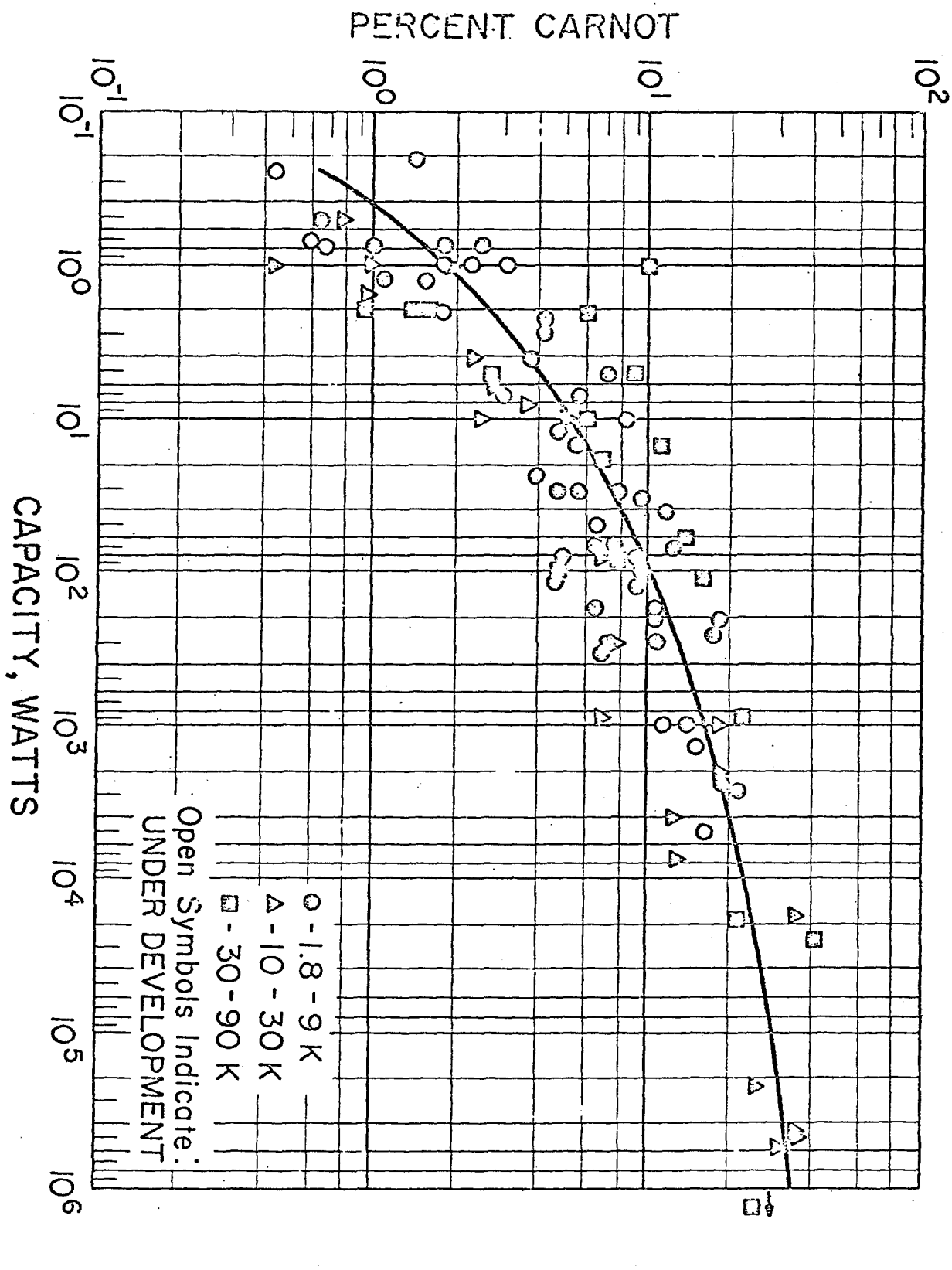

B-80086

Figure 12 (From Stobridge)

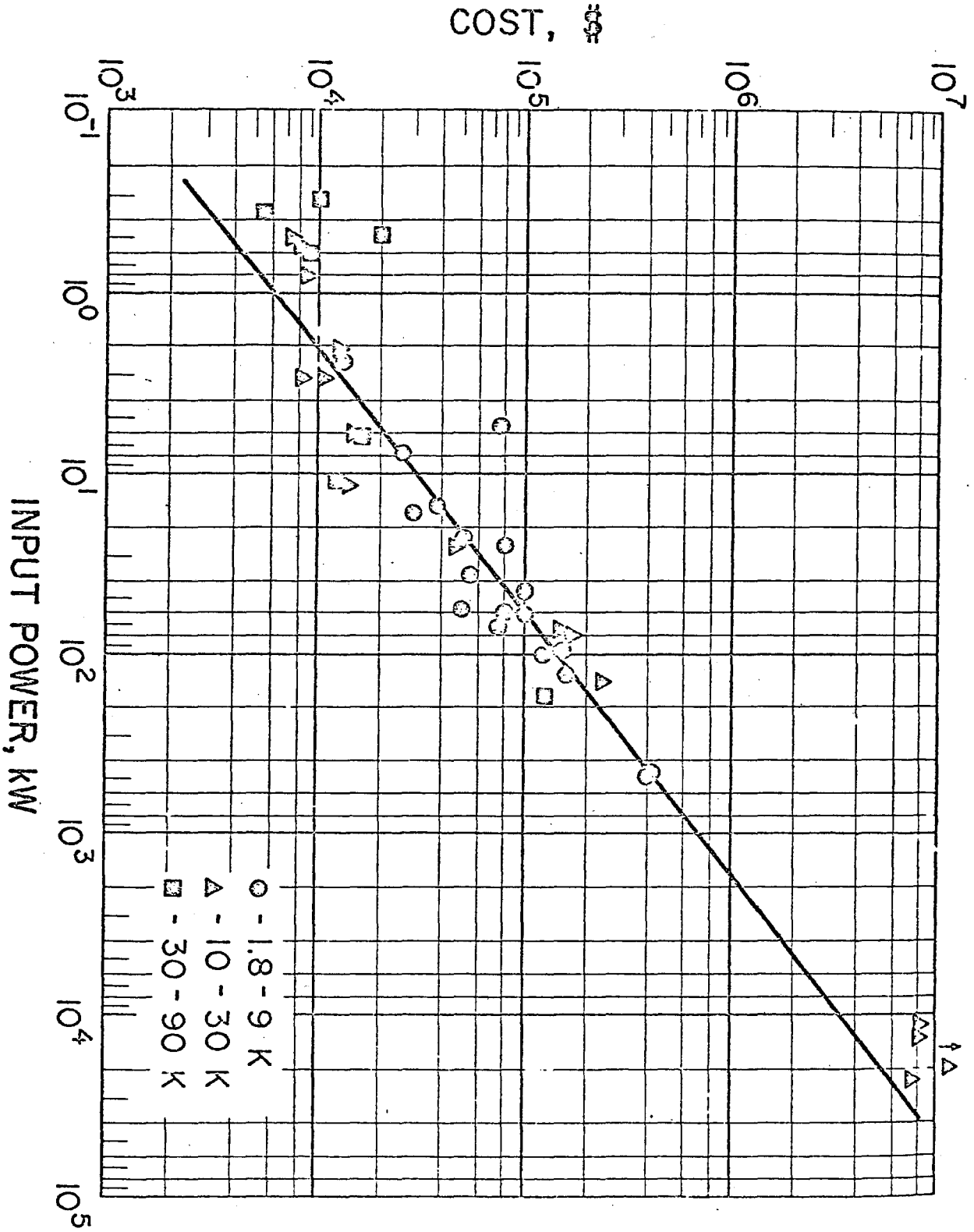

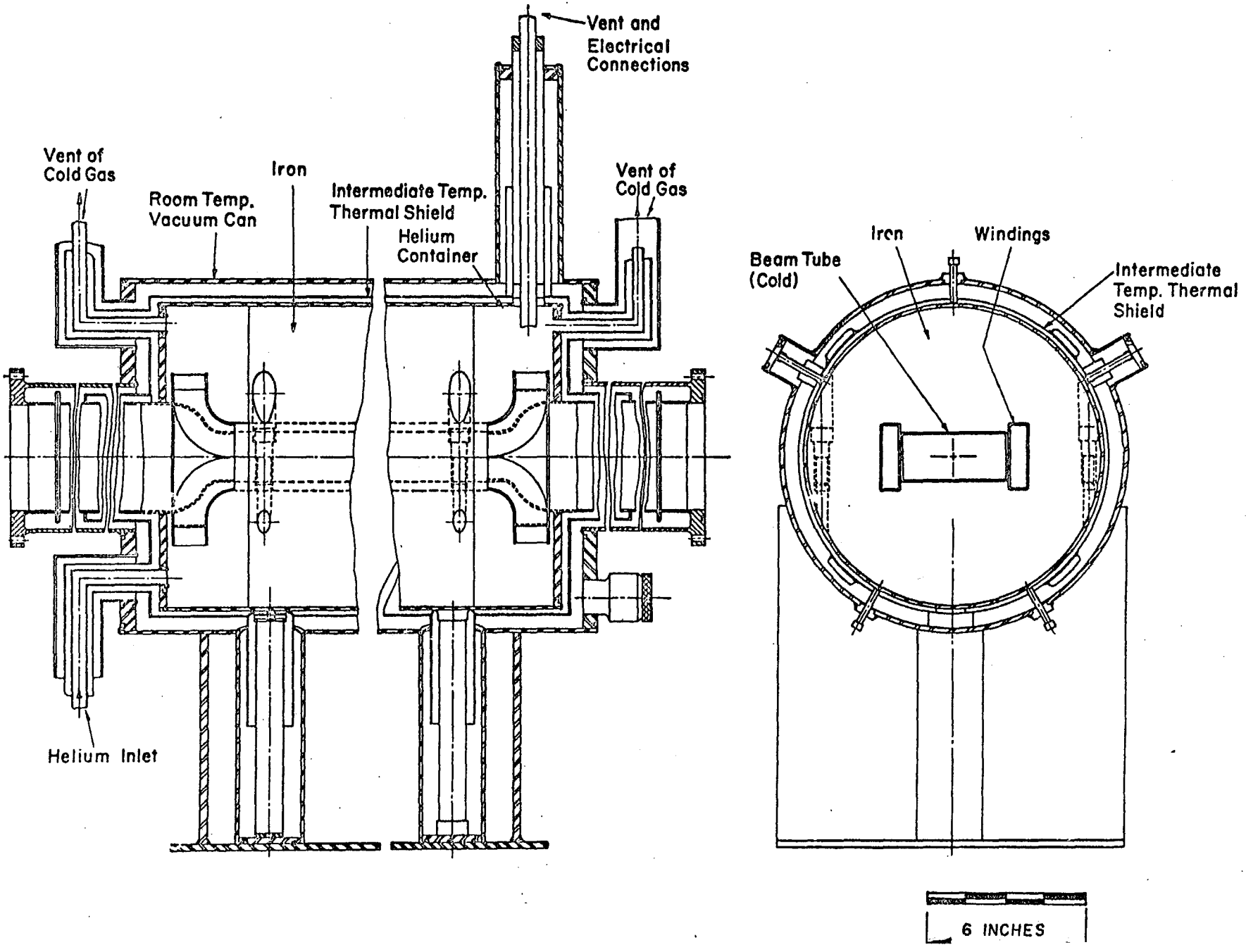
Vent and
Electrical
Connections
Vent of
Cold Gas
Iron
Intermediate Temp.
Thermal Shield
Vent of
Cold Gas
Room Temp.
Vacuum Can
Helium
Container
Helium Inlet
Iron
Windings
Beam Tube
(Cold)
Intermediate
Temp. Thermal
Shield
6 INCHES

Figure 13

APPENDIX VI

PROJECTED EXPERIMENTAL EQUIPMENT COSTS FY 1969-1975

E.J. Bleser and A.L. Read

February 21, 1969

An estimate has been made of the cost of the equipment that will be required for the initial implementation of a research program of the scope envisioned in the National Accelerator Laboratory's Design Report and in the Construction Data Sheets submitted for the 200 BeV accelerator. In order to develop this cost estimate a specific model of an experimental program has been designed, - a definite number of well-defined experiments simultaneously operating in a definite number of secondary beams. The specific experiments postulated have been selected largely as a result of a consideration of their representativeness of the variety of experiments which can now be expected to be undertaken during the first few years of operation of the accelerator. The choice does not reflect any significant decision with regard to an assignment of priorities among all of the experiments which might possibly be undertaken.

The total number of experiments is, of course, related to the total cost of the equipment to be purchased, and this number has been set in a manner that is consistent with previous estimates of the requirements of the overall program and with the scope established for the Laboratory's central facilities. Accordingly, we have assumed that by the end of FY 1975 the Laboratory will have about 16 beam lines, - 14 for counter experiments and 2 for a bubble chamber.

To set a time scale for our model, we have imagined that on beam day, July 1, 1972, there will be two experiments set up and ready to take data. Additional beams will become operable at a rate of about five a year until by the end of FY 1975 there will be the total of about 16 beam lines. The two beams designated bubble chamber beams are imagined to be a neutrino beam and a separated particle beam using superconducting R.F. cavities. These beams will be designed to serve counter experiments in addition to the bubble chamber.

One result of this study was the observation that the requisite momentum resolution for high energy, small phase space beams can be achieved with fewer bending magnets than are needed simply to spread the experiments out in a reasonable manner on the experimental floor. Therefore, in this study we have not considered the use of switching magnets so that one beam line can serve one or the other of two experiments. The resulting savings turn out to be quite small relative to the uncertainties of the present projection. Table I presents a list of the experiments that have been considered.

Table II gives an estimate of the equipment that each experiment might need. This list defines five general types of equipment, - beam transport magnets, spectrometer magnets, shielding, counters and electronics, and computers. In addition this report includes the neutrino and R.F. beams to the bubble chamber, film analysis equipment, a central computer for the Laboratory, and a large project not yet well defined, but taken to be some kind of spectrometer such as one of those proposed in the summer study.

This report does not concern itself with the provision of a large bubble chamber facility. This is assumed to be a separate construction project. Also not included are items required for proton beam transport, the associated tunnels, target stations and their shielding, and experimental buildings. These have all been provided as part of the accelerator construction described in the basic Construction Data Sheets for the Laboratory.

Table III gives the detailed cost estimate for equipping the experimental facilities of the Laboratory within the framework outlined above. The kinds and numbers of items have been estimated by the NAL staff. The costs of most items have been estimated by William M. Brobeck and Associates as given in their Report No. 200-1-R7. To a number of items, twenty-five per cent of the cost has been added for EDIA (Engineering, Design, Inspection, and Administration). The following notes and comments can be made on this table.

I. Beam Transport

1. Magnets are identified by the notation 20c-6-2-120, where 20 means the field in kilogauss, c means conventional iron and copper magnet, and the next three numbers give the width, height and length of the gap in inches.
2. Roughly, half the dipole magnets are needed not for momentum resolution, but to spread the beams out to give space between the experiments.
3. The aperture of the magnets has been chosen somewhat arbitrarily. A four inch aperture recommended in some studies instead of the

two inch aperture used here would add 50% to the cost for a total of $18 million instead of $12 million.

4. A 20 Kg iron superconducting magnet system is estimated to cost $15 million instead of $12 million, but may use only 10% of the power.

II. Spectrometer Magnets

1. This list is only a representative one -- what large magnets to actually purchase is a question open to considerable discussion.

2. These magnets are those called for by the spatial resolution of the present detectors. Improved detectors could save a great deal of money by reducing the size of these magnets.

III. Shielding

This is shielding for secondary beams only. It does not include the shielding of the primary beam or the primary target.

IV. Experimental Equipment

This list assumes that the laboratory will have a pool to provide the user not only with fast electronic modules, as is presently done, but also with other expensive and perhaps standardized items such as Cerenkov counters, wire spark chamber read-out systems, and scintillation counter hodoscopes.

V. Film Analysis

This is an estimate of the system needed to measure 300,000 neutrino pictures a year, plus a strong interaction program. The proposed scanning measuring chain is a three-phase process. The analysis machines provide high magnification observation of any particular region of the photograph.

VI. Computers

Since in 1969 Brookhaven is using two CDC 6600's, it seems very likely that by 1975, NAL will need at least three 6600's, or their equivalent. In addition to a central computer, the laboratory should have a set of standardized small and medium-sized computers, which might be connected to the central computer, to provide on-line-service for the experimenters. The specific computers named here are used only as examples.

VII. Neutrino Beam

The neutrino beam will be a major facility of the laboratory and will involve about a mile of tunnel, a large bubble chamber and perhaps several million dollars of steel shielding. None of these items are included in this report and since the project is as yet largely undefined, the only large item included has been a magnet, equivalent to the bubble chamber magnet, to sweep secondary muons out of the beam.

VIII. R.F. Beam

This project also requires a very long beam line and is still open to a great deal of development work.

IX. Multiparticle Spectrometer

Since large projects may be undertaken by the laboratory, this one, which was proposed in the summer study, has been included in this report as an example.

To the total of component and EDIA costs, 25% has been added for contingency. Twelve per cent of this total has been added for escalation estimated at approximately four per cent per year for an average period of three years.

Table IV uses the data of Tables II and III to estimate the cost of the equipment for each of the fourteen systems of beam transport and equipment. Each counter experiment needs on the average 2 million dollars worth of technical equipment. The equipment, of course, is reused many times in many experiments.

Graph I shows the number of beams operating as a function of time as discussed above. Graph II shows the costs per quarter year necessary to achieve the operating level in the time shown on Graph I. This curve peaks at the end of FY 1972 and levels off in 1974, 1975, at an annual rate of about $10 million, which is the proposed level of continuing expenditure after the laboratory is initially built and equipped. This curve is a smooth curve generated by considering the number of projects under construction at any given time and what fraction of the total effort they represent. Specific expenditures on large items which may make bumps in this curve have not been taken into account. Table V gives the costs and obligations per fiscal year for FY 1969 through 1975, with and without the Central Computing Facility. Table VI gives the breakdown of the obligations per fiscal year for the different types of equipment. The obligations projected for 1975 are for possible extensions of the laboratory beyond the scope detailed in this report.

Table I
Fourteen Possible Counter Experiments

1. Beam Survey - To measure secondary particle yields.
2. Quark Search - Look at the primary target with a DISC Cerenkov Counter.
3. W-Search - Look for muon pairs emerging from a beam dump.
4. Total Cross-Section Measurements - Transmission experiments using counter hodoscopes.
5. Large Angle Elastic p-p Scattering - Coincidences between two spectrometers looking at a hydrogen target.
6. Small Angle Elastic Scattering - One wire chamber spectrometer.
7. Backward π-p Elastic Scattering - A forward high energy spectrometer in coincidence with a large angle, low energy spectrometer using a very large magnet.
8. Rho-Production - A spectrometer to analyze the two pions from the decay of rho's produced at small angles.
9. Backward Inelastic π-p Scattering - One high resolution spectrometer to analyze the forward going proton.
10. W-Search - The muon decays of W's produced by a muon beam are analyzed.
11. Muon-Proton Elastic Scattering - Two wire chamber spectrometers.
12. n-p Scattering - A small angle neutral beam, a neutron detector and a recoil spectrometer.
13. K°-p Scattering - A large angle neutral beam with a wire plane spectrometer to measure $K^\circ_S \rightarrow 2\pi$ decays.
14. Multiparticle Spectrometer - A very large facility using bubble and spark chambers. The large items are listed in Section X.

Two Possible Bubble Chamber Beams

1. Neutrino Beam - Technical equipment is listed in Section VIII. In addition a large bubble chamber, 1.5 km of heavily shielded tunnel, and 0.5 km of earth absorber are needed.
2. High Energy Superconducting R.F. Separated Beam - Technical equipment listed in Section IX. In addition need 1.5 km of tunnel.

Equipment \ Experiment	1. Beam Survey	2. Quark Search	3. W-Search	4. Total Cross Section	5. Large angle p-p	6. Elastic	7. Backward π-p	8. Rho-production	9. Inelastic π-p	10. W-Search	11. μ-p Elastic	12. n-p Scattering	13. K°-p Scattering	14. Hybrid System	Total Items
Dipole Magnets	25	33		25	25	13	13	6	12	12	12	6	6	12	200
Quadrupole Magnets	14	16		14	14	8	6	4	6	6	6	0	0	6	100
20c-30-6-120	4					2			2	1	1				10
20c-24-12-120							2			1					3
20c-48-12-48								1							1
15c-24-24-48													1		1
10c-300-18-36							1								1
15c-72-36-48					2										2
15c-48-48-72												1			1
Concrete Walls	3	4		3	3	2	1	1	2	2	3	4	2	2	32
Steel Beam Stops	3	1		2	1	2			1	3	1	1	1		16
LiH_2 Targets	1			1	1	1	1	1	1		1	1	1	1	11
Fast Electronics Modules (In Hundreds)	1	1	1	2	2	1	1	1	2	2	2	1	1	2	20
Scintillation Counters	40	15	40	65	40	40	30	20	35	50	50	25	20	50	500
Beam Cerenkov				17	4	5	8	5	5					6	50
Large Cerenkov				3	3	2	4	3	2				1	2	20
DISC Cerenkov	1	1		1		1									4
Wire Planes					20	25	35	15	20	10	25	10	15	25	200
Readout Systems					1	1	1	1	1	1	1	1	1	1	10
Small Computer					1	1	1	1	1	1	1	1	1		9
Medium Computer						1				1				1	3

Table II

Table III
Technical Equipment Cost Estimates
For Experimental Facilities Section
(All Amounts in Thousands of Dollars)

	Cost	EDIA 25%	Total
Beam Transport			11,458
a. Dipole Magnets - 200 20c-6"-2"-120 @ $17.2	3,440	860	
b. Quadrupole Magnets - 100 15c-2"-Q-72" @ $17.2	1,720	430	
c. Power Supplies 41,000 kw @ $.09/kw	3,680	—	
d. Magnet Controls	329	82	
e. Cables	473	-	
f. Vacuum System	205	51	
g. Cooling Water System	150	38	
	9,997	1,461	

Comments: 1. 20 Kg iron superconducting magnets cost $15M
2. A 4" instead of a 2" high aperture adds 50% to the cost 12 + 6 = $18M

[. Spectrometer Magnets			8,454
a. 20c-30-6-120 - 10	1,099	275	
b. 20c-24-12-120 - 3	388	97	
c. 20c-48-12-48 - 1	125	31	
d. 15c-24-24-48 - 1	85	21	
e. 10c-300-18-36 - 1	475	120	
f. 15c-72-36-48 - 2	514	128	

Table III (cont.)
Technical Equipment Cost Estimates
For Experimental Facilities Section

	Cost	EDIA 25%	Total
g. 15c-48-48-72 - 1	325	81	
h. Power Supplies 15,000 kw	1,142		
i. Controls & Cables	51	13	
j. Moving Systems - for magnets based on 72" Bubble Chamber System	2,787	697	
	6,991	1,463	
Shielding			3,864
Heavy concrete blocks for each of 16 experiments assume two walls 2' wide, 8' high and 300' long, at $200/cy	1,300	-	
Steel Assume 16 beam stops 20' wide, 10' high and 20' deep at $1,000/cy	2,500	-	
Lead Bricks 4 cubic yards for each of 16 experiments at $1,000/cy	64	-	
	3,864		
Miscellaneous Equipment			1,249
Liquid Hydrogen Reservoirs & Dewars	90	23	
Monitoring, Measurements, Controls	403	101	
Fork Lifts, Trucks, Cranes	632	-	
	1,125	124	
Experimental Equipment			2,838
Fast Electronics 2000 assorted modules	904		

Table III (cont.)
Technical Equipment Cost Estimates
For Experimental Facilities Section

	Cost	EDIA 25%	Total
Oscilloscopes - 30 units	90	-	
Scintillation Counters - 500	300	75	
Wire Planes - 200	60	15	
Readout Systems - 16 units	300	75	
Gas Recovery & Purification Systems	150	38	
Beam Cerenkov Counters - 50 units	125	31	
Large Aperture Cerenkov Counters - 20	300	75	
Disc Cerenkov Counters - 4	120	30	
Trailers - 30 units	150	-	
	2,499	339	
I. Film Analysis			2,163
3 Measuring Machines	550	138	
10 Analysis Machines	500	125	
8 Scanning Machines	80	20	
Computer	350	88	
Developing Machine	250	62	
	1,730	433	
I. Computers			18,069
a. Central Computer 3 CDC 6600's	14,301	-	

'able III (cont.)
'echnical Equipment Cost Estimates
'or Experimental Facilities Section

	Cost	EDIA 25%	Total
b. Large on-line computers 3 Sigma-7 Systems	2,829	-	
c. Small on-line computers 9 Sigma-2 Systems	939	-	
	18,069		
. Neutrino Beam			3,375
a. Sweeping Magnet	3,000		
b. Focusing Devices	300	75	
	3,300	75	
. R.F. Superconducting Beam			3,637
a. Dipole Magnets - 20 20c-2-1-200 @ $11.4	228	57	
b. Quadrupole Magnets - 25 15c-2-Q-72 @ $17.2	430	107	
c. Power Supplies 5,400 kw @ $12/kw	627		
d. R.F. Separator System 3 Stations at $550/station +100	1,750	438	
	3,035	602	
. Multiparticle Spectrometer			9,500
a. 30" Hydrogen Bubble Chamber	3,000	750	
b. 30" Streamer Chamber	150	38	
c. 30" Superconducting Magnet 40 kg	450	112	

Table III (cont.)
Technical Equipment Cost Estimates
For Experimental Facilities Section

	Cost	EDIA 25%	Total
d. Superconducting Magnet 40 kg 50" gap 160" diameter	2,000	500	
e. Superconducting Magnet 40 kg 60" gap 100" diameter	2,000	500	
	7,600	1,900	
Totals	58,210	6,397	64,607
25% Contingency			16,152
			80,759
12% Escalation			9,691
			90,450

Table IV
Technical Equipment Cost per Experiment

	Experiments	Cost
1.	Beam Survey	3,000
2.	Quark Search	2,600
3.	W-Search	400
4.	Total Cross Section	2,600
5.	Large Angle p-p	4,000
6.	Elastic	1,800
7.	Backward π-p	3,300
8.	Rho-production	1,100
9.	Inelastic π-p	1,900
10.	W-Search	2,200
11.	μ-p Elastic	1,800
12.	n-p Scattering	2,000
13.	K^o-p Scattering	1,200
14.	Hybrid System	2,200
		30,100

Table IV (cont.)
Technical Equipment Cost per Experiment

	Special Apparatus	Cost
IV.	Miscellaneous	1,000
VI.	Film Analysis	2,000
VII.	Central Computer	14,000
VIII.	Neutrino Beam	3,000
IX.	R.F. Superconducting Beam	4,000
X.	Multiparticle Spectrometer	10,000
		64,100
	Contingency & Escalation	26,000
	Total	90,000

Table IV
Budget Summary
(In Millions of Dollars)

Fiscal Year	Obligations	Costs	Cumulative Total Obligations	Costs
1969				
1970	4	4	4	4
1971	23	15	27	19
1972	27	23	54	42
1973	26	24	80	66
1974	10	14	90	80
1975	10	10	100	90

Exclusive of Central Computing Facility

Fiscal Year	Obligations	Costs	Cumulative Total Obligations	Costs
1969				
1970	4	4	4	4
1971	18	12	22	16
1972	19	16	41	32
1973	19	18	60	50
1974	10	10	70	60
1975	10	10	80	70

Table VI
Estimated Obligations for Equipment 1969-1975
(In Millions of Dollars)

	Fiscal Year	1970	1971	1972	1973	1974	1975
I.	Beam Transport	2.5	4.0	4.0	3.0	3.0	4.5
II.	Spectrometer Magnets	.5	4.0	4.0	3.0	.5	2.5
III.	Shielding		1.5	3.0	1.5	1.0	1.5
IV.	Experimental Eqpt.	.5	.5	1.5	1.5	1.0	1.5
V.	Film Analysis	.5	.5	1.0	1.0	.5	
VI.	Computers						
	Large		5.0	8.0	7.0		
	Medium		1.5	1.5	1.0		
	Small	.2					
VII.	Neutrino Beam		4.0				
VIII.	R.F. Beam			1.0	3.0	1.0	
IX.	Multiparticle Spectrometer		2.0	3.0	5.0	3.0	
	Totals	4.2	23.0	27.0	26.0	10.0	10.0
	Accumulated Totals	4	27	54	80	90	100

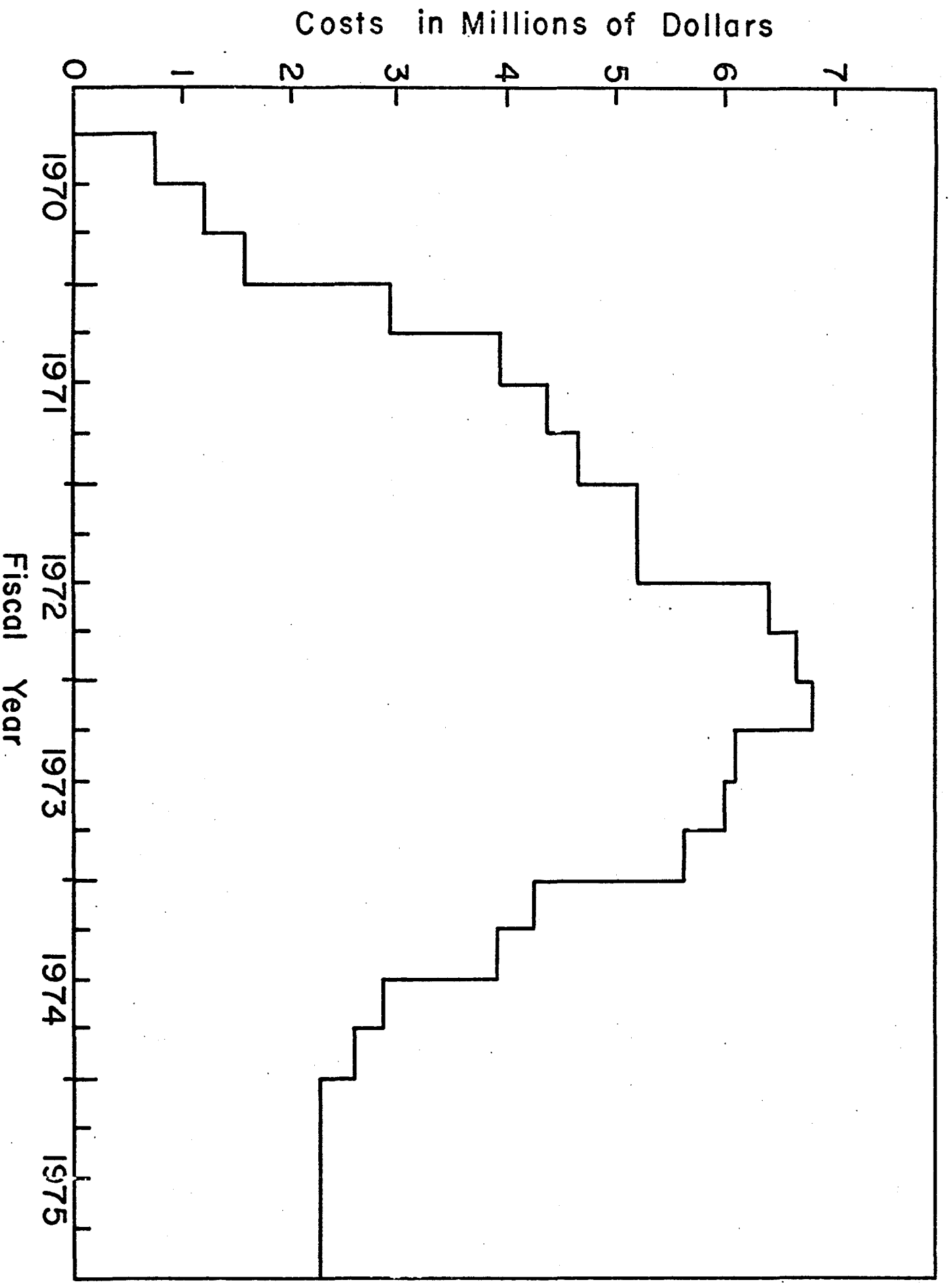
Costs in Millions of Dollars
0
1
2
3
4
5
6
7
Fiscal Year
1970
1971
1972
1973
1974
1975

Graph II

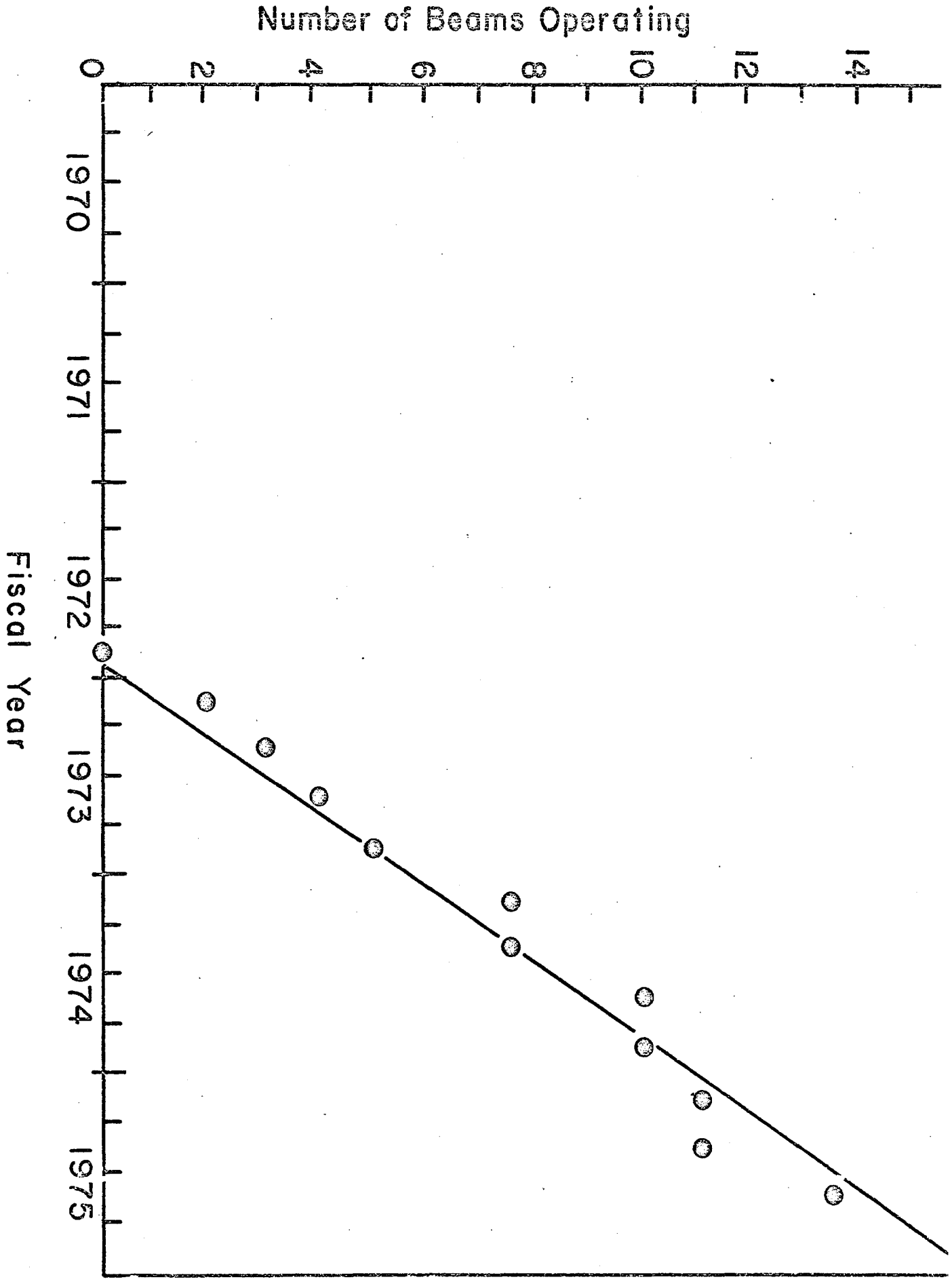
Number of Beams Operating
0
2
4
6
8
10
12
14
Fiscal Year
1970
1971
1972
1973
1974
1975

Graph I

APPENDIX VII

J. MacLachlan

CHARGED SECONDARY BEAMS USING MAIN RING MAGNETS

Purpose of the Study

This report describes a 200 BeV diffracted proton beam (3.5 mr) and an 80 BeV unseparated π beam (10 mr) designed around main ring components. It will be clear that these designs leave much to be desired, but the existence of concrete examples will hopefully ellicit explicit suggestions for improvement. The advantages of super-conducting magnets, for example, become clearer in comparing competing designs for the same intensity etc. Certainly general features of beams for this energy range are illustrated by these simple examples. Also the effort has been useful in evaluating NAL computer code resources. The techniques developed all appear to be helpful for satisfying more special or exacting design requirements.

There is, of course, good reason to capitalize on the development effort that has gone into main ring magnets if they are well matched to secondary beam needs. These examples are sufficiently realistic to show how good the match is. One general feature is the sagitta in the bending magnets which precludes their use for soft beams. The aperture loss

is already 3 cm at 80 BeV/c. Although the field quality is unnecessarily good the magnets would be available and units rejected for the ring could be used. Units used in a beam line could also serve as a secondary backup for components in service.

Design Goals

The desired beam properties are

	Beam I	Beam II
particle	p	π^-
momentum	200 BeV/c	80 BeV/c
prod. angle	3.5 mr	10 mr
momentum bite	.05-2.0%	.125-2%

The beams were to consist of two sections of the general form indicated in the diagram. The first drift from target to QD1 is 40 m minimum if the production angles are taken to opposite sides of the EPB line and 60 m minimum if both beams are on the same side. Much of the initial work was done for 40 m and some of it has not been repeated for the more realistic 60 m choice. Figure 1 is a beam schematic.

Outline of the Calculation

The emittance in the main ring is

$\varepsilon_V = .09\pi$ mm mr

Main Ring

$\varepsilon_H = .23\pi$ mm mr

FIGURE 1

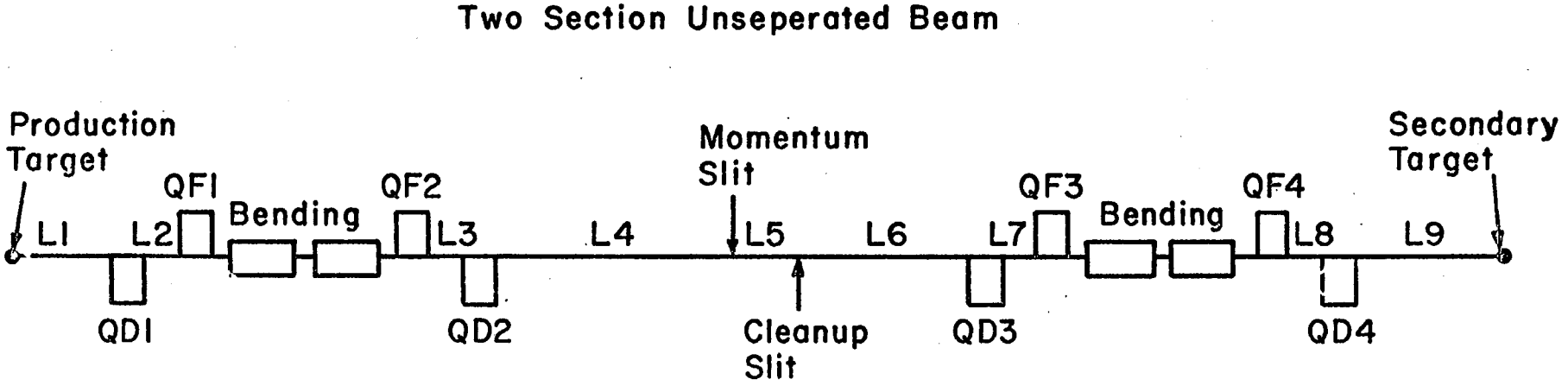
Two Section Unseperated Beam
Production Target
QF1
Bending
QF2
Momentum Slit
QF3
Bending
QF4
Secondary Target
L1
L2
L3
L4
L5
L6
L7
L8
L9
QD1
QD2
Cleanup Slit
QD3
QD4

but the effect of slow extraction on ε_H is largely a matter of guesswork. For present purposes the values

$$\varepsilon_v = .09\pi \text{ mm mr}$$

$$\varepsilon_H = .033\pi \text{ mm mr} \quad \text{EPB}$$

were chosen. It turns out that the size of the beam spot obtainable on the production target is likely to be fixed by other considerations such as regulation in the beam line bending magnets to values considerably larger than the minimum set by emittance. With reasonable optics one may obtain a spot radius of .1 mm, but regulation of $0(10^{-4})$ is required in the EPB bending magnet to hold the spot fixed to such tolerance. The spot radii were arbitrarily taken as 1 mm horizontal and 1.4 mm vertical. The larger blowup for horizontal gives some recognition to the fact that most of the bending is in the horizontal plane.

Using thin lens formulae the gradients and drifts were calculated for the layout shown to fill magnet aperatures and keep gradients in a range for D.C. excitation. No constraint was placed on lengths. The first order thick lens, finite emittance, results were then found from the TRANSPORT code. A sequence of runs was made to meet the aperture and gradient constraints.

Placement and regulation tolerances were determined by

a first order trace with TRANSPORT introducing a single displacement, rotation or gradient error in each run. Second order traces were run to get the effects of chromatic aberration and bending magnet sextupole. Confidence in the second order results and their interpretation is not too great at this time. Errors have been found in the TRANSPORT code, but no independent check has been made yet to show that they have all been found.

The TRANSPORT solution for the two beams is given in the table.

	Beam I			Beam II		
Element	length(m)	grad. (Kg/m)	angle (mr)	length(m)	grad. (Kg/m)	angle (mr)
L1	58.0			60.5		
QD1	2.1336	-145.2		2.1336	-124.1	
L2	7.8			.3		
QF1	2.1336	124.1		2.1336	119.3	
bending	38.524		49.17	13.052		40.98
QF2	2.1336	134.8		2.1336	95.1	
L3	7.0			3.07		
QD2	2.1336	-153.3		2.1336	-104.5	
L4	50.0			28.0		
L5	8.0			10.0		
L6	42.0			18.0		
QD3	2.1336	-164.5		2.1336	-150.3	

Element	length (m)	grad. (Kg/m)	angle (mr)	length (m)	grad. (Kg/m)	angle (mr)
L7	9.0			3.07		
QF3	2.1336	127.9		2.1336	112.6	
bending	38.524		49.17	13.052		40.98
QF4	2.1336	129.8		2.1336	116.4	
L8	10.0			1.5		
QD4	2.1336	-170.7		2.1336	-128.1	
L9	38.0			35.0		
Total	323.92		98.34	202.59		81.96

The solid angle accepted by the proton beam is .81 μ ster and by the π beam is .82 μ ster. In both cases the beam width at the momentum slit is about .8 mm and the first order resolution

$$\left(\frac{\Delta p}{p}\right)_{min} = \frac{\text{Image radius}}{\text{Dispersion}}$$

is just slightly greater than the limit

$$\frac{\Delta p}{p} = \frac{\Delta \theta}{\theta}$$

where θ is the bending angle and $\Delta\theta$ is the beam divergence in the bending magnets. For the 200 BeV beam Res = .022% and $\Delta\theta/\theta$ = .021%. The use of a doublet lens leads naturally to the separation of vertical and horizontal waists so that the cleanup slit is sufficiently downstream that it does not interfere with the momentum slit and is subjected to a somewhat broadened beam in the horizontal plane.

Tolerances

The effects of regulation, magnet displacement, and magnet rotation have been investigated for the 200 BeV beam with Ll = 42 m. The results should not be too different for Ll = 58 m.

1) Regulation

$$\underline{BM} \quad \frac{\Delta p}{p} = \frac{-\Delta\theta}{\theta} = \frac{-\Delta B}{B} = \frac{-\Delta I}{I}$$

Thus .05% resolution means $0(10^{-4})$ regulation in bending magnet supplies.

QM Each quad gradient was varied in turn by ± .1%

Quad in error	$\frac{\Delta p}{p}$ %
none	.0205
D1	.0206
F1	.0209
F2	.0209
D2	.0206

For such small changes the effect of similtaneous mis-settings will be additive.

2) Alignment

Alignment errors of .2 mm transverse displacement and 5 mr rotation were considered.

BM Δx and Δy affect aperatures only

Rotation about z-axis (roll):

$B_y = B_o \cos\delta$

$B_x = B_o \sin\delta$

The bend in the vertical direction is not critical; the change in B_y is second order and thus much smaller than regulation effects.

Rotation about x-axis (pitch):

The effect on B_y is again second order. The loss of vertical aperture from a 5 mr rotation is a non-trivial 3 cm.

Rotation about y-axis (yaw):

The loss of horizontal aperture is 3 cm for a 5 mr rotation.

QM

$$\Delta B_y = \frac{\partial B_y}{\partial x} \Delta x = 125 \text{ Kg/m} \times .0002 \text{ m} = .025 \text{ kg}$$

$$\Delta = \frac{\Delta B_y \times L_Q}{B\rho} = .008 \text{ mr}$$

$$\frac{\Delta p}{p} = \frac{\Delta}{\theta} = \frac{.008}{49.17} = .016\%$$

This added to the ideal first order resolution gives $\frac{\Delta p}{p}$ = .037%. Thus a horizontal displacement of .2 mm per quad is a bit large for .05% resolution. This high alignment tolerance is required only if the absolute value of the central momentum is needed to .05%; the width of the pass band is not affected by transverse displacement. This calculation assumes the bending increment is placed in the parallel beam where its disruptive effect is greatest. Because the divergence is greater in the regions where the quads are situated the effect calculated by TRANSPORT is a little smaller.

Quad rotated	$\frac{\Delta p}{p}$ %
none	.021
D1	.027
F1	.029
F2	.029
D2	.027

Δy introduces a non-critical vertical bending.

Rotation about z-axis (roll):

A coupling between x and y motions is introduced with consequences that are small. TRANSPORT gives a first order range of Res = .0205-.0210%.

Rotation about x & y (pitch and yaw). These are second order effects because the displaced equilibrium orbit is half the time to one side half the time to the other of the ideal orbit.

Second order effects

The principal second order effect is the change in image size due to the chromatic abberration term $\frac{\Delta p}{p} x'_{obj}$. This coupling is calculated by TRANSPORT to be

$$\Delta x_{image} = T_{126} \frac{\Delta p}{p} x'_{obj} = .35\ (.05\%)(.47\ mr) = .08\ cm$$

for the L1 = 58 m 200 BeV beam. This Δx amounts to 10% of the image size and therefore a 10% degradation of resolution. Runs with BM sextupole included and excluded look the same to two figures so that sextupole is apparently negligible.

There is sufficient uncertainty about the correctness of the second order features of the code to encourage some skepticism about these results.

Momentum Bite

Apparently because of the design symmetry the projection of the apertures onto the horizontal phase plane at the production target produces a very simple figure. Although there are eight vertices corresponding to the intersection of projections of entrance and exit apertures for the four focusing quads, these lie very nearly on four lines forming a parallelogram. Thus, for any momentum where opposite vertices lie over the target emittance the transmission is constant at its maximum value. For other momenta the transmission varies linearly because the parallelogram shape is nearly independent of momentum over the range of non-zero transmission. From Figure 2 one see that the actual momentum range Δp transmitted by the two beams is nearly the same. On the series of aperture projection plots from which this graph was made there are a few cases where BM apertures creep in to mess up the shape slightly, but generally the BM apertures lie just outside and parallel to the apertures of the focusing quadrupoles on either side of them. The graph has been drawn for $\Delta p>0$ only but is symmetric about $\Delta p = 0$.

FIGURE 2

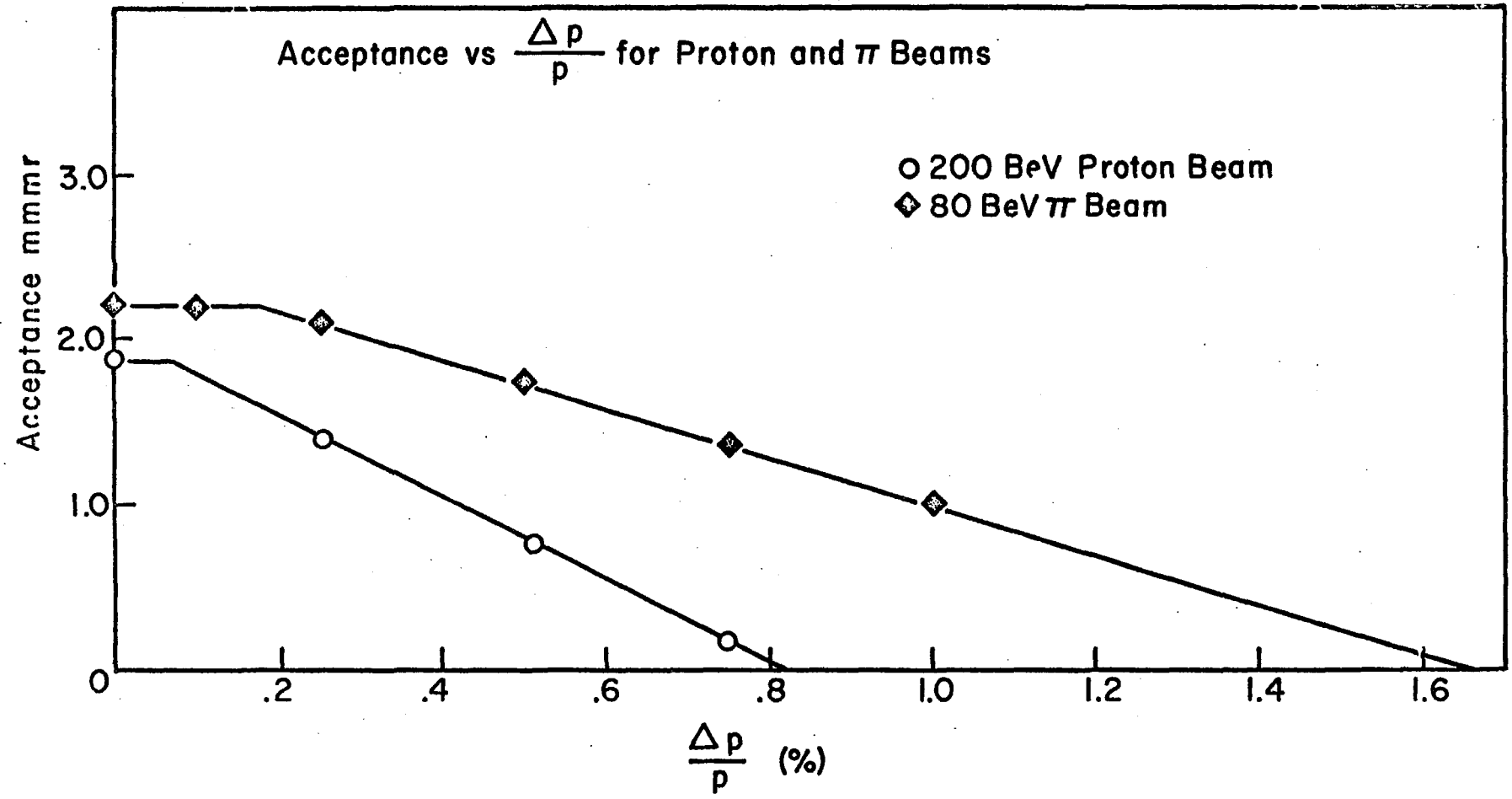
Acceptance vs Δp/p for Proton and π Beams
200 BeV Proton Beam
80 BeV π Beam
Acceptance mmmr
3.0
2.0
1.0
0
.2
.4
.6
.8
1.0
1.2
1.4
1.6
Δp/p (%)

APPENDIX VIII

A Preliminary Design of Target Station 2

A. W. Key

1. Introduction

This report lists the details of the beams which have been used in a preliminary design of an NAL target station. The scale drawing of this layout appears separately and Figure 1 presents a schematic diagram. Main Ring bending magnets and quadrupoles, with characteristics given in Table I, have been used throughout. All beams have been crudely scaled from two beams of maximum momenta 80 and 200 BeV/c provided by J. Maclachlan. (See Appendix VII.) Details of the methods of scaling are given in Section 4.

Since all beams have small angular deviations, complete licence has been used in changing all lengths, apart from the spacing of quadrupole doublets, as convenience in arranging the beams dictates. No effort has been made to optimize the beam designs or to shorten the lengths of the beams. In fact, more recent calculations by J. Maclachlan indicate that to achieve the performances assumed here, these beams would probably require more focusing power and sextupole corrections.

It has been assumed that a distance of at least 40 m is required between the target and the first beam element. Within this constraint some effort has been made to fit the six beams within reasonably small production angles without an excessive increase in beam length and resultant decrease in solid angle subtended at the first quadrupole. However,

no systematic optimization has been done, and doubtless the calculated intensities of these beams could be improved with some extra effort. It has been assumed that holes may not be bored in the magnets for insertion of beam pipes.

2. Details of Beams

A summary of the characteristics of the six beams is given in Table 2. Tables 3 through 8 present the same information in slightly more detail.

3. Calculation of Intensities

The intensities available in these beams as observed at the experimental target for protons and $\pi^{\pm}$ mesons are presented in Figures 2 through 4. The details of the methods of calculation are given in Sections 5 and 6.

It has been assumed in these calculations -

(a) that the calculations of Hagedorn-Ranft[1] as given by Walker[2] for p-p collisions are applicable.

(b) that 10^{13} protons at 200 BeV interact in the primary target.

(c) that the effective solid angle for acceptance of particles into a given beam line is that subtended at the target by the entire aperture of the first quadrupole in the beam. These are the solid angles $\Delta\Omega$ given in Table 2. (See Section 5.)

(d) that a momentum resolution of $\Delta p = 100$ MeV/c is applicable to all beams at all energies.

The figures in Walker's report[2] which have been used are:

(a) p production - Figure 9

(b) π^- production - Figure 6

(c) π^+ production - Figure 5

Since beams 3 and 6 use production angles of 3.5 mr, production curves have to be constructed and added to Walker's figures. The method used to do this is detailed in Section 6.

4. Scaling of beams

(a) The effective focal length, F, of a doublet of two quadrupoles of focal lengths, f, separated by a distance A is approximately $\frac{1}{F} = \frac{A}{f^2}$. The spacing of a quadrupole doublet A is scaled from that of a spacing from the relation $\frac{A}{A_o} = \left(\frac{f}{f_o}\right)^2 = \left(\frac{p}{p_o}\right)^2$ where p and p_o are the maxima momenta of the two beams.

(b) All other lengths have been changed at will to provide a desirable beam spacing. As far as possible higher momentum beams have been allowed longer drift spaces.

(c) J. Maclachlan's design of the 200 BeV beams required 12 bending magnets to achieve Δp = 100 MeV/c. It has been assumed that 2 bending magnets are sufficient for the 30 and 40 BeV beams and the bending magnets for the remaining beams have been arbitrarily chosen between 2 and 12. The sole exception to the general design is beam number 5 (120 BeV) which has had an extra magnet inserted at the front end for reasons of space. It was felt that greater intensity could be achieved in this beam by this procedure which, though it sacrifices solid angle, maintains a reasonable small production angle.

5. Calculation of Solid Angle Subtended by First Quadrupole at Target

Let R (m) be distance from target to entrance of first quadrupole. Than $\Delta\Omega = \frac{\pi x 2 x 5 x \frac{2.64^2}{2}}{(Rx100)^2} = \frac{50.7}{(R/10)^2}$ μsteradian.

6. Calculation of Secondary Particle Yields and Beam Intensities

Reference (2) does not reproduce curves for 3.5 mr. The points at this production angle have been scaled from those at 0 mr. production angle using the following approximation:

Trilling[3] shows that

$$\frac{d^2N}{dp\,d\Omega} \propto e^{-cp_T^2}$$

$$\propto e^{-cp^2\theta^2}$$

with $c = 3$

Thus

$$\left.\frac{d^2N}{dp\,d\Omega}\right)_{\theta=3.5\,mr} = e^{-3*p^2*(3.5*10^{-3})^2} \left.\frac{d^2N}{dp\,d\Omega}\right)_{\theta=0}$$

$$= e^{-0.003675(p/10)^2} \left.\frac{d^2N}{dp\,d\Omega}\right)_{\theta=0}$$

Table I

Details of Main Ring Magnets Used in Design

	Aperture (in^2)	Length (cm)	Width (cm)	Bend for 200 GeV (mr)
Bending Magnet (BM)	2x4	607	63.5	8
Quadrupole (DQ or FQ)	2x5	213	63.5	-

Table II

Summary of Beam Characteristics

Beam Number	Maximum Momentum (GeV/c)	Production Angle (mr)	Length of Beam (m)	No. of Dipoles	No. of Quadrupoles	(1) Δp %	$\Delta\Omega$ uster.	$\Delta p\,\Delta\Omega$ 10^{-7} GeV steradian
1	30	+20	121.58	2	8	.333	3.17	3.17
2	80	+10	186.37	4	8	.125	1.39	1.39
3	200	+ 3.5	309.78	12	8	.050	1.51	1.51
4	40	-20	141.58	2	8	.250	3.17	3.17
5	120	-10	229.87	7	8	.083	1.27	1.27
6	200	- 3.5	300.58	12	8	.050	1.39	1.39

(1) Assume Δp = 100 MeV/c for all beams.

Table 3

1. 30 BeV π, p beam.

(a) Production angle + 20 mradians. (b) Angle of bend in BM at 9kg = 53.3 mradians.

(c) Total length of beam = 121.58m (d) Total Bend = 106.6mr.

(e) Total number of dipoles = 2 (f) Total number of quadrupoles =

Component	Length (m)	Cumulative Distance (m)	Component	Length (m)	Cumulative Distance (m)
Tgt	0		DQ_5	2.13	87.92
0	40	40	0	.3	88.22
DQ_1	2.13	42.13	FQ_6	2.13	90.35
0	.3	42.43	0	.3	90.65
FQ_2	2.13	44.56	BM_2	6.07	96.72
0	.3	44.86	0	.3	97.02
BM_1	6.07	50.93	FQ_7	2.13	99.15
0	.3	51.23	0	.3	99.45
FQ_3	2.13	53.36	DQ_8	2.13	101.58
0	.3	53.66	0	15	116.58
DQ_4	2.13	55.79	2nd Momentum Slit		
0	15	70.79	0	5	121.58
Momentum Slit			Clean-up Slit and experimental target.		
0	5	75.79			
Clean-up Slit					
0	10	85.79			

Table 4

2. 80 Bev π, p beam.

(a) Production angle + 10 mradians.

(b) Angle of bend in BM at 9 kg = 20 mradians.

(c) Total length of beam = 186.32m

(d) Total bend = 80mr.

(e) Total no. of dipoles = 4

(f) Total no. of quadrupoles = 8

Component	Length (m)	Cumulative Distance (m)	Component	Length (m)	Cumulative Distance (m)
Target	0	0	DQ_5	2.13	133.89
O	60.5	60.5	O	2.5	136.39
DQ_1	2.13	62.63	FQ_6	2.13	138.52
O	2.5	65.13	O	.3	138.82
FQ_2	2.13	67.26	BM_3	6.07	144.89
O	5.0	72.26	O	.3	145.19
BM_1	6.07	78.33	BM_4	6.07	151.26
O	0.3	78.63	O	.3	151.56
BM_2	6.07	84.70	FQ_7	2.13	153.69
O	.3	85.0	O	2.5	156.19
FQ_3	2.13	87.13	DQ_8	2.13	158.32
O	2.5	89.63	O	20	178.32
DQ_4	2.13	91.76	2nd Momentum Slit		
O	20	111.76			
Momentum Slit			O	8	186.32
O	8	119.76	Clean up Slit and Experimental Tgt.		
Clean-up Slit					
O	12	131.76			

Table 5

3. 200 BeV p beam.

(a) Production angle + 3.5 mr. (b) Angle of bend in BM at 9kg = 8 mr.
(c) Total Length of Beam = 309.78m (d) Total Bend = 96 mr.
(e) Total number of dipoles - 12 (f) Total number of quadrupoles = 8

Component	Length (m)	Cumulative Distance (m)	Component	Length (m)	Cumulative Distance (m)
Target	0	0	DQ_5	2.13	204.87
0	58	58	0	9	213.87
DQ_1	2.13	60.13	FQ_6	2.13	216.00
0	9	69.13	0	.3	216.3
FQ_2	2.13	71.26	BM_7	6.07	222.37
0	12	83.26	0	.3	222.67
BM_1	6.07	89.33	BM_8	6.07	228.74
0	.3	89.63	0	.3	229.04
BM_2	6.07	95.70	BM_9	6.07	235.11
0	,3	96.00	0	.3	235.41
BM_3	6.07	102.07	BM_{10}	6.07	241.48
0	.3	102.37	0	.3	241.78
BM_4	6.07	108.44	BM_{11}	6.07	247.85
0	.3	108.74	0	.3	248.15
BM_5	6.07	114.81	BM_{12}	6.07	254.22
0	.3	115.11	0	.3	254.22
BM_6	6.07	121.18	FQ_7	2.13	256.65
0	.3	121.48	0	9	265.65
FQ_3	2.13	123.61	DQ_8	2.13	267.78
0,	9	132.61	0	34	301.78
DQ_4	2.13	134.74	2nd Momentum Slit		
Momentum Slit			0	8	309.78
0	8	176.74	Clean-up slit and Experimental target.		
Clean-up Slit					

Table 6

4. 40 BeV π, p beam.

(a) Production angle - 20 mr. (b) Bend in BM at 9 kg = 40 mr.

(c) Total length of beam = 141.58m (d) Total Bend = 80 mr.

(e) Total number of dipoles = 2 (f) Total number of quadrupoles = 8

Component	Length (m)	Cumulative Distance (m)	Component	Length (m)	Cumulative Distance (m)
Target	0		DQ_5	2.13	98.92
0	40	40	0	.8	99.72
DQ_1	2.13	47.13	FQ_6	2.13	101.85
0	.8	42.93	0	.3	102.15
FQ_2	2.13	45.06	BM_2	6.07	108.22
0	.3	45.36	0	.3	108.52
BM_1	6.07	51.43	FQ_7	2.13	110.65
0	.3	51.73	0	.8	111.45
FQ_3	2.13	53.86	DQ_8	2.13	113.58
0	.8	54.66	0	20	133.58
DQ_4	2.13	56.79	2nd Momentum Slit		
Momentum Slit			0	8	141.58
0	8	84.79	Clean-up Slit and Experimental target.		
Clean-up Slit					
0	12	96.79			

Table 7

5. 120 BeV π, p beam.

(a) Production angle = -10 mradians. (b) Bend in BM at 9 kg = 13.3 mradians

(c) Total length of beam = 229.87m (d) Total bend = 93.3mr

(e) Total no. of dipoles = 7 (f) Total no. of quadrupoles = 8

Component	Length (m)	Cumulative Distance (m)	Component	Length (m)	Cumulative Distance (m)
Target	0		DQ_5	2.13	154.13
O	53	53	O	6	160.13
BM_1	6.07	59.07	FQ_6	2.13	162.26
O	4	63.07	O	.3	162.56
DQ_1	2.13	65.20	BM_5	6.07	168.63
O	6	71.20	O	.3	168.93
FQ_2	2.13	73.33	BM_6	6.07	175.00
O	.3	73.63	O	.3	175.30
BM_2	6.07	79.70	BM_7	6.07	181.37
O	.3	80.00	O	.3	181.07
BM_3	6.07	86.07	FQ_7	2.13	183.80
O	.3	86.37	O	6	189.80
BM_4	6.07	92.44	DQ_8	2.13	191.93
O	.3	92.74	O	24	215.93
FQ_3	2.13	94.87	2nd Momentum Slit		
O	6	100.87	O	10	225.93
DQ_4	2.13	103.00	Clean up slit and		
O	24	127.00	Experimental Tgt.		
Momentum Slit					
O	10	137.00			
Cleanup Slit					

Table 8

6. 200 p beam

(a) Production angle = 3.5 mr. (b) Angle of bend in BM at 9kg = 8 m

(c) Total length of Beam = 300.58m (d) Total bend = 0 mr.

(e) Total number of dipoles = 12 (f) Total number of quadrupoles = 8

Component	Length (m)	Cumulative Distance (m)	Component	Length (m)	Cumulative Distance (m)
Target	0		DQ_5	2.13	195.67
0	60.5	60.5	0	9	204.67
DQ_1	2.13	62.63	FQ_6	2.13	206.8
0	9	71.63	0	.3	207.1
FQ_2	2 13	73.76	BM_7	6.07	213.17
0	.3	74.06		.3	213.47
BM_1	6.07	80.13	BM_8	6.07	219.54
0	.3	80.43		.3	219.84
BM_2	6.07	86.50	BM_9	6.07	225.91
0	.3	86.80		.3	226.21
BM_3	6.07	92.87	BM_{10}	6.07	232.28
0	.3	93.17		.3	232.58
BM_4	6.07	99.24	BM_{11}	6.07	238.65
0	.3	99.54		.3	238.95
BM_5	6.07	105.61	BM_{12}	6.07	245.02
0	.3	105.91	0	.3	245.32
BM_6	6.07	111.98	FQ_7	2.13	247.45
0	.3	112.28	0	9	256.45
FQ_3	2.13	114.41	DQ_8	2.13	256.58
0	9	123.41	0	34	292.58
DQ_4	2.13	125.54	2nd Momentum Slit		
0	34	159.54		8	300.58
Momentum Slit			Clean-up Slit and Experimental Target		
	8	167.54			
Clean-up Slit					
	26	193.54			

References:

[1] R. Hagedorn - J. Ranft CERN/ECFA 67/16 Vol 1, 70 (1967)

[2] T. G. Walker - Summer Study Report B.5-68-24.

[3] G. Trilling - UCRL 16830; UCID 10148, p. 25.

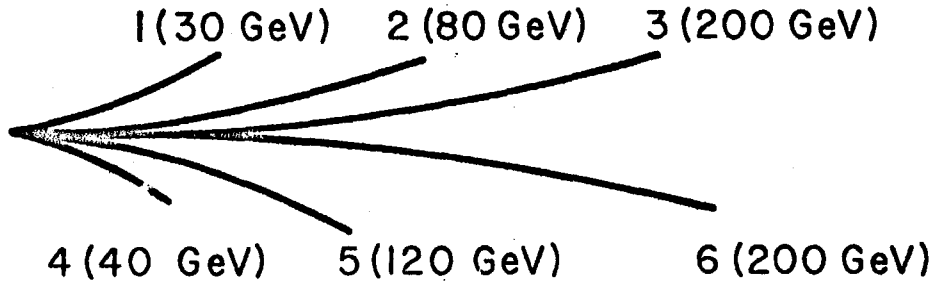

Figure 1
Experimental Area Layout

Figure 2 - Intensities per 10^{13} Interacting Protons at 200 GeV

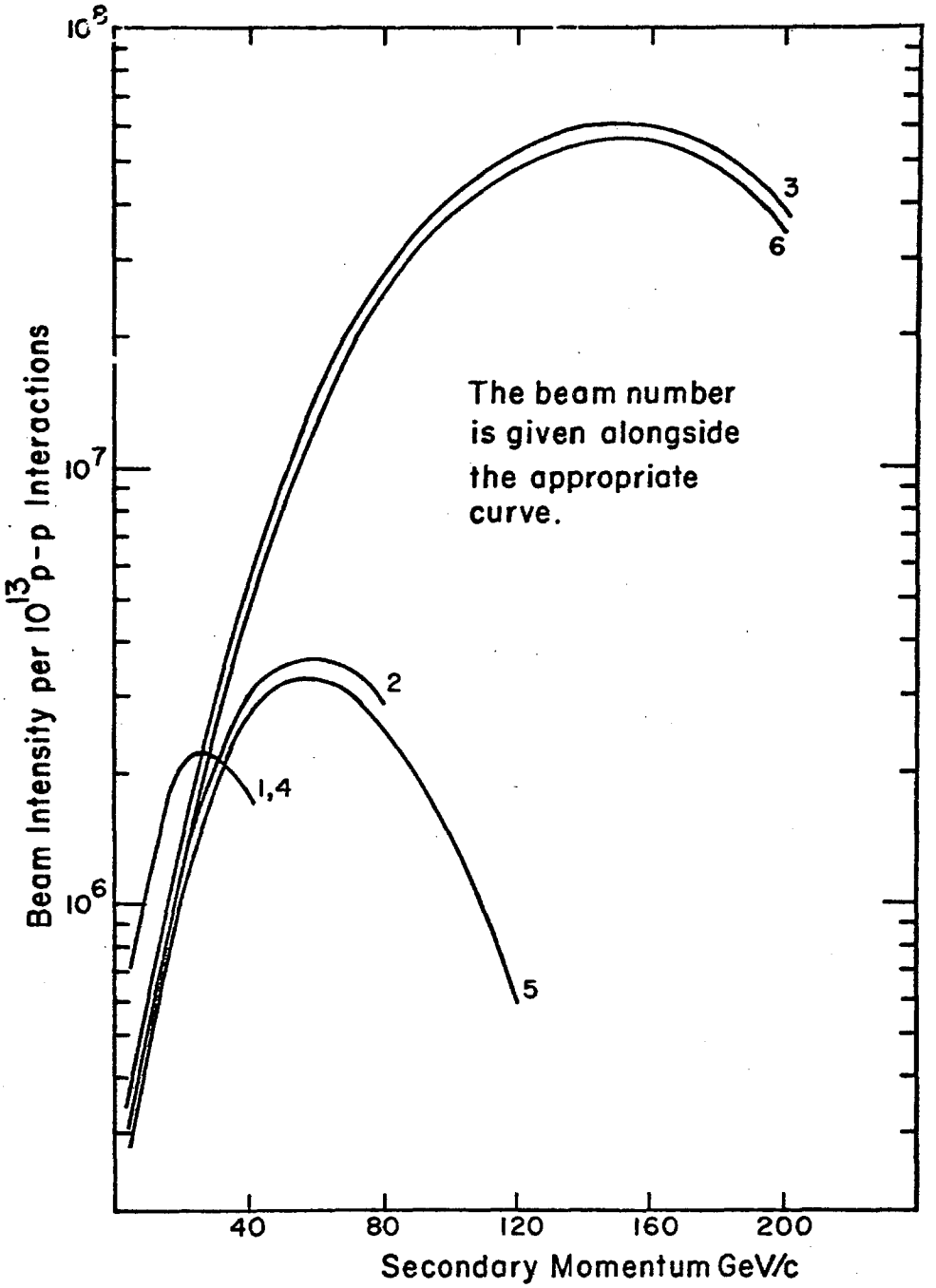

Figure 3 - π^- Intensities per 10^{13} Interacting Protons at 200 GeV

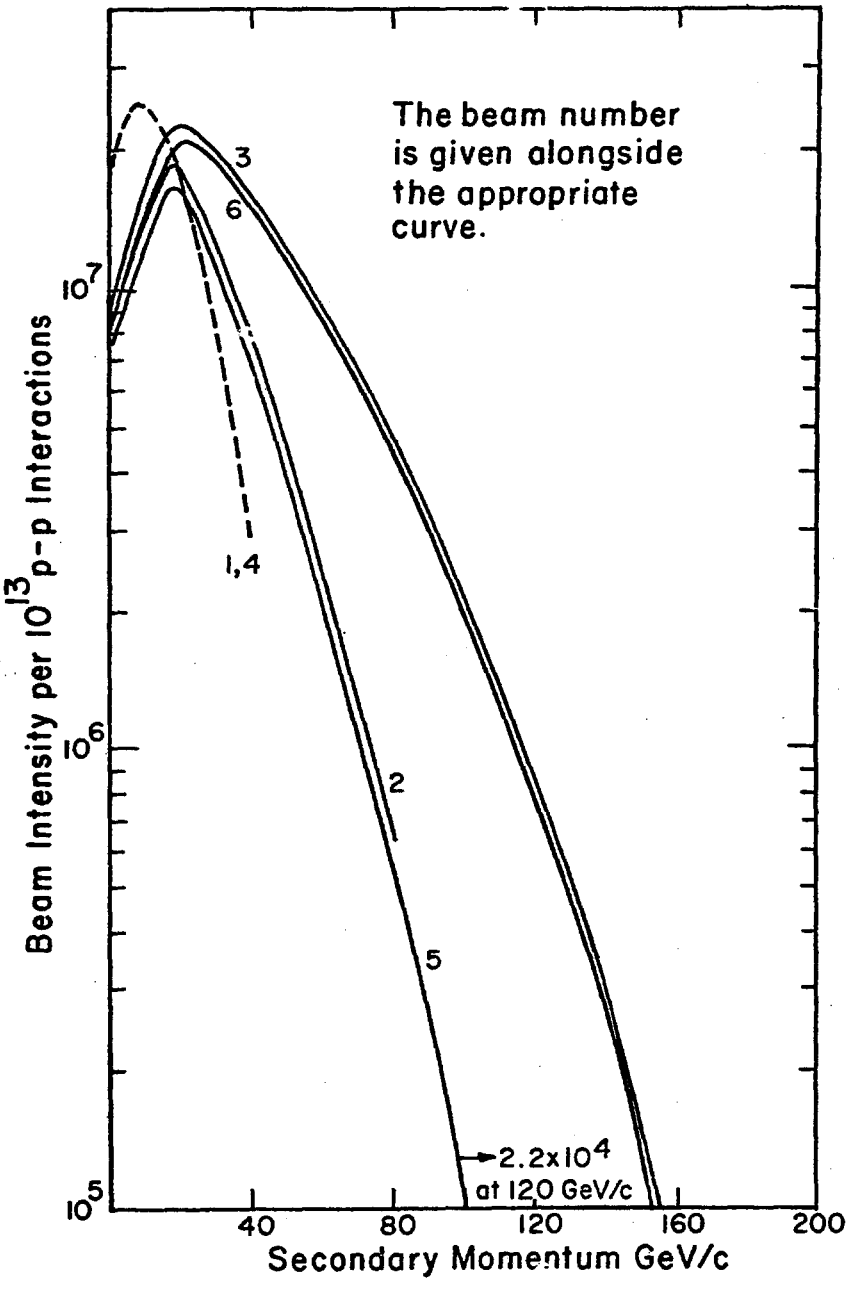

Figure 4 - π^+ Intensities per 10^{13} Interacting Protons at 200 GeV

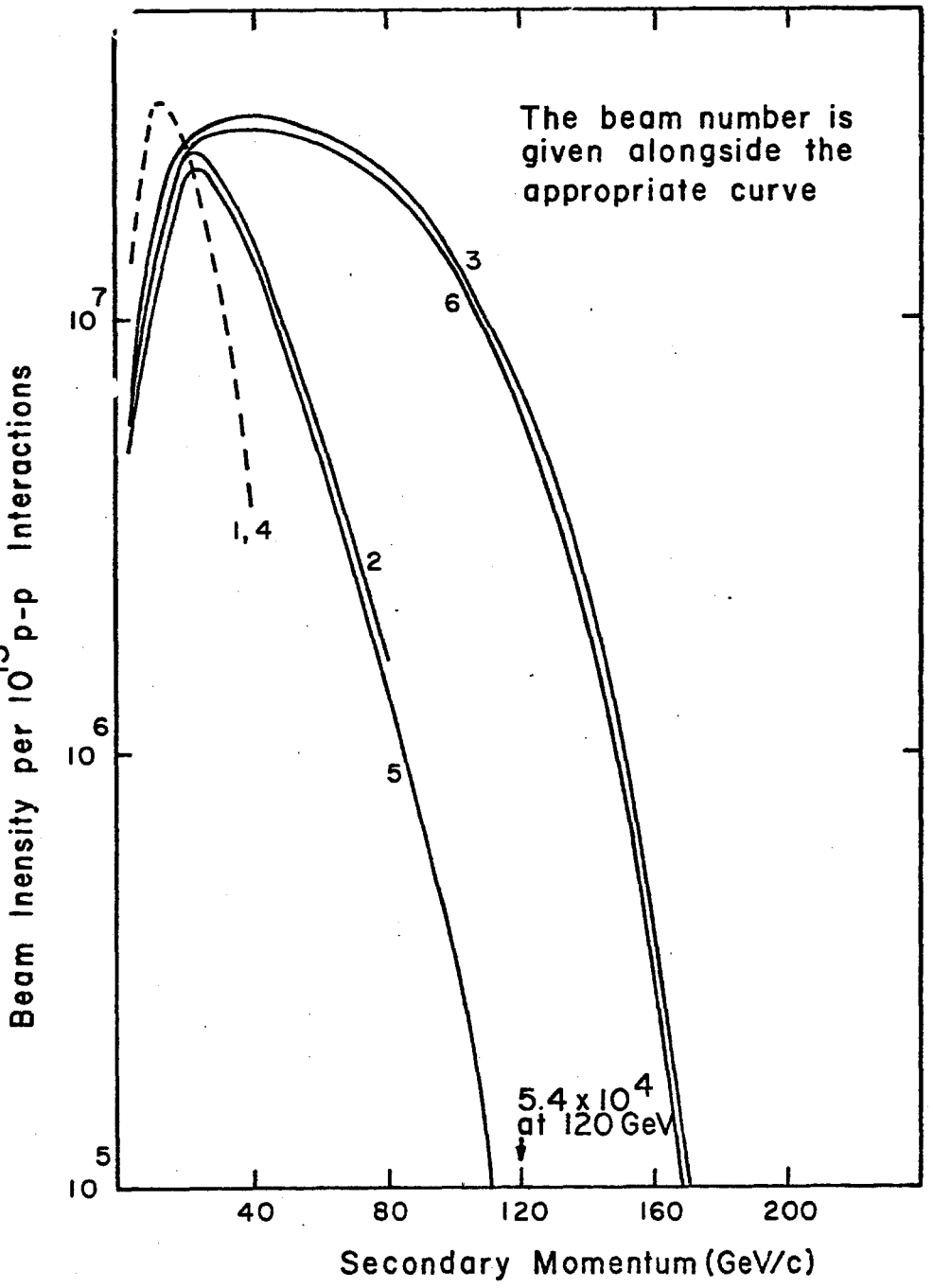

APPENDIX IX. NEUTRINO BEAM DESIGN

Y. Kang, F. Nezrick

ABSTRACT

The important parameters of a neutrino beam have been studied at NAL to develop a conceptual neutrino beam design. It has been found that a neutrino beam with a decay length of 600 m, a shielding thickness of 300 m, and a decay tunnel radius of 0.75 m is quite appropriate under either 200 BeV or 400 BeV operation of the NAL proton synchrotron. It appears useful to fill the decay tunnel with bags of He to substantially reduce the number of secondary beam (π or K) collisions in the decay tunnel. With a focusing system of two elements located inside target station T1, one elastic event in every four pictures of the 25' deuterium bubble chamber can be obtained.

NEUTRINO BEAM DESIGN

The important parameters in a neutrino beam design have been investigated by using a computer program[1] so that a conceptual neutrino beam for NAL could be developed. For the conceptual design work the CKP particle production formula with $K/\pi = 0.15$ has been used. Later in the more detailed design calculations, other particle production formula will be investigated. The π and K mesons with momenta from 7.5 BeV to 157.5 BeV within a maximum production angle of 60 mrad have been used in the calculations. A detector radius of 1.8 m and shielding thickness of 600 m, 150 m, and 70m for earth,

iron, and uranium, respectively were assumed.

A series of detailed calculations were performed to study the following problems:

1. The variation of neutrino flux with decay length for perfect focusing and different shielding materials, earth, iron, and uranium. The effects are illustrated in Figures 1 to 4.

2. The energy spectra for the three optimized geometries using the best decay length for each shielding thickness. (Perfect focusing.) See Figures 5 and 6.

3. The dependence of the neutrino flux on the detector radius. (Perfect, real, and no focusing.) See Figures 7 to 15.

4. The dependence of the neutrino flux on the decay tunnel radius. (Real focusing and no focusing.) See Figure 16 to Figure 18.

5. The neutrino energy spectra for the iron-shielded beam. (Perfect, real, and no focusing.) See Figure 19.

6. The dependence of neutrino flux on the number of focusing elements. (Real focusing.) See Figure 20.

7. Extension to 400 BeV: the dependence of neutrino flux on the decay length for the iron-shielded beam. (Perfect focusing.) See Figure 21 and Figure 22.

8. Optimization of the locations and currents for a two element focusing system.

9. Improvement in real focusing by meson ray traces.

10. The neutrino flux using a thick target. See Figure 23.

11. Neutrino energy spectra for specific pion and kaon momenta. See Figure 24.

12. Energy hardening of the neutrino beam.

13. Neutrino event rate in a deuterium bubble chamber.

A detailed discussion of each set of calculations will be given below.

1) The neutrino flux dependence on decay length for different shield materials - earth, iron and uranium. (Perfect focusing.)

For the assumed shield thickness of 600 m for earth 150 m for iron and 70 m for uranium, the integrated neutrino fluxes passing through the detector were calculated for different decay lengths. The integrated neutrino fluxes above different energies for the different shields are given in Figure 1 and Figure 2 for pion and kaon decays respectively as a function of decay length. The maximum production angle allowed was 20 mrad. The flux variation with decay distance can be understood by recalling that the mean decay distances for the pion and kaon are 55 m/BeV and 7.5 m/BeV respectively. In general, then, the integrated flux of neutrinos from the pion decays slowly increases with increasing decay length, while the integrated flux from the kaon decays decreases with decay length because of the solid angle factor.

For pion neutrinos, the integrated flux above 6 BeV for the iron-shield beam is about three times as large as that from the earth-shielded beam with a decay length of 600 m. The flux from the iron-shielded beam is only about 30% inferior to that from the uranium-shielded beam.

For the iron-shielded beam, the neutrino flux produced

from kaon decays becomes comparable to that produced from pion decays for the neutrino energies above about 25 BeV at a decay length of 600 m. The kaon neutrino flux above 35 BeV for an iron-shielded beam is about three times greater than that from the earth-shielded beam, while it is about 30% inferior to that for the uranium-shielded beam.

The integrated neutrino flux from π and K decays passing through the detector as a function of decay distance is given in Figure 3 for neutrino energies above 2.5 BeV and 40 BeV. Under the assumptions of the calculations an optimized decay length can be obtained from Figure 3 for each shield thickness and is given in Figure 4 for the integrated flux above 2.5 BeV. The optimal decay length increases with shielding thickness but its choice is not critical because of the flatness of the integrated flux curves in Figure 3. For our purposes a decay length of 600 m has been chosen because it produces a neutrino flux which is within 10% of being optimal for both high and low energy neutrinos.

2) The energy spectra for the three different muon-shielded beams with optimized decay lengths. (Perfect focusing.)

Using the optimum decay lengths from Figure 4 for the shields of uranium, iron and earth, the energy distribution of the neutrinos passing through the detector was calculated and is shown in Figure 5. The iron-shielded beam is inferior to the uranium-shielded beam in the energy regions below 7 BeV and around 30 BeV, while it is far superior to the earth-shielded beam below 15 BeV.

The solutions presented in Figure 5 use a maximum allowed production angle of 20 mrad. A slightly different set of decay lengths better illustrate the effect of the shield thickness on the neutrino energy distribution. Using a maximum allowed production angle of 60 mrad, Figure 6 gives the neutrino energy distribution for three different shield thicknesses for a fixed decay length and for the earth-shielded beam. For the fixed decay length one observes that as the shield thickness is increased one loses the neutrinos from the low energy pion and kaon decays while the neutrino flux from the higher energy pion decays remain essentially constant. If the decay length and shield thickness are both increased, then the neutrino flux contribution is reduced from the kaon decays and from the low energy pion decays but is increased from the higher energy pion decays. This is as expected from the ratio of the particle mean decay length to the length of the decay region.

3) The variation of the neutrino energy distribution with the detector radius. (Perfect, real, and no focusing.)

Using the iron-shielded beam with a 600 m decay length, the neutrino fluxes have been determined for different distances from the neutrino beam axis at the detector. We present nine graphs which give the radial dependence of the neutrino flux resulting from pion decays, from kaon decays, and from pion plus kaon decays, for perfect (Figures 7, 8, 9), real (Figures 10, 11, 12), and no focusing (Figures 13, 14, 15), respectively.

First consider the perfectly-focused case for pions,

Figure 7, for kaons, Figure 8, and for pions plus kaons, Figure 9. The general properties of these distributions can be roughly understood by considering the 6 BeV neutrino distribution from perfectly-focused pions, Figure 7. The flux per unit area has a maximum at about 1.5 m radius and it decreases for larger and smaller detector radii. These decreases reflect an interplay of the pion decay kinematics and the range of decay distances from the detector. For example, consider the decay of 20 BeV pions to give 6 BeV neutrinos, and which are copiously produced. The neutrino decay angle is 3.5 mrad so that it passes through the detector at radial distances from 3.1 m to 1.0 m depending on whether the pion decayed at the beginning or the end of the 600 m long decay region. In other words, fixed-energy neutrinos from a fixed-energy pion decay pass through a sharply defined radial band at the detector. The inside and outside radii of this region at the detector are determined by the shortest and longest pion decay distance from the detector. The distributions on Figure 7 do not have sharp limits because the energy spectrum of neutrinos is produced from a fixed-energy pion decay, and the pion production energy spectrum is broad and decreases logarithmically with increasing energy.

From Figure 7 we see that the pion neutrinos start to show a focused behavior at about 12 BeV while from Figure 8 the kaon neutrinos start showing a focused behavior at about 40 BeV. Combining the contributions of pion and kaon decays gives the distributions shown in Figure 9. The neutrino flux between 30 BeV and 40 BeV shows rather unusual variations when the kaon

contribution is included.

Using real focusing elements we obtain Figures 10, 11 and 12. The no-focusing case produces the distributions given on Figures 13, 14 and 15. The shapes of the no-focusing distributions can be understood in a manner similar to the perfect focusing case by including the decay angle from the meson production angle rather than from the neutrino beam axis. By comparing Figures 12 and 15 the advantages and quality of focusing are apparent.

4) The neutrino flux dependence on decay tunnel diameter. (Real- and no-focusing).

From Figures 16, 17 and 18 we see that a maximum useful decay tunnel diameter is 4 m for a non-focused beam and 3 m for a real-focused beam to optimize the flux in a detector 3.6 m in diameter. Making the tunnel radius a function of the distance from the target was also investigated. It was found that the decay tunnel could be appreciably reduced near the shield without a noticable flux loss. A tunnel diameter of 1.5 m reduces the flux at the detector by only 30%, but gives a considerable reduction of the transverse size of the muon shield.

5) The neutrino energy spectrum for the iron-shielded beam. (Perfect, real- and no-focusing.)

In Figure 19 we show a comparison of neutrino fluxes for the perfect, real- and no-focusing cases. The real-focusing calculation includes absorption in the horn material and target, while the perfect focusing includes only absorption in the target. On the average the real focusing is about 75% of perfect

focusing. The maximum production angle accepted was 20 mrad in the calculation.

6) The neutrino flux dependence on the number of the focusing elements.

A neutrino beam focusing system of three elements has been studied. A preliminary design of the first focusing element was made and the efficiency of the second and third elements was studied. From Figure 20, the two-element system is only 10% poorer than the three-element system, while the one-element system is 50% efficient. The first two-focusing elements are located inside the target station while the third element could be outside. During the first stages of the neutrino program at NAL a two-element system should be completely adequate.

7) Extension to 400 BeV: the flux dependence on decay length for the iron-shielded beam. (Perfect focusing.)

The 200 BeV accelerator will be extended to 400 BeV after several years' operation. We hope to extend the neutrino beam to 400 BeV with minimum modifications. Our main concern is not to change the location of the large bubble chamber, the beginning of the muon shield and the target station.

We see in Figure 21 that the optimum decay length would be 1,000 m but 600 m is also quite reasonable because of the broadness of the optimum. Figure 22 gives the dependences for the pion and kaon decays individually. With the decay length of 600 m, we have a high-energy flux (> 50 BeV) comparable to that at 1,000 m. Hence the selection of 600 m is quite adequate because we suppose that the higher energy neutrinos will be more important

than the low energy neutrinos when 400 BeV protons are available.

Therefore, the decay length of 600 m has been chosen in both 200 BeV and 400 BeV operations. The neutrino flux increase over the 200 BeV case is about a factor of two, as we expect.

8) Optimization of the locations and currents of the two focusing elements.

For focusing elements of a given shape we can find the best positions and current for the two elements to maximize the neutrino flux passing through the detector. Assuming the first element current, we calculated the neutrino flux as a function of the second element location and current. By a process of iterations we obtain the best values for the second element position and current. For a three-element system we proceeded in a similar way after we had fixed the location and current of the second element. However, we have not investigated the three-element system by optimizing simultaneously the currents in the three elements and the position of the second and third elements. The best parameters of the elements shown in Figure 23 were determined and are given in Table I.

TABLE I

	First Element	Second Element	Third Element
Location from target (m)	0	50	200
Current of focusing element (MA)	0.27	0.4	0.3

9) Efficiency improvement in real focusing by ray traces.

Up to this point the focusing system and flux distributions have been calculated without knowing in detail the individual pion and kaon trajectories in the decay tunnel. We have also

studied by ray traces how the individual particles with given momenta and production angles behave throughout the focusing system. The study of ray traces gives some idea of how the shape of the inner conductor of a focusing element should be modified to improve a particular momentum region at a particular production angle. By repeating ray traces and optimization of the focusing element parameters alternatively, we can improve the focusing systems.

10) The neutrino flux from a thick target.

We have calculated a neutrino flux efficiency as a function of position along the target and found that the flux was fairly uniform along the 2.5 m long target region. (See Figure 23.) We also calculated the fluxes for short and long targets (0.45 m long Cu and 2.5 m long Li target with the same radii of 2 mm). The Li target is better in the flux yield by 15% than Cu target. A flux distribution for a 2.5 m long thick target is given in Figure 24 and will be used for the estimate of a neutrino event rate.

11) The neutrino energy spectra for given pion or kaon momenta.

In Figure 25, we give the neutrino energy spectra passing through the detector for fixed pion or kaon momenta calculated for the real focusing case. The energy spectra taper off at the lower and higher energy ends. If we had 4π acceptance by the focusing elements, we would observe a rectangular spectrum.

12) The energy hardening of the neutrino beam.

In some experiments, only the high energy neutrinos (greater than 40 BeV) are desirable while the interactions of low energy neutrinos (less than 40 BeV) are regarded as background. In general, the low energy pions or kaons are very

sensitive to the focusing in the first element. With this aim in mind, we have calculated fluxes by changing the current signs of two elements with respect to the first. For one focusing and two defocusing elements, for example, the high energy neutrinos are reduced by a factor of two while the low energy neutrinos are reduced by a factor of four. The focusing effect on the oppositely-charged particles is found to be negligible. This was a very preliminary investigation but looks promising. Further improvement will be investigated by current variations and modifying the inner conductor shapes.

13) Neutrino elastic event rate.

A neutrino event rate in the 25-ft deuterium bubble chamber is determined on the basis of the flux yield shown in Figure 24. The 25-ft bubble chamber will have a usable fiducial volume of 70,000 litres with an approximate 7 m length. Since the inelastic cross section is less well known at present, only the elastic events will be considered with an assumed cross section of 10^{-38} cm^2. The actual event rate is expected to be much greater than we estimate here because of a large neglected inelastic event rate. The 200 BeV proton intensity is 5×10^{13} protons/pulse. The event rate is about one event every four pictures. In this estimate we included the attenuation effect in the decay tunnel (filled with bags of He), absorption effect in the focusing elements and the target, the target efficiency and also the reduction due to the tunnel radius being 0.75 m. We have also normalized the CKP formula to fit

the experimental data better, i.e., enhance by a factor of two the π^+ spectrum and give a K to π ratio of 10 percent. A further detail of the percent of events in different energy regions is given in Table II.

TABLE II

Neutrino Energy (BeV)	2.5-10	10-40	40-100
Pion (%)	80	20	-
Kaon (%)	-	70	30
Total (%)	78.9	20.6	0.5

Conclusions:

We have calculated the important parameters in a neutrino beam design to develop a conceptual neutrino beam at NAL. The parameters of the neutrino beam design follow:

1. The decay length: 600 m
2. The muon shielding thickness: 100 m of iron plus 200 m of earth under the 200 BeV operation and 300 m of iron shielding under the 400 BeV operation.
3. The radius of the decay tunnel: 0.75 m
4. The above parameters do not change in going from 200 BeV to 400 BeV operation. The positions of the target station, the beginning of the muon shielding, and the bubble chamber do not change.
5. During the first stage of the neutrino program, we will use a two-element focusing system which is located inside the target station.
6. When including the absorption effects in the focusing elements, the absorption in the target, the target

efficiency, the attenuation effect in the decay tunnel, the efficiency of a two-element focusing system, and the reduction due to the tunnel radius being 0.75 m, the elastic event rate is estimated to be one event in every four pictures of the 25-ft deuterium-filled bubble chamber.

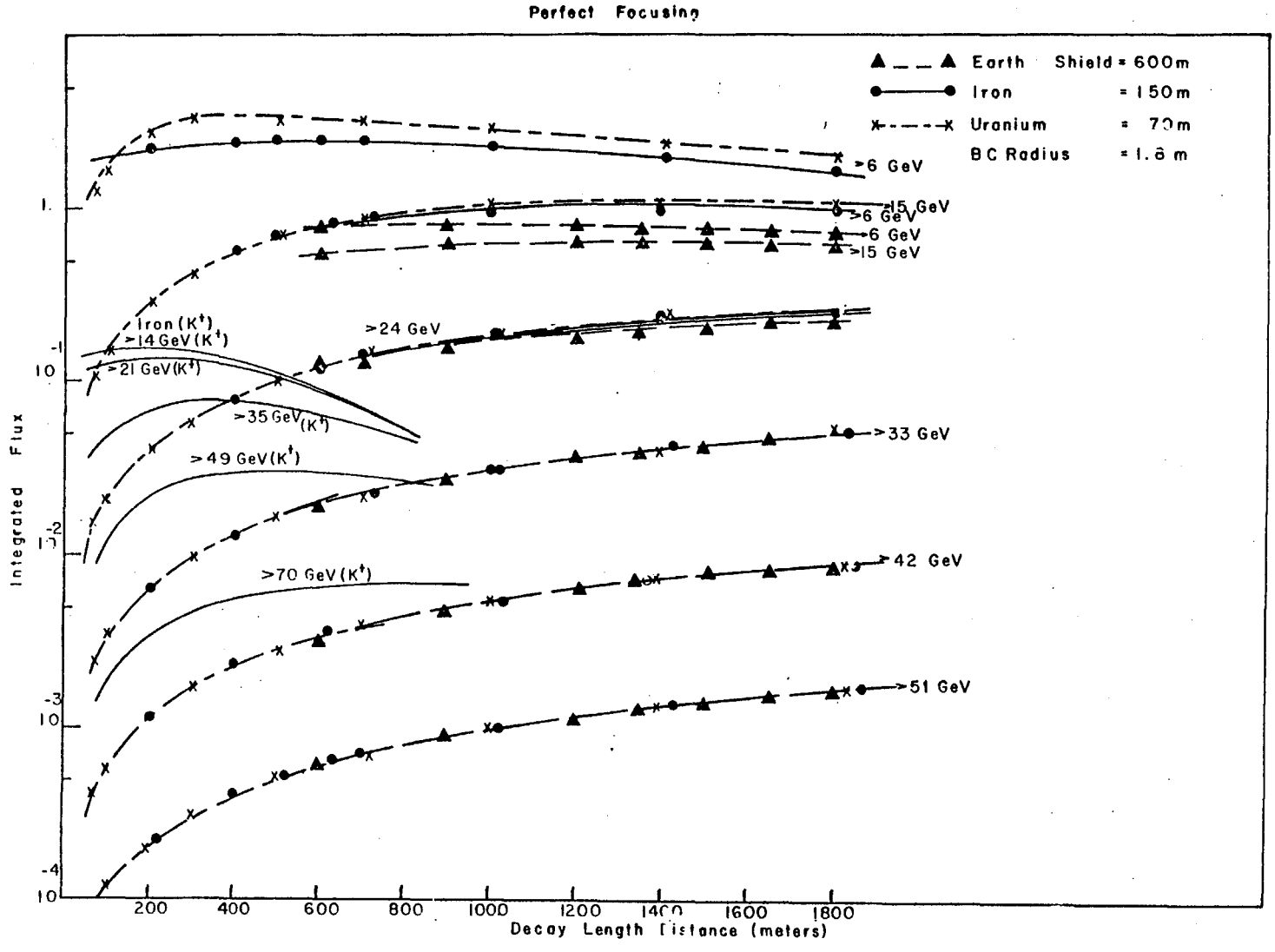
Perfect Focusing
Earth Shield = 600m
Iron = 150m
Uranium = 70m
BC Radius = 1.6 m
>6 GeV
>15 GeV
>6 GeV
>6 GeV
>15 GeV
Iron (K+)
>14 GeV (K+)
>21 GeV (K+)
>24 GeV
>35 GeV (K+)
>49 GeV (K+)
>33 GeV
>70 GeV (K+)
>42 GeV
>51 GeV
Integrated Flux
1
10-1
10-2
10-3
10-4
200
400
600
800
1000
1200
1400
1600
1800
Decay Length Distance (meters)

Figure 1

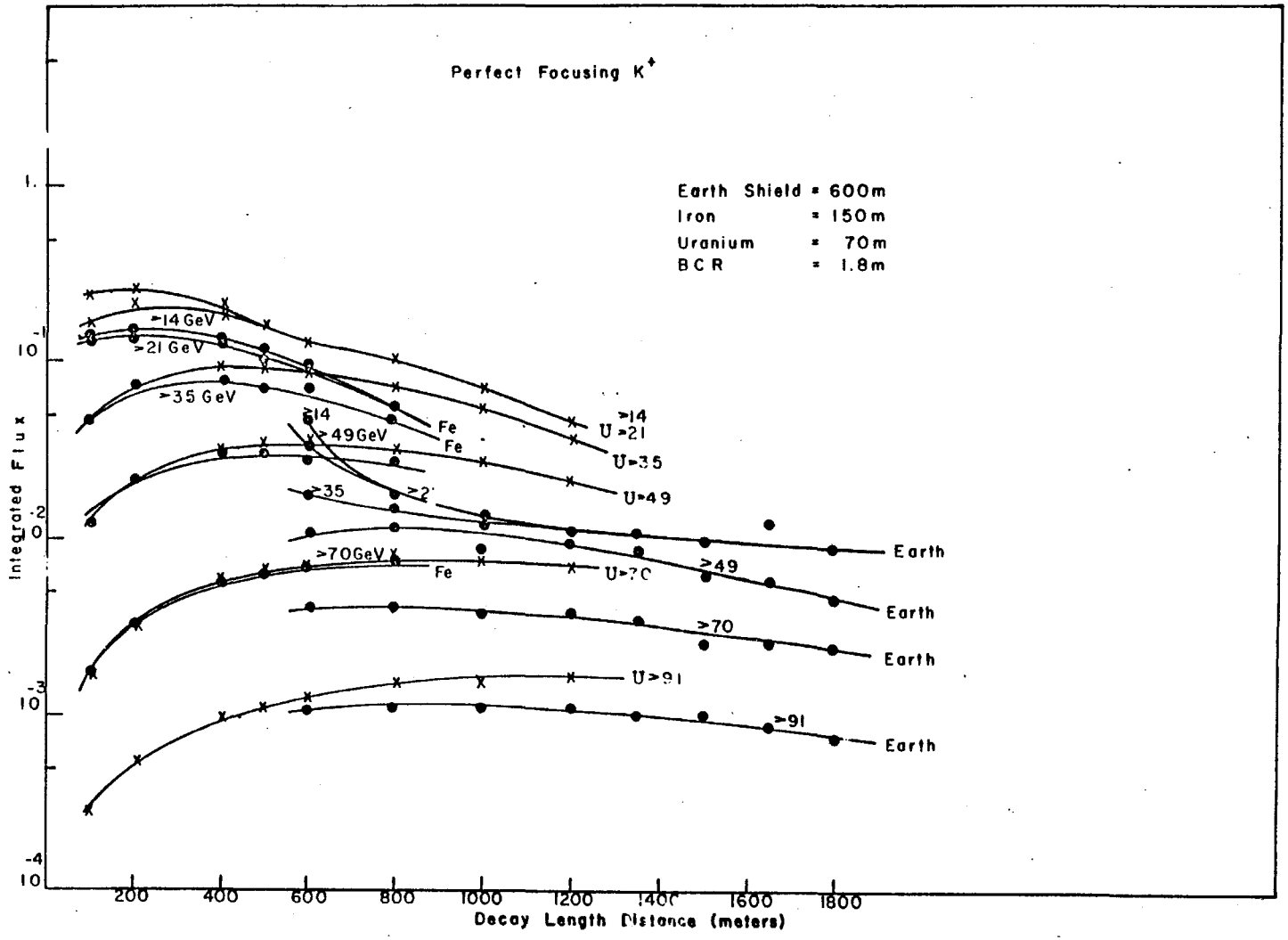
Perfect Focusing K+
Earth Shield = 600m
Iron = 150m
Uranium = 70m
BCR = 1.8m
Integrated Flux
Decay Length Distance (meters)
>14 GeV
>21 GeV
>35 GeV
>49GeV
>70GeV
>91
Fe
U>21
U>35
U>49
U>70
U>91
Earth

Figure 2

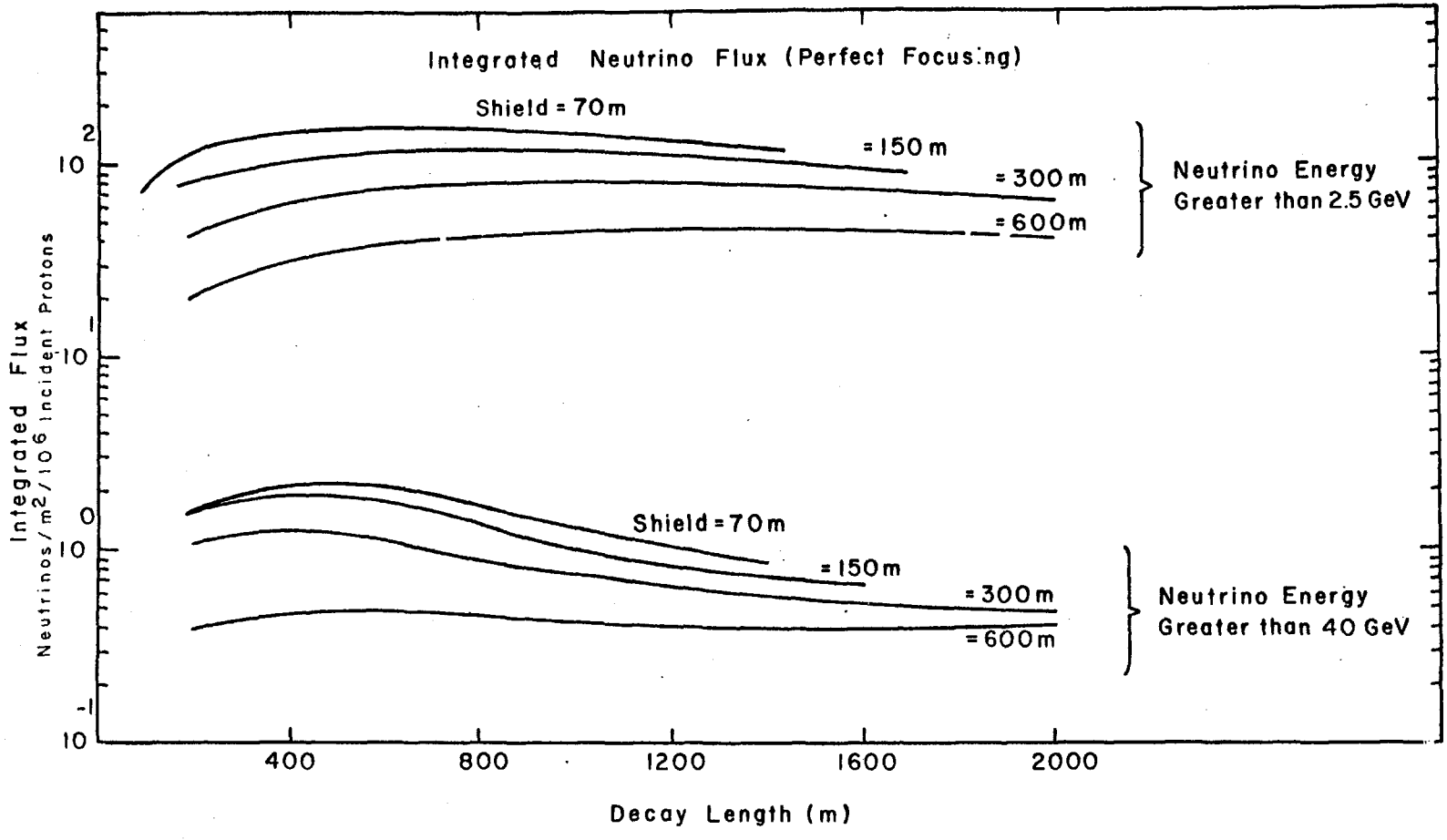
Integrated Neutrino Flux (Perfect Focusing)
Shield = 70m
= 150 m
= 300 m
= 600m
Neutrino Energy
Greater than 2.5 GeV
Shield = 70m
= 150m
= 300 m
= 600m
Neutrino Energy
Greater than 40 GeV
Integrated Flux
Neutrinos/m2/10^6 Incident Protons
2
10
-1
10
0
10
-1
10
400
800
1200
1600
2000
Decay Length (m)

Figure 3

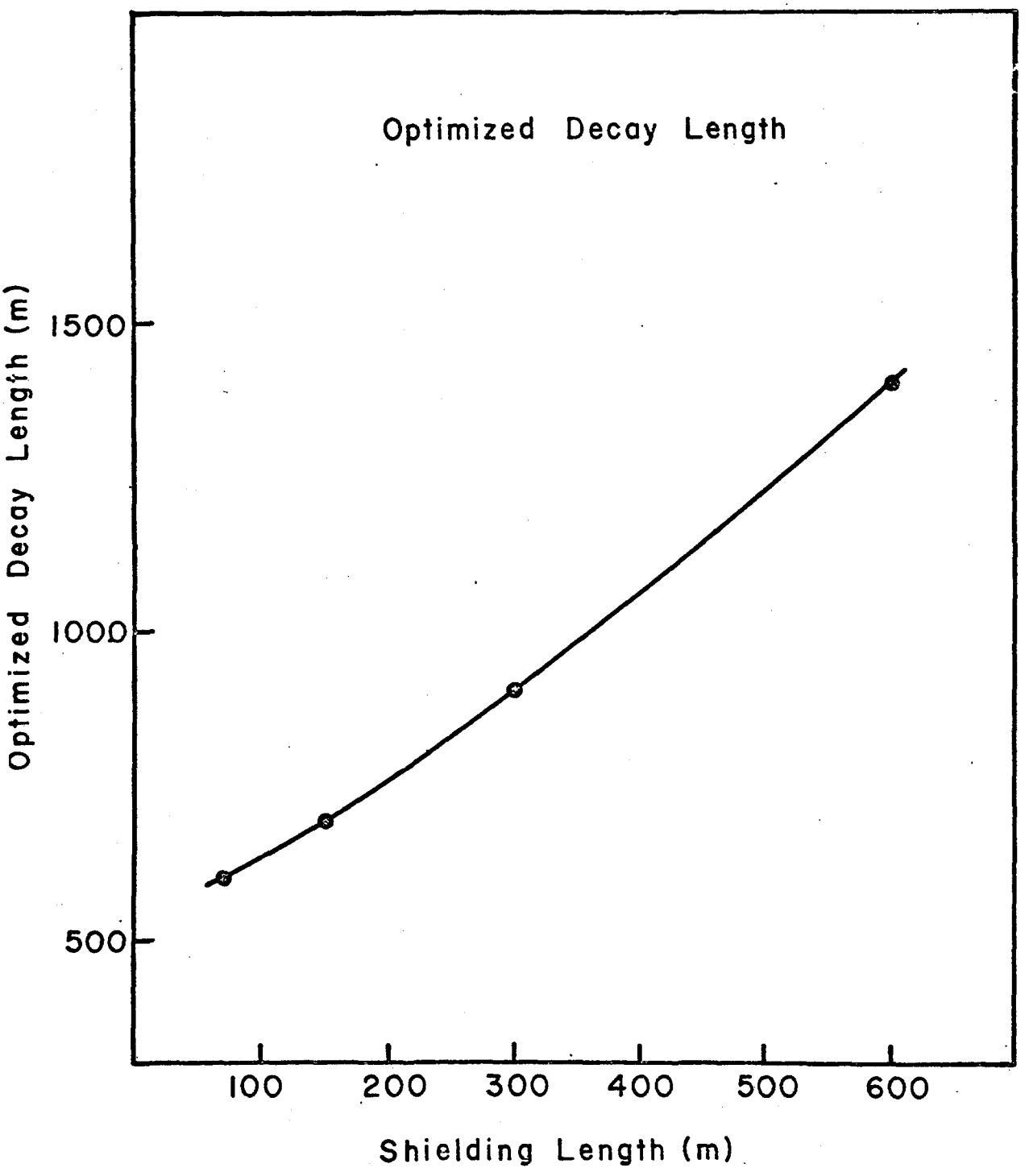
Optimized Decay Length
Optimized Decay Length (m)
1500
1000
500
100
200
300
400
500
600
Shielding Length (m)

Figure 4

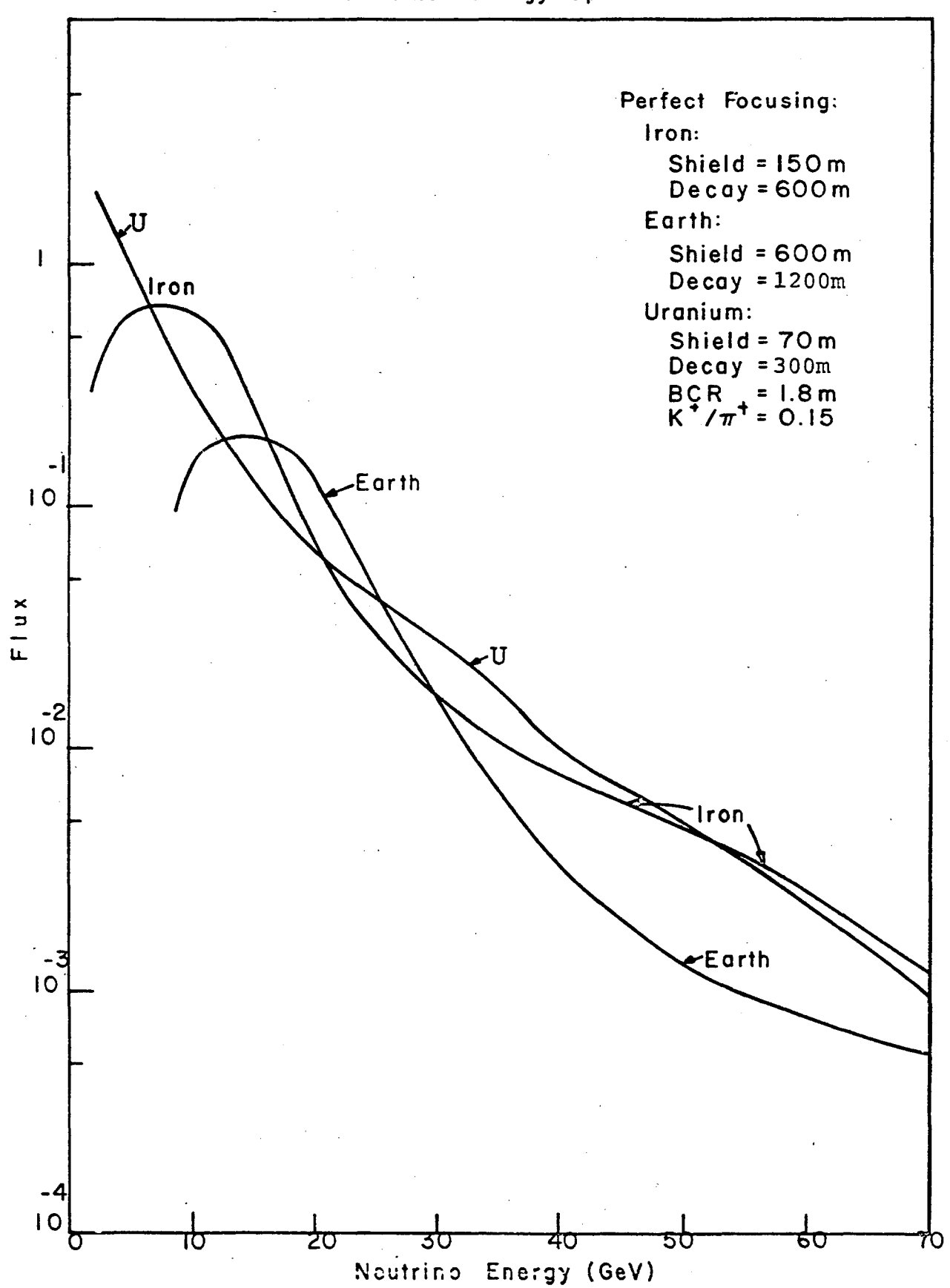
Neutrino Energy Spectrum
Perfect Focusing:
Iron:
Shield = 150 m
Decay = 600 m
Earth:
Shield = 600 m
Decay = 1200 m
Uranium:
Shield = 70 m
Decay = 300 m
BCR = 1.8 m
K+/π+ = 0.15
U
Iron
Earth
U
Iron
Earth
Flux
1
10^-1
10^-2
10^-3
10^-4
0
10
20
30
40
50
60
70
Neutrino Energy (GeV)

Figure 5

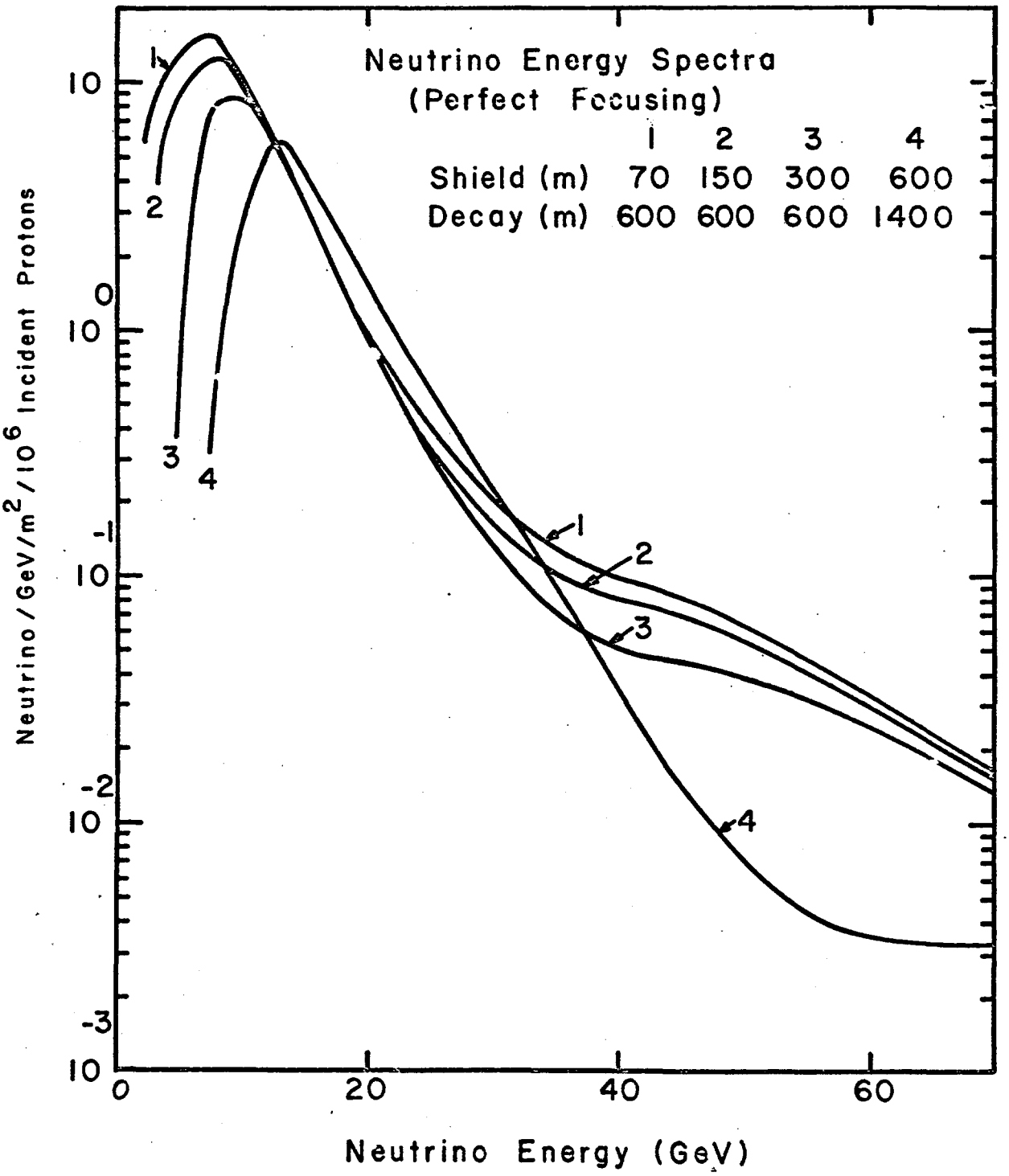
Neutrino Energy Spectra
(Perfect Focusing)
1 2 3 4
Shield (m) 70 150 300 600
Decay (m) 600 600 600 1400
Neutrino / GeV/m² / 10⁶ Incident Protons
Neutrino Energy (GeV)
10
0
10
-1
10
-2
10
-3
10
0
20
40
60
1
2
3
4

Figure 6

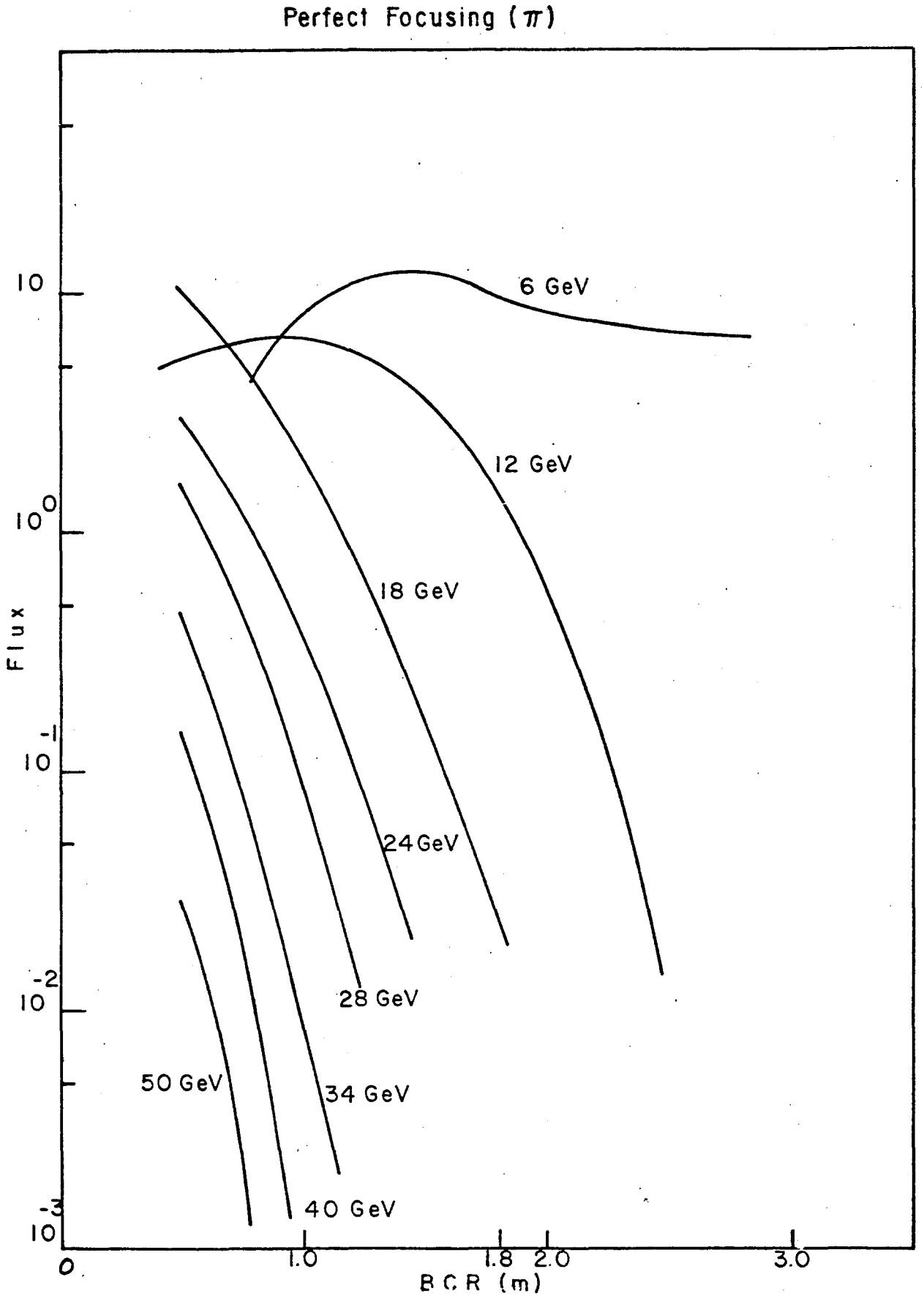
Perfect Focusing (π)
10
10^0
10^-1
10^-2
10^-3
Flux
6 GeV
12 GeV
18 GeV
24 GeV
28 GeV
34 GeV
40 GeV
50 GeV
0
1.0
1.8
2.0
3.0
BCR (m)

Figure 7

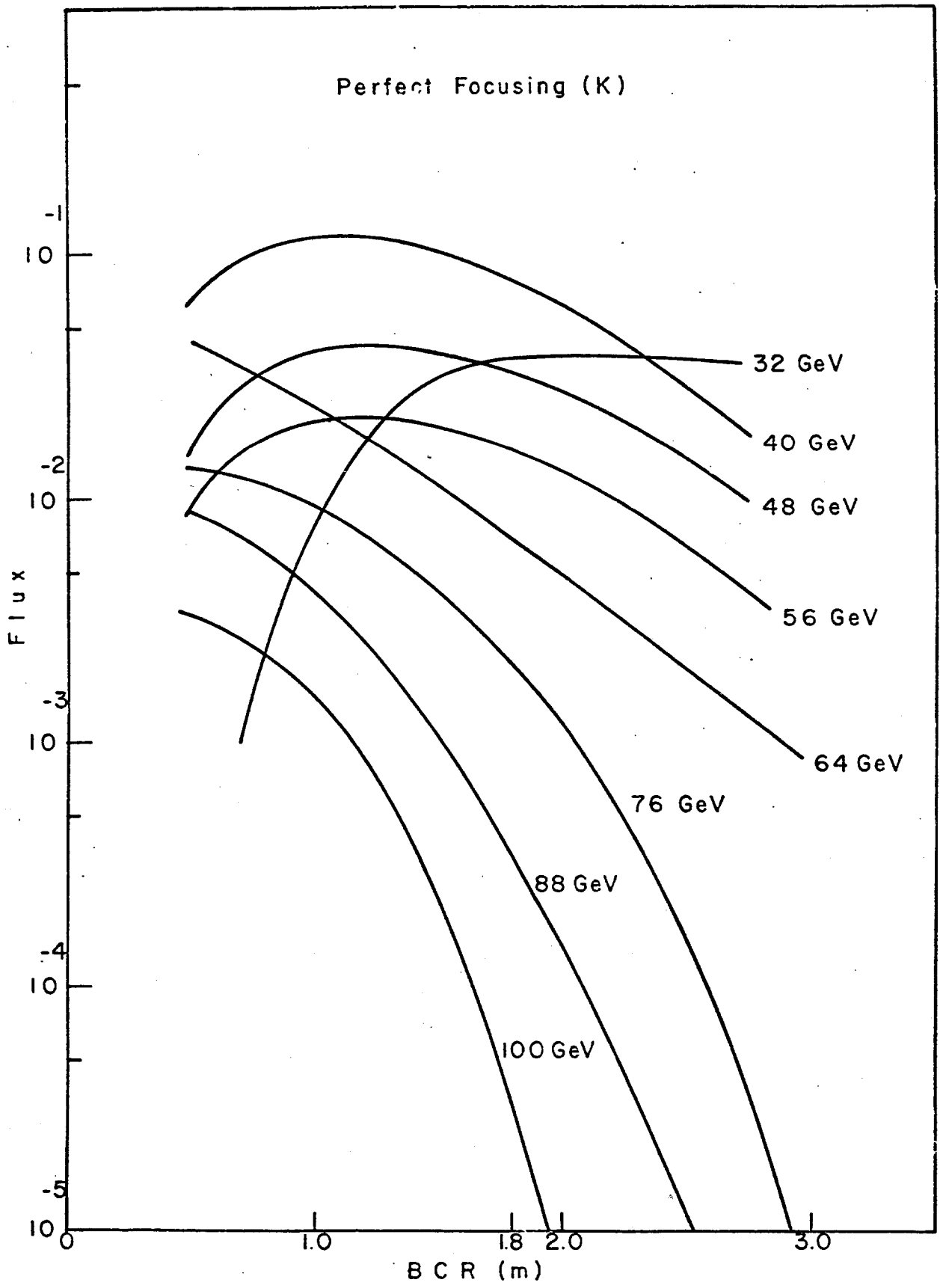
Perfect Focusing (K)
Flux
10^-1
10^-2
10^-3
10^-4
10^-5
32 GeV
40 GeV
48 GeV
56 GeV
64 GeV
76 GeV
88 GeV
100 GeV
0
1.0
1.8
2.0
3.0
BCR (m)

Figure 8

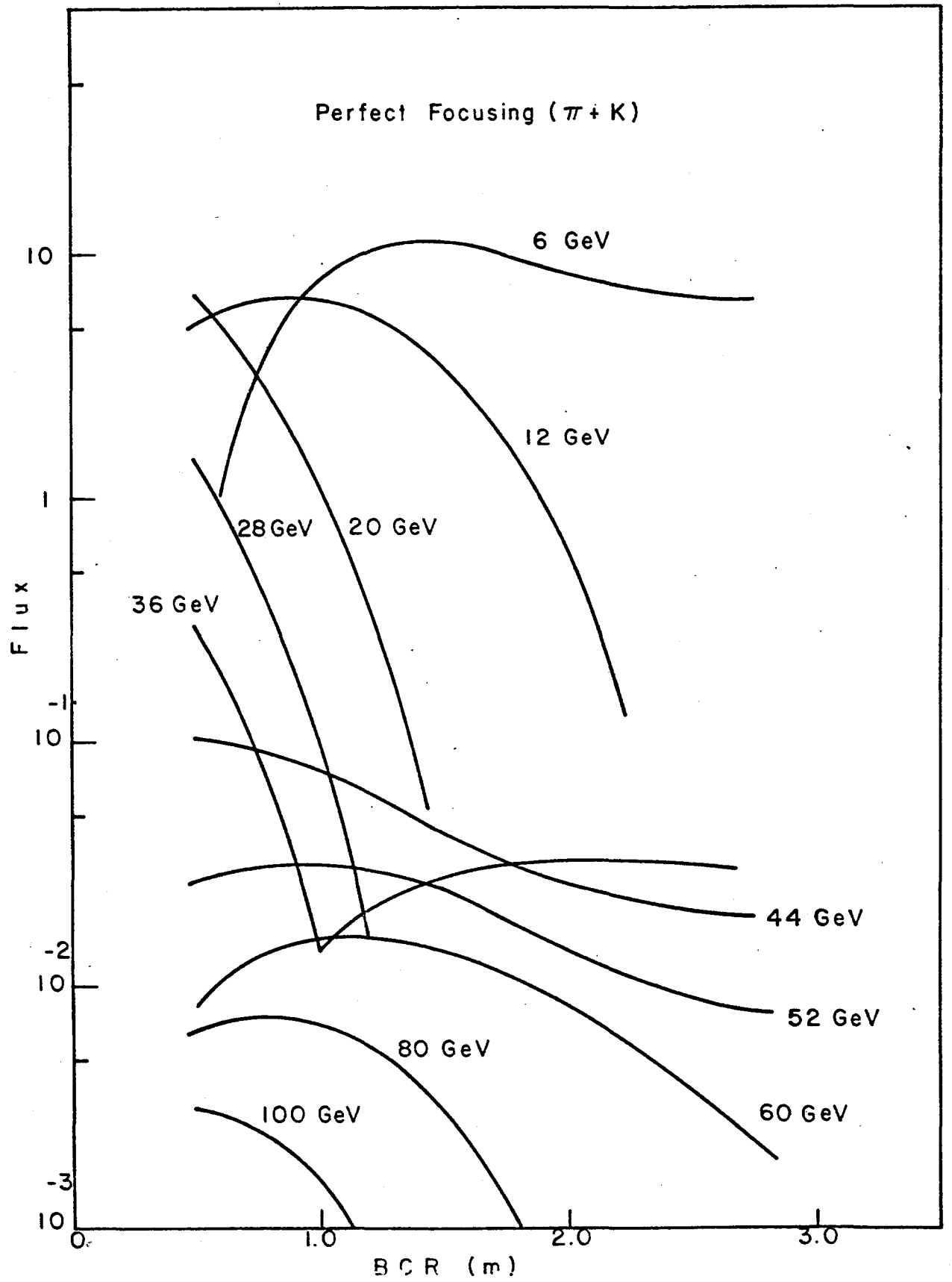
Perfect Focusing (π + K)
6 GeV
12 GeV
28 GeV
20 GeV
36 GeV
44 GeV
52 GeV
80 GeV
60 GeV
100 GeV
Flux
10
1
-1
10
-2
10
-3
10
0
1.0
2.0
3.0
BCR (m)

Figure 9

Real Focusing (Pions)

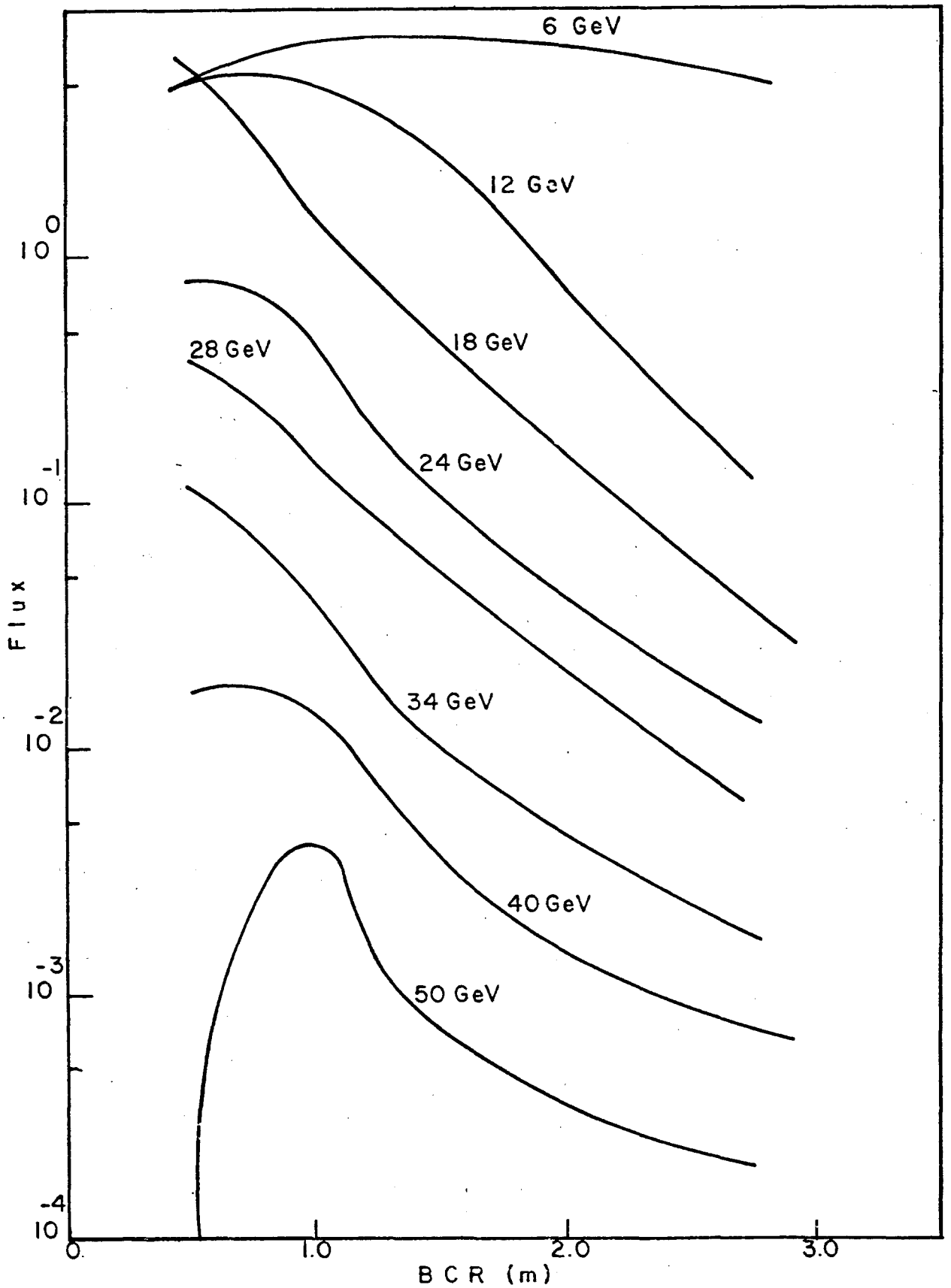

Figure 10

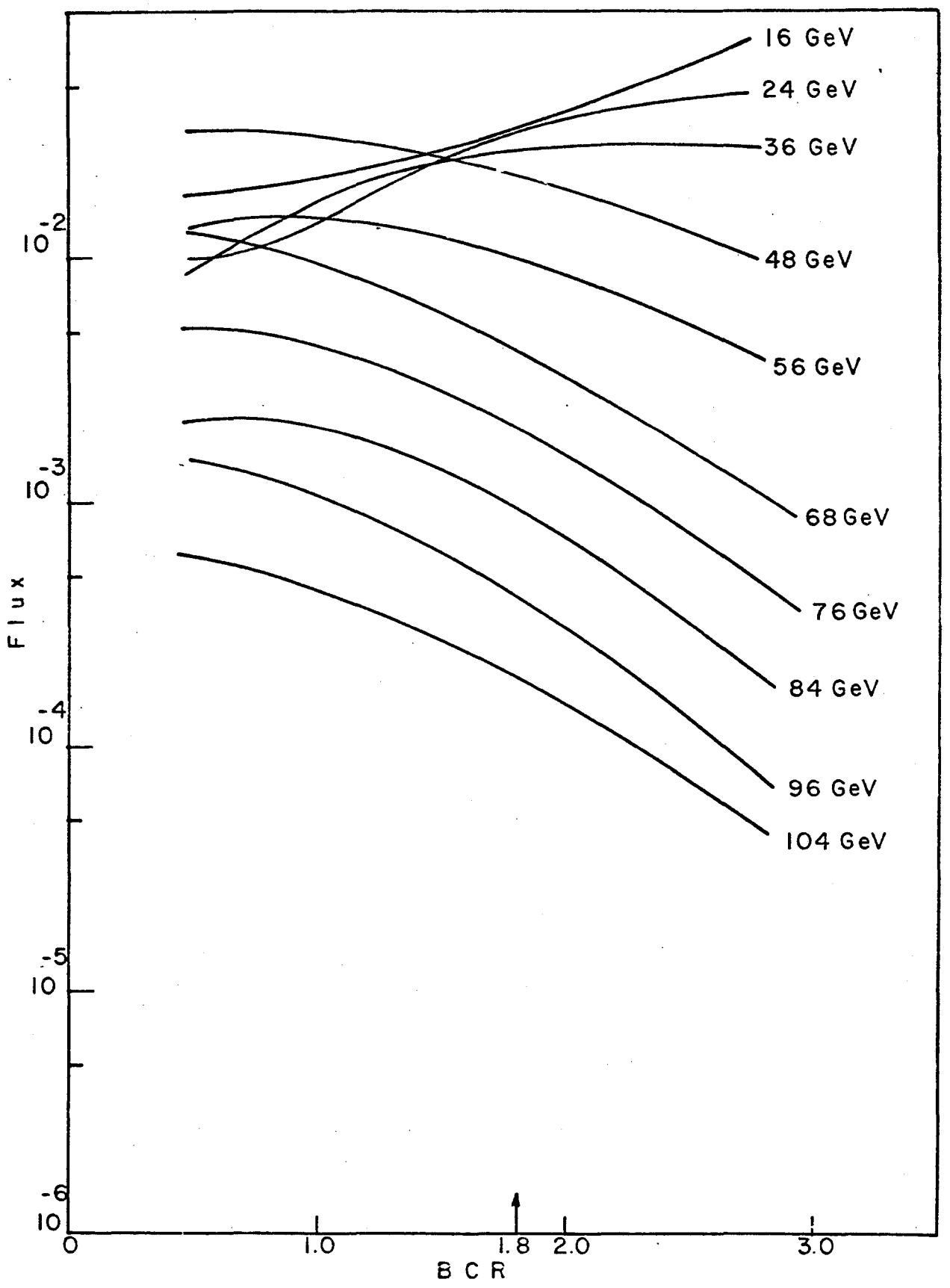
Real Focusing (Kaons)
16 GeV
24 GeV
36 GeV
48 GeV
56 GeV
68 GeV
76 GeV
84 GeV
96 GeV
104 GeV
Flux
10^-2
10^-3
10^-4
10^-5
10^-6
0
1.0
1.8
2.0
3.0
B C R

Figure 11

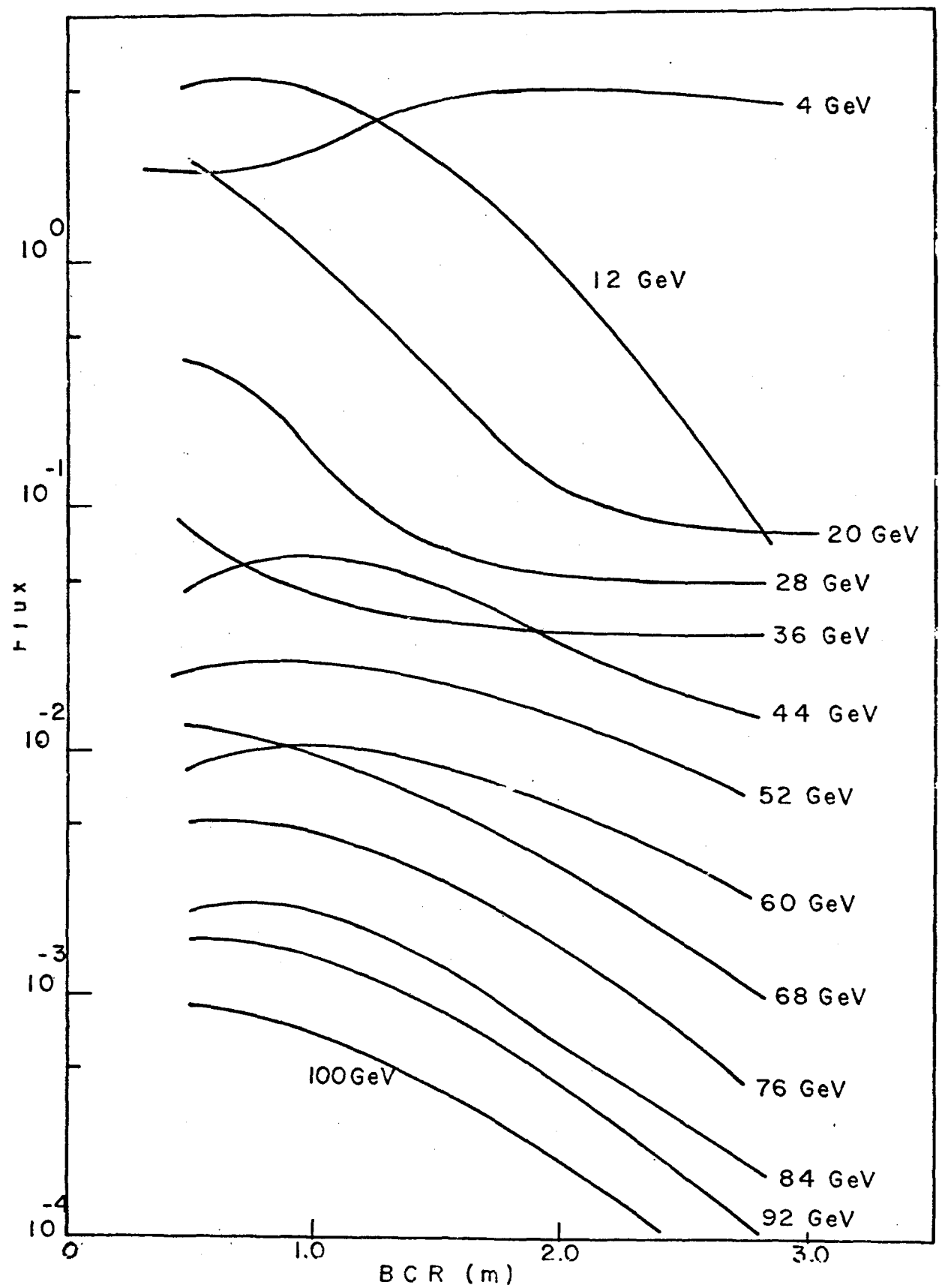
Real Focusing (π+K)
4 GeV
12 GeV
20 GeV
28 GeV
36 GeV
44 GeV
52 GeV
60 GeV
68 GeV
76 GeV
84 GeV
92 GeV
100GeV
Flux
10^0
10^-1
10^-2
10^-3
10^-4
0
1.0
2.0
3.0
BCR (m)

Figure 12

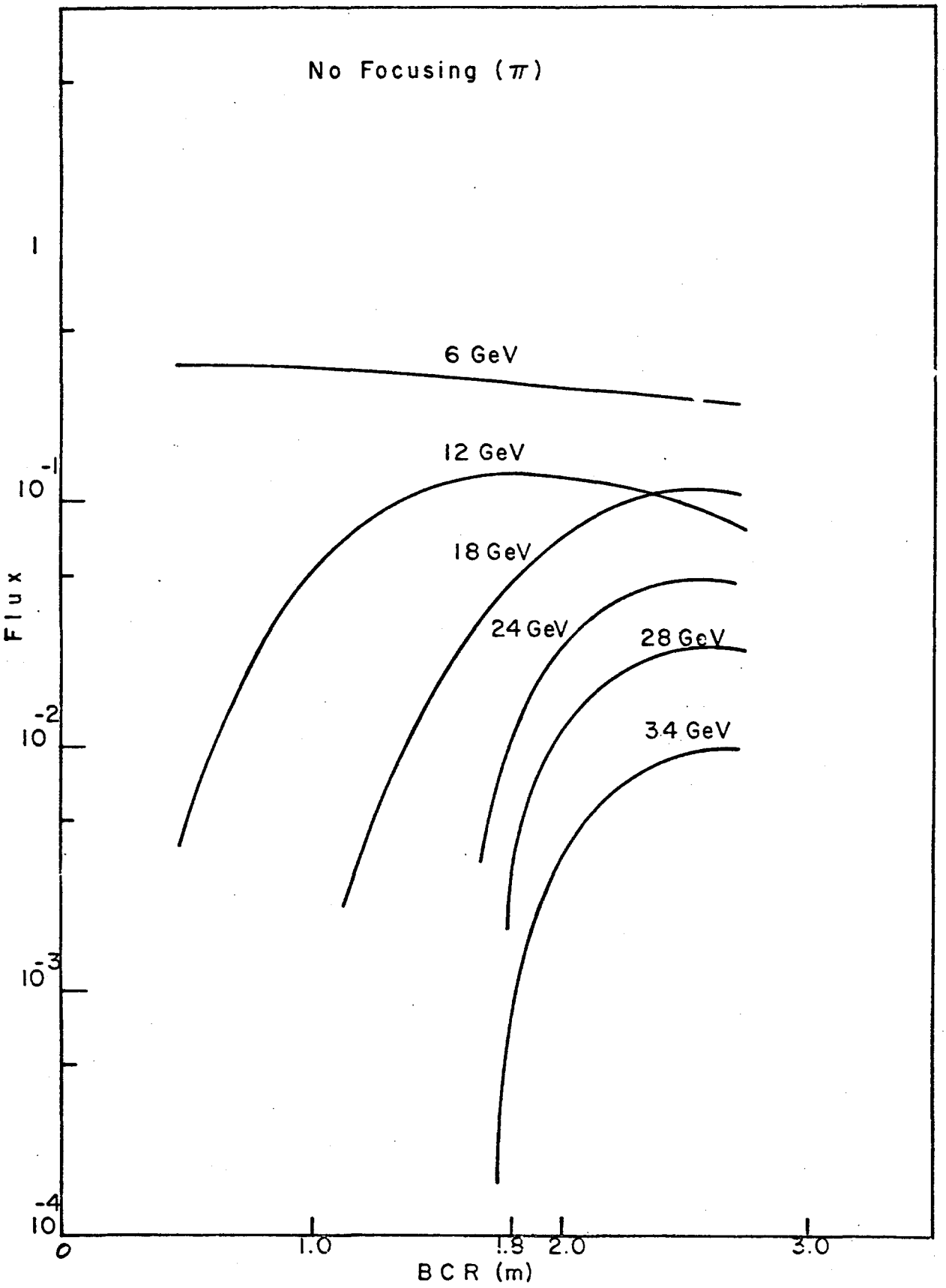
No Focusing (π)
6 GeV
12 GeV
18 GeV
24 GeV
28 GeV
34 GeV
Flux
1
10-1
10-2
10-3
10-4
0
1.0
1.8
2.0
3.0
BCR (m)

Figure 13

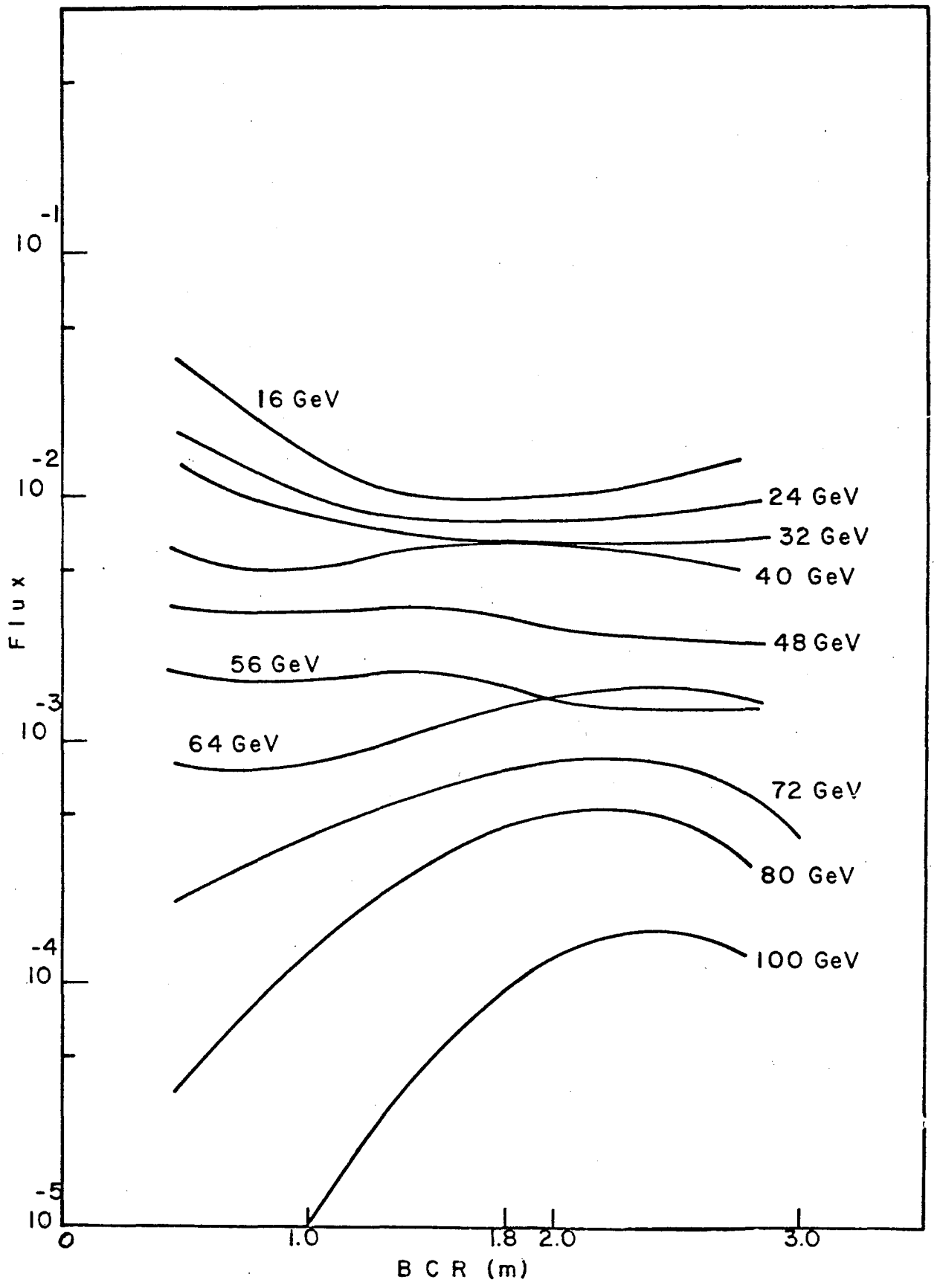
No Focusing (K)
Flux
10^-1
10^-2
10^-3
10^-4
10^-5
16 GeV
24 GeV
32 GeV
40 GeV
48 GeV
56 GeV
64 GeV
72 GeV
80 GeV
100 GeV
0
1.0
1.8
2.0
3.0
B C R (m)

Figure 14

No Focusing (π+K)

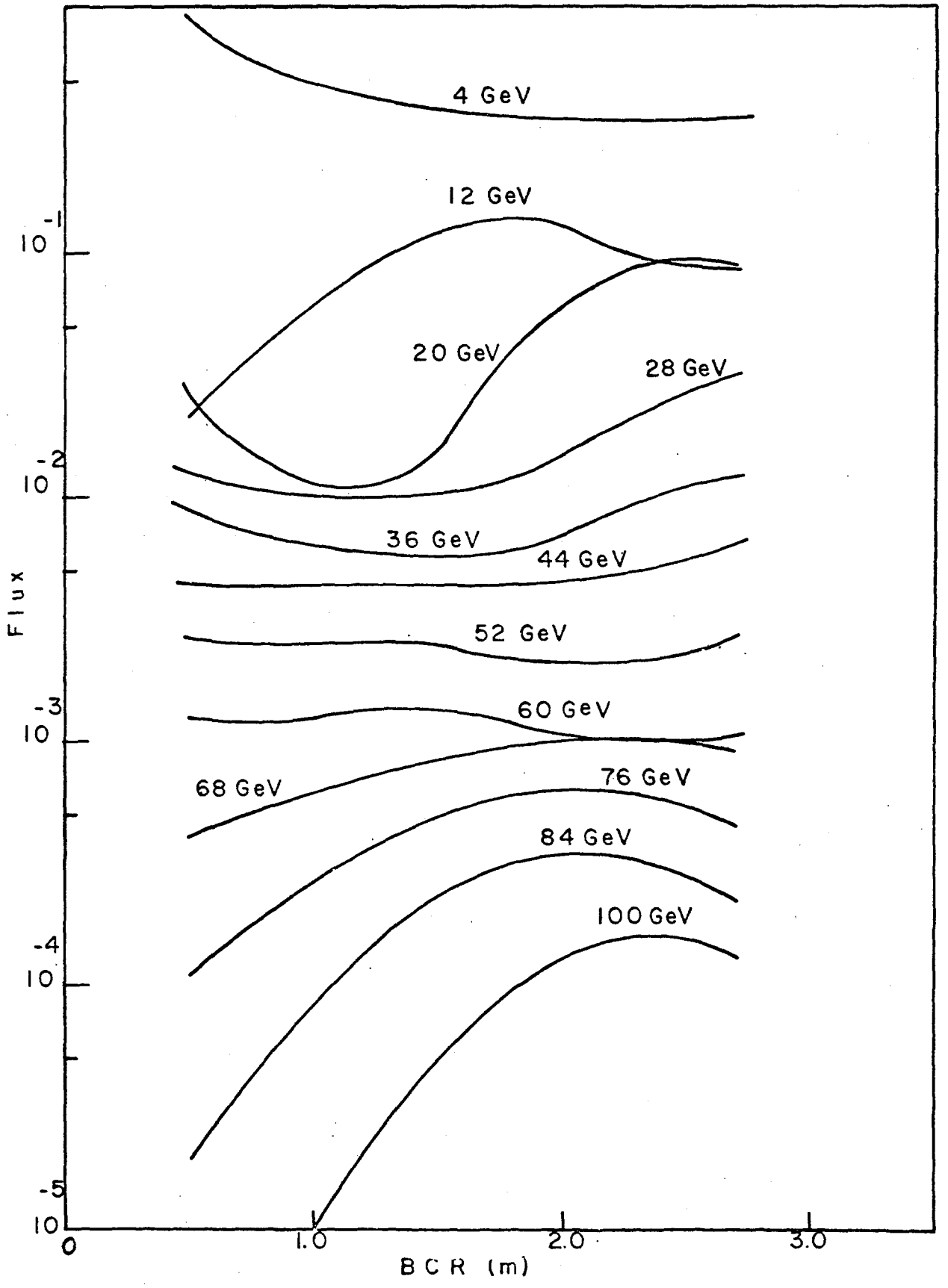

Figure 15

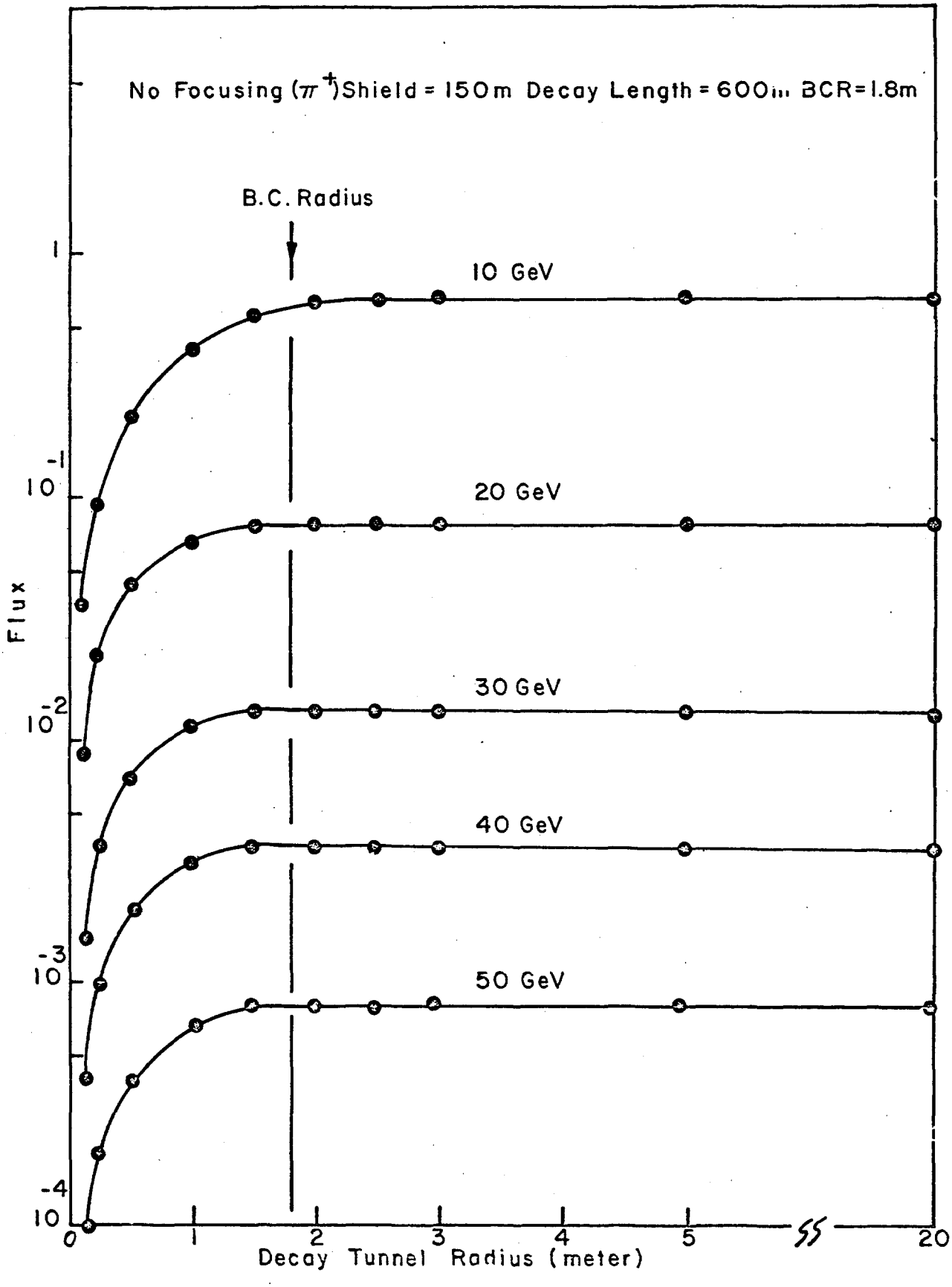
No Focusing (π^+) Shield = 150m Decay Length = 600m BCR = 1.8m
B.C. Radius
10 GeV
20 GeV
30 GeV
40 GeV
50 GeV
Flux
1
10^{-1}
10^{-2}
10^{-3}
10^{-4}
0
1
2
3
4
5
20
Decay Tunnel Radius (meter)

Figure 16

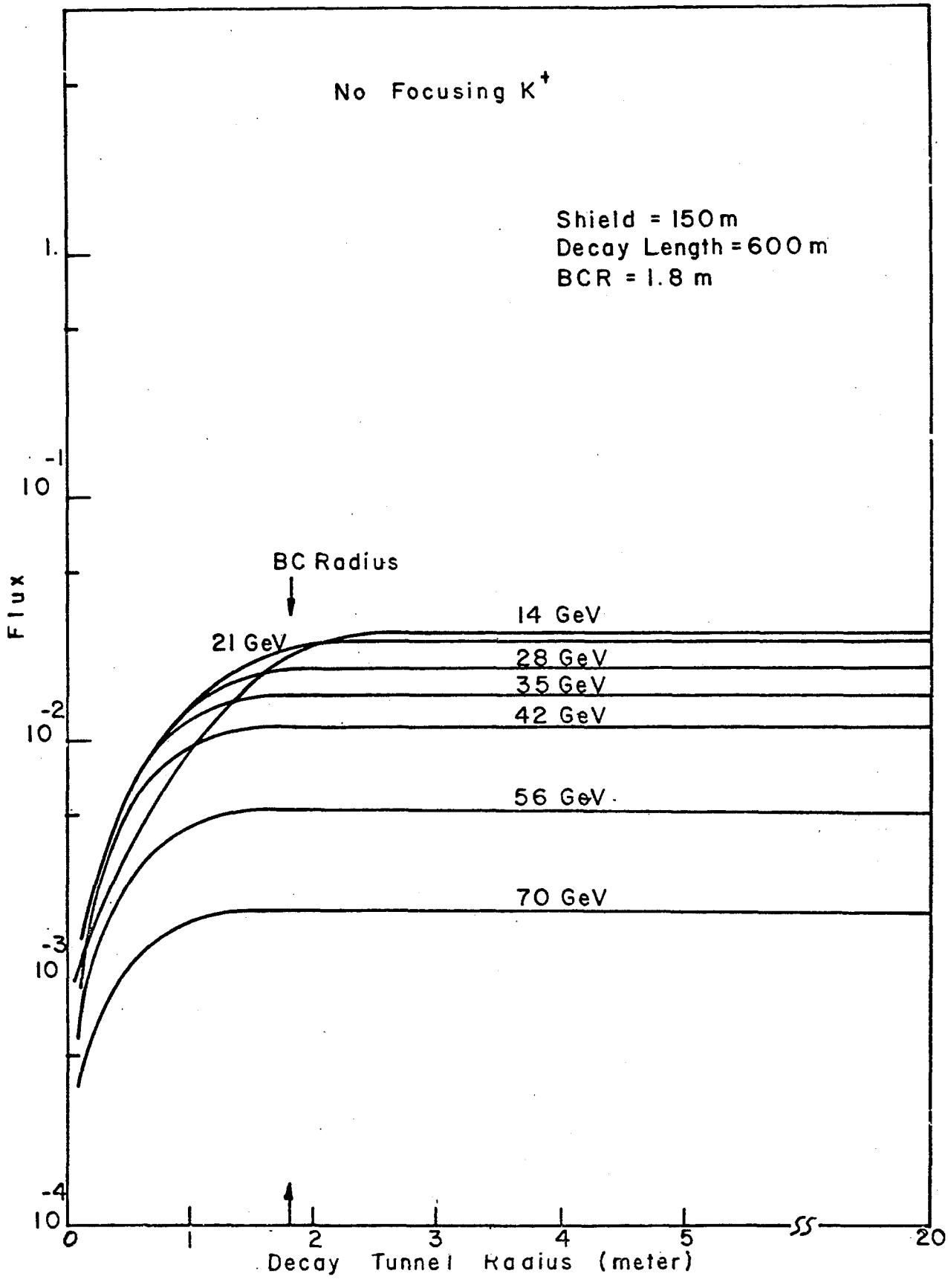
No Focusing K+
Shield = 150 m
Decay Length = 600 m
BCR = 1.8 m
BC Radius
14 GeV
21 GeV
28 GeV
35 GeV
42 GeV
56 GeV
70 GeV
Flux
1.
10-1
10-2
10-3
10-4
0
1
2
3
4
5
20
Decay Tunnel Radius (meter)

Figure 17

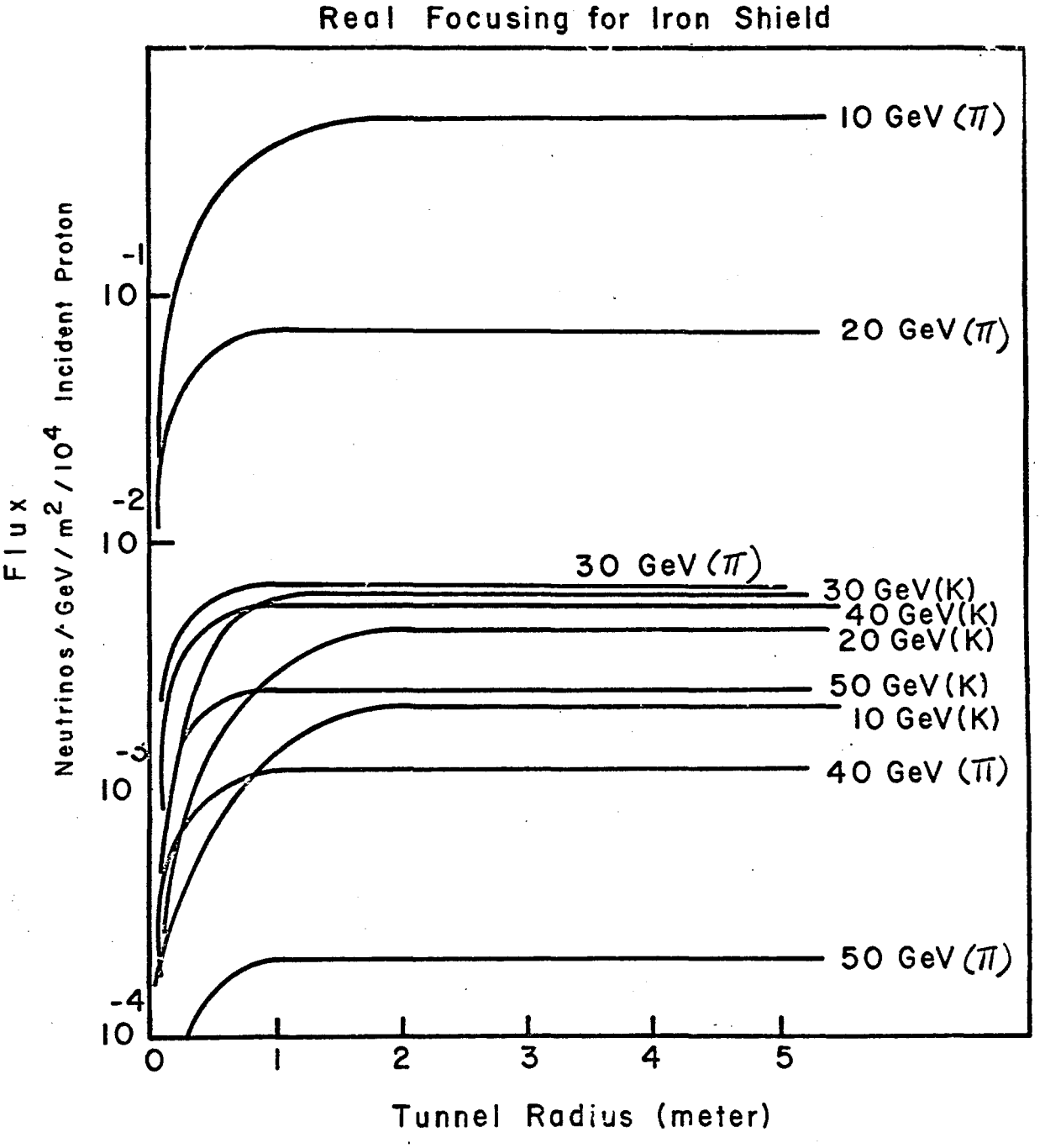
Real Focusing for Iron Shield
Flux
Neutrinos / GeV / m² / 10⁴ Incident Proton
10 GeV (π)
20 GeV (π)
30 GeV (π)
30 GeV(K)
40 GeV(K)
20 GeV(K)
50 GeV(K)
10 GeV(K)
40 GeV (π)
50 GeV (π)
10⁻¹
10⁻²
10⁻³
10⁻⁴
0
1
2
3
4
5
Tunnel Radius (meter)

Figure 18

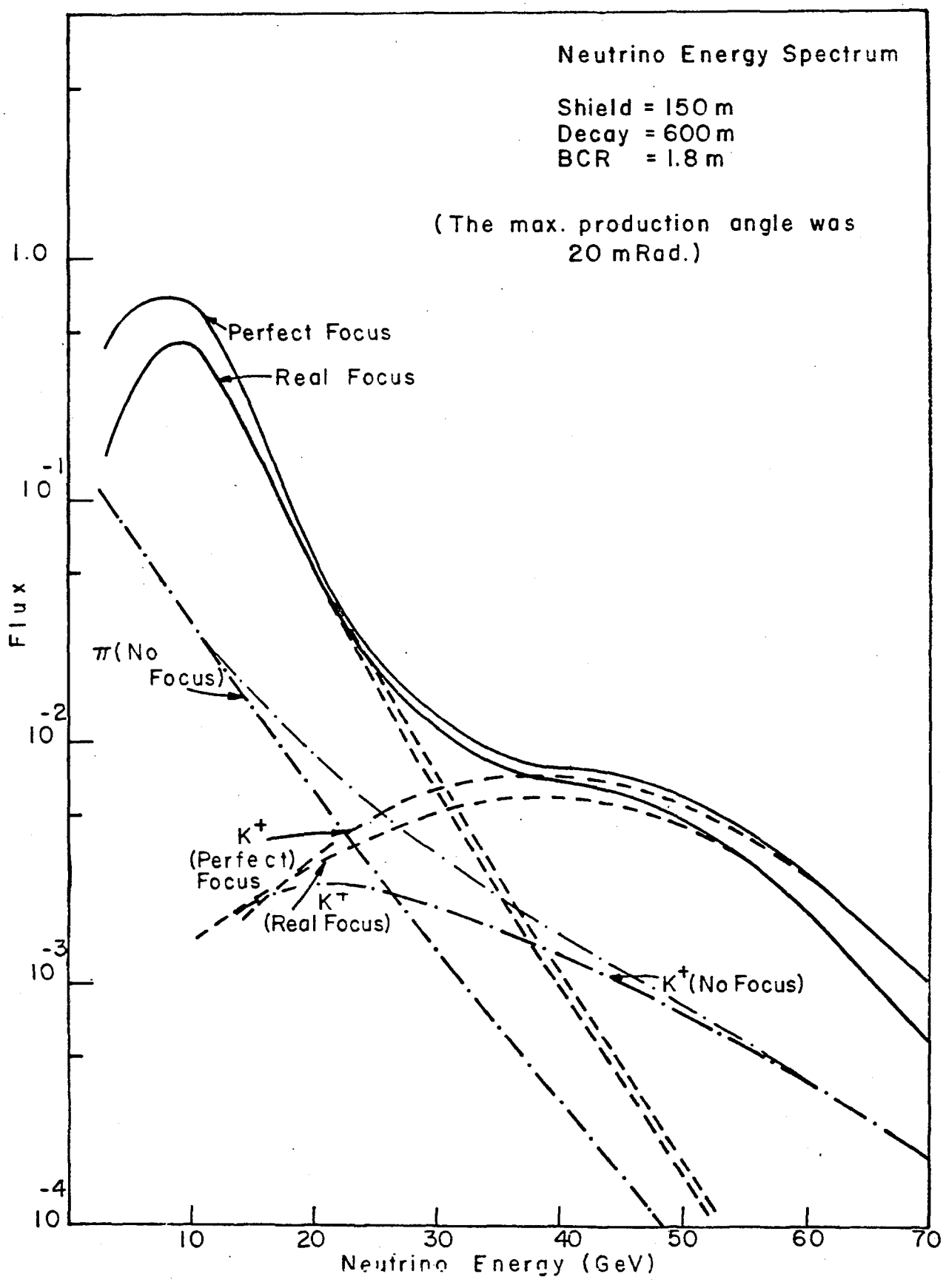
Neutrino Energy Spectrum
Shield = 150 m
Decay = 600 m
BCR = 1.8 m
(The max. production angle was 20 mRad.)
Perfect Focus
Real Focus
π(No Focus)
K+ (Perfect) Focus
K+ (Real Focus)
K+(No Focus)
Flux
1.0
10-1
10-2
10-3
10-4
10
20
30
40
50
60
70
Neutrino Energy (GeV)

Figure 19

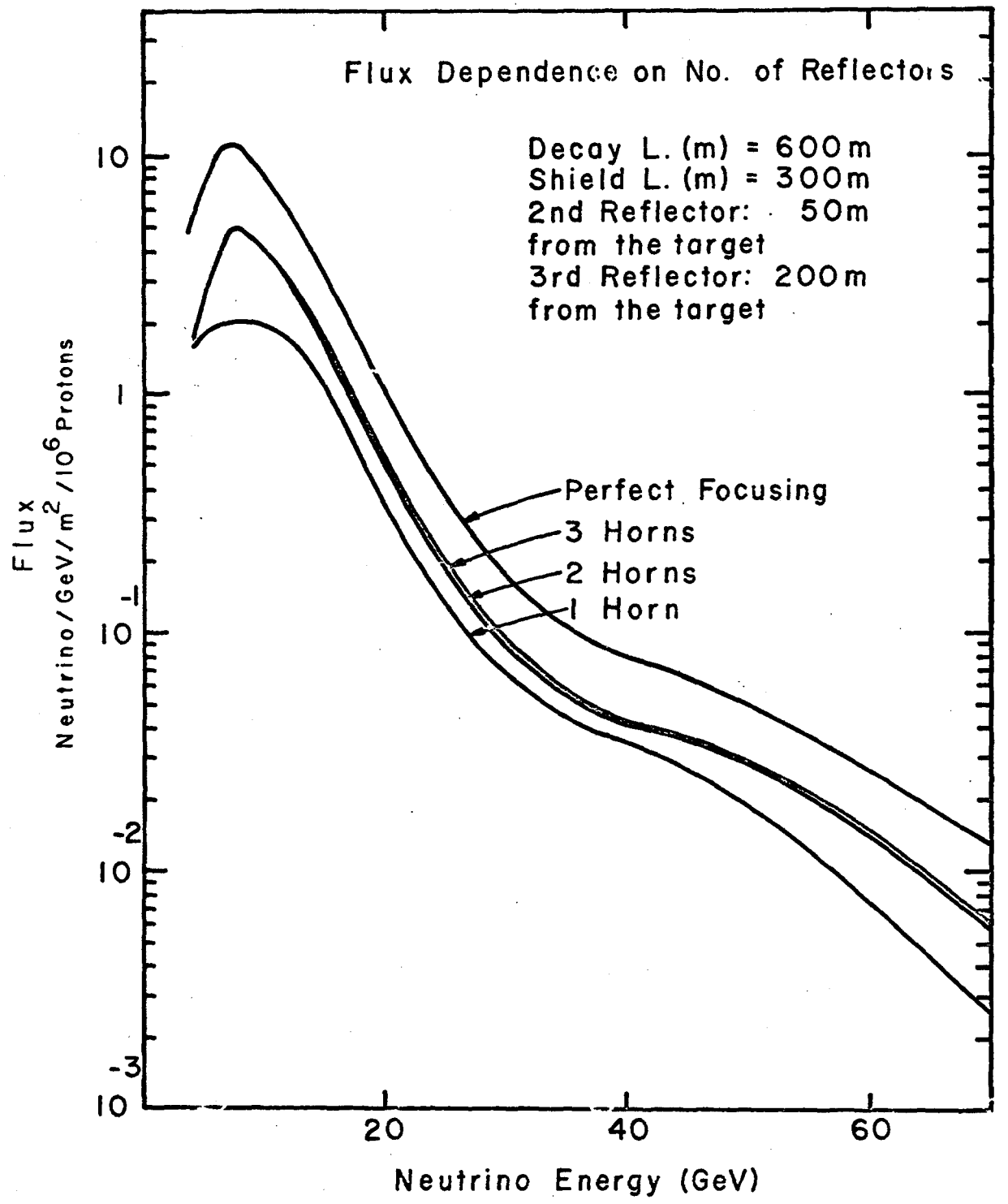
Flux Dependence on No. of Reflectors
Decay L. (m) = 600m
Shield L. (m) = 300m
2nd Reflector: 50m
from the target
3rd Reflector: 200m
from the target
Perfect Focusing
3 Horns
2 Horns
1 Horn
Flux
Neutrino/GeV/m^2/10^{6}Protons
10
1
10^{-1}
10^{-2}
10^{-3}
20
40
60
Neutrino Energy (GeV)

Figure 20

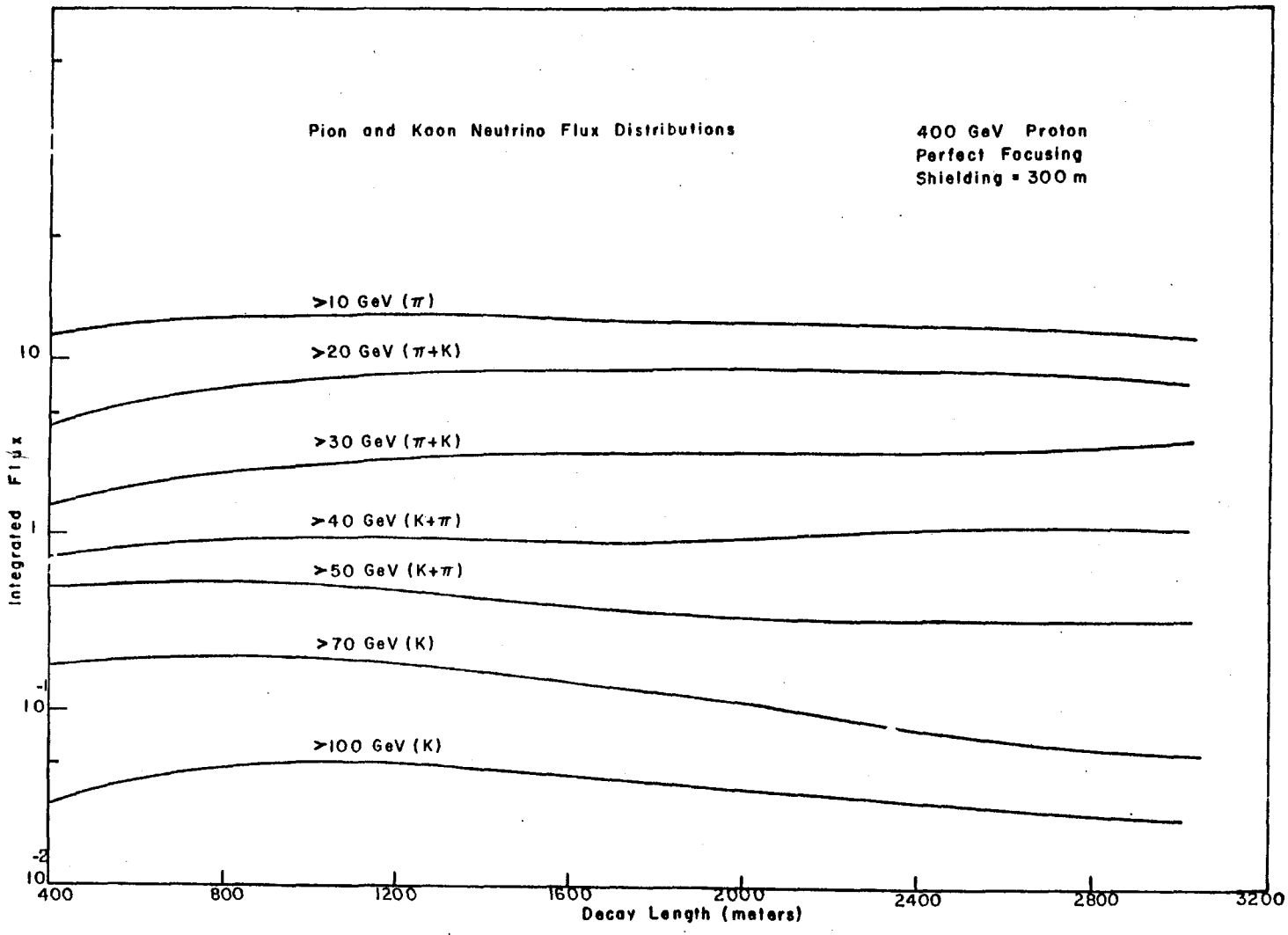
Pion and Koon Neutrino Flux Distributions
400 GeV Proton
Perfect Focusing
Shielding = 300 m
>10 GeV (π)
>20 GeV (π+K)
>30 GeV (π+K)
>40 GeV (K+π)
>50 GeV (K+π)
>70 GeV (K)
>100 GeV (K)
Integrated Flux
10
1
10⁻¹
10⁻²
400
800
1200
1600
2000
2400
2800
3200
Decay Length (meters)

Figure 21

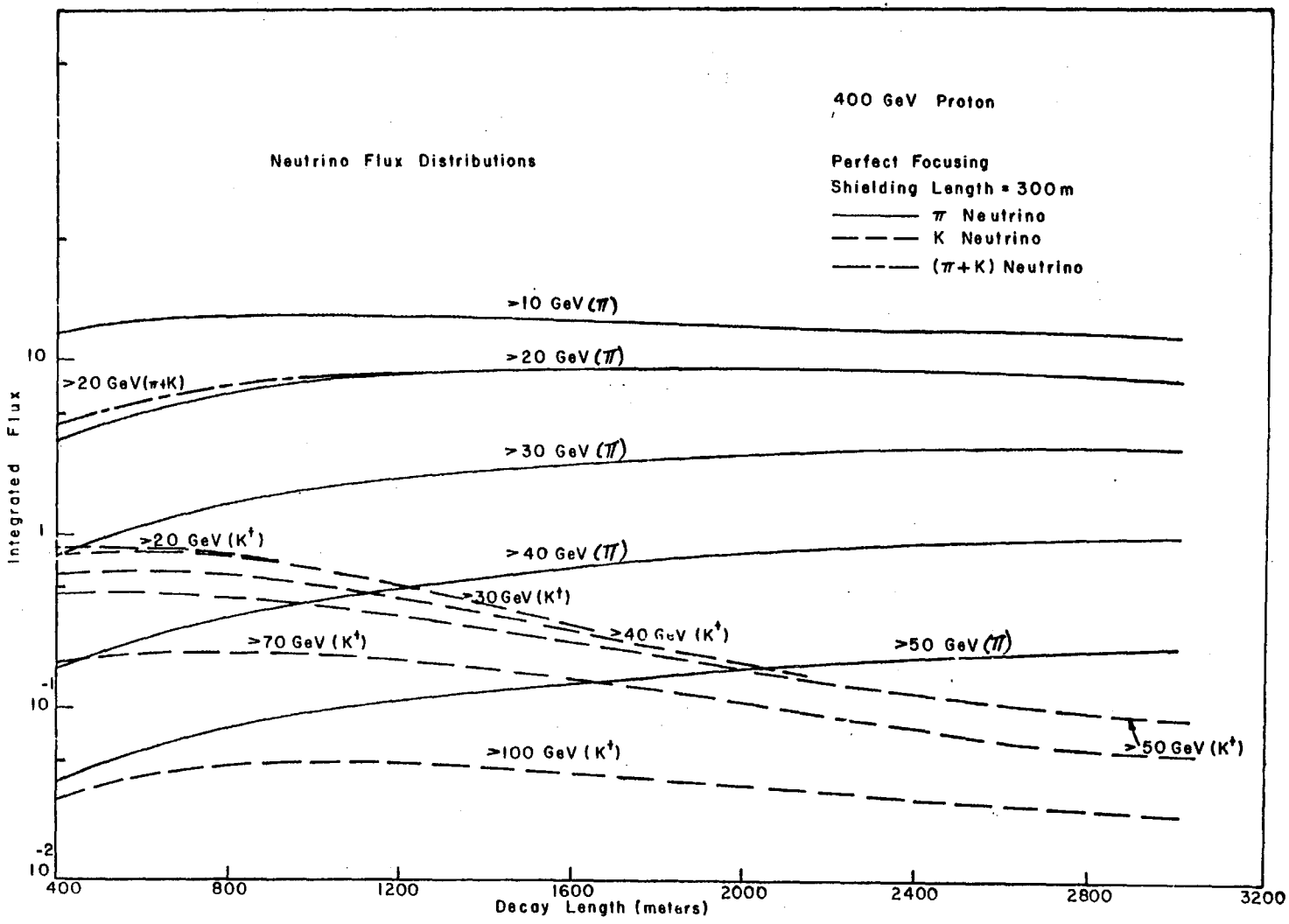
Neutrino Flux Distributions
400 GeV Proton
Perfect Focusing
Shielding Length = 300m
π Neutrino
K Neutrino
(π+K) Neutrino
>10 GeV (π)
>20 GeV (π)
>20 GeV(π+K)
>30 GeV (π)
>20 GeV (K+)
>40 GeV (π)
>30GeV (K+)
>40 GeV (K+)
>70 GeV (K+)
>50 GeV (π)
>50 GeV (K+)
>100 GeV (K+)
Integrated Flux
10
1
10-1
10-2
400
800
1200
1600
2000
2400
2800
3200
Decay Length (meters)

Figure 22

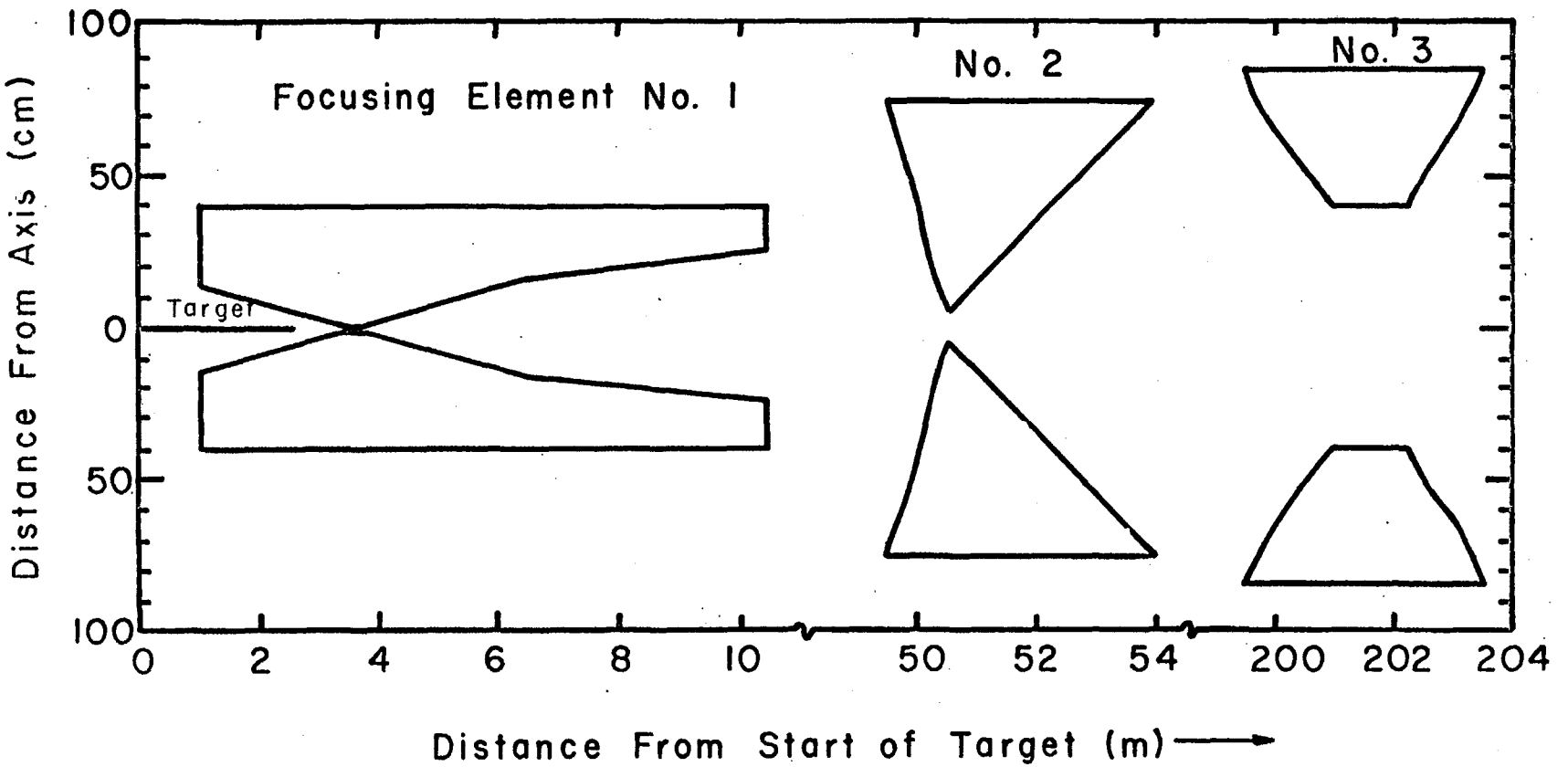
100
50
0
50
100
Distance From Axis (cm)
Focusing Element No. 1
Target
No. 2
No. 3
0
2
4
6
8
10
50
52
54
200
202
204
Distance From Start of Target (m)

Figure 23

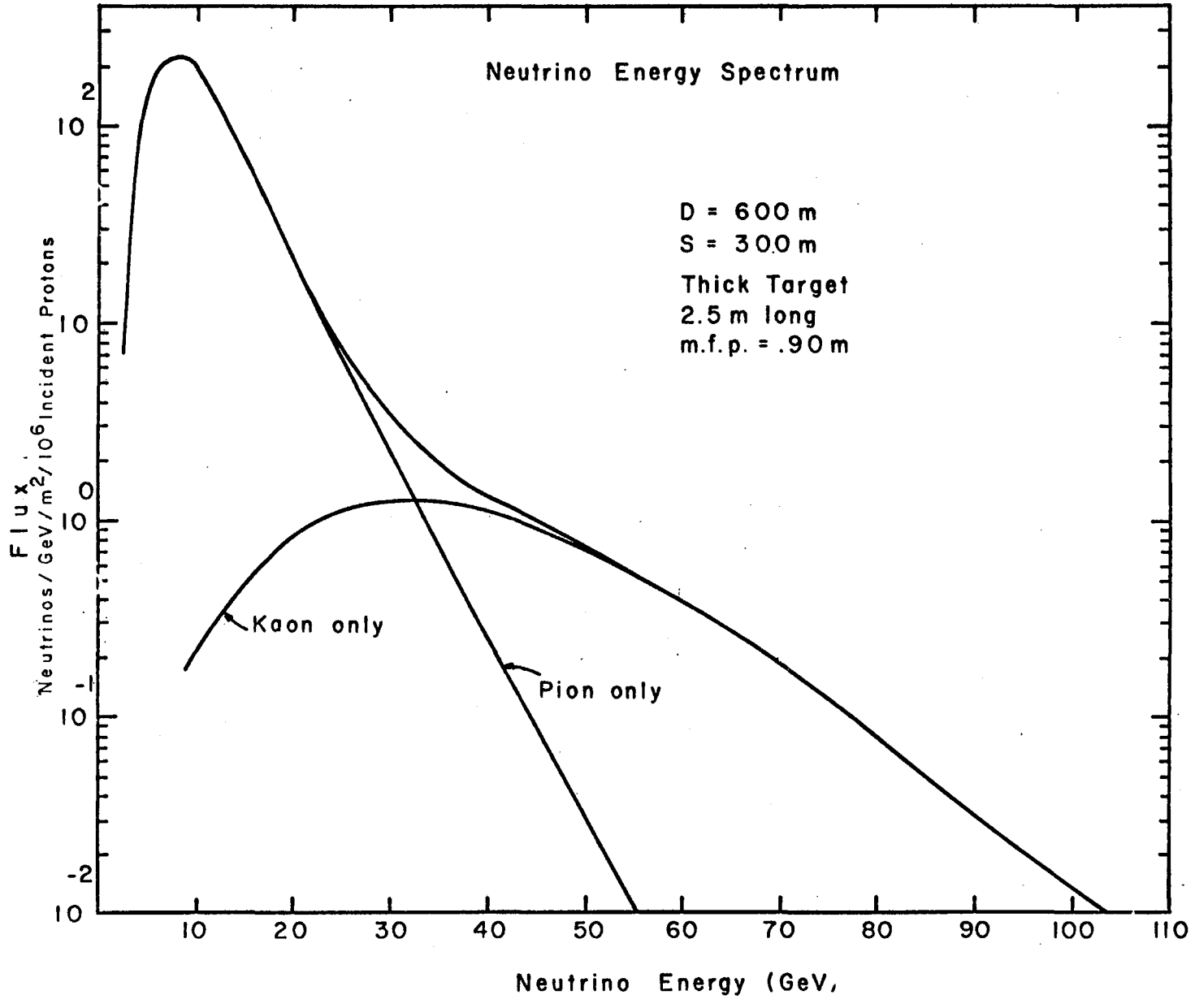
Neutrino Energy Spectrum
D = 600 m
S = 30.0 m
Thick Target
2.5 m long
m.f.p. = .90 m
Kaon only
Pion only
Flux
Neutrinos / GeV / m² / 10⁶ Incident Protons
Neutrino Energy (GeV)
10
20
30
40
50
60
70
80
90
100
110

Figure 24

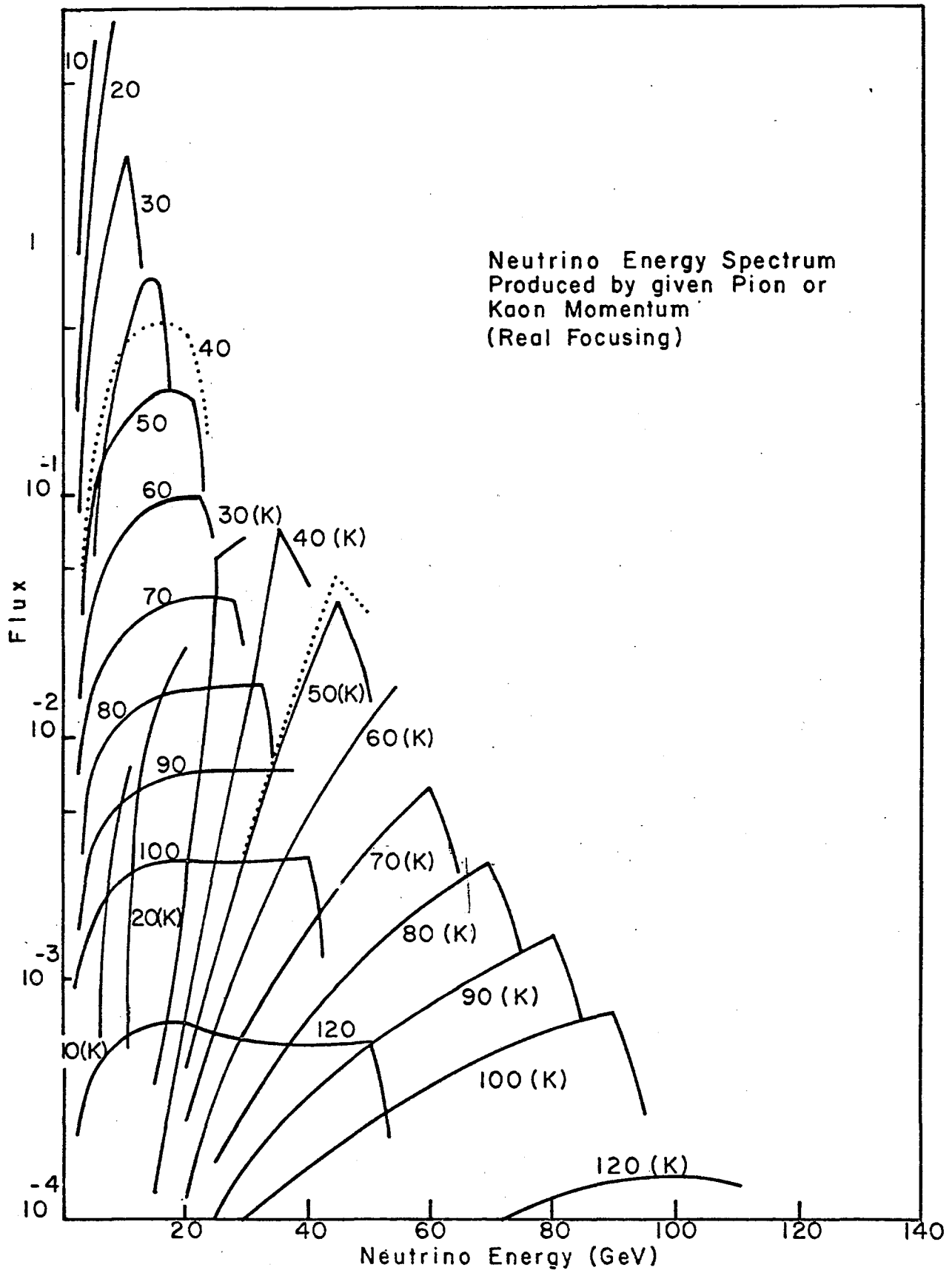
Neutrino Energy Spectrum
Produced by given Pion or
Kaon Momentum
(Real Focusing)
Flux
Neutrino Energy (GeV)
10
20
30
40
50
60
70
80
90
100
120
10(K)
20(K)
30(K)
40 (K)
50(K)
60(K)
70(K)
80 (K)
90 (K)
100 (K)
120 (K)
1
10^-1
10^-2
10^-3
10^-4
20
40
60
80
100
120
140

Figure 25

Reference 1. The neutrino flux program used at NAL is a variation of the CERN program. We wish to thank Dr. W. Venus for the private communication of the CERN program.

Figure Captions

Notes - Unless otherwise indicated, the target thickness is 0.033 interaction lengths (1cm) long. When the flux is dimensionless, it is to be considered as a relative flux.

Figure 1 The dependence of the integrated neutrino flux from pion decays on the decay length for different shield thicknesses. The flux from kaon decays and an iron shield are given for comparison.

Figure 2 The dependence of the integrated neutrino flux from kaon decays on the decay length for different shield thicknesses.

Figure 3 The dependence of the integrated neutrino flux from pion and kaon decays on the decay length for different shield thicknesses.

Figure 4 The dependence of the optimized decay length on the shield thickness.

Figure 5 Neutrino energy distributions from beams composed of uranium, iron or earth shields and their respective optimized decay lengths.

Figure 6 Neutrino energy distributions from four beams of different shield-decay length combinations.

Figures 7 through 15 These figures present the radial distribution of fixed energy neutrinos at the detector. The beam used was a decay length of 600 m and an iron shield thickness of 150 m. The figures present the distributions from the decays of different parents in different focused beams as given in the following table:

Figure	Parents	Parent focusing
7	π	perfect focusing
8	K	" "
9	π + K	" "
10	π	real focusing
11	K	" "
12	π + K	" "
13	π	no focusing
14	K	" "
15	π + K	" "

Figure 16 The dependence on the decay tunnel radius of the neutrino flux at various energies from a non-focused pion beam.

Figure 17 The dependence on the decay tunnel radius of the neutrino flux at various energies from a non-focused kaon beam.

Figure 18 The dependence on the decay tunnel radius of the neutrino flux at various energies from a real-focused pion and kaon beam.

Figure 19 The neutrino energy spectra for the iron shielded beam for perfect, real and no focusing.

Figure 20 The neutrino energy spectra for real focusing systems of one, two and three focusing elements and for a perfect focusing system.

Figure 21 The dependence of the integrated neutrino flux from pion and kaon decays on the decay length for perfect focusing.

Figure 22 The dependence of the integrated neutrino flux from pion and kaon decays individually on the decay length for perfect focusing.

Figure 23 The profile of the three element focusing system which optimizes the neutrino flux above 2.5 GeV passing through a detector of 1.8 m radius. The beam had a decay length of 600 m, and a shield thickness of 300 m.

Figure 24 The neutrino energy spectrum for the real focusing system using a 2.8 interaction length target 2.5 m long. Attenuation in the 3m diameter decay tunnel is not involved. This spectrum should be used for event rate calculations.

Figure 25 The neutrino energy spectra from the decays of fixed energy parents using real focusing.

APPENDIX X

NAL 1968 SUMMER

STUDY REPORTS

A. L. READ

NAL Summer Study Reports

Report Number	Date	Author	Title
B.6-68-1 (Stekly)	6/24/68	D. Keefe	Subgroup B.6 Superconducting Magnet Facilities, Meeting 1, June 20, 1968

Minutes of a meeting to discuss what would be profitable areas for summer physicists to explore--it was felt that guidance of particle physicists was needed in the following areas:

1. Operational specifications for cryogenic systems studies.
2. Specific input to magnet designers.
3. Arguments about advantages of higher fields.

B.6-68-2 (Stekly)	6/24/68	D. Keefe	Subgroup B.6 Superconducting Magnet Facilities, Meeting 2, June 24, 1968

Remarks by Fields on preliminary thoughts concerning the specification of magnet operation tolerances. Remarks by Steining on a first look at how beams would be modified if all magnetic fields and gradients were increased by a factor of 2.

B.6-68-3 (Stekly)	6/25/68	D. Keefe	Superconducting Beam-Transport Magnets at the 200 BeV Accelerator, Seminar presented June 25, 1968

Seminar presented by D. Keefe. Discussion of the state of the art of superconducting magnets. Description of superconductivity research programs presently in progress at LRL.

B.2-68-4 (Sculli)	6/26/68	W. Toner	Feasibility of Using High-Flux Muon Beams

Discussion of problems of performing experiments with high flux muon beams, based on experience of the author with a mu-p experiment presently in progress at SLAC.

B.6-68-5 (Stekly)	6/26/68	D. Keefe	Subgroup B.6 Superconducting Magnet Facilities, Meeting 3, June 26, 1968

Two areas for further superconducting magnet study were suggested:

1. Hyperon beams.
2. High field magnets in scattered-particle spectrometers.

B.5-68-6 (Bleser)	6/26/68	T.G. Walker	Subgroup B.5 Charged Particle Beams, June 25, 1968

List of topics to be studied by charge particle beams summer study group.

1. Background muon problems.
2. Ideas about typical secondary beam phase space characteristics.
3. Study of both high and low intensity beams.
4. Studies of two-body interactions.
5. Remarks on some parameters of target station layout and secondary beam layout.

Report Number	Date	Author	Title
B.5-68-7 (Bleser)	6/28/68	T.G. Walker	Subgroup B.5 Charged Particle June 28, 1968

List of reports to be prepared by members of the charged particle beams Summer S sub-group.

B.5-68-8 (Bleser)	7/1/68	W. Toner	General Ideas about Beam Desi for NAL

Discussion of miscellaneous points, mostly secondary beam phase space characteri and **B.dL** requirements in secondary beams.

B.4-68-9 (White)	7/1/68	W. Toner	Comments on Longo Neutral Bean

Discussion of Longo neutral beam report - topics include:

1. Front "porch" of accelerator cycle.
2. Layout of neutral beam experiment.
3. Shielding problems.
4. Protection against EPB getting down channel.
5. Alignment problems.

C.1-68-10 (Roberts)	7/3/68	J. Poirier	The Electromagnetic Form Factc the Charged Pion (Muon, Kaon, Electron)

An experimental layout is described to make a direct measurement of the pion-ele magnetic form factor, via elastic pion-electron scattering using atomic electron a target material in an intense beam of high momentum pions.

C.1-68-11 (White)	7/9/68	D.H. White	An Experiment to Look at Backw Peaks in π-p Scattering

An experiment is described to measure the energy dependence of the cross section the π-p backward elastic cross section and to detect the energy dependence in th shape of the cross section (shrinkage).

A.3-68-12 (Carrigan)	6/29/68	T. Fields A. Roberts D. Sinclair J. VanderVelde T.G. Walker	A High-Accuracy, Large Solid A Detector for Multiparticle Fin States at 100 GeV

A lengthy description of a possible hybrid configuration including a small bubbl chamber surrounded by a variety of thin and thick plate spark chambers and spectrometer magnets is described.

Report Number	Date	Author	Title
A.3-68-13 (Carrigan)	7/10/68	A. Roberts	Further Studies on a Combined Bubble-Spark Chamber High-Accuracy Detection System for Multiparticle Final States at 100 GeV

A modified version of the hybrid spectrometer system described in Summer Study report No. 12 is described.

A.1-68-14 (Key)	7/10/68	P. Condon	Some Notes on the Detection of Neutrals in a Large Bubble Chamber

Miscellaneous remarks on the detection of neutrals in a large bubble chamber.

C.1-68-15 (White)	7/10/68	J. Poirier T. Romanowski	Threshold Cerenkov Counters in Secondary Beams at NAL

The use of a vacuum pipe in a secondary beam for threshold Cerenkov counters is proposed and specific designs are described.

B.7-68-16 (Bleser)	7/9/68	D.H. White	A Proposal for a Unilateral Target Station Number 1

A specific layout of a target station and secondary beam front end, incorporating the Maschke box idea, is described.

B.4-68-17 (White)	7/10/68	J.H. Smith	Neutral Beams

Discussions of possible K^0 beams and neutron beams and a number of possible experiments to be done in such beams.

C.1-68-18 (Roberts)	7/10/68	J.H. Smith	Spark Chamber Experiments: $\pi^- + p \rightarrow K^0 + \Lambda^0$ at 100 GeV

Discussion of a spark chamber experiment to study associated production at 100 GeV.

C.1-68-19 (Nezrick)	7/10/68	T. Romanowski	Hyperon Beams at 200 GeV Weston Accelerator and Possible Experiments with These Beams

Discussion of beam transport for hyperon beams and possible strong interaction scattering experiments, mostly elastic scattering, using the spark chamber technique.

Report Number	Date	Author	Title
B.1-68-20 (Nezrick)	7/11/68	L. Hyman	Neutrino Beams at NAL

Calculation of some neutrino fluxes, using the CKP formula.

B.5-68-21 (Roberts)	7/8/68	R. Stiening	A Proposal for the Use of the 10 Be Booster Accelerator as a Source of Low Energy K^+ Mesons

Proposal to use the beam of the booster, when it is not being jected into the 200 BeV accelerator, to produce K mesons. A high flux of K mesons would be produced; a wide variety of possible experiments with low energy K's are discussed.

B.6-68-22 (Stekly)	7/2/68	R. Stiening	Effects of Super-Magnets on Experimental-Area Layout

The effect of the availability of high field supermagnets on the layout of 200 BeV experimental areas is considered. If it is possible to develop a 60 KG bending magnet, the length of some secondary beams may be reduced by a factor of 2. It appears that it is more important to develop high field bending magnets than high field quadrupoles.

B.5-68-23 (Bleser)	7/10/68	R. Stiening	A Proposal to Use Synchrotron Magne in Secondary Beams

It is shown that synchrotron bending magnets and quadrupoles can be used as beam transport elements in secondary beams. As these magnets are to be made in large quantities, their use as secondary beams may be very economical.

B.5-68-24 (White)	7/10/68	T.G. Walker	Secondary Particle Yields at 200 Ge

The predictions of the CKP, Trilling and Hagadorn-Ranft formulae are compared. It is concluded that the most reasonable predictions to use for studying the feasibility of particular beams and experiments are the Hagadorn-Ranft yields. Estimated yields of production of various particles in 200 GeV proton-proton collisions at angles up to 45 milliradians are plotted. The yields expected from targets other than hydrogen clearly requires further study.

M-68-25 (Carrigan)	7/9/68	J. Poirier	RELKIN: A Relativistic Kinematics Program

A brief description of a relativistic two-body kinematics program is given.

Report Number	Date	Author	Title
B.8-68-26 (Roberts)	7/12/68	A. Maschke A. Wattenberg D.H. White	Consideration of an Internal Target Facility

The plans for the 200 BeV machine do not include an operating internal target area or internal target experimental area. Some of the reasons for this decision are described in a note by Maschke. A second report by Wattenberg lists a number of experiments which under detailed study might argue for an internal target facility. At present, there is apparently no convincing argument in favor of building an internal target facility.

C.68-27 B.4-68-27 (White)	7/11/68	A. Wattenberg J.H. Smith	The Use of a High Energy K^o Beam to Study $K^o + p \rightarrow p + K^o$ Regeneration to Check the Pomeranchuk Theorem

Several high energy K^o_L experiments are considered. The possibility of a sensitive check of the Pomeranchuk (total cross section) theorem is investigated in detail. These studies have led the author to the recommendation that at least two neutral beams should be set up - a high energy neutron beam and a beam at a production angle of 7-10 milliradians, which is relatively richer in K^o's.

B.2-68-28 (Sculli)	7/11/68	K.W. Lai	Some Speculative μ Experiments

A number of speculative new experiments are discussed - tests of lepton quantum numbers, are they additive or multiplicative? Search for heavy leptons of new type; form factor study of nucleon isobars.

C.1-68-29 (Bleser)	7/11/68	T.G. Walker	Elastic Hadron Scattering at High Energies

Elastic hadron-hadron scattering at momenta of 100 GeV/c has been considered for the purpose of determining the specifications of suitable beams and spectrometer magnets. The angular distribution would be performed in three separate experiments: a) small angle scattering using a wire spark chamber spectrometer; b) intermediate scattering angles using a fixed counter spectrometer and a high intensity beam; c) large angle scattering using a double arm spectrometer.

30 - No Report.

B.9-68-31 (Roberts)	7/12/68	W. Toner	Electron and Photon Beams at NAL

In the 1966 LRL Summer Study, C. A. Heusch gave an extensive survey of methods to produce electron and proton beams at a 200 GeV accelerator. This note is a commentary on that paper and expands it somewhat.

Report Number	Date	Author	Title
B.2-68-32 (Sculli)	7/12/68	M. Tannenbaum	Muon Tridents at NAL

The direct production of muon pairs by muons in the field of a heavy nucleus is discussed. A number of comments are made about muon beams at NAL, notably, the importance of making very well collimated and very well momentum-defined muon beams, even at the expense of intensity, for the purpose of a large class of experiments.

A.3-68-33 (Carrigan)	7/10/68	P. Condon	Proposed Modification to Combined Bubble Chamber Plus Spark Chamber System

An alternative proposal to the bubble chamber-spark chamber hybrid system is discussed. Basically the idea is to make the bubble chamber with an axial magnetic field (B pointing along the beam axis).

B.5-68-34 (Bleser)	7/12/68	T.G. Walker	Charged Particle Beams

This is a list of written reports that Summer Study Subgroup B-5 (charged particle beams) intended to produce. A summary has also been made of beams and experiments proposed in the LRL, CERN, and NAL 1967 Summer Studies.

A.1-68-35 (Key)	7/12/68	M. Derrick R. Kraemer	Parameters of a Large Bubble Chambe Scaling of Momentum and Angle Errors

Parameters of large bubble chambers are considered, using FAKE-GRIND programs to simulate and fit events. Hand calculations were also made to provide orientation and to determine such quantities as optimum path length and optimum magnetic field. Some conclusions are drawn on the basis of this preliminary work.

C.1-68-36 (White)	7/12/68	P. Condon	Search for Long-Lived Heavy Particles

A straightforward beam-survey-type experiment is described, using momentum analysis and velocity measurement in some Cerenkov counters. It seems that the design requirements for the Cerenkov counter for this experiment are different from Cerenkov counters used for standard beam-survey measurements, so that the combination of the two tasks into one will probably involve putting different counters in the same beam in tandem.

Report Number	Date	Author	Title
B. 10-68-37 (Nezrick)	7/13/68	D. Berley J. Lach A. Maschke T. Romanowski	Hyperon Beams at a 200 GeV Accelerator

A number of possibilities to study hyperon interactions at the 200 GeV accelerator are discussed. The intent of the paper is to discuss experiments possible within the framework of our present knowledge of hyperons and to suggest further topics to be studied, which will also demonstrate how to implement a hyperon program at NAL.

B.2-68-38 (Sculli)	7/13/68	T. Yamanouchi	A Muon Beam at NAL

The purpose of this study is to investigate whether one can construct a simpler (cheaper) muon beam without too much loss in intensity compared with the muon beam proposed by Toohig in the LRL summer studies. A simple and short beam is described, which can produce 10^8 to 10^9 muons per pulse. This is still an adequate flux for many interesting experiments.

B.7-68-39 (Bleser)	7/13/68	A. Maschke	A Proposal for a Proton Beam Target Station

This paper gives a description of set-up for handling the front ends of secondary beams and the target and beam stop. The concepts are illustrated by a model, which follows the general philosophy, but none of the mechanical or dimensional features should be taken too seriously as these are details to be worked out later.

B.9-68-40 (Roberts)	7/13/68	W. Toner	Design of an Experiment to Measure $\sigma_{TOT}(\gamma p \rightarrow$ hadrons) at Very High Energies

Independently of immediate theoretical ideas, it is clear that a good measurement of σ_τ ($\gamma p \rightarrow$ hadrons) will be of interest at the highest possible energy. Likewise σ_τ ($\gamma n \rightarrow$ hadrons) via $H_2 - D_2$ difference.

B.3-68-41 (Key)	7/15/68	D. Berley	Modulated Proton Beams for an RF Separated Beam

This paper sketches a possible way of doing these experiments and goes into just enough detail to uncover the problems which arise in trying to obtain precision on the order of 1-2%. It has been suggested that some economy might be had in the construction of an RF separated beam by modulating the primary proton beam. The extent of the economy depends on how the modulation is performed. A possible beam modulation system is described. The problem of isochronism of the beam is also discussed.

Report Number	Date	Author	Title
B.1-68-42 (Nezrick)	7/15/68	M. Block	Neutrino Physics

This report concerns itself with possible neutrino and anti-neutrino experiments for the 200 BeV accelerator. This paper is limited to a discussion of two-body reactions. In particular, the ν_μ and $\bar{\nu}_\mu$ reactions are discussed in detail.

B.3-68-43 (Key)	7/16/68	J. Lach	100 BeV/c RF Separated Beam - 1968 Modification

The 1968 modification of the 100 BeV/c RF separated beam described in the LRL design study reports is discussed. Most of the previous work is still relevant. The author dwells in this note on those features which should be revised because of technological advances which have come about in the three years since the previous report was written.

B.3-68-44 (Key)	7/16/68	D. Berley	Note on Kadyk's Separated Beam

The author discusses Kadyk's separated beam described in the 1966 LRL Design Study. The technology required to construct such a beam is many years off and the author concludes that it is difficult to think about it in a realistic way. He argues that the idea will survive or be forgotten only on the basis of cost.

A.3-68-45 (Carrigan)	7/17/68	J. Lach	Comments on the Bubble Chamber Spark Chamber Detector Proposed by T. Fields, et al.

This is a set of random comments on the bubble chamber-spark chamber hybrid detector proposed by Fields, et al. These comments are not intended to be exhaustive and the limitations of the system rather than its merits are emphasized.

D.1-68-46 (Bleser)	7/13/68	M. Perl	Some Considerations on the Design of a Minimal NAL Target Station, Based on Experiments at SLAC.

The author presents some considerations of the design of a target station, based on his experience at SLAC. A minimal facility, involving two target stations, is discussed.

B.2-68-47 (Sculli)	7/19/68	M. Perl	Inelastic Muon and Proton Experiments at NAL

In this paper the author outlines two muon-proton inelastic scattering experiments for NAL, with two specific objectives in mind. First, to see what muon flux is needed, and, second, to see what size analyzing magnets would be needed.

Report Number	Date	Author	Title
B.9-68-48 (Roberts)	7/18/68	W. Toner	Problems in Attempting to Measure $\frac{d\sigma}{dt}$ ($\gamma p \to \gamma p$) Compton Scattering

These notes represent incompletely worked ideas on a number of questions: 1) Is it worthwhile to measure $\frac{d\sigma}{dt}$ at $\tau = 0$? 2) Can a single-arm spectrometer, which measures only the forward proton, work? 3) Will a double-arm spectrometer work? 4) What kind of event rates would we get?

B.9-68-49 (Sculli)	7/15/68	R. Wilson	Electromagnetic Physics at NAL

The contents of this report, although it was written at the start of the NAL 1968 Summer Study, should be considered as representative input data, rather than conclusions. The report presents a list of possible experiments to any of which the authors, all Harvard physicists, would be proud (sic) to contribute if the opportunity were to arise.

C.1-68-50 (Carrigan)	7/22/68	D. Meyer	Comments on Hybrid Spectrometer System

The purpose of this paper is not to present a spectrometer design but rather to set down criteria on which to judge ideas of spectrometers and to present some new ideas which must be investigated thoroughly before a sensible spectrometer design can be established.

B.7-68-51 (Bleser)	7/22/68	R. Wilson	Power Supplies for Magnets at NAL

This is propaganda for a point of view first expressed by the author in 1959; it did not find acceptance at CEA and the writer does not know why. So he starts again in the hope that it is of use at NAL. He proposes cheap, efficient and simple power supplies, and not to make them more complex than is needed.

D.1-68-52 (Bleser)	7/23/68	J. Sanford	Initial Program Capacity at NAL

This note attempts to estimate the number of secondary beams initially needed at the accelerator. The purpose is to size the experimental facilities at NAL to the number of groups which will be served, over and above those that are accommodated at other accelerators. No identification of specific beams is made, except that the gross number of secondary beams is specified.

S.68-53	7/24/68	G. Chew	A Simple Formula for the Distribution of Energetic Secondary Baryons from Proton Initiated Collisions

(Theory paper - no abstract for it.)

Report Number	Date	Author	Title
B.2-68-54 B.9-68-54 (Sculli)	7/25/68	R. Wilson M Perl	Progress Report on Muon and Electrc Beam for NAL

Progress of NAL Summer Study groups on a number of topics is discussed: 1) electron beams; 2) tagged gamma ray experiments; 3) muon beam design.

D.1-68-55 (Bleser)	7/26/68	J. Sanford T. Elioff	Plans for Experimental Areas at the NAL 200-400 BeV Accelerator

The purpose of this paper is to assemble the secondary beams and detectors proposed for NAL into the context of an overall experimental facility. The plans and layouts discussed can serve as a possible guide in the next round of beam and facility design. Hopefully, this work could reaffirm the correctness of plans made to date and suggest changes in particular features.

C.3-68-56 (Atac)	7/26/68	L. Yuan	Some New Developments and Proposals in High Energy Detectors

Some new developments in detectors are discussed: 1) transition radiation from relativistic charged particles; 2) surface plasma oscillations detector; 3) secondary emission detector; 4) time-of-flight measurement with p/sec time resolution.

C.4-68-57 (Roberts)	7/26/68	A. Odian F. Villa I. Derado	Proposal for 12 Meter Streamer Chamber

The observation and measurement of strong interactions at very high energies requires a detector which can be used at the high multiplicities common at these energies, including the cascading decays of high strangeness particles. The authors propose that the streamer chamber appears to fit the need and requirements of such a high energy detector.

S.68-58	7/29/68	M. Goldberger	Seminar

(theory paper)

A.1-68-59 B.1-68-59 (Nezrick)	7/29/68	G. Snow	Neutrino Physics and the 25-ft. Bubble Chamber

The author studies neutrino physics in large bubble chambers and concludes with a strong plea for high priority for construction of the 25-ft. bubble chamber.

Report Number	Date	Author	Title
D.1-68-60 (Bleser)	7/29/68	J. Sanford	Experimental Building Costs

This note concerns an analysis of the costs associated with the construction of a major experimental building at Brookhaven. Since similar buildings will be needed at the new accelerator, an examination of the features of the BNL building can provide information helpful for planning at NAL.

B.4-68-61 (White)	7/29/68	M. Perl	Progress Report on Group B.4, Neutral Beams

A report on the design and use of neutron beams has been given by Longo (NAL-FN-142). Toner has commented on this report.

Smith and Wattenberg have studied K_2 beams and experiments.

Detailed designs are needed for both K^o and neutron beams, particularly with respect to muon shielding. In collaboration with Longo, Perl plans to look into a specific 0 milliradien neutron beam. A smaller flux and consequently smaller hole in the muon shielding will be considered.

C.1-68-62 (White)	7/29/68	D. Meyer	Spark Chamber Experiment on $\pi^- + p \rightarrow N^* + p^o$

Two-body and quasi-two-body reactions at 100 GeV/c are considered. Details of a spark chamber experiment to investigate these reactions are outlined.

63 - No Report.

C.4-68-64 (Atac)	7/31/68	F. Villa	A Few Thoughts about High Energy Detectors

Problems associated with high energy detectors are discussed in a general way: 1) magnetic field mapping; 2) Study of limit of accuracy of spark chamber devices; 3) Study of very flexible, fast, electronics-hardware devices; 4) vidicons or other electronic scanning devices; 5) development and application of very accurate instruments for determining missing neutral energies and masses.

C.3-68-65 (Carrigan)	7/31/68	L. Lederman	Influence of Detector Spatial Resolution in the Scaling of NAL Experiments

The purpose of this note is to point out the enormous savings in cost, complexity, and flexibility that would flow from having detectors capable of improved spatial resolution. Among other conclusions, the author notes that at civilized apertures, cryo- and superconducting magnets become thinkable and give improvements in momentum resolution over AGS experiments.

Report Number	Date	Author	Title
B.1-68-66 (Nezrick)	8/5/68	D. Frisch	Beam and Spark Chamber Detector for Search for W's Produced by Neutrinos

An experiment to search for W's produced by neutrinos is described. The equipment for this search is also appropriate, with only small changes, for study of other high energy neutrino interactions; for instance, the quasi-elastic inverse-mu-capture reaction.

B.7-68-67 (Bleser)	7/31/68	T. Elioff	Memo to A. L. Read

Memo to A. L. Read concerning the jobs which, in the view of the author, need to be undertaken in the design of the EPB and its associated experimental areas.

B.5-68-68 (White)	8/7/68	D. Meyer	High Intensity π Beams

This is the result of a short investigation into the requirements and uses of a very high intensity π beam. No attempt is made to make detailed calculations. The purpose is to determine roughly what intensity is practically attainable and what components are needed to produce such a beam. The author also discusses whether, given such a beam, there are any insuperable problems in exploiting it using existing experimental techniques.

C.1-68-69 (Roberts)	7/22/68	R. Wilson	Comments on C.1-68-10 by J. Poirier

A number of comments on Poirier's article are made, in the form of suggested improvements, to the experimental layout.

C.1-68-70 (White)	8/6/68	A.D. Krisch	Remarks on π^-p Backward Scattering Experiments

This paper comments on the NAL report by H. White describing a possible layout for π^-p backward scattering measurements. The author suggests procedures which he claims will be both more economical and more successful.

B.1-68-71 (Nezrick)	8/8/68	A.D. Krisch	Low Cost High Quality ν Beam

Rather than using a large block of steel to filter out muons in the neutrino beam, another approach is suggested. A very large number of advantages are claimed for this beam design.

Report Number	Date	Author	Title
72 - No Report.			
B.1-68-73 (Nezrick)	8/9/68	L. Stevenson	Subgroup B.1 Neutrino Beams Meeting 3, July 11, 1968

Intermediate report on the neutrino beam design work of the Summer Study. Items such as neutrino yield calculations, chamber location considerations, choice of neutrino energy at which to optimize beam design, muon range spectrum calculations, are discussed.

B.2-68-74 (Sculli)	8/8/68	L. Lederman	Search for Intermediate Bosons Using Muons

A search for intermediate bosons using muons is described. The beam design by Yamanouchi appears to be adequate for this experiment. Since the detection of W production by neutrinos will be extremely difficult, the author concludes that this experiment is an essential component of the search for W's at NAL.

A.1-68-75 (Key)	8/9/68	U. Kruse	Analysis of Bubble Chamber Events Containing Neutral Pions

In this note the author considers the problem of analyzing events which have one π^o in them. He limits his analysis to the problem of energetic π^o's roughly 1 GeV or higher because in the relativistic limit one can make simple approximations for the pion kinematics. The problem of low energy π^o's is more difficult and will have to be handled in a more detailed analysis.

Report Number	Date	Author	Title
B.1-68-76 (Nezrick)	8/12/68	D. Cline	Study of the Four Fermion Weak Interactions and Exotic Beta Decay Using ν Scattering on High Z Mater

Our knowledge of the fundamentals of the weak interactions without the associated complication of strong interactions is grossly limited. One purely electronic proc has been studied so far, namely, mu decay. With the advent of high intensity, high energy neutrino beams, this situation will change. A number of experiments to study such reactions are discussed.

B.1-68-77 (Nezrick)	8/12/68	C. Schultz L. Lederman	Tests of Universality with Neutrin

The intensity of neutrino beams at NAL offers the opportunity of making a sensitive test of μ-e universality at high energy and high momentum transfer. This involves the preparation of a ν_e beam or at least a ν beam greatly enriched in ν_e's. Experim to discuss μ-e universality are discussed.

S.68-78 (Sculli)	7/15/68	D. H. White	Seminar: W's at the 200 BeV Accelerator

Searches for the intermediate vector bosons are discussed. Backward muons from back ward produced W's are to be detected.

B.1-68-79 (Nezrick)	8/9/68	U. Camerini S. Meyer	Flux Calculation for the So-Called "High Quality Low Cost Beam"

Neutrino spectra to be expected from a device proposed by Krisch are calculated. Be designs in holding iron block shields and earth shields are compared. With the adve of high energy, high intensity accelerators, it becomes reasonable to discuss the production of relatively high energy, exotic beams.

B.10-68-80 (Nezrick)	8/12/68	D. Cline	Tagged High Energy $\bar{n}$ Hyperon and Antihyperon Beams at NAL

In this note tagged high energy $\bar{n}$, hyperon and antihyperon beams are discussed. Experiments with these beams are discussed.

D.1-68-81 (Bleser)	8/12/68	A. Roberts	Comment on D.1-68-52, "Initial Pro Capacity at NAL." By J. Sanford

Comments on Sanford's note on "Initial Program Capacity at NAL" are made. The large uncertainties in estimations of "number of beams required" are pointed out.

Report Number	Date	Author	Title
B.1-68-82 (Nezrick)	8/8/68	U. Camerini S. Meyer	Neutrino Beams and Shielding

A number of problems of neutrino beams and shielding are discussed. Among them are the following: (1) Should NAL concentrate initially on a wide-band system or a narrow-band ν beam system? (2) Should one concentrate on a low-energy neutrino beam or a high-energy neutrino facility? (3) Does the facility require a full muon shield capable of ranging out muons at the maximum energy or will a combination of magnetized iron, earth, iron shield and magnetic field suffice? (4) Should the facility be primarily below ground or above? (5) Where should the facility be located? This matter must be settled at a fairly early date.

B.5-68-83 (White)	8/13/68	A. D. Krisch	Very High Intensity π Beams

Simple calculations show that it will be possible to obtain pion beams of very high intensity at NAL. Shielding problems connected with such high intensity secondary beams are discussed.

B.11-68-84 (Bleser)	8/6/68	A. D. Krisch	Thin Targeting Stations with Earth Shielding and Steering Magnets

This report is a proposal to have several thin-target stations placed in a row along one of the branches of the EPB at NAL. The employment of earth shielding rather than movable concrete shielding would drastically reduce the cost of each station. This might allow the construction of two or three such stations for the cost of one conventional thin station.

B.2-68-85 (Sculli)	8/9/68	L. Lederman	Beam Dump Experiment: Dimuons and Neutrinos

When the 10^{13} (tired) 200 BeV protons are finally brought to their last resting place in the beam dump, a judicious arrangement permits a sensitive search for neutral bosons in the mass range 5-20 BeV/c^2. This is patterned after the dimuon search experiments at the AGS. The dimuon search possibilities at NAL are discussed.

A.1-68-86 (Key)	8/14/68	G. Trilling	Strong Interactions in the 25-ft. Bubble Chamber

This paper looks in some detail to see if there is indeed a useful energy region in which a large bubble chamber can be used in the reconstruction of a sufficiently large range of types of strong interaction inelastic events to represent a useful technique.

Report Number	Date	Author	Title
B.1-68-87 (Sculli)	8/14/68	D. Cline	Lepton Conservation Tests at High Momentum Transfer Using the ν Shield

In this paper, the author supposes that the energy spectrum and charge spectrum of muons coming out of the back of the shield and passing through a large bubble chamber could provide the possibility of testing lepton conservation at high momentum transfer

C.3-68-88 (Atac)	8/14/68	D. Luckey	Tagging Counters for Electrons in the 100 GeV Range

The synchrotron radiation of electrons in the beam deflecting magnets of a beam transport system can provide an excellent tagging counter for electrons in the 100 GeV range. Special Cerenkov counters for electrons will require extreme lengths and differential Cerenkov counters are possible but difficult. This note discusses Cerenkov counter limitations and some of the design considerations for tagging counter using synchrotron radiation. This note also points out the use of synchrotron radiati in making a separated electron beam.

A.1-68-89 (Key)	8/14/68	M. Derrick T. O'Halloran R. Kraemer	Fake Studies on Some Strong and Weak Interactions in the 12-ft. and 25-ft Bubble Chambers (Not yet written)

Report not yet ready for distribution.

C.2-68-90 (White)	8/14/68	A. D. Krisch	Experiment on Proton-Proton Interactions

In a previous report, the author described the advantages of using a thin-target station to study p-p interactions. In this report he gives a more detailed account of the experimental procedure involved in these experiments.

A.3-68-91 (Carrigan)	8/14/68	D. Cline	Comments on Hybrid Visual-Magnetic Spectrometers

The comments include the following: (1) Comparison with large bubble chambers. (2) Complicated triggering problems. (3) Gamma-ray energy and direction measurements. (4) Use in hyperon beams. The importance of efficient gamma-ray detection in the larg bubble chamber and hybrid bubble chamber-spectrometer systems is discussed.

C.3-68-92 (Atac)	8/14/68	C. Schultz	Polarized Targets at NAL

The author discusses the kinds of experiments one can do with polarized targets at NAL and a variety of possible polarization techniques. He concludes with recommendati for an NAL polarized target program.

Report Number	Date	Author	Title
C.1-68-93 (Carrigan)	8/14/68	L. Rosenson	Further Comments on the Influence of Detector Spatial Resolution on Spectrometer Scaling

It was pointed out by Lederman that great cost savings and possible experimental simplicity would be achieved if one could improve the spatial resolution of the detectors used in high energy experiments at NAL. The purpose of this note is to point out some details and complications of such scaling of magnets using the Charpak technique to obtain the desired resolution.

C.2-68-94 (Bleser)	8/14/68	D. Frisch A. D. Krisch D. Meyer	Facilities for Small Experiments

The main conclusion reached by this group of authors is that in 1972, people will require equipment that the authors are not smart enough at this time to foresee. They apologize for this shortcoming, a shortcoming which was not apparent in other subgroups of the Summer Study. Nevertheless, they recommend that a fair sum of money should be made available in 1970-71 to purchase those small and intermediate size items whose need will become apparent at about that time.

A.3-68-95 (Carrigan)	8/14/68	R. Hulsizer	Comments on Substituting a Streamer Chamber for the Bubble Chamber in the Hybrid Bubble Chamber-Spark Chamber Detector Proposed by T. Fields et al. in NAL Summer Study Report A.3-68-12, June 29, 1968

This paper is a discussion of how a streamer chamber might replace a bubble chamber in the proposed hybrid chamber-spectrometer system.

A.1-68-96 (Key)	8/14/68	G. Trilling	Report of Group A Large Hydrogen Bubble Chamber Study

The purpose of this report is to examine what bubble chambers should be operated at NAL to fulfill both the neutrino program and the strong interaction program. The strong interaction program is discussed in some detail in this report.

B.1-68-97 (Nezrick)	8/16/68	J. Peoples	Background in the 25-ft. Chamber when Using Neutrino Physics

For the purpose of assessing the effect of background particles in a large bubble chamber, it is helpful to divide the background into charged and neutral particles. The level of a neutral background is evaluated in terms of the contamination it introduces into the measurement of a reaction like $\bar{\nu} + p \rightarrow n + \mu^+$. The charged particle background can normally be eliminated during scanning, and its principal effect would be to slow down the scanning process.

Report Number	Date	Author	Title
C.3-68-98 (Key)	8/16/68	K. Strauch	Remarks on Doing Strong Interaction Physics Involving Multiparticle Final States in the 100 BeV Region

This note attempts to use the results of the study of the π^-p inelastic interaction experiment at 13 and 20 BeV by the Harvard Bubble Chamber group to try to answer the question as to what will be the problems of doing strong interaction physics involving multiparticle final states in the 100 BeV region.

C.2-68-99 (White)	8/16/68	T. White	A Spectrometer for Measuring Inelastic Secondaries from 200 GeV/c p-p Collisions

One experiment which will be part of the early experimental program of the 200 GeV accelerator, will be aimed at a survey of inelastic production of secondary particles by 200 GeV protons on hydrogen and on heavy targets. This paper explores in some detail the possibilities of a relatively cheap and simple spectrometer which could measure yields of long-lived secondaries over a wide range of longitudinal and transverse secondary particle momenta.

A.3-68-100 (Carrigan)	8/20/68	W. D. Walker	On the Use of a Hybrid Bubble Chamber in the 100 BeV Region

The difficulty of area scanning for very high energy interactions in a bubble chamber is pointed out. A number of other problems in the use of a hybrid bubble chamber are discussed. The author concludes that more effort should be made than is proposed by Fields, et al, in angle measurement and less effort in longitudinal momentum measurement, for the high energy tracks.

C.1-68-101 (Sculli)	8/15/68	D. Luckey	Form-Factor Experiments

The form factors of unstable particles like the K and π can be determined by scattering off an electron target. Unfortunately, the only practical target is the electrons found in matter. Beams of electrons lack intensity by many orders of magnitude from being practical targets. Specific form-factor experimental layouts are discussed.

B.10-68-102 (Bleser)	8/13/68	D. Cline	Comments on Low Momentum High Intensity Beams at NAL

With the advent of the 200 GeV accelerator, it is reasonable to ask whether there will be a need for low-energy beams (5-15 GeV/c). The author concludes in the affirmative, and gives reasons.

Report Number	Date	Author	Title
B.10-68-103 (Nezrick)		M. Webster	Separated Σ^- Beams for Bubble Chamber

The intense fluxes of Σ-hyperons predicted by Hagedorn-Ranft encourage one to think about the possibility of making bubble chamber beams, despite the severe decay losses. The author discusses these beams, which would probably open up a whole new region of the strange particle resonances, since Y* might be produced as copiously as N* and Ξ^* as readily as Y* are produced in p-p interactions.

B.1-68-104 (Nezrick)	8/8/68	M. L. Stevenson	The Neutrino Facility at NAL

Report not yet ready for distribution.

B.6-68-105 (Stekly)	7/8/68	T. Fields	Field-shape Tolerances for NAL Superconducting Beam in Transport Elements

Unlike the situation with conventional beam transport magnets, there is little direct information available on the detailed properties, particularly field shape, of practical superconducting dipoles and quadrupoles. This note summarizes some brief thoughts and discussions aimed at providing information which will be useful to designers of secondary beam transport elements.

B.4-68-106 (Bleser)	7/10/68	J. H. Smith	Targeting for Neutral Beams

The author proposes targeting schemes for neutral beams. In particular, he discusses K^o_L beams.

T.68-107 (Theory)		S. D. Drell	Remarks on Experiments at NAL

Theory paper - no abstract.

B.7-68-108 (Bleser)		H. Frauenfelder W. A. Wenzel	Target Stations with Beam Multiplicity

A target station is proposed which produces many simultaneous charged particle beams of high intensity, high quality, and a reasonably high degree of flexibility and compatibility. It is suitable for use at an intermediate station in a way that does not destroy the EPB, or for use ahead of the beam dump with the simultaneous production of several neutral beams.

Report Number	Date	Author	Title
B.9-68-109 (Roberts)		C. Heusch	A Proposed Electron-Photon Facility for the National Accelerator Laboratory

Report not yet ready for distribution.

Report Number	Date	Author	Title
B.9-68-110 (Roberts)		C. Heusch	Photon Experiments Beyond the Reach of Present Day Machines

Report not yet ready for distribution.

APPENDIX XI
TARGET MODULATED RF SEPARATED BEAMS

J. Lach

May 1969

The basic features of the rf beam I would like to describe are shown in figure 1; I will refer to this as a target modulated rf beam to distinguish it from the more conventional type. In this design the angle of the external proton beam is modulated by passing it through the first rf deflector. The essential condition is that the angular deflection of the first deflector must be large compared to the natural angular divergence of the beam. Following the deflector is a lens which focusses all particles emerging from the deflector with a given angle into a given position at the target plane. Here, on the optical axis, we place a target having a very small vertical extent which is then swept by the proton beam twice for each rf cycle. The time that the proton beam spends on the target during each of these sweeps is small compared to the rf period which means that most of the protons miss the target and those that do interact do so in a time bunch very small compared to the rf period. The three long lived strongly produced secondaries (π, K, p) will have a time structure at the target identicle to that of the interacting protons. The secondary beam is momentum analyzed and after an appropriate drift distance from the target the secondary particles will become temporally separated due to their slightly different velocities. This temporal separation is converted to an angular separation by the second rf deflector which is phased relative to the first so that the wanted particles are undeflected but both contaminants recieve deflections. Following the second deflector is a lens which again converts a given angle in the deflector to a position at the stopper. Note that the stopper is now a slit which allows the wanted particles to pass but not the contaminants. Finally there is a second momentum analysis which removes those unwanted particles which emerge from the slit jaws.

Let us look at the above system in more detail. We define θ_n^m as the proton beam angular extent (½ angle) in the first deflector, rf-1, and θ_d^m as the amplitude of the transverse angular deflection of the proton beam. We also assume that this deflection is in the vertical plane. The lens following the first deflector has the property

$$\gamma = f_2 \tan\theta \simeq f_2\,\theta$$

f_2 = lens focal length

where Y is the vertical position at the target and θ is the angle with which a given proton emerges from the deflector. The angle θ can be written

$$\theta = \theta_n + \theta_d^m \sin 2\pi \frac{t}{T}$$

where θ_n is the proton angle before entering the deflector, T is the period of the deflecting field, and t is time. We can then write

$$Y = f_2 \theta_n + f_2 \theta_d^m \sin 2\pi \frac{t}{T}$$

or defining $\alpha = \frac{Y}{f_2}$

$$\alpha = \theta_n + \theta_d^m \sin 2\pi \frac{t}{T}$$

For simplicity let us assume that the protons have a flat distribution in θ_n between the limits $-\theta_n^m < \theta_n < \theta_n^m$. We can then plot the proton distribution in α as a function of time and this is the shaded region of figure 2. In this diagram protons which will interact in the target will be centered about $\alpha = 0$ and a width α_t which is then the target angular size. We now ask how short a time will the proton beam actually be on the target. Calling this time t_p and refering to figure 2 we see

$$\alpha_t = \theta_d^m \sin \frac{\pi}{T}(T - t_p) - \theta_n^m$$

or

$$\frac{t_p}{T} = \frac{1}{\pi} \sin^{-1}\left(\frac{\alpha_t + \theta_n^m}{\theta_d^m}\right)$$

$$\simeq \frac{\alpha_t + \theta_n^m}{\pi\, \theta_d^m} \quad \text{for} \quad \frac{t_p}{T} << 1$$

Defining $\delta_\omega \equiv \frac{t_p}{T}$ $\qquad \delta_\omega = \frac{\alpha_t + \theta_n^m}{\pi\, \theta_d^m}$

Looking at figure 2 we can ask ourselves what fraction of the proton beam actually strikes the target. This fraction, I_f, is given by

$$I_f = \frac{2}{\pi} \sin^{-1} \frac{\alpha_t}{\theta_d^m}$$

$$\simeq \frac{2}{\pi} \frac{\alpha_t}{\theta_d^m}$$

We can solve this for α_t and insert it into our previous expression

$$\epsilon_\omega = \frac{I_f}{2} + \frac{\theta_n^m}{\pi \theta_d^m}$$

which can be solved for θ_d^m

$$\theta_d^m = \frac{\theta_n^m}{\pi \left(\epsilon_\omega - \frac{I_f}{2} \right)}$$

If we are given the vertical emittance or the external proton beam, ϵ_v, and the aperture of the deflector, a, we see

$$\theta_n^m = \frac{\epsilon_v}{2a}$$

where the factor of ½ must be included since θ_n^m is the ½ width of the beam. The deflector aperture is related to the wavelength by the relation

$$a = 0.4 \lambda$$

hence

$$\theta_d^m = \frac{\epsilon_v}{0.8 \pi \lambda \left(\epsilon_\omega - \frac{I_f}{2} \right)}$$

The fractional pulse width, δ_w, will be determined by the condition that the pulses containing the various particles should be temporally separated after a determined drift distance, L. This is illustrated in figure 3. Here δ_s is the separation of the pulse centers and we will assume that our particles are temporally separated if

$$\delta_s \geq k\, \delta_w$$

and k will probably have to be at least 2. We can now rewrite our equation for θ_d^m

$$\theta_d^m = \frac{\varepsilon_v}{0.8\pi\lambda\left(\frac{\delta_s}{k} - \frac{I_s}{2}\right)}$$

We now must convert this temporal separation into a spatial one. To do we define D_d^m as the deflection amplitude of the second deflector and can write

$$D_d = D_d^m \sin 2\pi \frac{t}{T}$$

as the deflection recieved by a particle entering it at a time, t. In order to convert these very small temporal separations into spatial ones we want our pulse of particles to enter the deflector when D_d is most rapidly changing

$$\frac{d D_d}{dt} = \frac{2\pi D_d^m}{T} \cos 2\pi \frac{t}{T}$$

$$\left.\frac{d D_d}{dt}\right|_{max} = \frac{2\pi D_d^m}{T}$$

We can write this in a more convenient form

$$\Delta D_d = 2\pi\, \delta_s\, D_d^m$$

The quantity, ΔD_d, will be the angular separation of the wanted particles from the contaminants. In order for such a separation to actually exist the natural angular width of the beam in the deflector, D_n^m, must be small compared to ΔD_d.

We can probably still separated particles if

$$\Delta D_d \geq g D_m^m$$

but g will probably have to be at least 2.

If the vertical height of the target, Y_t, is given we have now fixed θ_v^t the vertical acceptance of our beam at the target since the target magnification at the second deflector, m_v, is

$$m_v = \frac{\frac{1}{2} 0.4\lambda}{Y_T} = \frac{\theta_v^t}{\Delta D_d}$$ Note: Y_t is ½ height

and

$$\theta_v^t = \frac{0.2\lambda \Delta D_d}{Y_T}$$

finally

$$\theta_v^t = \frac{0.2\pi \lambda g \delta_s D_d^m}{Y_T}$$

where θ_v^t is the vertical acceptance of the beam at the target.

One is now in a postition to draw a rather interesting conclusion about the frequency dependence of the intensity of such a beam. Assume we fix all the parameters of the beam, momentum, length, proton beam emittance, etc., excepting the deflector wavelength. The intensity of the wanted particles is proportional to the product of I_f and θ_v^t. Let us solve our equation for θ_d^m in terms of I_f.

$$I_f = \frac{2\delta_s}{k} - \frac{\varepsilon_v}{0.4\pi\lambda\theta_d^m}$$

and note that $\delta_s \sim \frac{1}{\lambda}$ so that

$$I_f \sim \frac{1}{\lambda}$$

Looking at our expression for θ_v^t we see that it is independent of λ. Hence the intensity of a target modulated rf beam is inversly proportional to the the wavelength and using a longer wavelength merely means a sacrifice of intensity.

Let us consider the expression for I_f as a function of the drift distance L. The only dependence on L is through δ_s and from the form of the equation there must be some δ_s below which separation is not possible. This minimum value, δ_s^{min}, is determined by setting $I_f = 0$

$$\delta_s^{min} = \frac{\varepsilon_v k}{0.8\pi\lambda\theta_d^m}$$

We define a time shift between our wanted and unwanted particles per unit drift distance, t_1, by the relation

$$\delta_s = \frac{L t_1}{T}$$

$$= \frac{L t_1 c}{\lambda}$$

or

$$L = \frac{\lambda \delta_s}{t_1 c}$$

There must be a L^{min} corresponding to δ_s^{min} given by

$$L^{min} = \frac{\lambda \delta_s^{min}}{t_1 c}$$

$$= \frac{\varepsilon_v k}{0.8\pi\theta_d^m t_1 c}$$

We note that <u>L^{min} is independent of wavelength</u>.

For a given set of deflector and external proton beam parameters, determine the minimum drift distance, L^{min}, below which separation is not possible. Let us

compute L^{min} for the following parameters. Assume a 3 meter deflector which is capable of imparting a transverse momentum of 18 MeV/c (the present BNL S-band deflectors are capable of this). For a 200 GeV/c beam this amounts to a deflection of

$$\theta_d^m = \frac{18\ MeV/c}{200\ GeV/c}$$

$$= 90\ \mu rad$$

Let us further assume

$$\varepsilon_v = 0.09\ \pi \text{ mm-mrad}$$

$$= 28.3 \text{ cm-}\mu\text{rad} \quad \text{(from NAL design study)}$$

$$k = 2$$

and that we wish a beam which will separate kaons from pions at 100 GeV/c. Figure 4 is a plot of t_1 as a function of momentum for the three possible particle combinations. We see from this plot that for K-π separation at 100 GeV/c

$$t_1 = 3.7\ 10^{-14} \text{ seconds/meter}$$

which gives

$$L^{min} = 225 \text{ meters}$$

which is a very reasonable beam length by NAL standards. Since for the above distance we will have zero flux, we will pick three longer distances for our sample calculations. These are 0.35 Km, 0.50 Km, and 0.65Km. For each of these distances we will consider λ = 3 cm (X-band) and λ = 10.5 cm (S-band) deflectors. The horizontal acceptance at the target will be taken, rather arbritrarily, at 1.0 mrad. We will assume a momentum bite of 0.1% (full width) and a target size of 0.5 mm (Y_t = 0.25 mm). The length of the second deflector will be assumed the same as the first which means that its deflection amplitude will be doubled that of the first since the secondary beam momentum is 100 GeV/c.

We will futher assume an external proton beam intensity of 10^{13} protons per pulse. To estimate the zero degree K^- flux we have used the Trilling curves from the LRL design study for pions and reduced it by a factor of 10. This give 0.2 K^- (sr-GeV/c-interacting proton)$^{-1}$. We have included an extra factor of 0.35 to account for targeting losses, beam shaping losses, etc. Note that the vertical acceptance of the beam at the target computed from the relation given on page 5 and shown in table 1, θ_v^τ, is probably larger than could be realized in practice and in the following flux computation we will assume the acceptance to be only 1 mr in the vertical plane. This gives us

$$\text{Flux} = (0.2)\,(0.1)\,(10^{13}\ \text{protons per pulse})\,(0.35)\,I_f\,\Delta\Omega$$

(0.2): K^- (sr-GeV/c-interacting proton)$^{-1}$

(0.1): ΔP (GeV/c)

(0.35): target efficiency, etc.

where $\Delta\Omega = \pi\,\theta_v^t\,\theta_h^t$

Table 1 is a summary of these parameters and fluxes for three drift distances and two deflector frequencies. Note that the length refered to here is the distance between the target and the second deflector and does not include the second momentum analysis section. One sees from this table that the available kaon fluxes are adequate for bubble chamber experiments but probably not useful for counter experiments.

How does this kind of rf beam differ in performance from a conventional two cavity system? The essential differences are that this beam has no stopper losses and the drift region begins at the target rather than at the first deflector. Similar separation with a conventional two deflector system can be achieved with the same deflectors and same drift lengths if one makes similar restrictions on the beam angular width in the deflectors. For the same number of <u>interacting</u> protons the target modulated beam will produce a higher flux of wanted particles because it does not have any inherent stopper losses and may have slightly lower decay losses because of the shorter overall length.

A final amusing point is that if rf-1 had a frequency which was ½ that of rf-2, it would be possible to make a simultaneous three way separation of our particles; i.e., kaons directly forward, pions above, and protons below!

Let me conclude by summarizing the good and bad points of a target modulated rf beam design.

GOOD POINTS

1. It provides a low flux separated beam in a length shorter than a conventional rf beam since the drift region starts at the target.
2. Since there are no inherent stopper losses, it makes extremely effective use of the interacting protons. For our 0.5 Km beam at S-band we only interact 2.8% of the proton beam. The rest passes above and below the target and can be used by downstream experimenters. If the slight increase in emittance imparted to the protons by rf-1 is objectionable to the downstream experimentors, another deflector after the target could be used to exactly cancel the deflection of rf-1 and reduce the proton beam emittance to what it was originally.
3. The beam operates over a continuous range of momenta. However this would also be true of a conventional two deflector system if it were operated in the same manner; that is, using a very small phase shift between wanted and unwanted particles, not the conventional 2π shift between the unwanted particles.

BAD POINTS

1. Inherently low fluxes.
2. Its performance will be very sensitive to the shape of the initial proton beam. Probably an additional optical system will be needed upstream of rf-1 to insure that the beam has the required emittance and has no 'halo'.
3. Uses very small deflection angles. This problem would still be with us, however, with a conventional beam operating with the same deflectors and drift space.

Summary of beam parameters and operation

LENGTH L	λ	δ_s	α_T	θ_m^m	ΔD_d	θ_v^π	$\Delta\Omega$	I_f	Flux
0.35 km	3 cm	0.129	6.4 μrad	11.8 μrad	146 μrad	11.0 mr	34.5 μsr	.045	3150. K^- per pulse
	10.5	0.036	1.7	3.4	40	11.0	34.5	.012	840.
0.50 km	3 cm	0.185	14.3	11.8	209	15.6	49.0	.101	7070.
	10.5	0.052	3.9	3.4	59	15.6	49.0	.028	1960
0.65 km 1.5	3.0 cm	0.240	22.1	11.8	271	20.4	64.0	.156	10900.
	10.5	0.068	6.4	3.4	77	20.4	64.0	.045	3150.

Parameters Used

$P = 150$ GeV/c

$\varepsilon_v = 0.09\,\pi$ mm-mrad
$= 28.3$ cm-μrad

$\theta_d^m = 90$ μrad

$D_d^m = 180$ μrad

$Y_T = 0.025$ cm.

$k = q = 2$

$\theta_h^\pi = 1.0$ mrad

$\frac{\Delta P}{P} = 10^{-3}$

Assume K^- flux at target at zero degrees of 0.2 K^- / sr/ GeV/c / interactiong proton

Note: In the Calculation of the Flux a solid angle bite $\Delta\Omega = 1$ μsr has been used since the values of θ_v^π listed above probably cannot be realized in practice. Even this smaller solid angle give fluxes which are adequate for bubble chamber experiment.

Figure 1

Target modulated rf beam illustrating K separation from π and p.

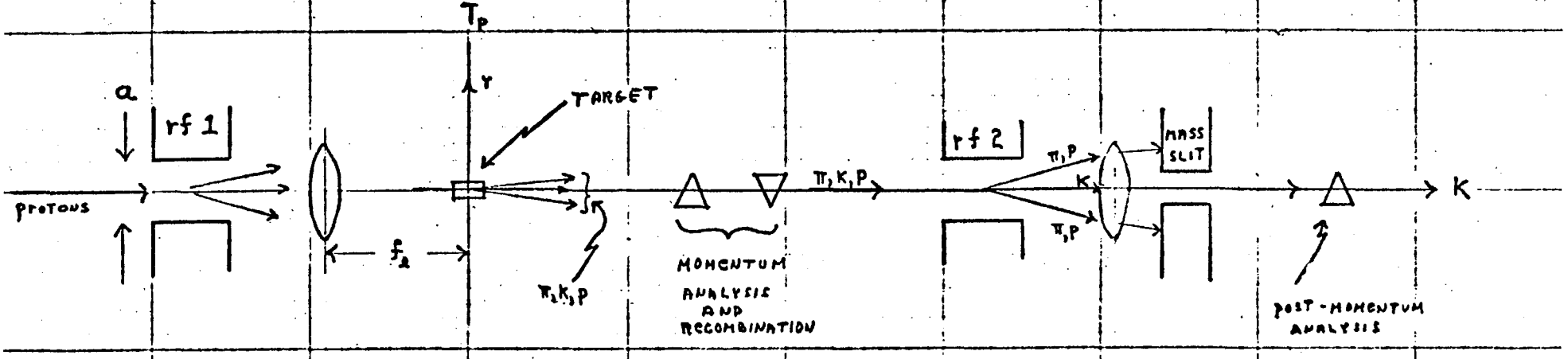

Figure 2

Time structure of protons on the target

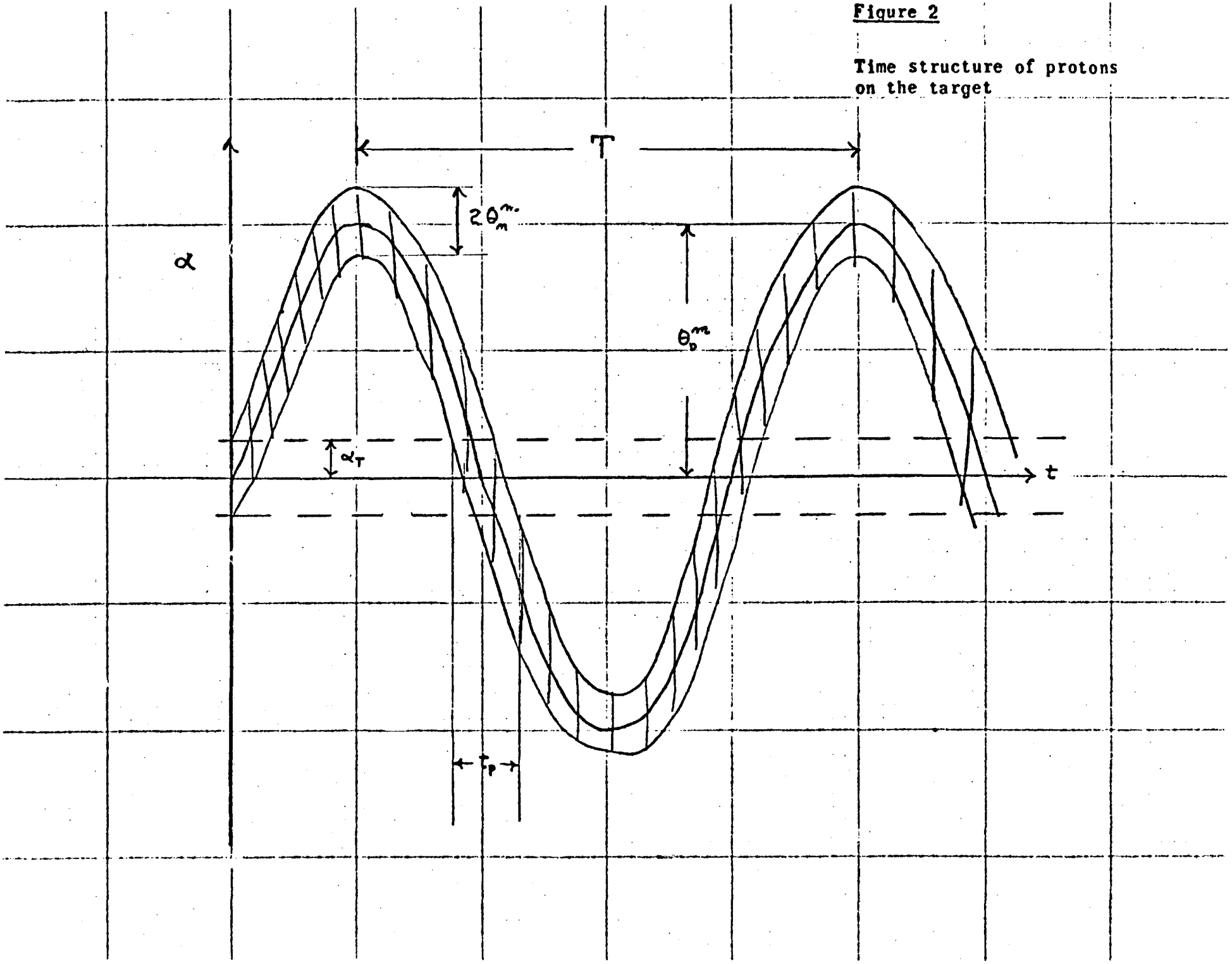

Figure 3

Time distribution of particles at rf-2

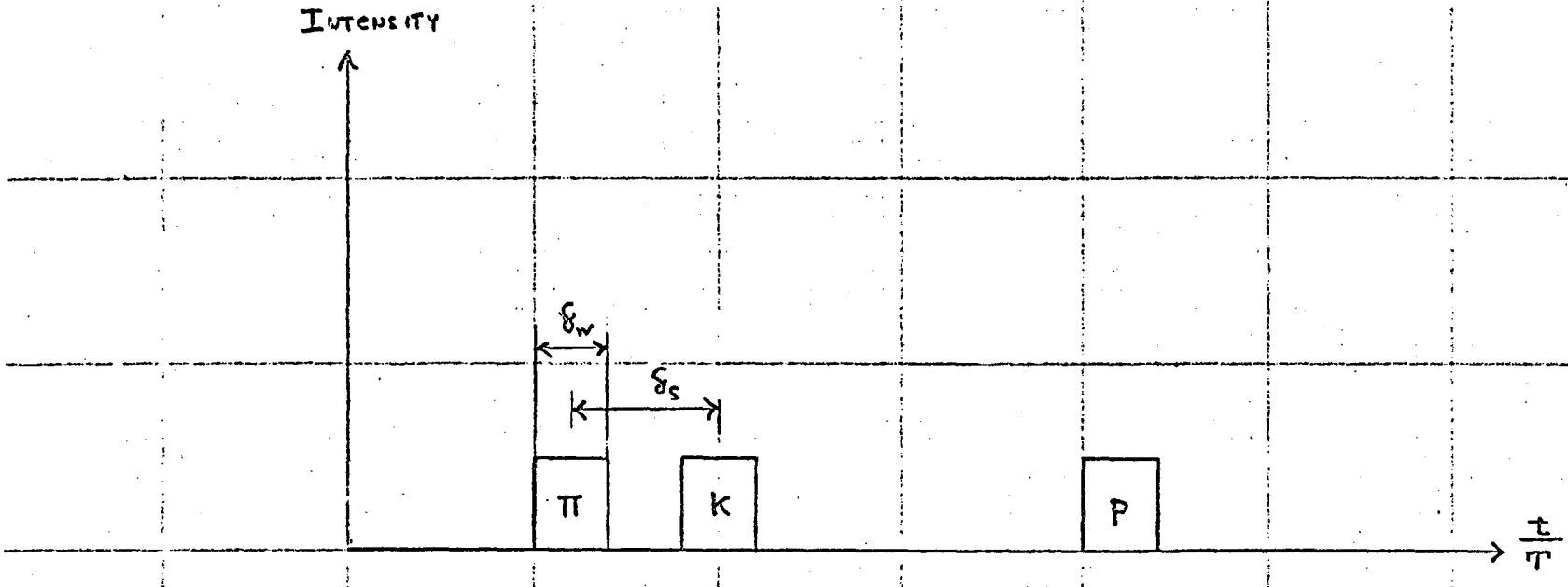

Transit time difference per meter vs Momentum

Frequency	Wavelength	Period	
2.85 GHz	10.5 cm	$3.5\ 10^{-10}$ sec	(S-ban
10.0	3.0	1.0	(X-ban
15.0	2.0	0.67